CHARLES UNIVERSITY

Faculty of Science

Department of Biochemistry

Doctoral study program: Biochemistry



Mgr. Kateřina Bělonožníková

Use of biochemical methods in the study of plant metabolism with emphasis on the defense system

Doctoral thesis

Supervisor: doc. RNDr. Helena Ryšlavá, CSc.

Consultant: RNDr. Daniel Kavan, Ph.D.

Prague, 2021

Prohlášení (In Czech):

Prohlašuji, že jsem závěrečnou práci zpracovala samostatně a že jsem uvedla všechny použité informační zdroje a literaturu. Tato práce ani její podstatná část nebyla předložena k získání jiného nebo stejného akademického titulu.

V Praze, ----------

Mgr. Kateřina Bělonožníková

Declaration:

I declare that I have prepared the doctoral thesis independently and that I have listed all used information sources and literature. Neither this work nor a substantial part of it has been submitted for another or the same academic degree.

In Prague, ----------

Mgr. Kateřina Bělonožníková

Declaration of authorship:

I declare that Mgr. Kateřina Bělonožníková contributed significantly to all the scientific publications in her doctoral thesis. She performed the specified experiments, substantially contributed to their planning, and took a significant part in the primary data interpretation and their preparation for publication.

In Prague, ----------

---

doc. RNDr. Helena Ryšlavá, CSc.

Abstract

As sessile organisms, plants cannot avoid being exposed to various biotic and abiotic stress factors. To defend themselves plants have developed complex and sophisticated defense mechanisms. In agriculture, pesticides are used for plant protection, but they can have undesirable side effects, and therefore attention is being paid to biological control agents.

One such agent is *Pythium oligandrum*, a soil oomycete that has a positive effect on plants at several levels. On the one hand, it secretes elicitins, which stimulate defensive responses and prepare the plant for possible infection (i.e., priming effect), and on the other hand, it produces tryptamine, a precursor of auxin, thus supporting the plant's growth. Furthermore, *P. oligandrum* directly acts as pathogen mycoparasite or evokes antibiosis, or competition for nutrients and space with other microorganisms.

The key research topic of this thesis was the analysis of the biochemical properties of eleven *Pythium* strains and their impact on plant metabolism. Our results showed that even closely related *P. oligandrum* strains significantly differ in the content of compounds secreted into the medium, including proteins, amino acids, tryptamine, and hydrolytic enzymes capable of degrading cell walls (endo-ß-1,3-glucanase, chitinase, and cellulase), exoglycosidases, proteases, and phosphatases. Rapeseed plants, seed-coated with *Pythium* strains, showed major differences in the phytohormone levels, i.e., increased concentrations of auxin and jasmonates (and salicylic acid in some strains), indicating plant growth promotion as well as readiness for effective defense response. The *Pythium* strains treated plants showed increased activities of isoforms of superoxide dismutase and peroxidase, involved in the plant antioxidant system, as well as shikimate dehydrogenase, one of the key enzymes in the secondary metabolite synthesis. The different behavior or "life strategy" of the *Pythium* strains may be crucial for selecting advantageous biological control agents.

Plant viruses are responsible for considerable economic losses. Various factors affect the virus propagation and plant defense responses. We followed the effect of two-hour long heat shock of 42°C on the course of potyviral (PVY^{NTN}) infection in *Nicotiana tabacum*. Heat shock protein (Hsp) expression plays an ambiguous role in viral infection. Hsp70 participates in plant defense response but also can interact with viral proteins and facilitate virus propagation. We detected that Hsp70 accelerated potyviral propagation in tobacco plants. The cytosolic and mitochondrial Hsp70 (~50-75 kDa) were present during the developed viral infection. Also, the plant defense response to PVY^{NTN} included an increase of salicylic and chlorogenic acids but decrease of quinic acid content. We also summarized the current scientific research about the mutual behavior of Hsp70 and viral infection in a review.

The plant protection still relies on the use of pesticides which represent a potential threat to the non-target organisms. The mechanism of triazole action lies in blocking the fungal sterol 14-α-demethylase (cytochrome P450 51A1), resulting in the depletion of ergosterol, and thus destabilization of the fungal plasma membrane. We observed that the foliar treatment by triazoles (fungicides) and their mixtures likely induces oxidative stress in tomato plants, resulting in alteration of some phenolic compound contents such as quercetin, *p*-coumaric acid,

and hesperidin in fruit. We studied the interactions of triazoles mixtures in the presence of copper and zinc cations that significantly change the compound reactivity. The triazole cocktails also showed a significant inhibition impact on the enzymes of the non-target organisms, such as cytochromes P450 19A1 (aromatase) and 3A4 that can cause significant health problems for humans and animals.

Herbicides like glyphosate target the shikimate pathway, which represents a metabolic route for the biosynthesis of aromatic amino acids and a connection to the production of various phenolics. We studied the mechanism of bisubstrate reaction and side reactions of the shikimate dehydrogenase from the root of *Petroselinum crispum*. We observed a feed-back regulation for one branch of phenylpropanoids on the shikimate dehydrogenase activity and that the compounds with higher number of hydroxyl groups showed higher inhibition impact.

Phenolics are undoubtedly the largest group of natural substances with antioxidant properties. We analyzed commonly available herbs in the form of teas and tinctures, with *Agrimonia eupatoria* showing the highest total phenolics content, also *Origanum vulgare* and *Mentha* × *piperita* possessing high antioxidant capacity in aqueous extracts.

Keywords: *Pythium oligandrum*, biological control agents, antioxidant system, phenolic compounds, viral infection, heat shock proteins, triazoles, fungicides.

Abstrakt (In Czech)

Rostliny, jako sesilní organismy, se nemohou vyhnout působení abiotických a biotických stresových faktorů. Z těchto důvodů se v rostlinách vyvinuly komplexní a sofistikované mechanismy obrany. V zemědělství se k ochraně rostlin používají pesticidy, které ale mohou mít nežádoucí vedlejší účinky, a proto se pozornost obrací na přípravky biologické ochrany rostlin.

Jedním z takových prostředků je *Pythium oligandrum*, půdní oomyceta, která pozitivně působí na rostliny v několika úrovních. Jednak vylučuje elicitiny, které stimulují obranné odpovědi a připravují rostlinu na případnou infekci (tzv. priming efekt), jednak sekretuje tryptamin, prekurzor auxinu, čímž podporuje růst rostliny. Kromě toho je *P. oligandrum* schopné mykoparazitismu vůči různým patogenům nebo antibiózy, přičemž také úspěšně soutěží s ostatními mikrooganismy o živiny a prostor. Klíčovým výzkumným tématem této práce byla analýza biochemických vlastností jedenácti izolátů *P. oligandrum* a jejich vliv na metabolismus rostlin. Naše výsledky ukázaly, že i blízce příbuzné izoláty *P. oligandrum* se významně liší v obsahu sloučenin sekretovaných do média, včetně proteinů, aminokyselin, tryptaminu a hydrolytických enzymů schopných degradovat buněčné stěny (endo-ß-1,3-glukanasa, chitinasa a celulasa), exoglykosidasy, proteasy a fosfatasy. Rostliny řepky, jejichž semena byla mořena izoláty rodu *Pythium*, vykazovaly velké rozdíly v hladinách fytohormonů, tj. zvýšené koncentrace auxinu a jasmonátů (v některých případech i kyseliny salicylové), což pravděpodobně přispívá k podpoře růstu rostlin a jejich připravenosti na efektivní obrannou odpověď. Rostliny ošetřené *P. oligandrum* vykazovaly zvýšenou aktivitu izoforem superoxiddismutasy a peroxidasy, které se podílejí na antioxidačním systému rostlin, a šikimátdehydrogenasy, jednoho z klíčových enzymů syntézy sekundárních metabolitů. Rozdílné chování neboli „životní strategie“ jednotlivých izolátů blízkých *P. oligandrum* je rozhodující pro výběr účinných prostředků biologické ochrany rostlin.

Rostlinné viry jsou odpovědné za významné ekonomické ztráty. Mnoho různých faktorů ovlivňuje šíření virů a obranné reakce rostlin. Sledovali jsme průběh infekce *Y virem bramboru* (PVY^{NTN}) v rostlinách *Nicotiana tabacum*, v souvislosti s dvouhodinovým teplotním šokem (42°C). Exprese proteinů teplotního šoku (Hsp) hraje dvojznačnou roli během virové infekce. Hsp70 se podílí na obranné reakci rostlin, ale také může interagovat s virovými proteiny a usnadňovat množení viru. Zjistili jsme, že některé izoformy Hsp70 urychlily šíření PVY^{NTN} v rostlinách tabáku. Cytosolové a mitochondriální formy Hsp70 (~50-75 kDa) byly přítomny během rozvinuté virové infekce. Obranná reakce rostlin vůči PVY^{NTN} zahrnovala zvýšení množství kyseliny salicylové a kyseliny chlorogenové, ale zároveň snížení obsahu kyseliny chinové. Problematiku vzájemného chování Hsp70 a virové infekce jsme shrnuli v přehledném článku.

Ochrana rostlin stále závisí na používání pesticidů, často ve směsích, které představují potenciální hrozbu pro necílové organismy. Podstatou účinku triazolů je, že blokují enzym sterol 14-α-demethylasu (cytochrom P450 51A1), což vede k nedostatku ergosterolu, a tedy k destabilizaci plazmatické membrány hub. Zjistili jsme, že ošetření listů triazoly a jejich kombinacemi pravděpodobně vyvolává v rostlinách rajčete oxidační stres, což v plodech vede ke změně obsahu některých fenolických látek, jako je kvercetin, kyselina *p*-kumarová a hesperidin.

Zaměřili jsme se také na interakce triazolových směsí v přítomnosti iontů mědi a zinku, které významně mění reaktivitu těchto sloučenin. Tyto triazolové koktejly také měly významný inhibiční dopad na enzymy necílových organismů, jako jsou cytochromy P450 19A1 (aromatasa) a 3A4, které mohou způsobit významné zdravotní problémy lidem a ostatním živočichům.

Herbicidy jako glyfosát cílí na šikimátovou dráhu, která představuje metabolickou cestu pro biosyntézu aromatických aminokyselin, a je také spojena s produkcí různých fenolických látek. Zaměřili jsme se tedy na studium kinetických parametrů a produkty vedlejších reakcí šikimátdehydrogenasy z kořene rostliny *Petroselinum crispum*. Pozorovali jsme regulaci zpětnou vazbou pro jednu větev skupiny fenylpropanoidů na aktivitu šikimátdehydrogenasy a to, že sloučeniny s vyšším počtem hydroxylových skupin vykazovaly vyšší inhibiční účinek.

Fenolické látky jsou nepochybně největší skupinou přírodních látek s antioxidačními vlastnostmi. Analyzovali jsme běžně dostupné byliny ve formě čajů a tinktur, přičemž nejvyšší celkový obsah fenolických látek vykazovala rostlina *Agrimonia eupatoria*, ale také *Origanum vulgare* a *Mentha* × *piperita* představovaly rostliny s vysokou antioxidační kapacitou ve vodných extraktech.

Klíčová slova: *Pythium oligandrum*, biologická ochrana rostlin, antioxidační systém, fenolické látky, virová infekce, proteiny teplotního šoku, triazoly, fungicidy.

Acknowledgement

Firstly, I would like to express my gratitude to my supervisor doc. RNDr. Helena Ryšlavá, CSc. for her professional guidance, valuable advice, willingness to always help in solving any problems, also for being always extremely kind and patient, and for encouraging me in every critical moment. This work is also her merit in many aspects. I also thank to RNDr. Veronika Hýsková, Ph.D. for being always friendly, hard-working, and ready to help, offer worthy advice and for her determination to successfully accomplish all the initiated projects. I thank to RNDr. Daniel Kavan, Ph.D. for being always ready to solve problems, offer help, give courage, support any idea, and conduct any experiments at any time. At the Institute of Experimental Botany, I thank to doc. RNDr. Noemi Čeřovská, CSc. for her enthusiasm, energic approach, help and support in the virology projects. I also thank to RNDr. Helena Synková, CSc. for her valuable advice, discussions about experiments on abiotic stress and for arranging my internship in Belgium. Also, I would like to thank to Lenka Kolčabová for being cheerful, friendly, and curious about the experiments and for looking after the plants in the greenhouses. At University of Hasselt in Belgium, I must thank to prof. Dr. Roland Valcke for letting me stay in his laboratory, for his support and interest in our research about abiotic stress factors and being very generous and benevolent. I also thank to doc. RNDr. PhDr. Ing. Jana Jaklová Dytrtová, Ph.D. for her contagious determination to elucidate the side effects of pesticides and for being always cheerful, helpful, and full of ideas. Also, I would like to mention Mgr. Martin Černý, Ph.D. for his enthusiasm, determination, and patience in our never-ending project about casein as a nitrogen source for plants. I would also like to thank to prof. RNDr. Petr Hodek, CSc. for showing interest and support of our research. I also very much thank and respect all my colleagues at Department of Biochemistry for creating a pleasant and gracious work environment.
Finally, I would like to express my deep gratitude to my family for their endless support and kindness.

This work was supported by the Czech Science Foundation (18-01710S), Technology Agency of the Czech Republic, program Zeta (TJ01000451), and the Charles University projects SVV260572/2020, GA UK No. 1304119, and partly by Ministry of Industry and Trade of the Czech Republic (FV20630). I would also like to thank to the foundation "Nadání Josefa, Marie a Zdeňky Hlávkových" for supporting my internship at University of Hasselt in Belgium.

Content

List of Abbreviations **1**

1 Introduction **3**

1.1 Plant antioxidant system *3*
1.1.1 Reactive oxygen species 3
1.1.2 Antioxidant enzymes 7
1.1.3 Antioxidants 10
1.1.4 Phenolic compounds 11
1.1.5 Reactive nitrogen species 14
1.1.6 Reactive sulfur species 15
1.1.7 Reactive carbonyl species 17

1.2 Environmental stress *19*
1.2.1 Biotic stress factors 19
1.2.2 Oxidative signaling 23
1.2.3 Viral infection 24
1.2.4 Abiotic stress factors 31
1.2.5 Pesticides 31

1.3 Sustainable agriculture *35*
1.3.1 Priming 36
1.3.2 Biological control agents 37
1.3.3 *Pythium oligandrum* 38

2 Aims of the thesis **42**

3 Results and discussion **43**

3.1 Publications *43*

3.2 Plant metabolism under stress conditions *45*
3.2.1 Novel insights into the effect of *Pythium* strains on rapeseed metabolism 45
3.2.2 Effects of heat treatment on metabolism of tobacco plants infected with *Potato virus Y* 75
3.2.3 Hsp70 plays an ambiguous role during viral infections in plants (Review) 90
3.2.4 How is the activity of shikimate dehydrogenase from parsley root regulated and which side reactions are catalyzed? 104
3.2.5 Side effects of triazoles on treated crops 150

3.3 Antioxidants and their impact on humans and the environment *162*
3.3.1 Characterization of some potential medicinal plants from Central Europe by their antioxidant capacity and the presence of metal elements 162
3.3.2 Does resveratrol retain its antioxidative properties in wine? Redox behaviour of resveratrol in the presence of Cu(II) and tebuconazole 172
3.3.3 Triazoles and aromatase: The impact of copper cocktails 179
3.3.4 Cocktail effects of triazoles and zinc on cytochrome 3A4 and 19A1 189

4 Conclusion **218**

5 References **221**

List of Abbreviations

ABA - abscisic acid
ACC - aminocyclopropane-1-carboxylic acid
ADP - adenosine diphosphate
AGO - argonaut protein family
AO - amine oxidase - EC 1.4.3.6
AOs - flavin-containing amine oxidases - EC 1.5.3.3
APX - ascorbate peroxidase - EC 1.1.11.1
ASC - ascorbate
Avr - avirulent factors
BCAs - biological control agents
CA - caffeic acid
CAT - catalase - EC 1.11.1.6
CDPKs - Ca^{2+}-dependent protein kinases
CERK1 - chitin elicitor receptor kinase
CGA - chlorogenic acid
cGMP - cyclic guanosine monophosphate
CuAOs - copper-containing amine oxidases - EC 1.4.3.6
CYP - cytochrome P450
DAMPs - damage-associated molecular patterns
DCL - Dicer-like protein - ribonuclease III-like protein
DHA - dehydroascorbate
DHAR - dehydroascorbate reductase - EC 1.8.5.1
DHD - 3-dehydroquinate dehydratase - EC 4.2.1.10
dsRNA - complementary double strand RNA
E4P - D-erythrose-4-phosphate
EFR - pattern-recognition receptor binding EF-Tu (elongation factor thermo unstable)
ESI-MS - electrospray ionization mass spectrometry
ET - ethylene
ETI - effector-triggered immunity
FA - ferulic acid
FALDH - glutathione-dep. formaldehyde dehydrogenase EC 1.2.1.46
FLS2 - pattern-recognition receptor for bacterial flagellin
GA - gallic acid
GPOX - guiacol peroxidase EC 1.11.1.7
GPX - glutathione peroxidase EC 1.11.1.9
GR - glutathione reductase EC 1.8.1.7
GSH - reduced glutathione
GSNO - S-nitrosoglutathione
GSSG - oxidized glutathione
GST - glutathione *S*-transferase EC 2.5.1.18
HCpro - helper component-proteinase
HR - hypersensitivity reaction
IAA - indole-3-acetic acid
JA - jasmonic acid
LAR - localized acquired resistance
LC-MS - liquid chromatography-mass spectrometry
LHC - light harvesting complex
LRR - leucine-rich-repeat
M - mock

MAMPs - microbe-associated molecular patterns
MAPK - mitogen-activated protein kinase
MCO attack - metal-catalyzed oxidative attack
MDA - malondialdehyde ($CH_2(CHO)_2$)
MDHAR - monodehydroascorbate reductase EC 1.6.5.4
MG - methylglyoxal (CH_3COCHO)
MPs - cell-to-cell movement proteins
Ni:NOR - nitrite-NO reductase
NLRs - nucleotide-binding domain and LRR containing proteins
NOS - NO-synthase EC 1.14.13.39
NR - nitrate reductase EC 1.7.1.2
PAMPs - pathogen-associated molecular patterns
Pas - polyamines
PCD - programmed cell death
PEP - phosphoenolpyruvate
PR proteins - pathogenesis-related proteins
PRX - peroxiredoxin EC 1.11.1.15
PTI - pattern triggered immunity
PXs - non-specific peroxidases
QA - quinic acid
R genes - resistance genes
RBOH - respiratory burst oxidase homologs (NADPH oxidase)
RCS - reactive carbonyl species
RDRs - RNA-dependent RNA polymerases
RIPs - ribosome-inactivating proteins
RISC - functional RNA-induced silencing complex
RLCKs - receptor-like cytoplasmic kinases
RLKS - leucine-rich-repeat receptor-like kinases
RNAi - RNA interference
RNS - reactive nitrogen species
ROS - reactive oxygen species
RSS - reactive sulfur species
Rubisco - ribulose-1-5-bisphophate carboxylase/oxygenase EC 4.1.1.39
SDH - shikimate dehydrogenase EC 1.1.1.25
siRNAs - 21-24-nucleotide short interfering RNAs
SA - salicylic acid
SKA - shikimic acid
SOD - superoxide dismutases EC 1.15.1.1
SRX - sulfinic acid reductases (sulfiredoxins)
TCV - turnip crinkle virus coat protein
TMV - tobacco mosaic virus
VSRs - viral suppressors of RNAi
WRKY - transcription factors with 1 or 2 WRKY (amino acids) protein domains
XO - xanthine oxidase EC 1.17.3.2

1 Introduction

1.1 Plant antioxidant system

Plants are sessile organisms, and thus, cannot avoid being exposed to unfavorable environmental conditions, i.e., various abiotic and biotic stress factors. Such exposure may lead to disruption of metabolic processes at the molecular, cellular, organismal, or even ecosystem level (Bartwal et al 2013). Therefore, during evolution, plants had to develop effective mechanisms that would eliminate or at least reduce this apparent disadvantage. They protect themselves with constitutive defense - pre-formed physical barriers (e.g., cuticle, cell wall, trichomes) and chemical barriers (e.g., secondary metabolites) (Huey et al 2002, Kliebenstein 2012). Plants also employ induced defense mechanisms, including the cell wall lignification, increased production of antimicrobials, defense proteins, and the enhancement of "chemical weapons" - reactive oxygen species (ROS) and nitrogen (RNS) levels, leading to oxidative or nitrosative ("nitro-oxidative") stress and sometimes even to triggering the programmed cell death (PCD). PCD may destroy the plant cell but also prevents further pathogen spread (Hasanuzzaman et al 2020, Janků et al 2019, Miller et al 2017).

1.1.1 Reactive oxygen species

The plant exposure to environmental stress results in oxidative burst and ROS play a dual role as both toxic (at high levels) and signaling (at low levels) compounds. Therefore, oxidative stress comes from the imbalance between ROS production and elimination (scavenging by antioxidants), representing a complex biochemical and physiological phenomenon (Hasanuzzaman et al 2020, Janků et al 2019, Soares et al 2019). ROS include the hydroxyl radical (•OH), which is highly dangerous, reacting quickly very close to its site of generation, superoxide radical ($•O_2^-$), perhydroxyl radical (•OOH), then hydrogen peroxide (H_2O_2), singlet oxygen ($^1O_2$) and ozone (O_3) (Hasanuzzaman et al 2020, Janků et al 2019, Kapoor et al 2019, Soares et al 2019). Free radicals have a short life span, and they readily react with most biological macromolecules (Janků et al 2019, Kapoor et al 2019).

They can damage nucleic acids (oxidation of deoxyribose, strand breaks, removal/degradation of nucleotides, modification of bases, and cross-linked protein-DNA), lipids (chain breaks and increase of the membrane fluidity and permeability), and proteins (site-specific amino acid modification, fragmentation of peptides, aggregation of cross-linked products, electric charge alteration, inactivation of enzymes, and increase in the protein susceptibility to proteolysis) and even activate PCD (Caverzan et al 2016, Janků et al 2019, Kapoor et al 2019). Oxidatively-damaged proteins are labeled and destined for degradation in the proteasome or for autophagy (Czarnocka & Karpiński 2018). ROS reactivity is significantly mediated by free Fe^{2+} ions which catalyze the Fenton reaction, producing ·OH radicals (Janků et al 2019).

ROS can be produced with varying magnitude from almost every cellular compartment, depending on the environmental and developmental conditions (Fig. 1, p. 6) (Bhattacharjee 2019). In chloroplasts, chlorophyll pigments and the reaction center of photosystem II are the main $^1O_2$ source. The Mehler reaction (photoreduction of oxygen), leading to the formation of $\cdot O_2^-$, occurs during low $NADP^+$ concentration in the presence of 2Fe-2S, 4Fe-4S clusters, reduced thioredoxin and ferredoxin in the photosystem I. The oxygenase activity of ribulose-1,5-bisphophate carboxylase/oxygenase (Rubisco - EC 4.1.1.39) produces 3-phosphoglycerate and 2-phosphoglycolate, that is metabolized further in the peroxisomes by glycolate oxidase (EC 1.1.3.15) resulting in H_2O_2 formation (Bhattacharjee 2019, Janků et al 2019). In the membrane of peroxisomes, NADH-dependent ferric-chelate reductase (EC 1.16.1.7) and cytochrome *b* form a short electron transport chain and produce $\cdot O_2^-$. In peroxisomes, xanthine oxidase (XO - EC 1.17.3.2) participates in $\cdot O_2^-$ generation during oxidation of xanthine/hypoxanthine to uric acid. Endoplasmic reticulum is a key compartment of xenobiotics biotransformation. The $\cdot O_2^-$ is a by-product of various oxidation and hydroxylation processes of cytochrome P450 and NAD(P)H-dependent cytochrome P450 reductase (Bhattacharjee 2019, Janků et al 2019).

In mitochondria, the NADH dehydrogenase (complex I), succinate dehydrogenase (complex II), ubiquinone-cytochrome (complex III) are considered

as the ROS source since they form and secure the electron transport chain to partially reduce O_2 (Bhattacharjee 2019, Janků et al 2019).

Cytoplasm is also important regarding to the fact that ROS signaling from the organelles and the apoplast must travel through to the nucleus (Janků et al 2019). Cytoplasmic NADPH helps to maintain the redox balance, the thiol/disulfide status, by participating in production of reducing substrates for antioxidant enzymes in the cytosol. Xanthine oxidase/dehydrogenase (EC 1.2.1.37), involved in plant purine metabolism, was shown *in vitro* to generate $\cdot O_2^-$ but not H_2O_2 in plants. Aldehyde oxidase (EC 1.2.3.1), involved in phytohormone biosynthesis, produces H_2O_2 (Hasanuzzaman et al 2020, Janků et al 2019)

In apoplast, the $\cdot O_2^-$ generation occurs predominantly *via* plasma membrane-localized NADPH oxidases (EC 1.6.3.1, also called as respiratory burst oxidase homologs, RBOHs) and the H_2O_2 production by amine oxidases, and cell wall peroxidases (Bhattacharjee 2019, Caverzan et al 2016, Hasanuzzaman et al 2020). RBOHs are the key factors and major ROS source in plant response to pathogen (Janků et al 2019). Environmental stress is directly correlated with increased accumulation of ROS (Caverzan et al 2016). Various biotic and abiotic stress factors such as pathogens, herbivores, insects, nutrient deficiency, salinity, heavy metals, drought, high or low temperature and light (radiation) conditions trigger the generation of ROS. Pesticides also induce the production of ROS and thus depletion of antioxidants (Caverzan et al 2016, Kapoor et al 2019).

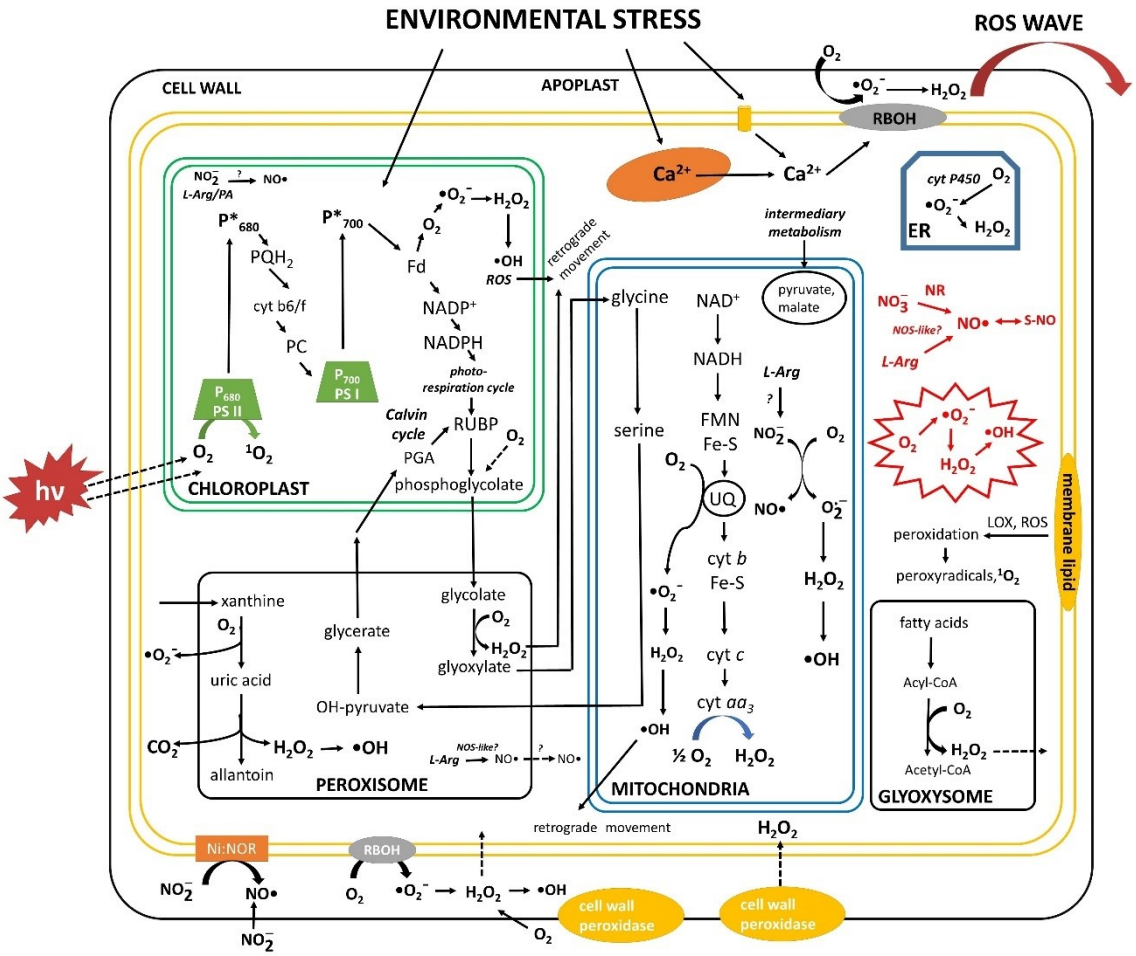


Fig. 1: Generation of ROS and NO in plant cells, modified (Bhattacharjee 2019, Janků et al 2019). The cell wall, apoplast and cytoplasmic membrane are important for ensuring cell integrity and for environmental interaction. Produced ROS can diffuse inside *via* the aquaporin-mediated pathway. Superoxide radical cannot surpass the membrane due to its negative charge but at pH 5 in the apoplast can be protonated. Nitrite is a reservoir to produce NO and RNS in the apoplast. For NO generation in mitochondria, the anaerobic conditions and availability of NO_2^- are crucial. Arg-dependent metabolism is closely related to NO signaling, since it is also a precursor for polyamines and a possible substrate for NOS-like activity. In soybean chloroplasts, NO was generated by NOS-like synthase (Arg/NADPH) and from NO_2^-. *Abbreviations: ER - endoplasmic reticulum, cyt - cytochrome, LOX, lipoxygenases (EC 1.13.11.-), NOS-like - NO synthase-like enzyme, PS - photosystem, PA - polyamines, PGA - 3-phosphoglycerate, RBOH - respiratory burst oxidase homologs (NADPH oxidase), RUBP* - ribulose-1,5-bisphophate.

1.1.2 Antioxidant enzymes

For the removal of ROS, plants developed an ingenious antioxidant system, containing both antioxidant enzymes and compounds (Bartwal et al 2013, Hasanuzzaman et al 2020). In plants, the ascorbate-glutathione cycle (Foyer-Halliwell-Asada pathway) plays a crucial role in controlling the ROS levels in chloroplasts, cytosol, mitochondria, and peroxisomes (Fig. 2, p. 8). This cycle involves consecutive oxidation and reduction of ascorbate (ASC), glutathione (GSH), and NADPH, catalyzed by ascorbate peroxidase (APX, EC 1.1.11.1), monodehydroascorbate reductase (MDHAR - EC 1.6.5.4), dehydroascorbate reductase (DHAR - EC 1.8.5.1), and glutathione reductase (GR - EC 1.8.1.7) (Caverzan et al 2016, Hasanuzzaman et al 2020, Janků et al 2019). APXs are enzymes that play a key role in catalyzing the conversion of H_2O_2 into H_2O and use ASC as a specific electron donor and turn it into the monodehydroascorbate radical (MDHA). Plants have four different APX isoforms distributed in subcellular compartments (thylakoid tAPX, chloroplast sAPX, cytosol cAPX and glyoxysome mAPX) (Janků et al 2019). MDHAR is a flavin-containing enzyme that transforms MDHA to dehydroascorbate (DHA), also uses NADPH to regenerate ASC from MDHA. DHAR catalyzes the renewal of DHA to ASC using GSH as a reducing substrate. GR is an NADPH-dependent enzyme and reduces the oxidized glutathione (GSSG) to GSH. A high GSH/GSSG ratio is essential for protection against oxidative stress (Caverzan et al 2016, Czarnocka & Karpiński 2018, Hasanuzzaman et al 2020, Janků et al 2019).

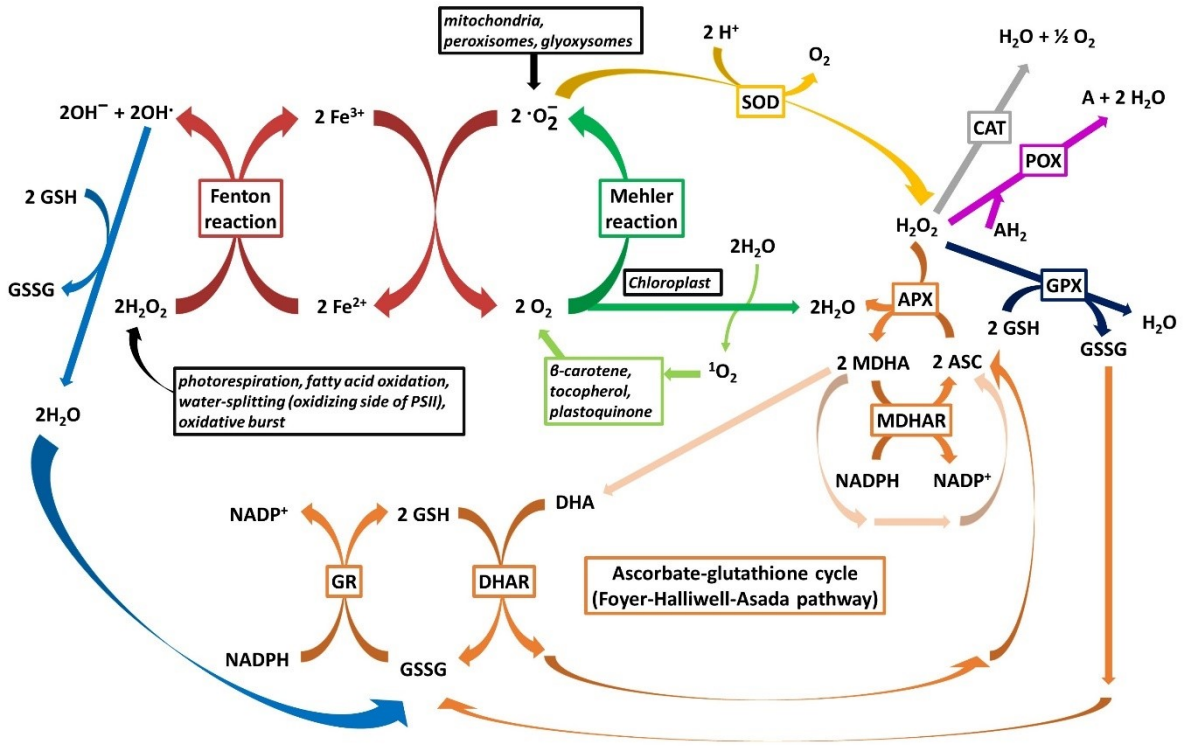


Fig 2: The ROS-scavenging pathways (Ciríaco da Silva et al 2013). The •OH generates by the Fenton reaction, $•O_2^-$ arises in the mitochondria, peroxisomes and glyoxysomes and by the Mehler reaction in chloroplasts, $^1O_2$ is produced in chloroplasts, and H_2O_2 by SOD, photorespiration, ß-oxidation of fatty acid or other reactions. SOD transforms H_2O_2, while CAT, PXs, GPX, and APX then detoxify H_2O_2. In contrast to CAT, APX requires ASC, PXs require phenolic compounds and/or ASC, and GPX requires GSH. H_2O_2 is also removed by the Ascorbate-glutathione cycle (NADPH dependent), ASC and GSH participate of the cyclic transfer of reducing equivalents. The •OH may be removed by GSH, resulting in GSSG that is then regenerated by GR. H_2O_2 can easily diffuse through membranes between the compartments and antioxidants such as GSH and ASC can be also transported (Ciríaco da Silva et al 2013). *Abbreviations: APX - ascorbate peroxidase, ASC - ascorbate, AH_2 - oxidizable substrate, DHA - dehydroascorbate, DHAR - dehydroascorbate reductase, GPX - glutathione peroxidase, PXs - peroxidases, GR - glutathione reductase, GSH - reduced glutathione, GSSG - oxidized glutathione, MDHA - monodehydroascorbate, MDHAR - monodehydroascorbate reductase, SOD - superoxide dismutase.*

Superoxide dismutases (SODs - EC 1.15.1.1) are enzymes that catalyze the dismutation of $•O_2^-$ to O_2 and H_2O_2. SODs are apparently the most important enzymes that decompose these radicals in cells. In plants, there are three isoforms named after their metal cofactors (copper/zinc, manganese, and iron). Cu/Zn-SOD is found in the cytosol, chloroplast, peroxisomes and apoplast, Fe-SOD in chloroplasts, mitochondria and peroxisomes, Mn-SOD occurs mainly in

mitochondria and peroxisomes (Hasanuzzaman et al 2020). In addition, Ni-SOD, was reported in *Streptomyces*. However, no evidence for Ni-SOD has been found in plants yet (Feng et al 2016). Plants have multiple genes encoding SODs that can be regulated by development, tissue-specific and environmental signals – biotic and abiotic stress factors (Caverzan et al 2016). Catalases (CATs, EC 1.11.1.6) reduce $2H_2O_2$ to $2H_2O$ and O_2. CATs are predominantly localized in peroxisomes and glyoxysomes (but also in chloroplast, mitochondria, and cytosol) to remove H_2O_2 that arise from photorespiration, ß-oxidation of fatty acids and purine catabolism (Caverzan et al 2016, Deisseroth & Dounce 1970). Peroxidases (PXs) possess a broad substrate specificity and participate on both ROS production and consumption. Also, they are involved in polymerization of suberin and lignin (passive defense) (Janků et al 2019). PXs can be divided into two main groups based on containing as a co-factor heme or not (non-heme, i.e., thiol PXs) (Soares et al 2019). Peroxiredoxins (PRXs - EC 1.11.1.15) are a family of thiol dependent peroxidases, catalyzing the decomposition of peroxides to their corresponding alcohols. Cysteine is in the active center of PRXs that during reaction with an oxidized substrate turns into a disulphide bond, thus resulting in an inactive form. Therefore, these enzymes are dependent on external electron donors to be regenerated, i.e., thioredoxin, that is then restored by NADPH-dependent thioredoxin reductase (EC 1.8.1.9) (Hasanuzzaman et al 2020). Glutathione peroxidases (GPXs - EC 1.11.1.9) are non-heme thiol peroxidases using GSH for detoxification of H_2O_2 and organic hydroperoxides (lipid peroxides). Also, they may be involved in regulation of the cellular redox homeostasis by maintaining the thiol/disulfide or NADPH/$NADP^+$ balance (Bela et al 2015, Dietz 2016). Guaiacol peroxidases (GPOXs - EC 1.11.1.7) are heme-containing enzymes, belonging to cell wall peroxidases. They are involved in the elimination of H_2O_2 in the lignification of the cell wall - electron donors for its reduction are in this case phenolics (e.g., guaiacol and pyrogallol). APXs, CATs, PRXs, GPXs, and GPOXs prevent excessive accumulation of H_2O_2 and thus the associated damage to organelles and membranes caused by oxidative stress (Caverzan et al 2016). Also, copper- and flavin- containing amine oxidases (CuAOs - EC 1.4.3.6, AOs - EC 1.5.3.3) catalyze oxidative deamination of biogenic polyamines to the respective aldehydes and

ammonia, accompanied by two-electron reduction of O_2 to H_2O_2. It was suggested that the H_2O_2 generated by AOs was important for cell wall maturation and lignification during wound-healing and reinforcement during pathogen invasion (Cona et al 2006, Janků et al 2019). Lastly, glutathione *S*-transferase (GST, EC 2.5.1.18), being responsible for the conjugation of GSH with various xenobiotics, particularly electrophilic substrates, belongs to antioxidant enzymes as well (Soares et al 2019).

1.1.3 Antioxidants

Antioxidants are compounds that possess the ability to reduce oxidants that are usually harmful to the organism. In plants, two main low mass metabolites play an irreplaceable role as antioxidants ASC (vitamin C) and tripeptide GSH, both of which are polar, and their fields of action thus lie mainly in the cytosol and inside the cell compartments. Both are crucial components of the Foyer-Halliwell-Asada pathway (Fig. 2, p. 8). ASC can reduce both $\cdot O_2^-$ and $\cdot OH$, and act as an electron donor for H_2O_2 reduction by APXs (Soares et al 2019). GSH (Glu-Cys-Gly) thanks to the presence cysteine and its thiol groups can enzymatically oxidize to form a disulfide bond – GSSG (Bhattacharjee 2019). Due to its structure, GSH contributes to the maintenance of the reduced state of several cell components during both normal and stressful conditions (Soares et al 2019).

The amino acid proline is a known osmoprotectant, however, is also linked with antioxidant properties. Proline can moderate ROS generation by NADPH consumption for its own synthesis and may undergo a reaction that converts it into γ-aminobutyric acid and thus scavenge $\cdot OH$ (Bhattacharjee 2019, Soares et al 2019, Soshinkova et al 2013). Free cysteine exhibits a reducing power since thiol groups are very susceptible sites for ROS attack, forming a disulphide bridge afterwards (Hasanuzzaman et al 2020, Soares et al 2019). Also, methionine exhibited a scavenger capacity for H_2O_2 under *in vitro* conditions and chelation of Cu^{2+} and Zn^{2+}, suggesting a possible role in antioxidant system (Soares et al 2019).

In lipid membranes, the hydrophobic substances like tocochromanols and partly also carotenoids act against oxidative stress (especially lipid peroxidation). Both groups of substances have a common isoprenoid origin, but in the case of

tocochromanol a part of the molecule is produced directly from the shikimate pathway. Tocochromanols (vitamin E) are divided into tocopherols with phytyl side chain and tocotrienols with geranylgeranyl side chain. In both groups, there are four structures (α, ß, γ, δ) based on the degree of methylation of the chromate skeleton (Bhattacharjee 2019, Blokhina et al 2003). Carotenoids are divided into carotenes, polyene hydrocarbons, and xanthophylls, i.e., various oxidized forms of carotene. Thanks to a relatively extensive system of conjugated double bonds, carotenoids can (in a process called non-photochemical quenching) take the excitation energy of $^1O_2$ or the triplet state of chlorophyll and thus go into the triplet state themselves. Then carotenoids are returned to the base state non-radiatively by means of rotational-vibrational transitions - this is how dissipation of excess energy occurs that would otherwise damage the photosynthetic processes (Janků et al 2019, Soares et al 2019).

Polyamines (Pas) are small aliphatic organic compounds, including putrescine, spermidine and spermine that are predominantly represented in plants. Directly, they protect the plant as powerful •OH scavengers and indirectly as polycations by binding to anionic macromolecules such as DNA, RNA, chromatin, and proteins (Soares et al 2019).

From the point of view of antioxidant capacity, some secondary metabolites, especially phenolic compounds (phenylpropanoids, hydroxyaryl-containing compounds) play an irreplaceable role in the antioxidant system.

1.1.4 Phenolic compounds

Phenolics are undoubtedly the largest group of natural substances with antioxidant properties (approx. thousands of structures described); they originate from phosphoenolpyruvate (PEP) and erythrose-4-phosphate (E-4-P, Fig. 3, p. 13) (Gülcin 2012, Tohge et al 2013). It is estimated that more than 30% of all fixed carbon passes through the evolutionarily very ancient and conserved shikimate pathway and this carbon is largely stored as lignin in the cell walls of plants (Tohge et al 2013). The shikimate pathway serves not only for the synthesis of a wide group of secondary metabolites, but also for the synthesis of important primary

metabolites such as aromatic amino acids phenylalanine, tyrosine, and tryptophan or pterin and quinone coenzymes (Herrmann & Weaver 1999).

The main functions of phenolic secondary metabolites include protection against UV radiation (thanks to a system of conjugated double bonds), chelation of a metal ions (Fe^{2+}, Cu^{2+}, Ni^{2+}, Cd^{2+} etc.) and antioxidant capacity (effective against all types of ROS) (Bartwal et al 2013). The amount of produced phenolics (especially flavonoids) increase during stress (Bartwal et al 2013, Gill & Tuteja 2010). Some of the phenolics are even considered to be more effective antioxidants than ASC or tocopherols (Blokhina et al 2003). This is supported by the fact that in these compounds there is often more than one hydroxy group (i.e., a potential hydrogen donor). The resulting radicals derived from these compounds are significantly stabilized (by delocalization of an unpaired electron throughout the conjugated system) and in addition some can form solid complexes with potentially pro-oxidative metal ions like Fe^{2+}. Flavonoids, coumarins, stilbenes and lignin are among the most numerous and at the same time the most important representatives of phenylpropanoids (Fig. 3A, p. 13). For the antioxidant properties of flavonoids, the presence of a specific structural motif is highly important (Fig. 3B, p. 13). The structural components are interconnected by conjugated double bonds (resonance) and as soon as one of the motifs is missing, the antioxidant capacity decreases. Modification of the 3-OH group by glycosylation or esterification is quite common, also the 7-OH group is often glycosylated (Blokhina et al 2003, Gülcin 2012, Rice-Evans et al 1996). The antioxidant effect of flavonoids also includes their ability to serve as substrate for different peroxidases (Soares et al 2019).

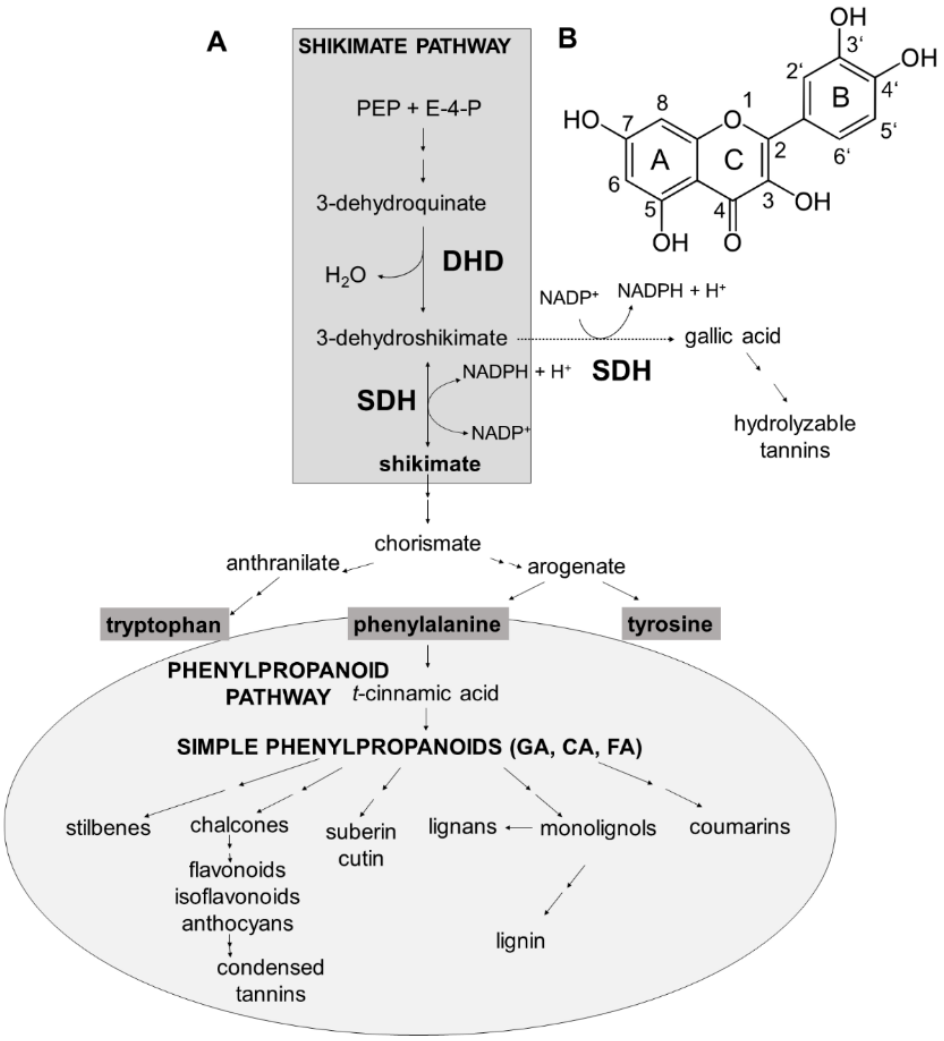


Fig. 3: Shikimate and phenylpropanoid pathways. A) Shikimate and phenylpropanoid pathways lead to production of various secondary metabolites (Hýsková et al 2021c). B) Structure and position numbering of the flavonoid quercetin. The typical antioxidant structural motifs that take place - 3',4'-catechol arrangement on ring B, then 2,3-double bond, 3-hydroxy group, and 4-carbonyl group on ring C and 5,7-dihydroxy arrangement on ring A (Gülcin 2012, Rice-Evans et al 1996). *Abbreviations: DHD - 3-dehydroquinate dehydratase, E4P - D-erythrose-4-phosphate, PEP - phosphoenolpyruvate, SDH - shikimate dehydrogenase, CA - caffeic acid, FA - ferulic acid, GA - gallic acid.*

1.1.5 Reactive nitrogen species

Unlike for ROS, production mechanisms of RNS in plants remain still in part unresolved (Turkan 2017). Free radical nitric oxide (NO•) is one of the three gaseous biological messengers (with H_2S and CO being the other two) with diverse functions in plant physiology and stress signaling (Hasanuzzaman et al 2020). Generally, RNS derived from NO include e.g., peroxynitrite ($ONOO^-$), nitrogen dioxide (NO_2), nitrous acid (HNO_2), dinitrogen tetroxide (N_2O_4), or S-nitrosothiols (RSNO) (Janků et al 2019, Kapoor et al 2019, Procházková et al 2015, Saddhe et al 2019). These molecules can react with a broad spectrum of molecules, and they may act as a transporters and reservoirs for NO in a broad range of plant cell signaling affairs. Some of these reactions, nitration and S-nitrosylation, may be as important as phosphorylation (Procházková et al 2015). The plant reductive enzyme pathways include reactions where NO is produced by nitrate reductase (NR - EC 1.7.1.2), nitrite-NO reductase (Ni:NOR - EC 1.7.2.1), mitochondrial electron transport chain or xanthine oxidoreductase (XOR - EC 1.17.3.2). On the other hand, the suggested oxidative pathways of NO synthesis involve NO synthase-like enzyme (NOS-like) utilizing arginine as a substrate, and insufficiently described metabolism of Pas (polyamines) or hydroxylamine (Janků et al 2019, Vishwakarma et al 2018). NO also arises from other pathways, where S-nitrosation of GSH yields to S-nitrosoglutathione (GSNO), a donor and a major reservoir of NO, providing the NO signal for protein nitrosation (Hasanuzzaman et al 2020, Janků et al 2019, Petřivalský et al 2015, Tichá et al 2016). Formation of GSNO proceeds indirectly through the formation of N_2O_3 or directly by the reaction of NO with the glutathionyl radical (Janků et al 2019). NO readily reacts with molecules, which are likely to be produced temporally and spatially close. A simultaneous generation of NO and $\cdot O_2^-$ in plant peroxisomes, mitochondria and chloroplasts results in the formation of $ONOO^-$ (Hasanuzzaman et al 2020, Procházková et al 2015). A major biological function of $ONOO^-$ may be to react with tyrosine within proteins to form 3-nitrotyrosine. This occurs *via* addition of a nitro group in the ortho position of the aromatic ring in tyrosine. The formation of nitrotyrosine represents an irreversible oxidative modification that is accepted as a biomarker of nitrosative stress. Nitration is a mechanism distinct from

S-nitrosylation where NO can covalently but reversibly oxidize the thiols groups of reduced reactive cysteine residues in proteins. S-Nitrosylation (-SNO) can activate or repress protein function, resulting in possible signal transduction. In peroxisomes, NO nitrosylates enzymes such as CAT, glyoxylate oxidase (EC 1.2.3.5) and NAD-dependent malate dehydrogenase (EC 1.1.1.37) that are involved in the photorespiration, ß-oxidation, and ROS detoxification (Hasanuzzaman et al 2020, Procházková et al 2015, Vishwakarma et al 2018). Besides S-nitrosylation, increasing interest and evidence point at the important role of protein denitrosylation as a feedback mechanism controlling NO signaling. The removal of NO group from proteins might occur through different enzyme systems of which especially GSNO reductase and thioredoxin play a predominant role (Jahnová et al 2019, Kovacs & Lindmayr 2013).

1.1.6 Reactive sulfur species

Reactive sulfur species (RSS) are defined as sulfur-containing compounds that can either reduce or oxidize various compounds, also contribute to the redox state of the cell. RSS are strongly connected with ROS and due to their reactions, sulfur atoms are oxidized (Gruhlke 2019). Thiols are key molecules with formal oxidation states of S^{-II} and are an important source to produce RSS (Fig. 4, p. 16). Under stress conditions, thiols may oxidize into sulfenic acids (RSOH) which can act as both reductants and oxidants. When it goes through a reduction reaction, it regenerates thiol or disulfide molecule while on oxidation it produces a sulfinic acid (RS(O)OH) or sulfonic acid ($RS(O)_2OH$) (Ijaz et al 2019). Sulfenic acids are found in protein-thiols, e.g., in peroxiredoxins as reversible oxidation state, and can easily be re-reduced to thiols by thioredoxins or glutaredoxins. In glutathiolation (-SSG), sulfenic acids of proteins are important targets for attaching thiol-containing molecules such as GSH, which also influences protein function and stability (Gruhlke 2019). Sulfinic acid reductases (Sulfiredoxins - SRX - EC 1.8.98.2) are ATP-dependent enzymes that can convert sulfinic acids to sulfenic acids. The oxidation to a sulfonic acid is not reversible and requires degradation of the protein (Gruhlke 2019).

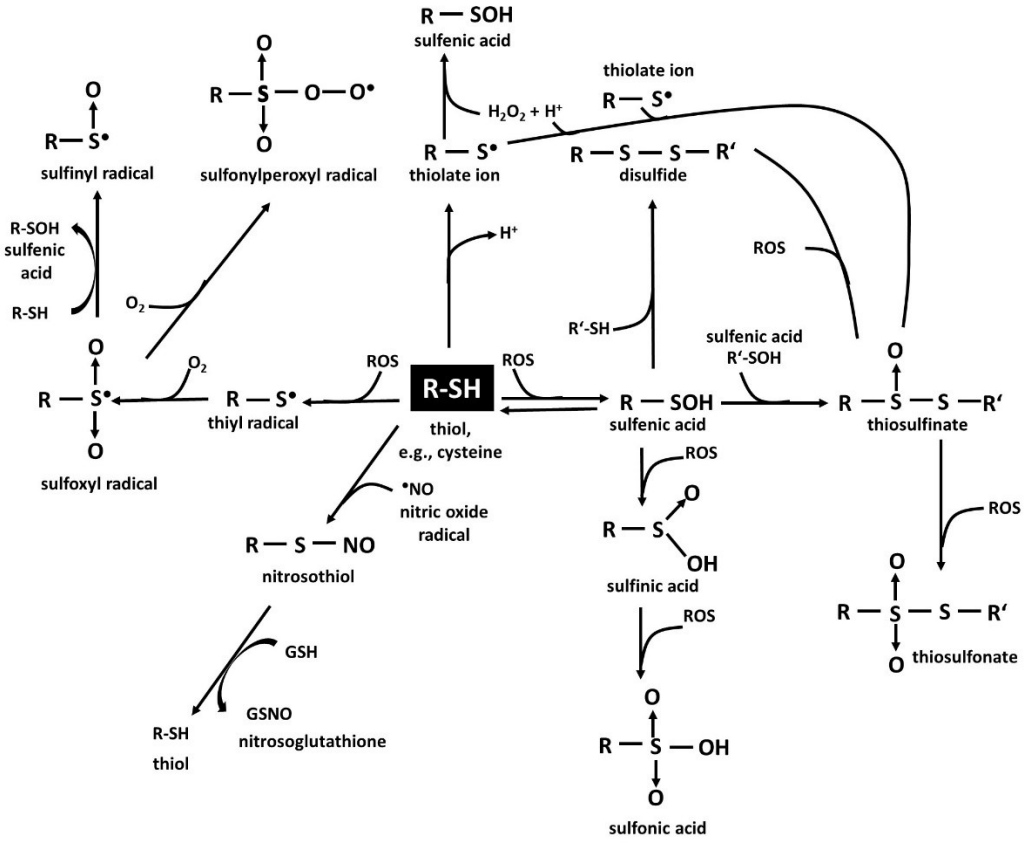


Fig. 4: Generation of various RSS from compounds containing a thiol group (Gruhlke & Slusarenko 2012).

In plants, many abiotic and biotic stressors cause the release of H_2S which signals protein sulfhydration (various cysteine persulfides, RSSH), i.e., a post-translational modification like nitrosylation. PRXs are the most abundant sulfhydrated proteins, important enzymes in ROS degradation. Protein sulfhydration very likely protects protein-thiols from further oxidation, e.g., caused by either ROS or RNS. Also, the formation of disulfides protects the thiols from oxidation to corresponding acids (Gruhlke 2019).

Hydrogen sulfide (H_2S) actively interacts with ROS to regulate the plasma membrane antiporter (Na+/H+) system, in contrast it activates antioxidant SOD, CAT, and APX and enhances GSH content (influences GSH:GSSG ratio), thus reducing oxidative damages (Fig. 5, p. 18). Moreover, H_2S is involved in production, perception, and further signal transduction of ROS as well as RNS (Hasanuzzaman et al 2020).

The last non-discussed gaseous messenger is carbon monoxide (CO), which arises in biological systems (both plant and animal) during heme degradation as

the oxidation product of the α-methene bridge of heme, and this process is catalyzed by heme oxygenase enzymes (EC 1.14.14.18) as the major production route (Wang & Liao 2016). For soybean plants the lipid peroxidation and ureide metabolism were considered as potential sources of CO (Zilli et al 2014). In low concentration CO acts as a compound with hormonal effects, affecting seed germination, root development, and inducing stomatal closure (Wang & Liao 2016).

1.1.7 Reactive carbonyl species

The oxidations products of carbohydrates as well as oxidized lipids form reactive carbonyl species (RCS). Therefore, ROS and RCS are tightly bound (Fig. 5, p. 18). More or less, all the forms of reactive species are somehow intertwined (Hasanuzzaman et al 2020). Lipid-derived aldehydes or ketones come from peroxidation and breakdown of polyunsaturated fatty acids (e.g., linoleic acid). The lipid peroxidation products are mobile and may diffuse across membranes and covalently modify proteins which are localized far from the ROS generation site. RCS can modify proteins by adding carbonyl compounds (e.g., acrolein, 4-hydroxy-(E)-2-nonenal). Carbonyl groups can be attached by a metal-catalyzed oxidative (MCO) attack in the presence of reduced metal ions (e.g., Fe^{2+}, Zn^{2+}, Cu^{+}) and H_2O_2 (producing ·OH) on amino acids residues such as Asn, Lys, Arg, Pro or Thr (Ciacka et al 2020, Hasanuzzaman et al 2020, He et al 2018, Mano et al 2019). RCS may also reversibly modify cysteine in proteins and thus regulate their activity, e.g., CAT, APX and SOD (Hasanuzzaman et al 2020).

In RCS, malondialdehyde (MDA, $CH_2(CHO)_2$) and methylglyoxal (MG, CH_3COCHO) have been drawing attention (He et al 2018). MG may over-accumulate as a by-product in some metabolic pathways (e.g., glycolysis from glyceraldehyde-3-phosphate and dihydroxyacetone phosphate) under stress condition and can be produced by the auto-oxidation of ketone bodies and sugars and the Maillard reaction (i.e., reaction between the sugar carbonyl group with the nucleophilic amino group of the amino acid). MG can form glycation end-products and contribute to the ROS formation by catalyzing photoreduction of O_2 to $\cdot O_2^-$ in chloroplasts. Plants deal with MG toxicity *via* glyoxalase system (glyoxalase I,

i.e., lactoylglutathione methylglyoxal lyase, EC 4.4.1.5 and glyoxalase II, i.e., hydroxyacylglutathione hydrolase; EC 3.1.2.6) using GSH as a co-factor. However, at low levels MG can act as a signaling molecule (Mostofa et al 2018).

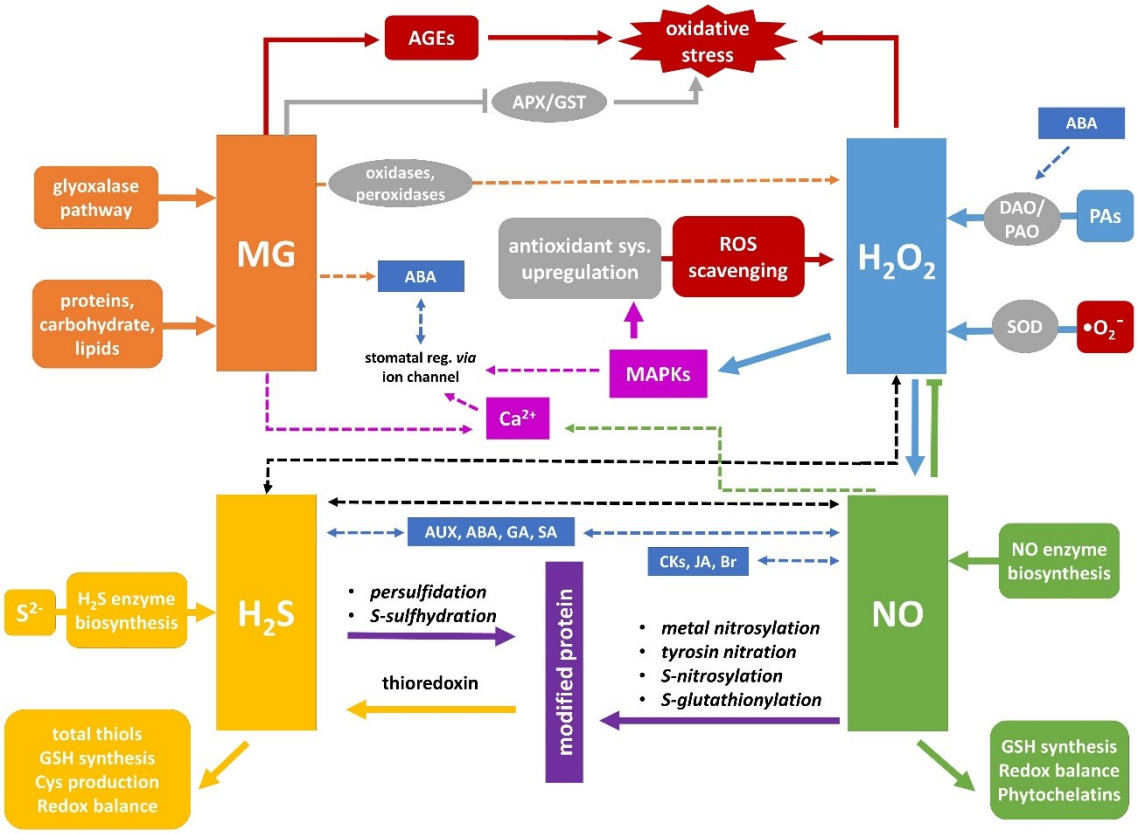


Fig. 5: Crosstalk among the key ROS (H_2O_2), RNS (NO), RSS (H_2S), and RCS (MG) in plants during oxidative stress and defense response, slightly modified, (Hasanuzzaman et al 2020). *Abbreviations: ABA - abscisic acid, AEGs - advanced glycation end products, APX - ascorbate peroxidase, AUX - auxin, ET - ethylene, GSH - reduced glutathione, JA - jasmonates, MAPKs - mitogen-activated protein kinases, MG - methylglyoxal, ROS - reactive oxygen species, SA - salicylic acid, PAs - polyamines. Dotted lines represent activation/enhancement.*

1.2 Environmental stress

1.2.1 Biotic stress factors

The action of viruses, bacteria, pathogenic fungi, herbivores, and other factors of biotic stress affects the plant growth and metabolism, and often leads to the formation of chlorotic and necrotic sites (lesions). The spectrum of plant responses to biotic stress is wide and specific. Each plant has both constitutive and inducible defense systems (Fig. 6) (Benhamou & Nicole 1999, Ding et al 2018, Saijo & Loo 2020).

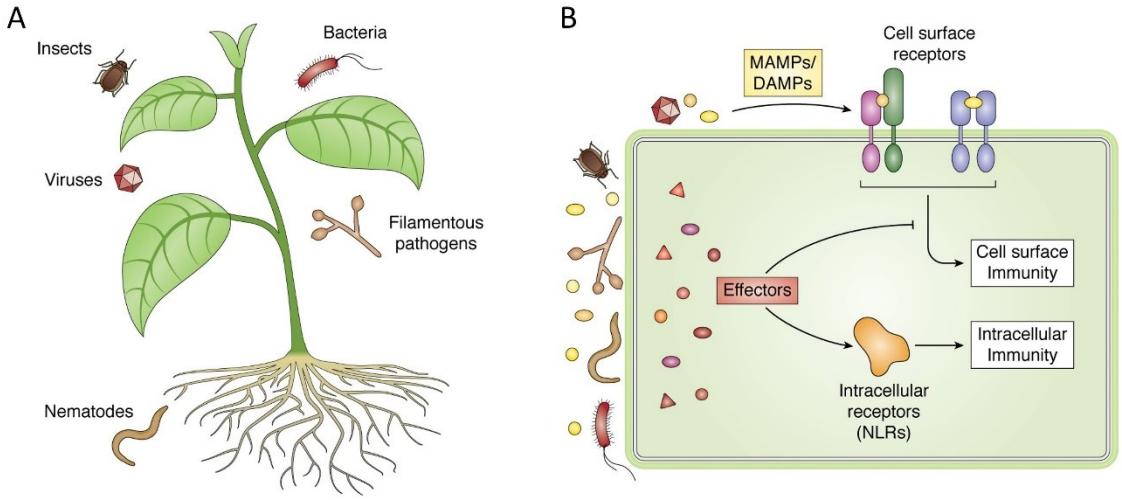


Fig. 6: Brief overview of plant immunity (Bentham et al 2020). A) Various pathogens and pests that may endanger the plant. B) MAMPs/DAMPs, received by receptors, may initiate cell-surface immunity. Effectors can act on host systems to their benefit, including the suppression of signaling pathways downstream of cell-surface receptors. Effectors can be received by intracellular immune receptors (NLRs) to initiate intracellular immunity. *Abbreviations: DAMP, damage-associated molecular patterns, MAMP - microbe-associated molecular patterns, NLR - nucleotide-binding leucine-rich repeat receptors.*

Cells on the plant surface may contain different amounts of hydrolytic enzymes (e. g., glucanases, chitinases), some of which, can disrupt the cell wall of the pathogen and thus contribute to resistance to infection (Agrios 2005, Fotopoulos et al 2003, Hammond-Kosack & Jones 2000, Salas-Marina et al 2011).

The mechanical form of defense against the entry of a pathogen into a cell is the cell wall, which can be further strengthened during infection by increased deposition of lignin and callose. PXs located on the cell wall may crosslink the

proline-rich glycoprotein and induce the production of callose (Brown et al 1998, Deepak et al 2006, Patykowski 2006, Peng & Kuc 1992). Lignification and callose deposition make the cell wall more resistant to microbial penetration and enzyme degradation (Hammond-Kosack & Jones 2000).

Plant immunity relies on innate immune receptors expressed in each cell, which recognize invasion signals to initiate pattern triggered immunity (PTI) or effector-triggered immunity (ETI). PTI connected with pattern recognition receptors (PRRs) on the cell surface, which detect typical molecular structures called microbe-, pathogen- and damage-associated molecular patterns (MAMPs, PAMPs and DAMPs). PRRs include the leucine-rich-repeat (LRR) receptor-like kinases (RLKs), e.g., FLS2 and EFR that recognize bacterial flagellin and EF-Tu (elongation factor thermo unstable), respectively, and the lysin-motif (LysM) RLK CERK1 (chitin elicitor receptor kinase 1) required for recognition of fungal chitin-oligomers and bacterial peptidoglycans (Saijo & Loo 2020). Ligand-bound receptors form complexes with coreceptor/adapter kinases of the same extracellular domain class, thereby triggering protein phosphorylation cascades through RLKs and receptor-like cytoplasmic kinases (RLCKs). PRR signaling then involves cytosolic Ca^{2+} and apoplastic ROS bursts, Ca^{2+}-dependent protein kinases (CDPKs), mitogen-activated protein kinase (MAPK) cascades, defense hormone networks and extensive transcriptional, translational, and metabolic re-programming (Fig. 7, p. 21). These outputs collectively contribute to PTI, which prevents infection of most pathogens (Bhattacharjee 2019, Saijo & Loo 2020). To avert PTI, pathogenic as well as mutualistic microbes have evolved a wide range of effectors that circumvent host immunity and susceptibility. ETI, the second layer of plant immunity, functions directly by recognizing pathogen secreted effectors (virulence-factors, that are intended to inhibit PTI) with plant intracellular immune receptor proteins. For example, plant intracellular receptors such as nucleotide-binding domain and LRR containing proteins (NLRs) amplify defense response, leading to hypersensitive reaction (HR) and PCD. ETI represents a more specific immune response than PTI, and usually initiates HR and PCD (Saijo & Loo 2020, Yan et al 2019).

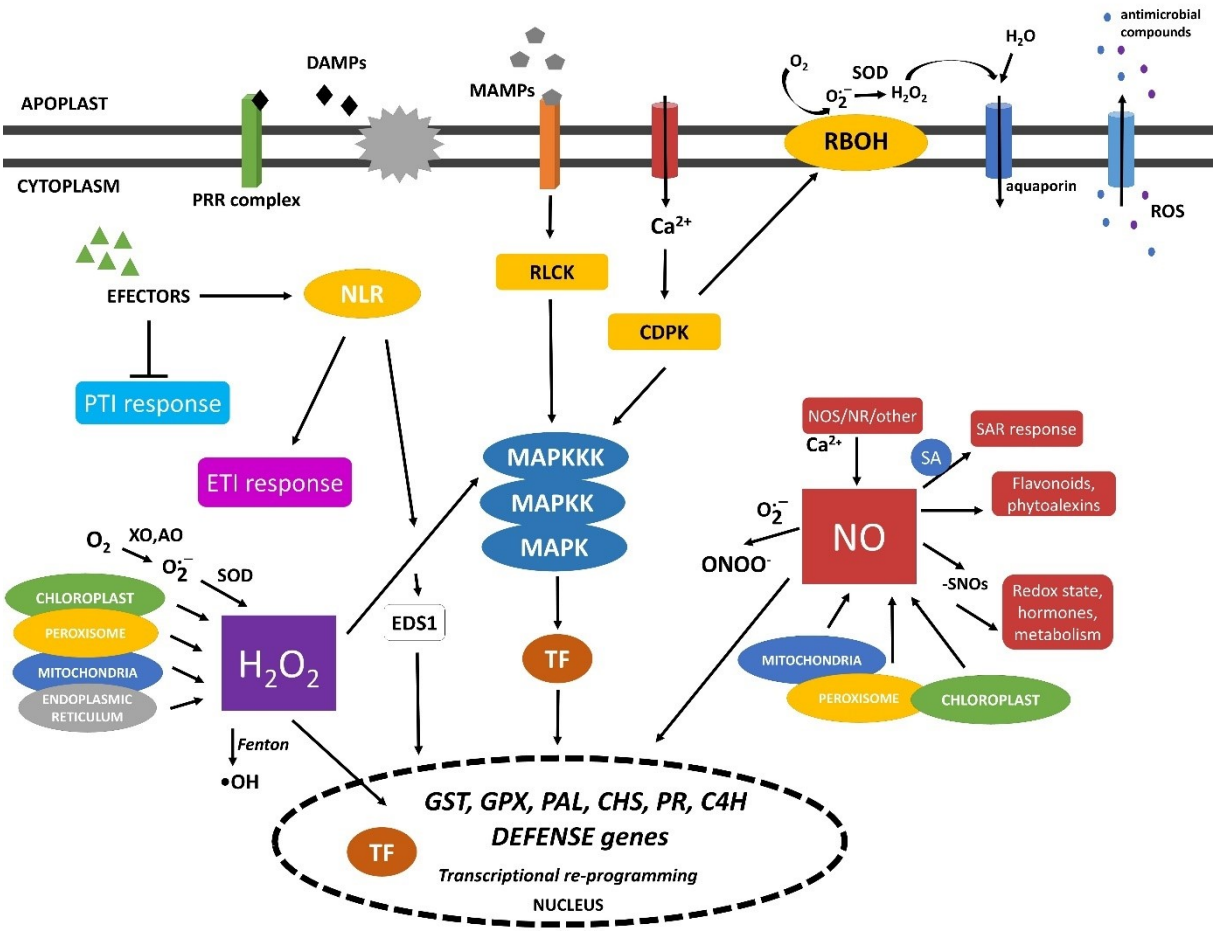


Fig. 7: A brief glimpse into the plant immune signaling, modified, (Janků et al 2019, Miller et al 2017, Molina-Moya et al 2019, Saijo & Loo 2020). The perception of MAMPs and DAMPs induces formation of the receptor complexes. PRR activation initiates Ca^{2+} signaling, CDPKs, MAPK cascades and defense-related TF leading to transcriptional re-programing. Effectors are supposed to be recognized by NLR proteins involving EDS1 and SA-dependent regulators to activate defense signaling. ROS and RNS (NO) signaling takes place early in the PTI immunity and may lead to HR in order to pathogen removal in the ETI response. RBOHs and peroxidases produce most ROS, while NR and NOS-like are responsible for NO production. *Abbreviations: C4H - cinnamate-4-hydroxylase, CDPK - Ca^{2+}-dependent protein kinases, DAMP, damage-associated molecular patterns, EDS1 - enhanced disease susceptibility 1 protein, ETI - effector-triggered immunity, GPX - glutathione peroxidase, GST - glutathione-S-transferase, CHS - chalcone synthase, MAMP - microbe-associated molecular patterns, MAPK - mitogen-activated protein kinase, NLR - nucleotide-binding leucine-rich repeat receptors, NOS - NOS-like synthase, NR - nitrite reductase, PAL - phenylalanine ammonia lyase, PR - pathogenesis related proteins, PRR - pattern recognition receptor, PTI - pattern triggered immunity, RBOH - respiratory burst oxidase homologs (NADPH oxidase), RLCK - receptor-like cytoplasmic kinases, ROS - reactive oxygen species, SA - salicylic acid, SOD - superoxide dismutase, TF - transcription factor.*

HR is the result of a receptor-ligand interaction based on the specific pairing of plant resistance (R) and pathogenic avirulence (Avr) gene products. This type of pathogen-plant interaction is called incompatible, meaning that the plant can recognize the pathogen and after penetrating the host, the infection is suppressed (Pieterse et al 2009). HR is often related to salicylic acid (SA) dependent response - systemic acquired resistance (SAR), accompanied with initiation of necrosis, protecting the plant mainly against biotrophs (Ding et al 2018, Saijo & Loo 2020). SAR is also associated with the accumulation of PR proteins (mainly acid forms) such as PR-1 (various antifungal proteins), PR-2 (ß-1,3-glucanases) and PR-5 (antifungal, thaumatin-like proteins) (Balint-Kurti 2019). PR proteins occur both within the cell and in the intercellular space. Several groups of PR proteins have been described according to function, amino acid sequence, molecular weight, serological and other properties. Likely, the most known PR proteins are ß-1,3-glucanases (PR-2), chitinases (PR-3, 4, 8 and PR-11), defensins (PR-12), thionins (PR-13), proteinase inhibitors (PR-6) and peroxidases (PR-9) (Hammond-Kosack & Jones 2000, Van Loon & Van Strien 1999).

Localized acquired resistance (LAR) occurs in the place of infection, persists shortly, and is accompanied with HR (Cordelier et al 2003, Costet et al 1999).

On the other hand, induced systemic resistance (ISR) is typically activated upon colonization of plant roots by beneficial microorganisms (e.g., rhizobacteria). Like in SAR, a long-distance signal travels through the vascular system to activate systemic immunity in above-ground parts. ISR is commonly regulated by jasmonic acid (JA)- and ethylene (ET)-dependent signaling pathways (SA independent) and associated with activation of alkaline forms of PR proteins. ISR-expressing plants are primed for accelerated JA- and ET-dependent gene expression, which becomes evident only after pathogen attack. ISR is usually not accompanied by necrosis and very likely involved in protection against different necrotrophs and insects (Pieterse et al 2009).

1.2.2 Oxidative signaling

Oxidative signaling is an early response to stress, it shifts redox balance, thus ROS/RNS accumulate, either through an increase in their production or a decrease in antioxidant capacity (Fig. 7, p. 21). The resulting enhanced oxidation entrains PCD and/or acclimation and improved stress tolerance, according to its intensity (Noctor et al 2018). RNS (especially, NO) and ROS (especially, H_2O_2) have been associated in signal transduction as secondary messengers because of their generation at the time of activation of receptor and short-life span (Bhattacharjee 2019). ROS and calcium waves constitute important components of rapid systemic signaling in plants. ROS production leads to changes in Ca^{2+} transport and protein phosphorylation. In addition, NO and abscisic acid (ABA) play an important role in mediating systemic responses to biotic and abiotic stress (Neill et al 2003, Sewelam et al 2016). NO regulates calcium channels by means of cGMP and ADP-ribose, through which it increases the cytoplasmic concentration of Ca^{2+} from intracellular stores, and thus activates signaling cascades. Together with MAPK cascades, it promotes the synthesis of phytoalexins (various secondary metabolites) and is involved in the initiation of PCD. A precise control of the NO concentration is thus necessary for its function as a signal molecule. Glutathione-dependent formaldehyde dehydrogenase (FALDH - EC 1.2.1.46), which reversibly binds NO to glutathione, is involved in controlling cellular NO concentration. NO can be eliminated by oxidation to nitrate (Neill et al 2003).

1.2.3 Viral infection

Viruses represent not just another group of pathogens, but rather a fundamentally different form of life. Mature virus particles come alive and reproduce only inside infected cells. All viruses lack protein-synthesizing and energy-producing machinery. Plant cells are protected by a cell wall that can also be covered with cuticle and waxes; and since viruses have no mechanism to actively penetrate the cell, they must rely on the aid of carriers (e.g., aphids, whiteflies) or mechanical wounding (Agrios 2005, Gergerich & Dolja 2006, Hammond-Kosack & Jones 2000, Wu et al 2019). Most viral infections cause restrictions on plant growth (malformation), various dwarfism, and shortening of plant life in general. The most noticeable are the symptoms on the leaves, however, they can also appear on stems, fruit, and roots. Symptoms are either only at the site of infection and appear as chlorotic or necrotic lesions, or systemic influencing the whole plant. Systemic infections are most often manifested by mosaics and ring spots, and accompanied also by chlorosis, necrosis, yellowing, and veining (Agrios 2005, Hammond-Kosack & Jones 2000). Once the virus enters the plant cell, it multiplies using the host's translational apparatus and the resulting virus particles spread to other cells through plasmodesmata (Henlein 2015). The virus movement is allowed by cell-to-cell movement proteins (MPs) encoded by the virus (Ivanov et al 2014, Lucas 2006). Viral MPs bind RNA/DNA to nucleoprotein protein complexes. The host proteins then participate in the relocation of MPs and nucleoprotein complexes to the plasmodesmata estuary. Transport of nucleoprotein complexes by plasmodesmata involves three phases, in which MPs (a) interact with a putative complex in the estuary of plasmodesmata, (b) induce expansion of the plasma microchannels; and (c) bind to the internal translocation system and penetrate the cytoplasm of neighboring cells (Ivanov et al 2014, Ivanov & Makinen 2012, Lucas 2006). The virus multiplies in an infected parenchymal cell. In most economically significant infections, the virus particles get into the phloem, from where they spread rapidly at greater distances, especially in the direction to developing parts of the plant (apical meristems) or nutrient-receiving parts (rhizomes) (Agrios 2005).

The main plant defense mechanisms against viral infection are RNA silencing (i.e., RNA interference, RNAi), innate immunity, translational repression, and ubiquitination- and autophagy-mediated protein degradation (Fig. 8, p. 27), (Calil & Fontes 2017, Moon & Park 2016, Wu et al 2019).

Most viruses have RNA genomes containing imperfect regulatory stem-loops, that are copied into complementary double strand RNA (dsRNA) replication intermediates by virus-encoded RNA-dependent RNA polymerases (RDRs). In RNAi, the dsRNAs are then recognized by a host ribonuclease III-like protein, Dicer-like (DCL) protein, and then processed into 21-24-nucleotide short interfering RNAs (siRNAs). The siRNAs are then recruited to a functional RNA-induced silencing complex (RISC) and act as guides to direct RISC to their target viral RNA molecules, which have complementary sequences. Consequently, viral RNAs are degraded by the core components of RISC which are members of the Argonaut (AGO) protein family (Calil & Fontes 2017, Moon & Park 2016). However, plant viruses may encode viral suppressors of RNAi (VSRs) that perturb the plant RNAi pathway, e.g., potyviral HCPro, *Turnip crinkle virus* (TCV) coat protein (Moon & Park 2016, Wu et al 2019).

In plants, some studies regard dsRNAs as viral PAMPs and therefore, claim that these compounds initiate PTI. Viral proteins such as MPs and replicase proteins act as Avr factors. Also, the coat proteins of *Tobacco mosaic virus* (TMV) and *Potato virus X* (PVX) triggered PTI-like responses in *Arabidopsis* and tobacco. Plants also employ R genes to mediate ETI leading to HR as the direct consequence of defense in most R-mediated resistance (Calil & Fontes 2017, Wu et al 2019). R genes such as tobacco “N” against TMV, “Rx1/2” in potato against PVX, “HRT” and “RCY1” in *Arabidopsis* against *Turnip crinkle virus* (TCV) and *Cucumber mosaic virus* (CMV) were regarded with resistance against viral pathogens (Moon & Park 2016, Wu et al 2019). Since viruses essentially rely on the plant translation machinery, its repression is another way to achieve antiviral resistance. For example, ribosome-inactivating proteins (RIPs) inhibit protein synthesis by depurinating the sarcin/ricin loop of rRNA, e.g., pokeweed antiviral protein. However, RIPs show cytoplasmic toxicity for the plant itself (Wu et al 2019). Recently discovered nuclear shuttle protein (NSP) interacting kinase 1 may

repress the expression of ribosomal protein genes, leading to the shutdown of global cellular and viral protein synthesis. Specific direct translation inhibition may also take place by small RNAs (i.e., repression determined by its sequence) that result from RNAi (Wu et al 2019). Ubiquitination-mediated protein degradation is crucial for cellular protein homeostasis and may also be employed for viral proteins (e.g., MPs) degradation (Calil & Fontes 2017, Wu et al 2019). The same goes for the autophagy that transports misfolded proteins or degraded defense-related proteins to the vacuole for degradation and recycling. In a sort of selective autophagy, plants degrade viral protein aggregates, ribonucleoproteins and even viral particles as reported for *Cauliflower mosaic caulimovirus* (CaMV) (Wu et al 2019).

On the other hand, plant viruses have been engineered and developed as vectors for biopharmaceutical protein production (e.g., subunit vaccines or presenting epitopes), and as research tools for plant functional genomics studies (Hefferon 2014). Plant virus-based vectors (containing a gene of interest) are a useful tool for expression of recombinant proteins at high levels in plants (Hefferon 2014, Lico et al 2008). For example, *Potato virus A* and *Potato virus X* vectors were shown to express epitopes from *Human papillomavirus* type 16 (Čeřovská et al 2008, Čeřovská et al 2013, Plchová et al 2011, Vaculík et al 2015).

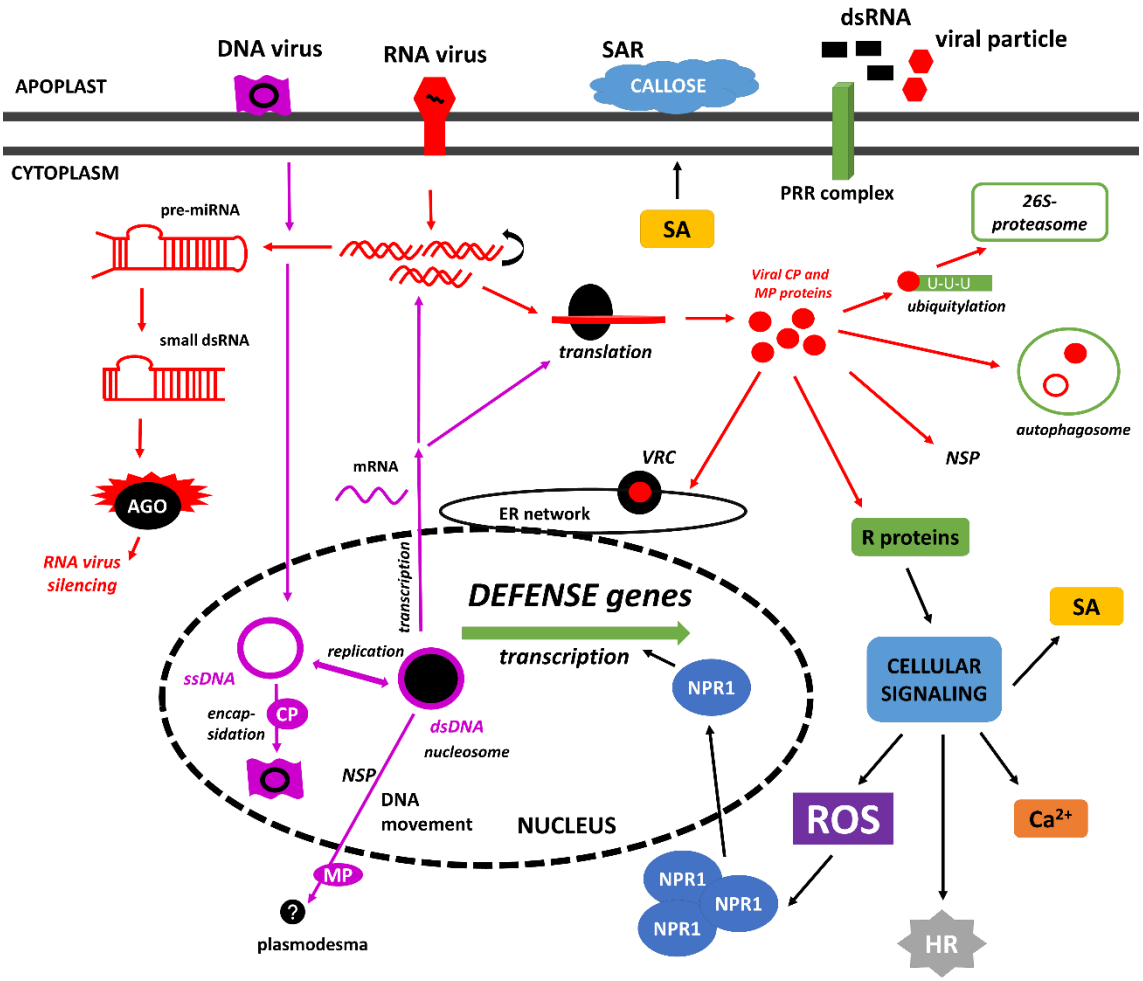


Fig. 8: **Routes of viral infection in plants**, modified (Hanley-Bowdoin et al 2013, Hýsková et al 2021b, Miller et al 2017, Wu et al 2019). Most plant viruses contain ssRNA genome but also dsRNA, ssDNA and dsDNA plant viruses exist. In red, RNAi silencing may avert the viral infection. In green, the ubiquitination and autophagy may degrade viral proteins. Also, dsRNAs as viral PAMPs may initiate PTI-like responses resulting in various cellular signaling. In purple, there is shown a simplified scheme of the begomovirus cycle (ssDNA). The ssDNA is released from virions and copied to generate dsDNA (assembled in nucleosomes). NSP binds viral DNA and moves it with MP through plasmodesmata. After encapsidation of circular ssDNA by CP, virions can be transmitted by whiteflies (Hanley-Bowdoin et al 2013). *Abbreviations: CP - coat protein, ER - endoplasmic reticulum, HR - hypersensitive response, MP - movement protein, NPR1 - nonexpresser of PR genes 1, NSP - nuclear shuttle protein, PTI - pattern triggered immunity, ROS - reactive oxygen species, SA - salicylic acid, SAR - systemic acquired resistance, U - ubiquitin, VRC - virus replication complex.*

In 2011, Scholthof et al. conducted a survey among scientists to compile a list of top ten plant viruses (Table 1). Although many of the included viruses cause significant problems in terms of economic losses of crops, it is predominantly their use as scientific tools that regarded them as most important (Rybicki 2015, Scholthof et al 2011). Therefore, Rybicki (2015) put together another list of viruses that cause severe hardship and affect large numbers of people, especially in developing countries (Table 2).

Table 1: Top ten viruses according to the survey among scientists by Molecular Plant Pathology (Scholthof et al 2011). Symptoms and signs of virus infection are often dependent on the host plant, plant developmental stage, virus strains, environmental conditions. In the table, the most common symptoms were gathered from various publications and databases. *Abbreviations: MP, movement protein, CP, coat protein.*

virus	type	symptoms	possible reasons
Tobacco mosaic tobamovirus (TMV)	+ssRNA	stunting, leaves: mosaic pattern malformation, yellow streaking, yellow spotting, veins: distinct yellowing (Scholthof 2004)	1st plant virus RNA sequenced, 1st defined MP, 1st demonstration of the efficacy of transgenic CP expression for protection from infection, 1st evidence of a gene-for-gene resistance interaction, 1st proof-of-principle platform for both nanodevices and the expression of therapeutic monoclonal antibodies and other pharmaceutically relevant proteins
Tomato spotted wilt tospovirus (TSWV)	-ssRNA	necrotic/chlorotic rings and flecking on leaves, stems, and fruits, with early infections leading to one-sided growth, leaves dropping reminiscent of vascular wilt, stunting or death (Scholthof et al 2011, Sherwood et al 2003)	virions enveloped in a host-derived membrane studded with two viral glycoproteins and contain one negative-sense, and two ambisense single-stranded RNAs encapsidated in multiple copies of the viral nucleocapsid protein (unique among plant viruses)
Tomato yellow leaf curl begomovirus (TYLCV)	DNA	severe stunting, reduction of leaf size, upward cupping/curling of leaves, chlorosis on leaves and flowers, and reduction of fruit production (Cathrin & Ghanim 2014)	1st begomovirus shown to possess a single genomic component, rapid spread caused by whiteflies *Bemisia tabaci*

virus	type	symptoms	suggested reasons
Cucumber mosaic cucumovirus (CMV)	+ssRNA	severe stunting, prominent yellow foliar mosaic, mottling malformation, and stunting due to drastic reduction of leaf size and stem internodes (El-Borollosy 2013)	broad, collective host range, infecting more than 1200 plant species in over 100 families, transmitted by more than 80 species of aphid (Aphidoidea)
Potato virus Y (potyvirus, PVY)	+ssRNA	leaf/tuber necrotic symptoms, mosaic, leaf drop, mottling, vein necrosis (Čeřovská 1998)	PVY isolates (PVY^0, PVY^N, PVY^{NTN}) highly differ at the biological, serological, and molecular levels
Cauliflower mosaic caulimovirus (CaMV)	DNA	chlorosis (loss of green leaf color), mosaic (patches of light and dark green on leaves), vein clearing (abnormal clear or translucent color of veins), and/or stunting (Bak & Emerson)	1st identified as plant DNA virus, 1st plant virus genome sequenced, 1st plant virus shown to be replicated by reverse transcription.
African cassava mosaic begomovirus (ACMV)	DNA	dwarfing, stunting, distortion, rosetting, malformation and abnormal colors of leaves, reduced root system (Legg & Winter 2021)	1st geminiviruses to be molecularly characterized, forms the staple food for nearly 80% of the African population, cassava is not so studied as other staple crops such as rice, maize, and wheat
Plum pox potyvirus (PPV)	ssRNA	fruit: malformation, lesions, premature drop, leaves: malformation, abnormal color and patterns, seed: discolorations, stems: dieback (Levy et al 2000)	highly studied, causes Sharka - the most important viral disease of "stone fruit crops" such as peaches, plums, apricots, and cherries, transmission by aphids, severe symptoms, over 800 isolates, almost impossible to stop, treatment only slows down the spread,
Brome mosaic bromovirus (BMV)	+ssRNA	stunted growth, lesions, mosaic leaves (He et al 2021)	1st eukaryotic viral RNA-dependent RNA polymerase extract with marked specificity for its cognate viral RNAs, 1st definition of a eukaryotic ribosome binding site, revealing the linkage of eukaryotic translation initiation to mRNA 5′ ends, 1st plant RNA virus for which infectious transcripts were designed from cloned viral cDNA, 1st demonstration of plant viral RNA recombination, and many other detailed analyses, primarily infects grasses (inc. cereals), rarely causing significant crop losses
Potato virus X (potexvirus, PVX)	+ssRNA	vary cyclically or seasonally and may disappear soon after infection, may cause necrosis, ringspot, or dwarf symptoms in a wide range of plant species (Ryu & Hong 2008)	development of PVX-based vectors for expression in transgenic plants was essential for RNA silencing discovery and mechanisms of pathogen-derived resistance in transgenic plants

Table 2: Top ten economically important plant viruses according to (Rybicki 2015). In the table, the most common symptoms were gathered from various publications and databases.

virus	type	symptoms	suggested reasons
African cassava mosaic disease (ACMD) begomovirus complex	DNA	dwarfing, stunting, distortion, rosetting, malformation and abnormal colors of leaves, reduced root system (Legg & Winter 2021)	devastating effects for cassava in Africa, major threat to food security there
Banana bunchy top nanovirus (BBTV)	ssDNA	Dark green broken streaks on leaf veins, midribs, petioles, pseudostem with clustered leaves ("bunchy"), short chlorotic plants, leaves curl upwards (Elayabalan et al 2015)	devastating effects in developing countries in Africa, Asia, and South Pacific
Banana streak badnavirus (BSV)	dsDNA	symptoms range from occasional chlorotic streaking to lethal systemic necrosis, chlorotic and brown necrotic streaks (Lockhart 2000)	
Barley yellow dwarf disease luteovirus complex (BYDV)	ssRNA	variable, chlorosis, stunting, photosynthesis inhibition, discoloration, thick leaves (Kaddachi et al 2014)	complex of ssRNA viruses, worst viral pathogen of wheat
Cucumber mosaic cucumovirus (CMV)	ssRNA	severe stunting, prominent yellow foliar mosaic, mottling malformation, and stunting due to drastic reduction of leaf size and stem internodes (El-Borollosy 2013)	infects almost anything, including maize and most vegetables
Maize streak mastrevirus (MSV)	ssDNA	leaves: yellow streaks on veins, veinal swelling, impaired chloroplast formation, stunting, curling, midribs (Monjane et al 2020)	worst viral pathogen of maize in Africa which is most common staple food
Maize dwarf mosaic (MDMV) / Sugarcane mosaic potyviruses (SCMV)	ssRNA	MDMV: chlorotic spots and short streaks followed by typical mosaic or mottle, SCMV: distinct mosaic, strong chlorosis, sometimes together with a red striped pattern (Signoret 2008)	wide-spread maize disease, often impossible to distinguish MDMV and SCMV based on symptoms
assoc. with rice tungro disease badnavirus (RTBV, dsDNA) and rice tungro spherical waikavirus (RTSV, ssRNA)	dsRNA and ssRNA	orange-yellow leaves, rust-colored spots, discoloration, delayed flowering, stunted (Hibino & Cabunagan 1986)	most important virus disease of rice in South and Southeast Asia
Rice yellow mottle sobemovirus (RYMV)	+ssRNA	streaking, mottling, discoloration, and malformation of leaves as well as death of infected young plants (Salaudeen et al 2009)	impacts crops of great importance in Asia and Africa
Sweet potato feathery mottle potyvirus (SPFMV)	+ssRNA	mottling, general chlorosis, chlorotic or purple ring spots (Tugume et al 2008)	worst pathogen of this crop world-wide

1.2.4 Abiotic stress factors

High temperature, water availability, wind, soil fertility, salinity, heavy metals, ultraviolet radiation, ozone are major abiotic factors influencing plant growth and development. Plants even must cope with their combinations including biotic stressors (He et al 2018, Velásquez et al 2018). Various xenobiotics such as pesticides, although applied to protect plants, also represent a wide group of abiotic stressors causing oxidative stress, reduction of chlorophyll, alteration in phenolics and protein content (Jakl et al 2021a, Sharma et al 2017, Sharma et al 2019).

1.2.5 Pesticides

Agricultural pesticides are used to kill crop pests, inhibit their growth, or decrease the harmful effects. Different classes of pesticides include fungicides, herbicides, insecticides, nematicides, molluscicides (snails), piscicides (fish), avicides (birds), rodenticides, bactericides, virucides, algicides (algae), miticides (mites), slimicides (slime-producing microorganisms), animal repellents, and antimicrobials. Pesticides are characterized by various toxicity to target and non-target organisms. Many pesticides accumulate, thus circulate in ecosystems, and endanger many living organisms as shown in Fig. 9 (Bhagat et al 2021, Lushchak et al 2018, Sharma et al 2020).

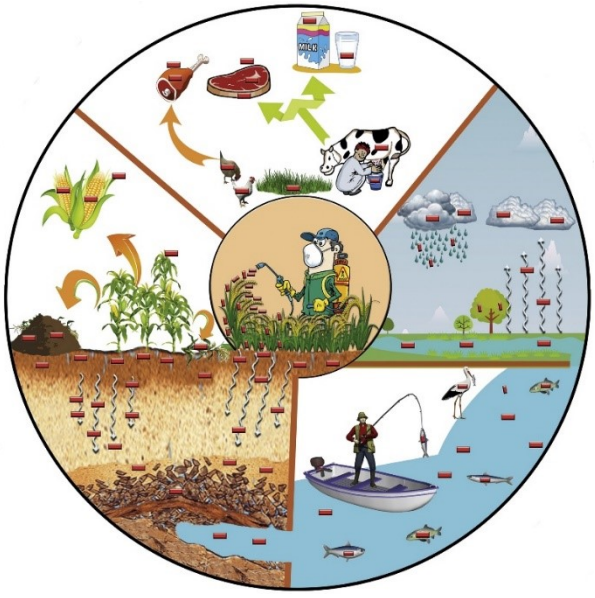


Fig. 9: The circulation and accumulation of pesticides and their residues, visualized as dark red rectangles (Vaezi et al 2018).

Fungicides can be divided into two classes - contact and systemic ones. In agricultural systems, they are widely used to control diseases and preserve the yield and quality of crops (Brauer et al 2019, Petit et al 2012). However, the extensive use raises public concern because of the harmful potential of such substances in the environment and human health (Dias 2012, Petit et al 2012).

Contact fungicides (e.g., copper, sulfur) remain on the treated surface and do not penetrate the plant tissue. They kill or inhibit fungi or fungal spores before the mycelia can grow and develop within the plant tissue, while the systemic ones (e.g., triazoles, benzimidazoles) target the fungus after the mycelia has penetrated the parenchyma of plant tissue to stop the infection (Dias 2012). Fungal plant pathogen species are primarily in the phyla Ascomycota (e.g., *Dothideomycetes, Sordariomycetes*, and *Leotiomycetes*) and Basidiomycota (e.g., the rusts and smuts) (Doehlemann et al 2017). Fungicides target various metabolic pathways or processes in fungal pathogens. They can be classified according to their mode of action: a) nucleic acid metabolism, b) cytoskeleton and motor proteins, c) respiration, d) amino acid and protein synthesis, e) signal transduction, f) lipid synthesis or transport/membrane integrity of function, g) sterol biosynthesis in membranes, h) cell wall biosynthesis, i) melanin synthesis in cell wall, j) host plant defense induction, k) chemicals with multi-site activity, l) biologicals with multiple modes of action, and m) unknown mode of action (FRAC 2020, Riah et al 2014). It is expected that in soil they may have non-target effects on soil microbes other than the crop pathogens (Duke 2018), i.e., on species essential for soil processes and processing nutrients crucial for plants. Some analogous pathways can be found also in plants. Therefore, pesticides generally represent a potential risk of phytotoxicity. Undesirable inhibition of photosynthesis, mitosis, cell division, enzyme function, root growth, or leaf formation; interference with the synthesis of pigments, proteins; or DNA damage, destruction of cell membranes were reported for a great number of pesticides (Dias 2012, Parween et al 2016).

Copper can be used as both fungicide (e.g., Bordeaux mixture, i.e., $CuSO_4$+$Ca(OH)_2$) and algicide (e.g., $CuSO_4$) in agriculture. Copper is also an essential plant micronutrient as a component of various proteins, particularly those involved in both photosynthetic (plastocyanin) and the respiratory

(cytochrome oxidase) electron transport chain (Petit et al 2012). However, its excess is highly phytotoxic, resulting in photosynthesis inhibition likely due to fatal changes in chloroplast ultrastructure which was observed in green algae. Copper was shown to alter the lipid content in chloroplast membrane, inhibit pigment accumulations and integrate into the photosystems in barley (Petit et al 2012). It inhibits both the synthesis of the chlorophyll precursor, δ-aminolevulinic acid and the activity of protochlorophyllide reductase (EC 1.3.1.33 - enzyme important in chlorophyll biosynthesis) (Stiborová et al 1986). Other effects of copper fungicides were reported such as suppression of oxygen evolution, photosystem II inactivation, Mg^{2+} substitution, interaction with -SH groups of ATPase and more.

Sulfur again functions both as a plant nutrient and a fungicide. Adverse effects on plants related to photosynthesis decrease and reduced stomatal conductance were reported (Petit et al 2012).

Triazole fungicides such as triadimefon, propiconazole, hexaconazole, and paclobutrazol inhibit the biosynthesis of steroids (Egbuta et al 2014, Zarn et al 2003), namely they block sterol 14-α-demethylase (CYP51, EC 1.14.14.154) leading to destabilization of fungal plasma membranes (Dvořák 2011, Lepesheva et al 2003). They are usually applied as foliar spray and probably represent the largest and most important group of systemic compounds developed for control of crop fungal (e.g., *Fusarium* sp. and *Erysiphe necator*) and yeast diseases. Also, triazoles can create complexes with copper ions (and probably other metal ions as well) and change their behavior in the environment, i.e., accumulation in soils, degradation, mobility, and stability (Arias et al 2006, Jakl et al 2017, Jakl et al 2021b, Jaklová Dytrtová et al 2011, Jaklová Dytrtová et al 2018). Although originally used in agriculture, triazoles easily spread through the soil; and contaminate groundwater and even reach urban centers (Valadas et al 2019). Moreover, they are also used in therapeutic and personal care products (e.g., shampoos, dermal creams, and soaps) and can be found in surface water and sediment of the aquatic environment (Bhagat et al 2021, Casida 2009, Chen & Ying 2015, Schmidt et al 2016).

Various developmental and morphological malformation and other toxic effects on non-targets like zebrafish (*Danio Rerio*), were documented if exposed to

triazoles such as tebuconazole, cyproconazole, clotrimazole and ketoconazole (Cao et al 2019, Chen & Ying 2015, Li et al 2019). In healthy non-target organisms, azoles may act as potential endocrine disruptors (Taxvig et al 2008, Trösken et al 2006, Zarn et al 2003).

Some triazoles were regarded with both phytotoxic and stimulant effects on plant physiology (Petit et al 2012). Triazoles were shown to have increased the level of cytokinin, likely resulting in stimulation of chlorophyll biosynthesis, then acceleration of chloroplast differentiation, and protecting the integrity of chlorophyll (Fletcher et al 2000, Jaleel et al 2008), presence of cyproconazole and penconazole after application into soil decreased the amount of green biomass of tomato plants, influenced the phenolic content in fruit, increased the fruit size and yield, and reduced the mobility of some essential elements (Fe, Cu, Zn) (Jakl et al 2021b)

An urgent problem with fungicides (pesticides in general) emerges because there is an unpleasant struggle with developing fungal resistances. Fungi may defend themselves by modification of sensitive sites, exclusion of fungicide or its detoxification (Brauer et al 2019, Esquivel B.D. & White 2017). Therefore, as various mixtures of fungicides increase in the environment, the more frequent and larger the exposure to non-target organisms is (Bhagat et al 2021). Plants can respond to xenobiotics e.g., pesticides in a three-phase detoxification system (Fig. 10, p. 35). In the phase I, the reactions are primarily catalyzed by cytochrome P450, but also by other enzymes such as amidases, reductases, esterases, PXs. They all participate in the transformation of the xenobiotics into a more water-soluble and usually a less toxic product. The next phase II (conjugation) produces compounds with higher molecular weight, reduced biological activity and mobility and further increased water solubility. This detoxification process involves conjugation with GSH, glucose, amino acids, and malonic acid, performed by different enzymes, especially glutathione and glycosyl transferases. In the phase III, the compounds can be either stored in the vacuole, translocated to the cell wall where they co-polymerate with lignin or are transported through the phloem (Singh et al 2016).

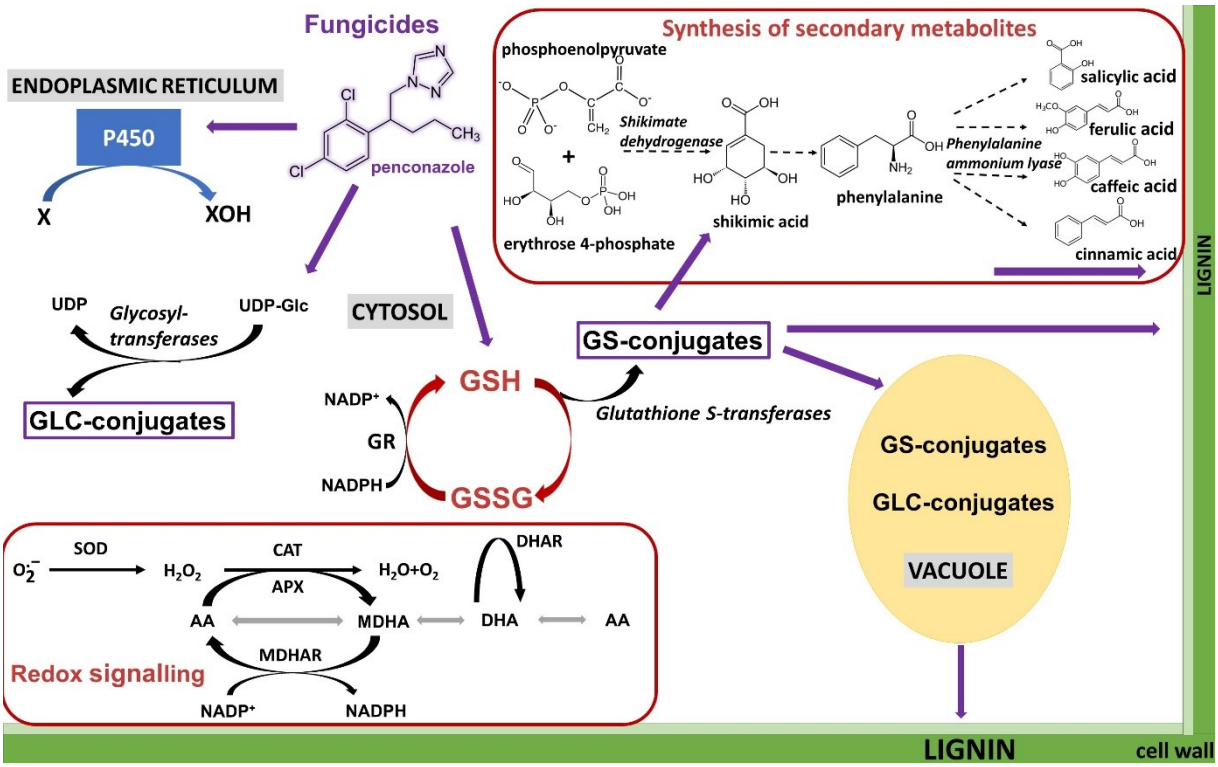


Fig. 10: Metabolic pathways of processing fungicides, modified, (Singh et al 2016). The dashed line indicates multi-step reactions. *Abbreviations: ASC - ascorbate, APX - ascorbate peroxidase, CAT - catalase, DHAR - dehydroascorbate reductase, GLC - glucose, GR - glutathione reductase, GSH - glutathione, MDHAR - monodehydroascorbate reductase, SOD - superoxide dismutase.*

1.3 Sustainable agriculture

Naturally, the demand for food, animal feed, bioenergy feedstocks, and biomaterials increases on the global level, pushing the crop harvest to its limits. However, high yields are often redeemed with application of excessive amounts of fertilizers, which apart from high costs contribute to environmental damage through eutrophication, soil acidification and air pollution (Brodt et al 2011, Chen & Liao 2017). In sustainable agriculture, the use of synthetic pesticides and fertilizers is abandoned. Instead, farmers plant a variety of plants together to promote biodiversity and repel pests and pathogens (Nicholls & Altieri 2013). Also, other ways of plant protection open using priming effects and biological control agents (BCAs).

1.3.1 Priming

Concisely, priming means that a mild exposure to stress can activate stress responses of plants, leading to various types of induced resistance (Fig. 11). Thus, it provides the plant with an increased capacity for rapid and effective activation of cellular defense responses and allows the plant to respond more effectively and readily to the action of the subsequent stress factor. Altogether, when biotic and abiotic stresses repeat, the plant recalls past molecular experiences and engage the saved information ("stress memory") for life-saving adaptation to new conditions (Bertini et al 2018, Conrath et al 2015, Turgut-Kara et al 2020).

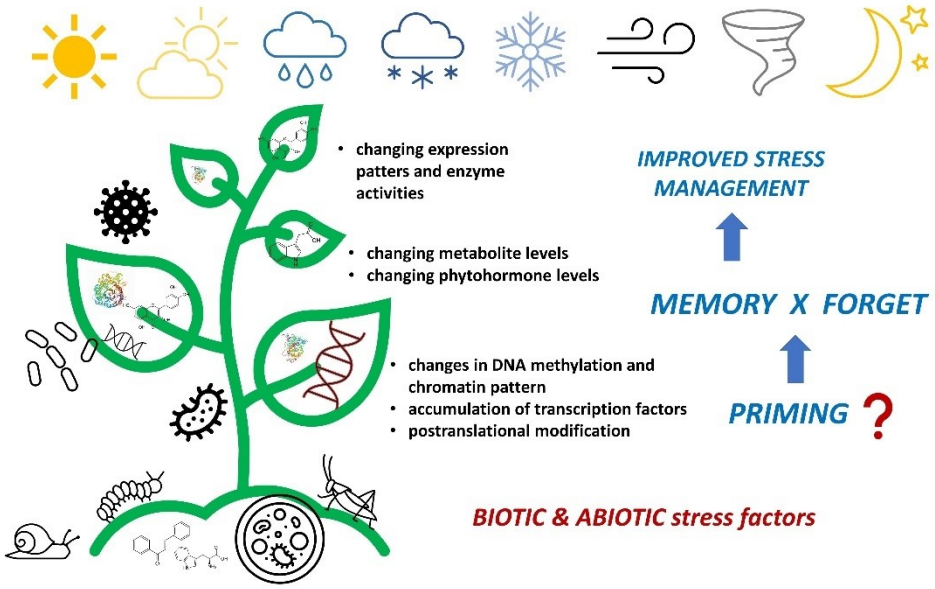


Fig. 11: The plant faces various stress factors. The plant responses may lead to improved stress management after priming and forming a "memory" of a stress factor. One of the mechanisms that can be involved in "forgetting" a stress response is autophagy, modified, (Hilker & Schmülling 2019).

A range of priming strategies such as modification of regulatory proteins *via* epigenetic mechanisms, accumulation of various cellular compounds, and the phosphorylation of MAPKs have been identified (Bertini et al 2018, Turgut-Kara et al 2020).

Epigenetic modifications are unique mechanisms for responding to the changing conditions at both in somatic and transgenerational states, and they seem to be critical for the plant survival and quick response to unfavorable conditions (Turgut-Kara et al 2020). All-chemical changes on the DNA and histone proteins are included in the epigenome. Plants use all major epigenetic

mechanisms present in eukaryotes. DNA methylation relies on several plant-specific proteins associated with gene silencing including a few proteins likely specific for demethylation. Also, histone modifying enzymes that modulate the chromatin structure in plants are present and frequently encoded by relatively large gene families (Espinas et al 2016, Turgut-Kara et al 2020). The histone modifications on the promoters of transcription factors (e.g., methylation and acetylation on promotors of WRKY genes, histones H3 and H4) are related to defense and priming promotion of gene expression (Bertini et al 2018, Espinas et al 2016, Turgut-Kara et al 2020).

Beneficial microorganisms are related to ISR initiation, which is often regulated by SA-independent mechanisms. However, several plant-growth promoting rhizobacteria have been reported to trigger a SA-dependent type of ISR that resembles pathogen induced SAR (Djellout et al 2020, Pieterse & Van Wees 2015). ISR is associated with the synthesis of defense related enzymes, such as PR proteins, and to the accumulation of PXs, polyphenol oxidase and phenolics as plant response to various stresses (Magnin-Robert et al 2007). This way of priming plant defense can be maintained for the plant whole life and protect it effectively against a wide range of pathogens (Djellout et al 2020, Wallis & Galarneau 2020)

Not only the exposure of plants to pathogens or beneficial microorganisms, but also some natural and synthetic chemicals may cause the priming effect after application (Mauch-Mani et al 2017). Natural occurring compounds with priming effects belong chitosan, caproic acid and SA, and those of synthetic origin include various SA analogs (e.g., benzothiazole - a fungicide), ß-aminobutyric acid, 2,6-dichloroisonicotinic acid and its methyl ester (Bertini et al 2018, Burketová et al 2015, Zhou & Wang 2018). Also, proteinaceous elicitors oligandrin from *Pythium oligandrum* and ß-cryptogein from *Phytophthora cryptogea* induced expression of many defense genes in tomato plants (Ouyang et al 2015, Satková et al 2017, Starý et al 2019).

1.3.2 Biological control agents

BCAs represent a promising, environmentally friendly approach to protecting plants against various pathogens. These agents include fungi,

oomycetes, and bacteria, and their positive effect originates from interactions that prime defense responses and enhance plant resistance to future stressors (Gerbore et al 2014a, Le Hesran et al 2019). Therefore, the repeated use of chemical agents (i.e., pesticides) might be decreased as well as the workforce dedicated to the treatment.

The philosophy of BCA usually follows one of the three major ways: importation of exotic species into a new habitat, augmentation of established species by increased production and periodic colonization or their conservation through manipulation of the environment, i.e., plant and habitat diversification, cropping intensity reduction, and increased landscape complexity (Begg et al 2017, Le Hesran et al 2019).

For example, the oomycete *Pythium oligandrum* is a world-wide soil organism (Takenaka 2015) that was first described by the American mycologist Charles Drechsler in 1930 (Drechsler 1930). This organism can be found on the surface of plant roots (in the rhizosphere) where it may interact with numerous plant pathogens and the plant itself (Brožová 2002, Gerbore et al 2014a). Among the organisms serving as BCAs, some species of the genus *Trichoderma* (e.g., *T. asperellum* and *T. atroviride* act as fungicides) or certain species genus *Bacillus* (e.g., *B. thuringiensis* acts as an insecticide) can be found (Gerbore et al 2014a).

1.3.3 *Pythium oligandrum*

Pythium oligandrum, a soil-inhabiting oomycete, has been reported to be an effective BCA (Benhamou et al 2012). *P. oligandrum* produces two types of proteinaceous elicitors (Masunaka et al 2010, Takenaka et al 2006). One type of elicitors represents cell wall protein in mycelial mats of *P. oligandrum* and has several members (Takenaka et al 2003, Takenaka & Tamagake 2009, Takenaka et al 2011). Another type of elicitor in *P. oligandrum* are oligandrins, extracellular proteins that can induce resistance in many plants against *Phytophthora* species, bacterial and fungal pathogens (Benhamou et al 2001, Mohamed et al 2007). Oligandrins are low molecular mass proteins (10 kDa) with characteristic structure containing six α-helixes, two short ß-sheets, and ω-loop, which is

important for sterol binding. Oligandrins have a conserved sequence within elicitins, which is stabilized by three disulphide bridges, but without homology to plant proteins. Oligandrins (OLI-S1, OLI-D1, OLI-D2) and cell wall proteins (POD1, POD1a, POD1b, POD2, and POS1) are elicin and elicitin-like proteins that were reported to be produced by various *P. oligandrum* strains (Derevnina et al. 2016).

The effect of *P. oligandrum* on plant is a complex process, which results either in direct or indirect protection of plants against pathogens. *P. oligandrum* interacts with other soil microorganisms (pathogens) in a mycoparasitic process, involving a secretion of cell wall degrading enzymes, such as chitinases and cellulases, and use target's carbon compounds for its own growth and development. Simultaneously, it also competes for nutrients and space with its target organism. Its penetration into pathogen cells is associated with a complete destruction of the cytoplasm in the target cells and finally the whole cell, *e.g*., of *Fusarium oxysporum* f. sp. *radices-lycopersi* or *P. ultimum*. Further analysis of *P. oligandrum* transcripts showed genes for proteases, protease inhibitors, glucanases, putative effectors, and elicitors that were also found in the interaction with *Ph. infestans* hyphae (Gerbore et al 2014a).

It is known that *P. oligandrum* can interact with plant roots. It was reported that *P. oligandrum* quickly and massively colonizes root tissues, but its colonization is associated neither with host wall disruption nor host cell alterations and is followed by induction of several host defense reactions (Takenaka et al 2011). The details of the process were observed in tomato plants. *P. oligandrum* penetrates root tissues rapidly but it cannot survive in plants. The first events include the penetration of *P. oligandrum* into the root epidermis and colonization of the cortex, where the hyphae are metabolically active. After 12-14 h, structural changes and cytoplasm disintegration occur. After 48 h, the cells of *P. oligandrum* look like empty shells surrounded by enlarged oogonia. The above processes are accompanied by changes in plant metabolism, particularly, the phenylpropanoid pathway is stimulated to synthetize defense compounds (Benhamou et al 2012). The fact that the invading hyphae of *P. oligandrum* degenerate concomitantly with the accumulation of plant defense compounds strongly suggests that

P. oligandrum is not able to short-circuit plant defense responses as do most other mutualistic agents through the production of effector-like molecules.

Plants contain receptors for elicitins and thus the defense response can be activated, and local induced resistance can occur to a broad spectrum of pathogens (Derevnina et al 2016, Du et al 2015). The plant encounter with *P. oligandrum* and its secreted products may lead to priming.

P. oligandrum also stimulated growth of tomato plants. Since *P. oligandrum* can produce tryptamine (auxin precursor), which is then readily absorbed by root system, resulting in an increase of root mass associated with an enhanced formation of secondary roots (Benhamou et al 2012, Le Floch et al 2003). Roots are very sensitive to even a low auxin concentration, a mild but frequent production of auxin of fungal origin may have a key impact on root physiology (Le Floch et al 2003). In greenhouse experiments with pepper grown in soil infested with *Verticilium dahliae* (wilt disease), shoot and fruit masses were significantly higher in the presence of *P. oligandrum* than in its absence. Disease losses caused by *V. dahliae* were conclusively reduced by *P. oligandrum* which promoted plant growth (Al-Rawahi & Hancock 1998).

The treatment with *P. oligandrum* oospores induced defense reactions against *Botrytis cinerea* infection in strawberry. It was found that this treatment reduced the severity of grey mold in field tests. The efficiency of the treatment was ca. 90% and 60% for low and high disease intensity, respectively. But in both cases, the treatment reached the same or only a little lower efficiency compared to standard chemical fungicides (Meszka & Bielenin 2010). Furthermore, the elicitor oligandrin induced expression of several defense genes against *B. cinerea* and *Oidium neolycopersici* in tomato plants (Ouyang et al 2015, Satková et al 2017).

The application of a cell wall protein fraction of *P. oligandrum* to sugar beet plants induced plant defense reaction and increased resistance against seedling diseases caused by *Aphanomyces cochliodes* and *Rhizoctonia solani* AG2-2. Also, the early colonization of sugar beet seeds by *P. oligandrum* protected seedlings against subsequent infection by *P. ultimum*, a reason for this seems to be a competition for space and nutrition between both microorganisms (Takenaka & Ishikawa 2013).

The complex relationship between *P. oligandrum*, plants, and pathogens is shown in Fig. 12. It seems that an impressive number of diseases in various plants can be controlled by *P. oligandrum*. The reduction of pathogenic attacks varies from 15–100%, depending on the host plant, the target pathogen, and the application method (Gerbore et al 2014a, Gerbore et al 2014b). The ability of *P. oligandrum* to enter and colonize the root system before rapidly degenerating is one of the most striking features that differentiate this organism from all other known biocontrol fungal agents.

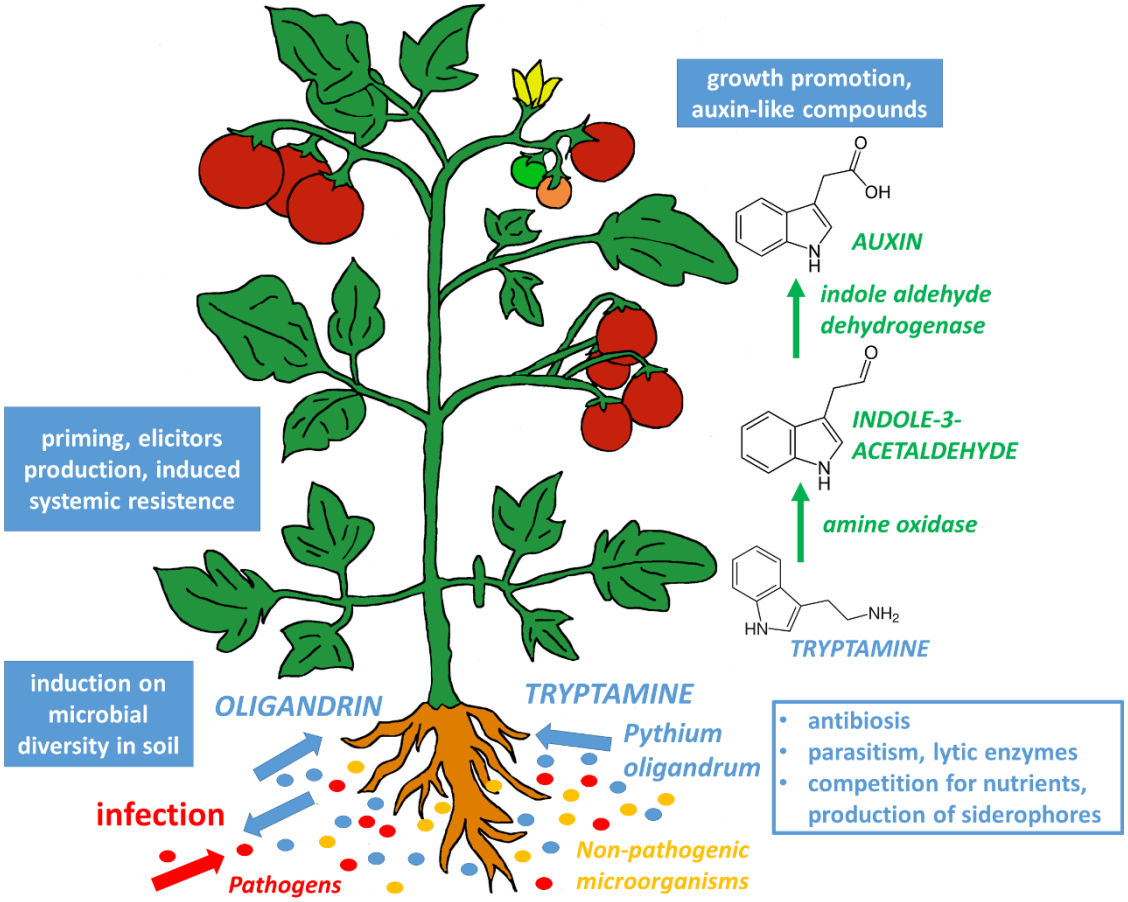


Fig. 12: Schematics of *P. oligandrum* interactions modified from (Gerbore et al 2014a). *P. oligandrum* appears to be a promising BCA, as it operates on several levels (Benhamou et al 2012): 1. It acts against pathogens in the soil by occupying the rhizosphere, and thus by competing for space and nutrients. 2. It directly attacks some plant pathogens living in the soil. 3. It increases the resistance of plants because it induces their defense system. 4. Through the production of tryptamine, a precursor of auxin, it promotes plant growth (Le Floch et al 2003).

2 Aims of the thesis

The thesis can be divided into two major sections. The first part represents an insight into the plant metabolism exposed to biotic and abiotic stress factors. We focused on the features of *Pythium* strains and their use in seed-coating as an environmentally friendly way of plant protection. Plant viruses represent major economic losses in agriculture and are affected by several factors. Thus, we followed the impact of elevated temperature on viral propagation in plants. In contrast with biological control agents, we observed some adverse effects of fungicides in plants. In the analyses, we always observed changes of phenolic compounds in plant metabolism. Thus, we also paid attention to the kinetic parameters of shikimate dehydrogenase. The second part of this thesis focuses on the antioxidant capacity involved either in plants or occurring *in vitro* during triazoles (fungicides) interactions. Triazoles also represent a potential threat to non-target organisms.

The aim of the thesis was:

I.

- To analyze the biochemical properties of *Pythium* strains, related to the oomycete *Pythium oligandrum*.
- To characterize the metabolism of the rapeseed plants grown from the seeds coated with *Pythium* strains.
- To evaluate the effect of heat shock on the course of viral propagation.
- To assess the side effects of fungicides on crop plants.
- To study the regulation and side reactions catalyzed by shikimate dehydrogenase, a key enzyme of the shikimate pathway.

II.

- To evaluate the connections between antioxidant capacity, total phenolic content, and key nutritional minerals of medicinal plants.
- To analyze the interactions between plant antioxidants and triazoles.
- To evaluate the impact of triazoles on the enzymes of non-target organisms.

3 Results and discussion

3.1 Publications

The participation of **Kateřina Bělonožníková** in preparation of all manuscripts (specified for each in "My contribution") was approved by the supervisor doc. RNDr. Helena Ryšlavá, CSc. and the consultant RNDr. Daniel Kavan, Ph.D. The results of this thesis are summarized in 7 published and 2 submitted manuscripts. Currently, we also have 2 manuscripts in preparation, but they are not a part of the thesis. The following publications can be divided into two major parts. The first group of articles focuses on the plant metabolism under stress conditions and the second one concentrates on the antioxidants and their resulting impact on humans and the environment.

I) Plant metabolism under stress conditions

Bělonožníková, K., Vaverová, K., Vaněk, K., Kolařík, M., Hýsková, V., Vaňková, R., Dobrev, P., Křížek, T., Hodek, O., Čokrtová, K., Štípek, A., Ryšlavá, H.: **Novel insights into the effect of *Pythium* strains on rapeseed metabolism,** Microorganisms, 8:1472, 2020, IF 2019 = 4.152, https://doi.org/10.3390/microorganisms8101472

Hýsková, V., **Bělonožníková**, K., Čeřovská, N., Ryšlavá H.: **HSP70 plays an ambiguous role during viral infections in plants, (Review)**, Biologia Plantarum, 65:68-79, 2021, IF 2019 = 1.602, https://doi.org/10.32615/bp.2021.001

Hýsková, V., **Bělonožníková, K.**, Doričová, V., Kavan, D., Gillarová, S., Henke, S., Synková, H., Ryšlavá, H., Čeřovská, N.: **Effects of heat treatment on metabolism of tobacco plants infected with *Potato virus Y,*** Plant Biology, 2021, IF 2019 = 2.167, https://doi.org/10.1111/plb.13234

Hýsková, V., **Bělonožníková, K.**, Šmeringaiová, I., Kavan, D., Ingr, M., Ryšlavá, H.: **How is the activity of shikimate dehydrogenase from parsley root regulated and which side reactions are catalyzed?** *Submitted: Phytochemistry, March 2021*

Jakl, M., Ćavar Zeljković, S., Kovač, I., **Bělonožníková, K.**, Jaklová Dytrtová, J.: Side effects of triazoles on treated crops, Chemosphere, 277:130242, 2021, IF 2019 = 5.778, https://doi.org/10.1016/j.chemosphere.2021.130242

II) Antioxidants and their impact on humans and the environment

Tupec, M., Hýsková, V., **Bělonožníková, K.**, Hraníček, J., Červený, V., Ryšlavá H.: **Characterization of some potential medicinal plants from Central Europe by their antioxidant capacity and the presence of metal elements,** Food Bioscience, 20:43-50, 2017, IF 2019 = 3.067, https://doi.org/10.1016/j.fbio.2017.08.001

Jaklová Dytrtová, J., Straka, M., **Bělonožníková, K.**, Jakl, M., Ryšlavá, H.: **Does resveratrol retain its antioxidative properties in wine? Redox behaviour of resveratrol in the presence of Cu(II) and tebuconazole,** Food Chemistry, 262:221-225, 2018, IF 2019 = 6.306, https://doi.org/10.1016/j.foodchem.2018.04.096

Jaklová Dytrtová, J., **Bělonožníková, K.**, Jakl, M., Ryšlavá, H.: **Triazoles and aromatase: The impact of copper cocktails,** Environmental Pollution, 266:115201, 2020, IF 2019 = 6.792, https://doi.org/10.1016/j.envpol.2020.115201

Jaklová Dytrtová, J., **Bělonožníková, K.**, Jakl, M., Ryšlavá, H.: **Cocktail effects of triazoles and zinc on cytochrome 3A4 and 19A,** *Submitted: Food and Chemical Toxicology, February 2021*

III) Manuscripts in preparation, not included in the doctoral thesis

Bělonožníková, K., Černý, M., Hýsková, V., Kavan, D., Křížek, T., Hodek, O., Valcke, R., Synková, H., Vaňková, R., Dobrev, P., Schnablová, R., Ryšlavá, H.: **What is the impact of organic nitrogen sources on tobacco metabolism?** *In preparation: 2021*

Bělonožníková, K., Kavan, D., Hýsková, V., Hraníček, J., Ryšlavá, H.: **Fruit and vegetable juices: effects of antioxidants on metabolic enzymes,** *In preparation: 2021*

3.2 Plant metabolism under stress conditions

3.2.1 Novel insights into the effect of *Pythium* strains on rapeseed metabolism

The search for economically and environmentally friendly crop protection is getting more and more attractive and likely even necessary for sustainable agriculture. In 2017, we successfully applied our grant proposal "Industrial research for universal seed and seedlings treatment that protects against fungal, bacterial and other pests" (TJ01000451) in the project Zeta of the Technology Agency of the Czech Republic. During the collaboration with Biopreparáty spol. s r.o. we began to analyze the unique features of *Pythium* isolates and tested the influence of seed coating on metabolism and defense reactions of young rapeseed plants (*Brassica napus*). Although *Pythium* genus is mostly known for the pathogenic *P. ultimum* and *P. insidiosum*, the beneficial effects of *P. oligandrum*, but also *P. acanthicum*, *P. periplocum* and *P. nuun* against various fungal diseases have been continuously reported (Benhamou et al 1999, Brožová 2002, Gerbore et al 2014a, Sankaranarayanan & Amaresan 2020). The overview of our publication is summarized in the graphical abstract (Fig. 13).

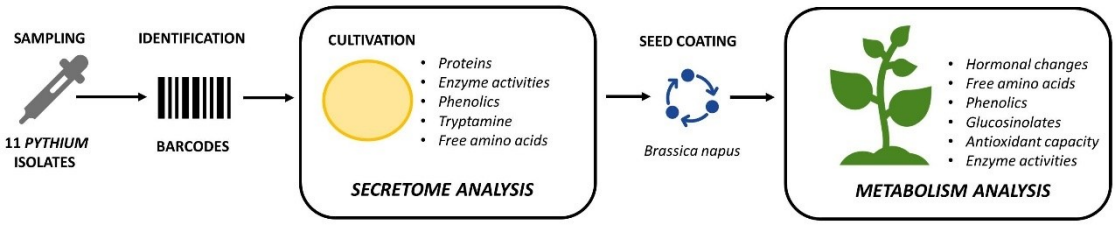


Fig. 13: Graphical abstract of the publication about *Pythium* strains (Bělonožníková et al 2020). *Pythium* strains were labeled as M1, 00X5, 00X11, 00X23, 00X30, 00X34, 00X40, 00X42, 00X48, X40 and X42. All the strains were identified as *P. oligandrum*, except for X42 which was shown as a novel *Pythium* strain. For the metabolism analysis, we also grew untreated (C, control) plants.

Firstly, we identified eleven *Pythium* isolates (strains) from the collection of Biopreparáty spol. s r.o. The ten *Pythium* strains were identified as *P. oligandrum* and one isolate was regarded as a previously undescribed *Pythium* sp. (called X42). Also, one of the tested isolates, called M1 (ATC 38472), was the commercially used agent (Vesely 1978) (Table 1, Fig. 1, in Bělonožníková et al 2020). In the first part of the project, we focused on the analysis of secretomes of *Pythium* strains. Although the composition of the cultivation medium was identical for all of them,

we discovered significant differences in the contents of proteins, free amino acids, and phenolic compounds (Fig. 2 in Bělonožníková et al 2020). *P. oligandrum* may produce tryptamine, an auxin precursor, that promotes plant growth (Benhamou et al 2012, Le Floch et al 2003). Surprisingly, the X42 secretome showed the highest tryptamine content, approx. 5.5 times higher than the commercial strain M1 (Fig. 2b in Bělonožníková et al 2020).

Naturally, we focused on the detection of oligandrin, a secreted elicitin, that is known to induce resistance in many plants and to initiate plant priming, leading to restriction the pathogen growth and development (Benhamou et al 2001, Lherminier et al 2003, Picard et al 2000, Satková et al 2017). This was also another striking evidence of X42 peculiarity since its secretome showed unique protein profile in comparison with other tested *Pythium* strains in the Tricine electrophoresis. In addition to oligandrin (~10 kDa), likely significant amounts of several peptides (<6.5 kDa) was detected, that may be either just degradation products or other elicitors (Fig. 3 in Bělonožníková et al 2020). Elicitins form a family of oomycete proteins, including cryptogein, capsicein, parasiticein and INF1 from pathogens *Phytophthora cryptogea, Ph. capsici, Ph. parasitica,* and *Ph. infestans* (Derevnina et al 2016). They typically induce HR and subsequently PCD in some plant species, e.g., capsicein and cryptogein in tobacco (Ricci et al 1989). On the other hand, elicitin-like cell wall protein fraction (POD1 and POD2) from *P. oligandrum* activated JA- and ET- pathways and did not induce HR (Takenaka et al 2006, Takenaka et al 2003). Also, oligandrin-treated tomato plants did not exhibit necrotic features typically associated with HR. However, oligandrin treatment significantly reduced disease severity provoked by *Ph. parasitica* (Picard et al 2000). It was also presented that ultrastructural modifications in tomato cells upon oligandrin treatment that correlated with restriction of pathogen *Fusarium oxysporum* f. sp. *radicis-lycopersici* ingress to the vascular stele (Benhamou et al 2001). However, they suggested the metabolic changes do not follow a general pathway upon signal recognition (Benhamou et al 2001). The plant receptors implicated in the defense responses independent of HR still need to be identified (Derevnina et al 2016).

Subsequently, we analyzed the hydrolytic enzymes that are important for facilitating the cell wall penetration during mycoparasitism (Brunner et al 2002). Numerous pathogenic fungi and oomycetes produce saponin-detoxifying glycosidases (Bowyer et al 1995, Ivanov & Bernards 2012). Also, for example ß-glucosidase could modulate O-glycosylated cytokinins to alter the phytohormonal levels in plants (Le Roy et al 2016). Most information about various hydrolytic enzymes of *Pythium* spp. derives from genomic analyses (Faure et al 2020, McGowan & Fitzpatrick 2017) without the substrate specificity of the enzyme. Therefore, we measured enzyme activities of endoglycosidases (celullase EC 3.2.1.4, chitinase EC 3.2.1.14, and ß-1,3-glucanase EC 3.2.1.6) and exoglycosidases (α-glucosidase EC 3.2.1.20, ß-glucosidase EC 3.2.1.24, ß-galactosidase EC 3.2.1.23, α-mannosidase EC 3.2.1.24, α-galactosidase EC 3.2.1.22, and ß-hexosaminidase EC 3.2.1.52). Some *Pythium* strains (00X5, 00X30, 00X48, X40) showed higher endoglycosidase activities than the commercially used M1 strain, while the exoglycosidase activities were the highest in the M1 secretome, except for α-mannosidase which was the most active in the X40, X42 secretomes. We detected no activities of α-galactosidase and ß-hexosaminidase. On the other hand, we observed an unexpected activity of ß-galactosidase in alkaline pH (Fig. 4 in Bělonožníková et al 2020). Interestingly, in the total proteolytic activity measurement of the secretomes, the M1 strain did not show as significantly high activity as the X42. Acid and alkaline phosphatases were also present in the *Pythium* strain secretomes. These enzymes could be interesting for plants as they remove phosphates from various organic sources and increase the nutrient availability (Fig. 5 in Bělonožníková et al 2020). In average, alkaline phosphatases showed higher activity than the acid forms. The strains M1 and 00X5 showed significantly high activities of both forms in the secretomes. We also supposed that the enzyme activities could be induced by a different composition of the cultivation medium. In the future research, we would test various substrates in the media to promote the secretion of hydrolytic enzymes. For the mycoparasitism, the carbohydrate hydrolytic enzymes are especially important. However, they must be tightly regulated and compartmentalized to prevent self-degradation. *P. oligandrum* behaves parasitically even to *P. ultimum*

from its own genus (Ali-Shtayeh & Saleh 1999, Brožová 2002). Therefore, one of the key questions that remains is how the recognition between self and non-self occurs (Liang et al 2020). *P. oligandrum* performs a strong mycoparasitism against more than 50 fungal and oomycete species and thus is also used as an effective agent against various dermatophytoses in human and animals (Gabrielova et al 2018, Načeradská & Mencl 2010).

The impact of rapeseed inoculation with *Pythium* strains was followed in 3-week-old plants. Seed coating represents a convenient tool to implement beneficial microorganisms into the soil and rhizosphere or plant tissue (Ma 2019). We did not observe any significant changes in the rapeseed growth parameters as expected by tryptamine supplementation by *Pythium* strains. The tryptamine content was also followed in the rapeseed leaves, but it was rather low and only the plants treated with 00X30 significantly differed from the control (untreated) plants (Fig. 6c, in Bělonožníková et al 2020). We suggested that a further biotransformation to auxin could take place (Fig. 12, p. 41). In the future research, we would focus on the analysis of roots and conduct a time-dependent experiment to investigate the metabolic changes. We also followed the content of free amino acids in the rapeseed leaves (as well as in the secretomes, Table 2, Fig. 7 in Bělonožníková et al 2020). The interaction between the plant and *Pythium* strain may also include the exchange of the plant tryptophane for tryptamine as shown for rhizobacteria and *P. oligandrum* (Kravchenko et al 2004, Le Floch et al 2003). We observed a decrease in the tryptophan content, especially in the plants treated with 00X40, 00X5, and X42 strains. Also, the content of other aromatic amino acids, phenylalanine and tyrosine were decreased in all plant groups. Therefore, we expected to see a connection with the phenolic content, but we found no significant differences among the plant groups in the total phenolics as well as the antioxidant capacity (Fig. 6 in Bělonožníková et al 2020). However, the measurements encompass only the soluble phenolics content. We suggested that some of the phenolics could impregnate the cell wall in the form of lignin, providing a reinforcement and significant improvement of the defense barrier against biotic stressors.

The plant metabolism as well as the plant-environment interaction is regulated by phytohormones. The strains X42 and 00X11 belonged to the candidates that could significantly alter the indole-3-acetic acid (IAA, auxin) content since they both produced significant amounts of tryptamine in the secretome and decreased the tryptophan content. Not only IAA content was altered (significantly increased in plants treated with 00X11, 00X30, X42 and M1), but also the contents of indole-3-acetamide, indole-3-acetonitrile (precursors of IAA in different biosynthetic pathways) and phenylacetic acid (Fig. 8a,b in Bělonožníková et al 2020). We proposed that this could mean that *Pythium* strains influence the auxin metabolism by multiple ways. We also observed a sort of "acceleration" of the cytokinin metabolism in the treated plants since high concentrations of precursors and degradation products were detected (Fig. 8c in Bělonožníková et al 2020). In accordance with literature, we detected high levels with JA, JA-Ile, and aminocyclopropane-1-carboxylic acid (ACC, ET precursor) in the treated plants (Fig. 8d in Bělonožníková et al 2020). Also, Yacoub et al highlighted the promotion of JA- and ET-signaling pathways with certain genes induced (e.g., ACC synthase, allene oxide cyclase) early after *Phaeomoniella chlamydospora* attack if grapevine roots had been inoculated with *P. oligandrum* (Yacoub et al 2020). However, we also detected higher levels of SA in the plants treated with 00X30 and 00X11 in comparison with the control plants. It could be related to the species specificity or maybe readiness for faster response. Similar differences were found for the ß-cryptogein treatment which activated the ET- and JA-signaling pathways in tomato plants (Starý et al 2019) and SA-signaling in tobacco plants (Keller et al 1996).

Brassicaceae plants are famous for their glucosinolate content that protects them from herbivores and other pathogens. Since the project was dedicated to the plant protection, we also investigated if *Pythium* strains could alter their composition and content. In the leaves of experimental plants, glucobrassicin and progoitrin were the most abundant. The low levels of tryptophan in the treated plants could also indicate its involvement as precursor of not only auxin but also of glucobrassicin (Fig. 7 in Bělonožníková et al 2020). Glucoraphanin was detectable only in the treated plants (Table 3 in Bělonožníková et al 2020).

Methionine as a precursor of both glucoraphanin and progoitrin was detected in significant amounts in the *Pythium* secretomes (Fig. 7 in Bělonožníková et al 2020), thus may have stimulated the Met-dependent pathways, including ET biosynthesis, S-adenosylmethionine (Pieterse et al 2012).

Using native electrophoretic methods, we detected the isoforms of antioxidant enzymes SOD and PX which were increased in all plants treated with *Pythium* strains (Fig. 9a,b in Bělonožníková et al 2020). Also, we observed an increased activity of SDH, one of the key enzymes for the phenylpropanoid synthesis, in the plants treated with *Pythium* strains (Fig. 9c in Bělonožníková et al 2020).

In conclusion, we showed that the *Pythium* strain secretomes varied significantly based on various protein content, hydrolytic enzyme activities and tryptamine production. We employed seed coating as an economically friendly way to treat plants with a BCA. Our findings suggest that the differences in the *Pythium* strains "metabolic behavior" or "life strategy" are of great importance for finding a novel and effective BCA.

My contribution:

I analyzed the protein content of secretomes, measured most enzyme activities, prepared all the figures and tables, helped to analyze the data, and to write the manuscript.

microorganisms

MDPI

Article

Novel Insights into the Effect of *Pythium* Strains on Rapeseed Metabolism

Kateřina Bělonožníková [1], Kateřina Vaverová [1], Tomáš Vaněk [2], Miroslav Kolařík [3,4], Veronika Hýsková [1], Radomíra Vaňková [5], Petre Dobrev [5], Tomáš Křížek [6], Ondřej Hodek [6], Kateřina Čokrtová [6], Adam Štípek [2] and Helena Ryšlavá [1,*]

[1] Department of Biochemistry, Faculty of Science, Charles University, Hlavova 2030, 128 43 Prague 2, Czech Republic; katerina.belonoznikova@natur.cuni.cz (K.B.); katerina.vaverova@natur.cuni.cz (K.V.); veronika.hyskova@natur.cuni.cz (V.H.)
[2] Biopreparáty, spol. s r.o., Tylišovská 1, 160 00 Prague 6, Czech Republic; vanek@biopreparaty.eu (T.V.); stipek@biopreparaty.eu (A.Š.)
[3] Institute of Microbiology, Academy of Sciences of the Czech Republic, Vídeňská 1083, 142 20 Prague 4, Czech Republic; mkolarik@biomed.cas.cz
[4] Department of Botany, Faculty of Science, Charles University, Benátská 2, 128 01 Prague 2, Czech Republic
[5] Institute of Experimental Botany, Academy of Sciences of the Czech Republic, Rozvojová 263, 165 02 Prague 6, Czech Republic; Vankova@ueb.cas.cz (R.V.); Dobrev@ueb.cas.cz (P.D.)
[6] Department of Analytical chemistry, Faculty of Science, Charles University, Hlavova 2030, 128 43 Prague 2, Czech Republic; tomas.krizek@natur.cuni.cz (T.K.); ondrej.hodek@natur.cuni.cz (O.H.); katerina.cokrtova@natur.cuni.cz (K.Č.)
* Correspondence: helena.ryslava@natur.cuni.cz

Received: 20 August 2020; Accepted: 23 September 2020; Published: 25 September 2020

Abstract: *Pythium oligandrum* is a unique biological control agent. This soil oomycete not only acts as a mycoparasite, but also interacts with plant roots and stimulates plant defense response via specific elicitors. In addition, *P. oligandrum* can synthetize auxin precursors and stimulate plant growth. We analyzed the secretomes and biochemical properties of eleven *Pythium* isolates to find a novel and effective strain with advantageous features for plants. Our results showed that even closely related *P. oligandrum* isolates significantly differ in the content of compounds secreted into the medium, and that all strains secrete proteins, amino acids, tryptamine, phenolics, and hydrolytic enzymes capable of degrading cell walls (endo-β-1,3-glucanase, chitinase, and cellulase), exoglycosidases (especially β-glucosidase), proteases, and phosphatases. The most different strain was identified as a not yet described *Pythium* species. The changes in metabolism of *Brassica napus* plants grown from seeds coated with the tested *Pythium* spp. were characterized. Enhanced levels of jasmonates, ethylene precursor, and salicylic acid may indicate better resistance to a wide variety of pathogens. Glucosinolates, as defense compounds against insects and herbivores, were enhanced in young plants. Altogether, *P. oligandrum* strains varied in their life strategies, and either they could perform equally as plant growth promoters and mycoparasites or they had developed one of these strategies better.

Keywords: *Pythium*; secretome; cultivation medium; plant metabolism; phytohormones; rapeseed; enzyme activities

1. Introduction

Biological control agents (BCAs) represent a promising, environmentally friendly approach to protecting plants against a vast array of pathogens. These agents include fungi, oomycetes, and bacteria, and their positive effect stems from interactions that prime defense responses and enhance plant resistance to future stressors [1]. For example, soilborne plant pathogens can be biologically controlled by treating seeds with antagonists [2]. In particular, a striking number of soilborne diseases of various plants can be controlled by *Pythium oligandrum*, including ascomycetes, basidiomycetes, and pathogenic oomycetes [3].

P. oligandrum is a nonpathogenic soil inhabitant with worldwide distribution, which belongs to the class of filamentous eukaryotic microorganisms (oomycetes) and stands out among promising licensed biological agents. *P. oligandrum* has numerous beneficial effects on plant fitness, which result from the synergistic action of direct and indirect mechanisms on plant protection. *P. oligandrum* directly attacks the aforementioned pathogens via mycoparasitism or antibiosis, even attacking pathogenic oomycetes of its own *Pythium* genus [1,3–5]. Simultaneously, *P. oligandrum* also competes for nutrients and/or space with its target organisms.

P. oligandrum as a BCA can colonize plant root systems without damaging plant tissues, produce elicitors, secrete different hydrolases, and trigger signaling cascades and defense gene expression, thus indirectly activating localized and systemic induced resistance [3]. It produces two types of proteinaceous elicitors including the extracellular protein oligandrin (10.5 kDa) and cell wall protein fractions [6,7]. Oligandrins function like sterol carrier proteins and pick up sterols from plasma membranes, because oomycetes are unable to synthesize sterols but require an exogenous source of β-hydroxy sterols for sporulation [6].

Therefore, the treatment of plants with *P. oligandrum* functions by priming and activating the plant immune system, and thus providing increased protection against fungal and bacterial diseases [1,3]. In the rhizosphere, *P. oligandrum* supports the plant root system by producing tryptamine (auxin precursor), which is readily absorbed, thereby increasing the root mass through enhanced secondary root formation [3,8]. Since roots are highly sensitive to auxin, even at low concentrations, a mild but frequent exogenous auxin production may have a strong impact on root physiology [8].

The aim of this work was to find new *Pythium* strains exhibiting unique beneficial properties suitable for use as BCAs. For this purpose, we compared the activities of enzymes related to mycoparasitism or competition for nutrients (glycosidases, proteases, phosphatases, etc.), the amount of excreted oligandrins, and the amount of tryptamine as an auxin precursor and plant growth promoter. The secretomes of 11 *Pythium* spp. were analyzed in terms of protein profiles, total and individual free amino acids, and activity of both endo- and exoglycosidases, proteases, and phosphatases. In addition, we evaluated the effect on the metabolism of *Brassica napus* plants after seed coating. We found significant differences, especially in the contents of tryptamine, auxin, and other phytohormones, and free amino acids.

2. Materials and Methods

2.1. Isolation and Selection of Pythium Isolates

Approximately 20 g of soil sample was mixed thoroughly with 15 mL of sterilized (121 °C; 30 min) 15 g L^{-1} tap water agar (TWA) [9]. Then, it was poured into a Petri dish and left to solidify. After that, the surface of the Petri dish was covered with pure TWA, incubated in the dark at 24 °C, and observed daily.

After 5 days of incubation, the Petri dish with the soil sample was microscopically observed. In the case of ornamental oogonia detection, a small plug of agar medium with the oogonia was transferred to a Petri dish with TWA, followed by 24-h incubation at an elevated temperature (36–37 °C). After the incubation, a small plug of TWA with one separated growing hypha was transferred, using a sterile preparation needle and microscope, to a Petri dish with TWA and incubated for 24 h at 24 °C. After this last incubation period, a small plug of TWA with one separated hypha was transferred with a sterile needle to a Petri dish with malt extract agar (MEA, Merck, Darmstadt,

Germany). After 7 days of incubation at 24 °C, the plugs of MEA with growing oomycete biomass were stored in paraffinic oil at 10 °C.

Only the strains with in vitro mycoparasitic abilities were selected for further study. The competition tests were conducted in triplicates on 9 cm diameter Petri dishes with MEA medium (25 °C, dark) using plant pathogenic fungi *Alternaria alternata*, *A. brassicicola*, *Verticillium albo-atrum*, and *Phoma lingam*. First, the plant pathogens were inoculated on one side of the plate and allowed to grow for 2–5 days, producing colonies 20–25 mm in size. Thereafter, the agar block with particular *Pythium* strain was placed onto the opposite side of the Petri dish, and the continuation of the growth of the tested mold and *Pythium* were evaluated every 2 days until 10 days. The ability of individual strain to parasitize the pathogens was assessed on the basis of visible overgrowth of the pathogen colony by *Pythium* hyphae, cessation of pathogen hyphae growth and loss or inability of the pathogen colony to change pigmentation compared to control growth without *Pythium* sp. Another characteristic feature of parasitism, which was evaluated using an optical microscope, was the ability of *Pythium sp.* hyphae to encircle the pathogen hyphae at sites of early contact between the two colonies.

2.2. Cultivation of Pythium Isolates

Eleven strains exhibiting spiny spores, a typical feature of *P. oligandrum*, and mycoparasitism ability were selected for the study. The composition of cultivation medium was 1000 g millet grain mixed with 500 mL of 2% (*w*/*v*) sucrose solution containing 30 μM cholesterol as a source of sterols. A quantity of 30 g of the solid cultivation medium was placed in a 250-mL Erlenmeyer flask, sterilized, inoculated by 5 small plugs of *Pythium* isolates, and incubated at 24 °C for 7 days. After the cultivation period, the biomass of growing mycelium and remnants of cultivation media were diluted 1:5 with sterile deionized water and centrifuged (8000× *g*, 15 min). The upper phase was used for the determination of secreted compounds. The biomass of *Pythium* was freeze-dried. The number of oospores was determined after lyophilization, and the inoculum concentration for further use (seed coating) was set to 12.0×10^6 oospores.g^{-1} using sterile carrier silicon dioxide powder. Control (negative control) represents a sterile, non-inoculated cultivation medium cultivated under the same conditions. The M1 strain of *P. oligandrum* was provided by the company Biopreparáty, Ltd. (Únětice, Czech Republic) and corresponds to strain ATCC 38472. This oomycete was isolated from sugar beet [10].

2.3. Identification of Pythium Isolates

Partial sequences of cytochrome c oxidase subunit I (COI), which is recommended as the main marker for oomycete identification [11,12], were studied in all strains. In addition, internal transcribed spacer (ITS) rDNA, another recommended barcode [12], was sequenced in the strains representing unique COI haplotypes. Genomic DNA was extracted using a DNeasy UltraClean Microbial Kit (Qiagen, Germantown, MD, USA). The ITS region was amplified with the primers ITS4 and ITS5 [13]. The COI gene was amplified with the primers Fm85mod and OomCoxI-Levup [12]. Amplification conditions were set as in [14]. The PCR products were purified and sequenced in Macrogen, Europe. The dataset for the phylogenetic analyses was assembled using reference sequences generated by [12,14] and supplemented with best Blast hits from NCBI GenBank. The other two *P. oligandrum* sequences were extracted from the whole genomic data of ATCC 38472 [15] and Po37 [16]. Sequence alignments was performed in MAFFT 6 using the G-INS-i strategy [17]. Maximum Likelihood phylogenetic analyses were done in PhyML 3.1. [18] using 500 bootstrap replicates and default settings. The COI gene alignment had 28 sequences and 680 characters, of which 91 were variable and 46 were parsimony informative. The ITS alignment had 29 sequences and 755 positions, of which 24 were variable and 12 parsimony informative. Barcode sequences were deposited in the EMBL sequence database (Table 1).

Table 1. Summary of *Pythium* spp. and their identification parameters (internal transcribed spacer (ITS) rDNA and cytochrome c oxidase subunit I (COI)).

Identity	Strain	Accession No.	
		ITS rDNA	COI
P. oligandrum	00X5	*LR760206*	*LR760205*
P. oligandrum	00X11	*MT249384*	*LR760204*
P. oligandrum	00X23		*LR760202*
P. oligandrum	00X30		*LR760200*
P. oligandrum	00X34		*LR760199*
P. oligandrum	00X40	*LR760209*	*LR760201*
P. oligandrum	00X42	*LR760210*	*LR760197*
P. oligandrum	00X48	*LR760208*	*LR760198*
P. oligandrum	X40	*LR760207*	*LR760196*
Pythium sp.	X42	*LR760211*	*LR760203*

2.4. Plant Material

Brassica napus (rapeseed) seeds were treated with lyophilized *Pythium* spp. inoculum (oomycete biomass with medium inoculum) containing 12.0 × 10^6 oospores.g^{-1}. The inoculation of seeds was performed in a rotating seed machine at the concentration of 5 g of the inoculum on 1 kg of seeds. The mixture was moistened with deionized water and exposed to continuous rotation for 5 min. Then, it was left to dry and stored at room temperature.

Brassica napus treated and nontreated seeds were sown in pots with soil and grown for three weeks in growth chambers under 16/8 h light/dark period, ca. 150 µmol (photon) m^{-2} s^{-1} irradiance, at 20 °C, and 60% relative humidity. The samples of all mixed leaves from each group were immediately frozen in liquid N_2 and kept at −80 °C.

Frozen leaf samples (0.5 g) were ground in liquid N_2 with 1% polyvinylpyrrolidone. Then, 0.5 mL of extraction buffer (0.1 M Tris–HCl, pH 7.8, 1 mM EDTA, 10 mM DTT, 5 mM $MgCl_2$; except for glycosidases and proteases—100 mM MOPS-NaOH, pH 5) was added to the ground tissue. The homogenate was centrifuged at 13,000× *g* for 10 min, and the resulting supernatant was used for measurements.

2.5. Protein Content

Protein measurements of all samples were performed spectrophotometrically at 595 nm using Protein Assay solution (Bio-Rad, Hercules, CA, USA) with bovine serum albumin as a standard [19].

2.6. Electrophoretic Separation

Tricine-SDS-electrophoresis was performed to detect small molecules (such as oligandrins) secreted into the medium [20]. The gels consisted of 4% focusing and 16% separating layers. Medium samples were dissolved 1:1 in reducing sample buffer (6% (*w*/*v*) SDS; 3% (*v*/*v*) mercaptoethanol; 15% (*w*/*v*) glycerol; 0.025% (*w*/*v*) Coomassie Blue G-250; 150 mM Tris-HCl, pH 7.0). The proteins contained in the medium were separated by an SDS-PAGE run in 4% focusing and 15% separating gels [21].

2.7. Free Amino Acids and Tryptamine Content

Free proteinogenic amino acids and tryptamine were determined by capillary electrophoresis [22]. All electrophoretic experiments were conducted in a fused-silica capillary (Polymicro Technologies, Phoenix, AZ, USA) using a G7100A Capillary Electrophoresis Instrument (Agilent Technologies, Waldbronn, Germany) with a contactless conductivity detector. The detector consisted of two 4-mm-long cylindrical electrodes, with a 1-mm insulation gap. The inner diameter of the electrodes was 400 µm. The detection limits of all amino acids were in the range of 6 µg g^{-1} to 33 µg g^{-1}. The limit of detection was calculated as 3-fold the standard deviation of the noise.

2.8. Phenolics and Antioxidant Capacity

The total phenolic content was determined using the standard Folin-Ciocâlteu colorimetric method [23,24]. Free Radical Scavenging, with the 2,2-diphenyl-1-picrylhydrazyl (DPPH) radical, and the Ferric Reducing Antioxidant Potential (FRAP) assays were used to determine the antioxidant capacity [23,24].

2.9. Phytohormone Analysis

In rapeseed leaves, indole-3-acetic acid (IAA), IAA-aspartate (IAA-Asp), indole-3-acetamide (IAM,), indole-3-acetonitrile (IAN), oxo-IAA (OxIAA), oxo-IAA-glucose ester (OxIAA-GE), phenylacetic acid (PAA), salicylic acid (SA), jasmonic acid (JA), JA-isoleucine (JA-Ile), and cytokinins (CKs) were determined. Frozen samples (ca. 50 mg fresh weight (FW)) were homogenized and extracted with cold (−20 °C) methanol/water/formic acid (15/4/1, *v*/*v*/*v*), as described previously [25–27]. The following isotope-labeled internal standards (10 pmol/sample) were added: $^{13}C_6$-IAA (Cambridge Isotope Laboratories); 2H4-SA (Sigma-Aldrich); $^{2}H_3$-PA, $^{2}H_3$-DPA (NRC-PBI); ^{2}H6-ABA, $^{2}H_5$-JA, $^{2}H_5$-transZ, $^{2}H_5$-transZR, $^{2}H_5$-transZ7G, $^{2}H_5$-transZ9G, $^{2}H_5$-transZOG, $^{2}H_5$-transZROG, $^{2}H_5$-transZRMP, $^{2}H_3$-DZ, $^{2}H_3$-DZR, $^{2}H_3$-DZ9G, $^{2}H_6$-iP, $^{2}H_6$-iPR, $^{2}H_6$-iP7G, $^{2}H_6$-iP9G, ^{2}H6-iPRMP (Olchemim). Phytohormones were separated with a reverse-phase cation exchange SPE column (Oasis-MCX, Waters) into the acid fraction by elution with methanol (auxins, ABA, SA, JA), and into the basic fraction by elution with 0.35 M NH_4OH in 60% methanol (CKs and aminocyclopropane-1-carboxylic acid (ACC)). Fractions were analyzed using HPLC (Ultimate 3000, Dionex, Sunnyvale, CA, USA) coupled to a 3200 Q TRAP hybrid triple quadrupole/linear ion trap mass spectrometer (Applied Biosystems, Waltham, MA, USA). Hormone quantification was performed using the isotope dilution method with multilevel calibration curves ($r^2 > 0.99$). Data processing was performed with the Analyst 1.5 software package (Applied Biosystems).

2.10. Extraction and Separation of Glucosinolates

Glucosinolates were extracted from 100 mg of lyophilized leaves ground in 1500 µL methanol/water (70/30, *v*/*v*). Then, the sample was shaken for 10 min (Vibramax 100 vibration platform shaker, Heidolph, Schwabach, Germany) and sonicated for 10 min (Elmasonic S 15, Elma, Germany). After centrifugation (10 min at 9000 rpm), 1200 µL of supernatant was evaporated and dissolved in 200 µL of background electrolyte (100 mM sodium tetraborate dissolved in water) and filtered through a 0.45-µm PVDF filter [28]. Again, the sample was shaken for 10 min and sonicated for 10 min. After centrifugation, 30 µL of supernatant was mixed with 5 µL of 1.8 mM sorbic acid as an internal standard.

Electrophoretic experiments were performed on an Agilent 7100 CE system (Agilent Technologies, Waldbronn, Germany) equipped with a UV/VIS detector. An unmodified fused-silica capillary of 50 µm ID and 375 µm OD (Polymicro Technologies, Phoenix, AZ, USA) was cut to 70.0 cm total length (effective length of 61.5 cm). Before the first measurement of the day, the capillary was flushed for 10 min with 1M NaOH and 10 min with deionized water. Between individual runs, the capillary was flushed with 1M NaOH for 2 min, and with background electrolyte for 2 min as well. Samples were injected using 5 kPa pressure for 5 s. Voltage of 20 kV (current approx. 76 µA) was applied during the 45-min analysis, and absorbance was detected at λ = 225 nm. The capillary temperature was 25 °C. The detection limits of glucosinolates were from 1 µg g^{-1} to 2 µg g^{-1}. The limit of detection was calculated as 3-fold the standard deviation of the noise.

2.11. Enzyme Activities

Generally, enzyme activities were determined spectrophotometrically (Helios α, Thermo-Spectronics, Waltham, MA, USA) and expressed as activity in µmol of the respective product formed (substrate decreased) per min per mL of growth medium or per g of fresh plant weight (FW).

Catalase (CAT, EC 1.11.1.6) was detected at 240 nm as a H_2O_2 decomposition rate. Total ascorbate peroxidase (APOD, EC1.11.1.11) activity was determined as a decrease in the absorbance of ascorbate

at 298 nm. Malic enzyme (NADP-ME, EC 1.1.1.40), glucose-6-phosphate dehydrogenase (EC 1.1.1.49), shikimate dehydrogenase (EC 1.1.1.25), and glutathione reductase (GR, EC 1.8.1.7) activities were assayed as NADPH production at 340 nm [29,30].

Proteolytic activity was determined using azocasein substrate or Nα-benzoyl-DL-arginine 4-nitroanilide [31,32]. Endo-β-1,3-glucanase (EC 3.2.1.6), cellulase (EC 3.2.1.4), and chitinase (EC 3.2.1.14) activities were determined based on the quantification of reducing sugars (products) with 3-methyl-2-benzothiazolinone hydrazone [33].

α-Glucosidase (EC 3.2.1.20), β-glucosidase (EC 3.2.1.21), α-galactosidase (EC 3.2.1.22), β-galactosidase (EC 3.2.1.23), α-mannosidase (EC 3.2.1.24), and β-N-acetylhexosaminidase (EC 3.2.1.52) activities were determined using the end-point method with specific synthetic *p*-nitrophenyl (*p*-NP-) substrates (*p*-NP-α,D-glucopyranoside, *p*-NP-β,D-glucopyranoside, *p*-NP-α,D-galactopyranoside, *p*-NP-β,D-galactopyranoside, *p*-NP-α,D-mannopyranoside, and *p*-NP-N-acetyl-β-D-glucosaminide, respectively). The reaction mixture contained a 50 mM citrate buffer, pH 4.5, 0.5 mM *p*-NP-substrate, and 10 µL of enzyme extract in total 40 µL volume. The reaction was stopped with 80 µL of 0.25 M borate buffer, pH 9.0. The hydrolyzed *p*-nitrophenol in the alkali region was quantified by measuring absorbance at 405 nm against a blank in which the enzyme was previously inactivated by the high pH of the borate buffer. Acid (EC 3.1.3.2) and alkaline phosphatase (EC 3.1.3.1) activities were determined with *p*-NP-phosphate at pH 5.5 and 9.0, respectively, modified from [34].

Superoxide dismutase (SOD, EC 1.15.1.1) isozyme patterns and activities were assessed after separation by 10% native PAGE [35,36].

Peroxidase (POD, EC 1.11.1.7) isozyme pattern was assessed after separation by 10% native PAGE. POD isozymes were detected in situ by staining gels in 1 M acetate buffer, pH 4.6, with 0.04% benzidine and 10 mM H_2O_2 [37].

Shikimate dehydrogenase (SDH, EC 1.1.1.25) isoenzyme pattern was detected after separation by 10% native PAGE by staining in 3 mM shikimate, 0.2 mM $NADP^+$, 0.1 mg mL^{-1} nitroblue tetrazolium, and 5 µg mL^{-1} phenazine methosulfate.

2.12. Carbon, Nitrogen, and Sulfur Content Analysis

The lyophilized samples of leaves were used for elementary analysis of C, H, N, and S, which was performed on a Thermo Finningan Flash FA 1112 series CHNS/O analyzer.

2.13. Statistical Analysis

All measurements were performed at least in triplicate. Each plant experimental group consisted of three biological samples. Each sample represented mixed leaves of 30 plants. Three biological replications (i.e., independently cultured strains) were studied for each strain. Data were analyzed by one-way ANOVA (Bonferroni method) and *t*-test; differences were considered significant at $p \leq 0.05$. The different letters in figures and tables denote significant differences ($p \leq 0.05$).

3. Results and Discussion

3.1. Identification of Tested Pythium spp. Revealed not yet Described Pythium Species

In response to demands from many regulatory authorities and professional agricultural institutes, scientists have intensified the search for new and more effective biological control agents, which requires characterizing not only the specific organisms but also their effects on plant metabolism. As *Pythium oligandrum* is well-known for its beneficial features, we searched for other *Pythium* oomycetes with high potential for use as BCAs. For this purpose, we collected soil samples from different areas to identify new suitable organisms with unique properties (Table 1, Figure 1). We selected the strains that after cultivation showed ornamental oogonia and also behaved as mycoparasites. The mycoparasitism tests of the M1 strain as an example are shown in the Supplementary Materials (Figures S1–S4). Then, we characterized unknown *Pythium* strains by COI and ITS rDNA barcode genes.

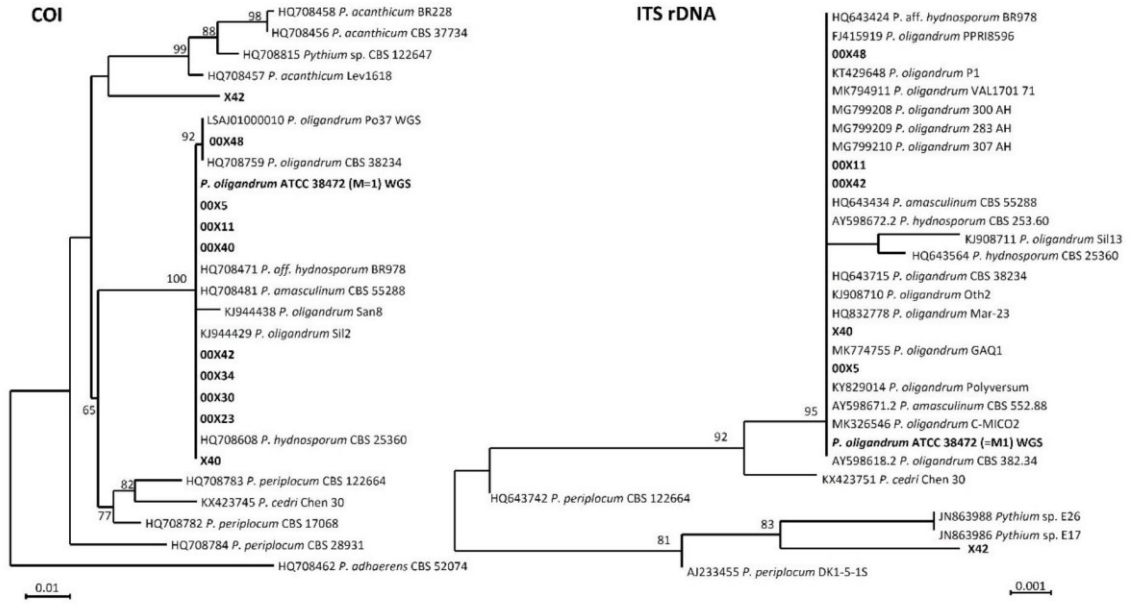


Figure 1. Maximum likelihood (ML) tree of *Pythium* spp. based on COI (left) and ITS rDNA (right) barcode genes. The bootstrap values are indicated at the nodes. The strains used in this study are printed in bold. The tree was rooted with *P. adherens* HQ708462 and *P. periplocum* AJ233455, respectively. Each code (00X5, 00X11, 00X23, 00X30, 00X34, 00X42, 00X48, X40, X42, and M1) represents a *Pythium* strain.

Based on the COI gene, we determined that our study strains belonged to three unique haplotypes: (1) X42, (2) 00X48, and (3) others. Phylogenetically, the two latter haplotypes belonged to the well-supported clade consisting of sequences deposited as *P. amasculinum* (HQ708481, [12]); *Pythium* aff. *hydnosporum* (HQ708471, [12]); *Pythium hydnosporum* (HQ708608, [12]); and *P. oligandrum* (HQ708759, [12]; KJ944429, [14]) (genomic data from strains Po37 and ATCC 38,472 = M1) (Figure 1). The sequence of strain X42 showed a separate position, with the closest affinity to sequences deposited as *Pythium acanthicum.* Based on the ITS, all but one (X42) of the strains belonged to a single haplotype. The main haplotype belonged phylogenetically to the well-supported clade of *P. oligandrum*, *P. hydnosporum*, and *P. amasculinum*, whereas strain X42 showed a separate position with the closest affinity to *Pythium* sp. E26 JN863988 (97.50% sequence similarity).

Most of our isolates fit into the *P. oligandrum* clade consisting of *P. oligandrum*, *P. hydnosporum*, and *P. amasculinum* sequences. All three species have spiny oogonia and are morphologically related. For these reasons, *P. oligandrum* has been often misidentified as *P. hydnosporum. P. amasculinum* is considered a likely synonym of *P. oligandrum* [38].

There is a general consensus that the species inside this clade cannot be recognized based on the widely used barcode genes ITS and COI and should be formally synonymized pending more thorough investigations with multiple hypervariable genes [11,12,14]. Our strains morphologically fit into *P. oligandrum*, and accordingly we are designating them using this name. The strain of X42 has a separate position, sister to the *P. oligandrum* clade and *P. acanthium*. This strain is not ascribable to any sequenced species of *Pythium*. Morphologically, it is an ornamented oogonia, like *P. oligandrum*.

3.2. Secretomes Contained Proteins, Amino Acids, and Phenolic Compounds

The main goal of this study was to find out the biochemical background of the *Pythium* spp. life strategies, i.e., mycoparasitism and/or promoting plant growth. The oomycetes depend on their hosts in acquiring β-hydroxy sterols for sporulation [6] and thus produce extracellular protein elicitors (oligandrin and cell wall protein fractions) such as sterol carriers. A side effect of these elicitors is plant priming and activation of plant defense responses, which is advantageous during interaction

with real pathogens [1]. In addition, *Pythium* spp. as mycoparasites secrete a large arsenal of effector proteins that allows the penetration of the host cell wall [39] (Figures 2–5). Although the composition of the medium was identical among all studied *Pythium* strains, the contents of proteins, amino acids, and phenolic compounds in secretomes varied considerably (Figure 2). All *Pythium* strains secreted proteins into the medium; the highest content was in M1 and the lowest in 00X40 (Figure 2a). Differences were also found in the proportion of individual proteins analyzed by SDS-electrophoresis (Figure 3). Most proteins were of a molecular weight lower than 30 kDa, but proteins were also detected in the regions around 85 kDa and 55 kDa. Strains 00X40 and X40, and strains 00X23 and 00X42 showed similar protein profiles. However, the protein profile of X42 was quite unique; the relative molecular weights of its most abundant proteins differed from those of other strains analyzed in this study. By Tricine electrophoresis, suitable for separating small proteins and peptides, we identified molecules of approximately 10 kDa, which could correspond to oligandrins. In addition to oligandrins, X42 medium contained several peptides (<6.5 kDa), which could be either elicitors or degradation products (Figure 3).

One of the significant properties of *P. oligandrum*, which is responsible for plant growth promotion, is the production of tryptamine, the precursor of the phytohormone auxin. Thus, we determined the concentrations of tryptophan and tryptamine in the medium (Table 2, Figure 2b). Although we found low tryptamine concentrations and no free tryptophan in the control medium (without *Pythium*), after *Pythium* cultivation, tryptophan was present and tryptamine concentrations were significantly elevated, especially in X42 (5.5 times more than M1). The lowest tryptamine concentration was found in 00X23 medium, whose value was only 6% of that in X42 (Table 2, Figure 2b). Considering the amount of tryptophan and tryptamine provided in their secretomes, strains X42, 00X42, and 00X11 appear to have good predispositions to increase plant growth and fitness (Table 2, Figure 2b).

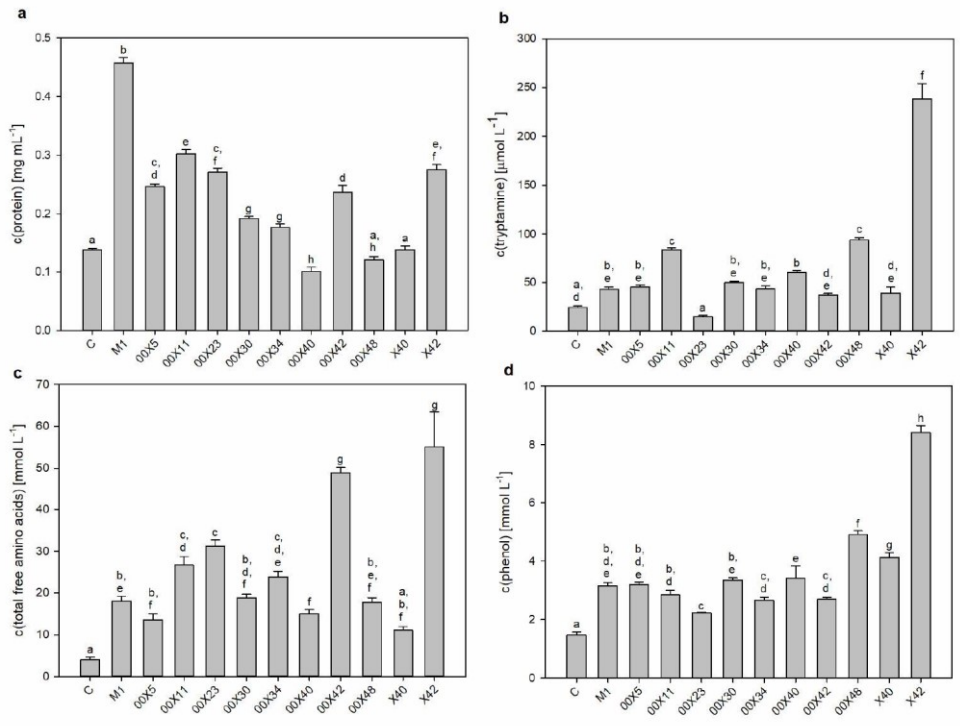


Figure 2. Characterization of compounds secreted into the medium by *Pythium* strains: protein content (**a**), tryptamine content (**b**), total free amino acids (**c**), total phenolics (**d**). Each code (00X5, 00X11, 00X23, 00X30, 00X34, 00X40, 00X42, 00X48, X40, X42, and M1) represents a *Pythium* strain. Control (C) is a sterile, non-inoculated cultivation medium. The different letters above each bar denote significant differences ($p \leq 0.05$) between groups according to one-way ANOVA (Bonferroni method).

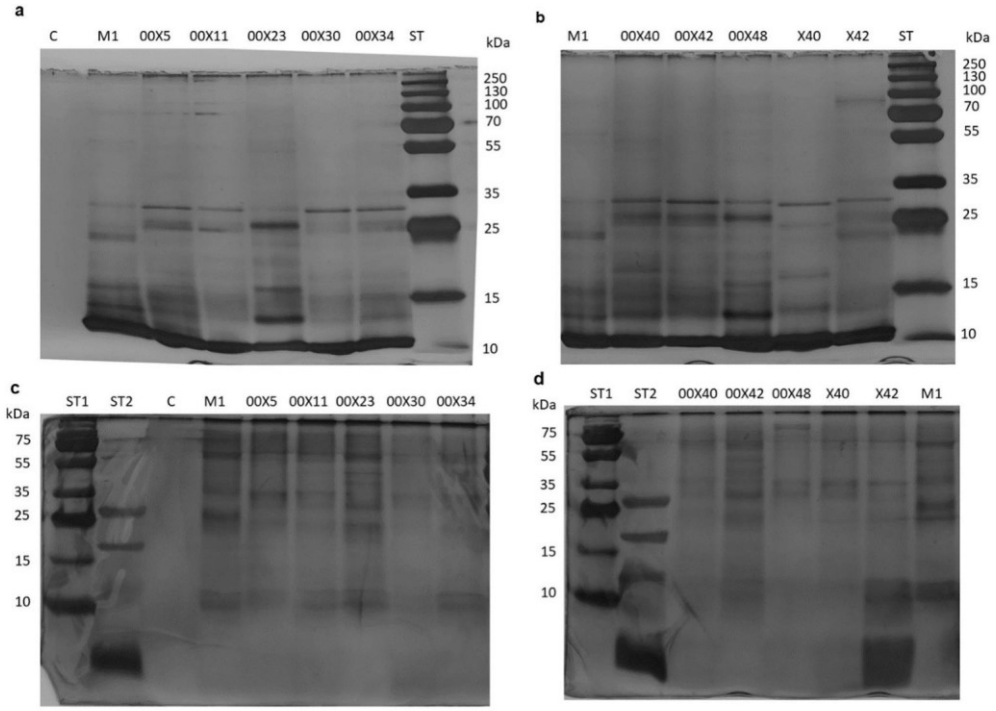


Figure 3. Electrophoretic separation of proteins secreted into the medium by *Pythium* strains. The proteins were separated by 15% SDS-PAGE (**a**,**b**) and 16% Tricine-SDS-PAGE (**c**,**d**). ST1-Thermo Scientific PageRuler Plus Prestained Protein Ladder (kDa): 250; 130; 100; 70; 55; 35; 25; 15; 10. ST2-Polypeptide SDS-PAGE Bio-Rad (kDa): 26.6; 17; 14.4; 6.5; 3.5; 1.4. Each code (00X5, 00X11, 00X23, 00X30, 00X34, 00X40, 00X42, 00X48, X42, and M1) represents rapeseed plants treated with a *Pythium* strain. Control (C) was prepared as untreated rapeseed plants.

Table 2. The free amino acid content in the medium. <LOD, under the limit of detection. Each code (00X5, 00X11, 00X23, 00X30, 00X34, 00X40, 00X42, 00X48, X40, X42, and M1) represents a *Pythium* strain. Control (C) is a sterile, non-inoculated cultivation medium.

	C [µmol.L^{-1}]											
	C	**M1**	**00X5**	**00X11**	**00X23**	**00X30**	**00X34**	**00X40**	**00X42**	**00X48**	**X40**	**X42**
Ala	993 ± 70	2578 ± 134	1523 ± 120	3055 ± 199	7391 ± 198	1951 ± 52	2984 ± 61	1625 ± 32	9734 ± 6	1832 ± 37	1130 ± 45	8088 ± 1769
Arg	32 ± 8	975 ± 50	1274 ± 42	1507 ± 66	457 ± 25	1272 ± 21	1036 ± 41	820 ± 8	908 ± 59	2039 ± 89	1057 ± 83	1088 ± 89
Asn	345 ± 39	685 ± 97	482 ± 109	1167 ± 80	784 ± 14	812 ± 43	1056 ± 65	794 ± 19	1171 ± 54	623 ± 92	442 ± 28	1462 ± 183
Asp	<LOD	426 ± 33	181 ± 50	1077 ± 219	709 ± 157	353 ± 130	854 ± 85	455 ± 98	2027 ± 67	295 ± 113	225 ± 131	2552 ± 120
Cys	<LOD	<LOD	<LOD	<LOD	<LOD	<LOD	<LOD	<LOD	<LOD	<LOD	<LOD	<LOD
Gln	<LOD	1207 ± 24	771 ± 12	2555 ± 241	2486 ± 65	1488 ± 116	2410 ± 102	2169 ± 115	3609 ± 94	777 ± 36	797 ± 47	4169 ± 630
Glu	63 ± 31	1731 ± 59	1208 ± 112	2737 ± 132	3332 ± 90	1934 ± 7	2806 ± 87	1415 ± 79	7537 ± 106	1106 ± 30	991 ± 30	8597 ± 937
Gly	276 ± 31	1223 ± 60	476 ± 69	1638 ± 137	2445 ± 107	861 ± 69	1726 ± 28	806 ± 17	4364 ± 181	778 ± 43	417 ± 83	4338 ± 927
His	1 ± 0	251 ± 13	204 ± 35	383 ± 37	128 ± 8	249 ± 1	337 ± 23	199 ± 27	351 ± 8	250 ± 46	163 ± 14	360 ± 111
Ile	106 ± 64	650 ± 71	471 ± 81	1038 ± 48	705 ± 45	645 ± 15	901 ± 87	517 ± 19	1365 ± 70	533 ± 47	371 ± 12	1662 ± 147
Leu	659 ± 43	1237 ± 12	1068 ± 161	1895 ± 67	1367 ± 109	1311 ± 52	1602 ± 87	1014 ± 132	2513 ± 66	1193 ± 92	811 ± 121	3099 ± 514
Lys	26 ± 7	900 ± 113	750 ± 26	1327 ± 32	779 ± 53	935 ± 20	1096 ± 17	679 ± 11	1408 ± 55	896 ± 27	546 ± 19	1669 ± 100
Met	134 ± 28	352 ± 10	323 ± 45	498 ± 147	313 ± 47	386 ± 31	331 ± 84	256 ± 27	640 ± 55	316 ± 29	251 ± 14	737 ± 129
Phe	138 ± 67	521 ± 47	374 ± 84	904 ± 182	476 ± 127	534 ± 43	748 ± 69	460 ± 116	910 ± 82	510 ± 38	354 ± 19	1441 ± 240
Pro	573 ± 146	2030 ± 155	2080 ± 292	1970 ± 163	4881 ± 89	2866 ± 115	1494 ± 105	1199 ± 102	3888 ± 108	3829 ± 138	1677 ± 89	6118 ± 983
Ser	228 ± 45	879 ± 22	558 ± 99	1331 ± 67	1865 ± 102	809 ± 44	1249 ± 78	734 ± 79	2859 ± 77	715 ± 133	470 ± 12	3113 ± 393
Thr	170 ± 42	846 ± 0	520 ± 63	1211 ± 102	1358 ± 47	793 ± 35	1116 ± 125	633 ± 28	2068 ± 42	712 ± 43	420 ± 22	2417 ± 452
Trp	<LOD	122 ± 12	50 ± 15	141 ± 56	87 ± 56	89 ± 17	127 ± 24	81 ± 14	266 ± 46	82 ± 21	60 ± 20	250 ± 61
Tyr	<LOD	419 ± 65	378 ± 78	676 ± 26	339 ± 26	440 ± 34	555 ± 58	351 ± 55	842 ± 32	376 ± 31	277 ± 32	1118 ± 238
Val	302 ± 31	1058 ± 158	821 ± 35	1623 ± 47	1353 ± 88	1095 ± 11	1443 ± 102	784 ± 113	2461 ± 71	884 ± 41	656 ± 41	2806 ± 347

Due to differences in tryptophan content, we also determined other free amino acids and total amino acids (Table 2, Figure 2c). In the control medium, tyrosine, glutamine, and aspartate were absent, whereas histidine, lysine, and arginine were found in very low concentrations (Table 2). Key amino acids that could affect plant metabolism (tryptophan, methionine, phenylalanine, and partly tyrosine) were most abundant in secretomes of *Pythium* spp. X42, 00X42, and 00X11 (Table 2). The only absent amino acid in all media was cysteine, which has a reactive thiol group and therefore is likely bound in other compounds such as glutathione. The concentration of all free amino acids increased in the medium after *Pythium* cultivation; in X42, the increase was 14 times in comparison with the control (Figure 2c). Although the specific secondary metabolites that *Pythium* spp. produce remain somewhat unclear, we tested for the presence of phenolic compounds (Figure 2d). The highest value was determined in strain X42, 2.7 times exceeding M1. The presence of phenylpropanoid compounds is unlikely because we did not find the initial enzyme catalyzing the conversion of phenylalanine to cinnamic acid, phenylalanine ammonium lyase, in the published genome of the *P. oligandrum* strain ATTC 38,472 [15]. However, the synthesis of isoprenoids is probable because in the abovementioned genome, we found genes for enzymes capable of synthesizing mevalonate, isopenthenyldiphosphate, geranyldiphosphate, farnesyldiphosphate, and geranylgeranyldiphosphate from an acetyl-CoA precursor. This is in agreement with other oomycetes [40].

3.3. Pythium Secretes a Cocktail of Host Cell Wall-Degrading Enzymes

Hydrolytic enzymes facilitate cell wall penetration for host colonization. These enzymes include cutinases, glycosidases, pectinases, and proteases. A "cocktail" of different hydrolytic enzymes with overlapping substrate specificities apparently enables the formation of proper infection structures [41]. Most information about these enzymes in oomycetes derives from genomic analysis of *Pythium* spp. [15,39]. The glycoside hydrolases and proteases were represented in high numbers. Among oomycete effector proteins, glycoside hydrolases belong to the most abundantly secreted proteins (79 for *P. oligandrum*). Based on sequence analysis, glycoside hydrolases can be assigned to families [39], but their true substrate specificity and activity cannot be ascertained. This is the first study providing a comprehensive survey of enzyme activities of plant and fungal cell wall-degrading enzymes across the variety of *Pythium* strains. We showed that there is a high difference in the quantity and quality of the presented enzymes, even across strains of the same species (Figures 4 and 5), and proper strain selection is crucial in searching for BCAs.

In comparison with M1, higher activities of 12ellulose (3–4-fold), chitinase (3-fold), and endo-β-1,3-glucanase (1.5-fold) were found in 00X5, 00X30, 00X48, and X40 media (Figure 4a).

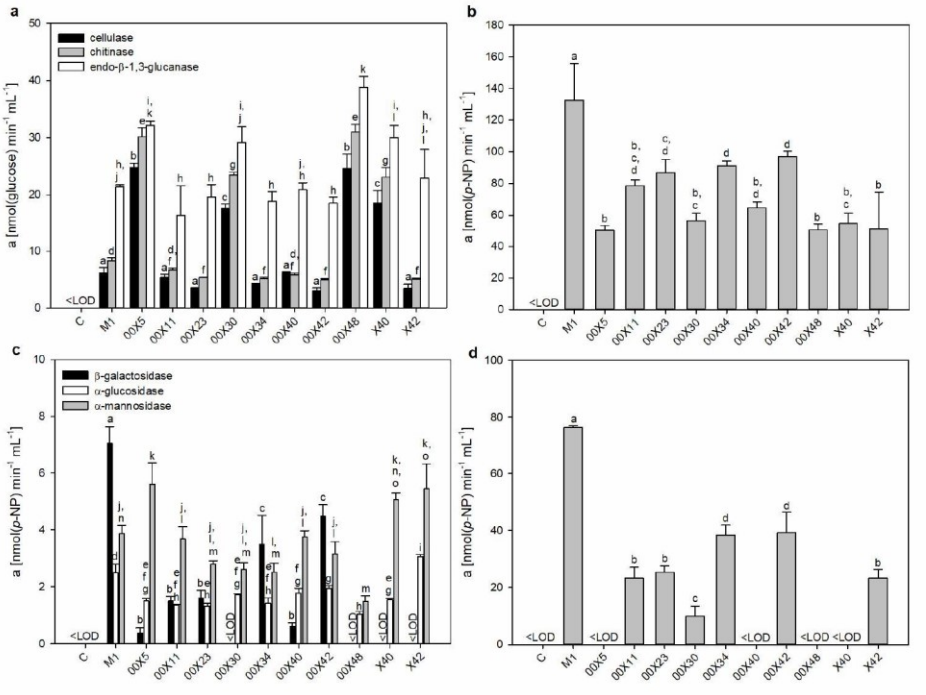


Figure 4. Activities of endo- and exoglycosidases secreted into the medium by *Pythium* strains. Cellulase, chitinase, and endo-β-1,3-glucanase activities (**a**); β-glucosidase activity (**b**); β-galactosidase, α-glucosidase, and α-mannosidase activities (**c**); β-galactosidase activity in alkaline pH 9.0 (**d**). Each code (00X5, 00X11, 00X23, 00X30, 00X34, 00X40, 00X42, 00X48, X40, X42, and M1) represents a *Pythium* strain. Control (C) is a sterile, non-inoculated cultivation medium. The different letters above each bar denote significant differences ($p \leq 0.05$) between groups according to one-way ANOVA (Bonferroni method).

In addition to endoglycosidases, exoglycosidases also complete the degradation of glycoconjugates. Thus, we measured the activity of α-glucosidase, β-glucosidase, β-galactosidase, α-mannosidase (Figure 4), α-galactosidase, and β-hexosaminidase. β-Glucosidase degrading β-oligoglucans into glucose monomers, used as a source of energy, showed the highest activity, especially in M1 (Figure 4b). The other strains' media reached only 40–70% of M1 activity. α-Glucosidase activity was approx. 45 times lower than β-glucosidase activity, as expected because substrates such as α-glucans are a much less commonly found source in the natural environment. α-Mannosidase may degrade mannan structures, glycoproteins, or glycolipids in host cell walls or membranes. The activity of α-mannosidase in 00X5 and X42 media exceeded M1 by 40–45%; and X40 by 30%. (Figure 4c). β-Galactosidase activity at pH 4.5 was found only in some *Pythium* spp. (Figure 4c). Interestingly, even though exoglycosidases generally have an acidic optimum pH, β-galactosidase showed activity when measured under alkaline reaction conditions; the highest activity at pH 4.5 was found in M1, with no activity in 00X30, 00X48, X40, or X42 (Figure 4c). This enzyme may have a very broad optimum pH, but the 00X30 and X42 media showed activity only under alkaline conditions, reaching only 10% and 30% of M1, respectively. Therefore, we cannot rule out an alkaline β-galactosidase isoform (Figure 4d). Various glycoconjugates containing galactose, hemicelluloses, and pectins in plant cell walls, glycolipids, and glycoproteins could be substrates of this enzyme. No activity of α-galactosidase or β-hexosaminidase was detected, but the activity of these enzymes could be induced by the presence of an appropriate substrate. As far as we know, this is one of the first studies concerning the determination of exoglycosidase activity in *Pythium* spp.

Numerous pathogenic fungi and oomycetes produce saponin-detoxifying glycosidases, which are able to deglycosylate saponin molecules for their detoxification (degradation) [42–44]. Another role of exoglucosidases, namely β-glucosidase, could be the re-activation (deglycosylation) of O-glycosylated cytokinins, thus modulating the phytohormonal levels in planta [45]. Glycosylation is

also the key regulating factor of the phenylpropanoid pathway by changing the solubility, stability, and toxicity of secondary metabolites. A vast array of glycoside hydrolases could help oomycetes to alter host metabolism, especially the level of defense compounds [46].

In addition to glycosidase activity, proteolytic activity is important for the ability of *Pythium* to penetrate the cell wall of the host. Accordingly, total proteolytic activity was assessed using azocasein as a substrate. All *Pythium* strains secreted proteases into the medium, and the highest activity was found for X42, whereas the lowest activity was found for M1. The activity was almost 4 times higher in X42 than in M1 (Figure 5a). In addition to X42, 00X11 strains also showed high activity of serine proteases in the media (both ca. 4-fold higher than M1) (Figure 5b), with significant differences in the proportion of individual classes of proteases in *Pythium* spp.

Phosphatases are enzymes with broad substrate specificities. Both alkaline and acidic phosphatases were present in all *Pythium* spp. media (Figure 5c). Alkaline phosphatase activity was much higher than acidic phosphatase activity. The highest differences between them were found for 00X23 (19-fold) and 00X42 (26-fold). Phosphatases remove phosphate groups from small organic molecules or polymers, which are then used to meet their own needs. This feature could also be useful for increasing nutrient availability for plants when phosphate is released near the roots.

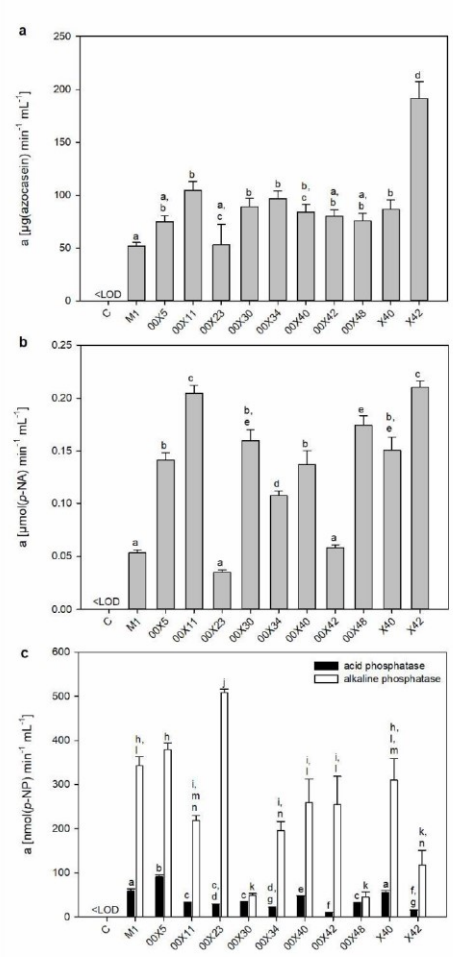


Figure 5. Activities of proteases and phosphatases secreted into the medium by *Pythium* strains. Total proteolytic activity (**a**), serine proteases (**b**), acid and alkaline phosphatases (**c**). Each code (00X5, 00X11, 00X23, 00X30, 00X34, 00X40, 00X42, 00X48, X40, X42, and M1) represents a *Pythium* strain. Control (C) is a sterile, non-inoculated cultivation medium. The different letters above each bar denote significant differences ($p \leq 0.05$) between groups according to one-way ANOVA (Bonferroni method).

3.4. How Do Pythium spp. Affect Metabolism in Inoculated Rapeseed Plants?

The impact of inoculation of *Brassica napus* seeds with ten *Pythium* species on plant metabolism was followed in 3-week-old plants. Seed coating represents an efficient and convenient tool for introducing beneficial microorganisms into the soil and consequently into the rhizosphere or plant tissues [47]. Although most growth parameters were not affected in young plants, many metabolic pathways showed significant changes even within individual isolates. The inoculated plants showed no visible differences when compared to the control samples, or to each other. Similarly, the elementary analysis of dried leaf samples showed no significant differences in the content of carbon, nitrogen, or sulfur between plants treated with *Pythium* spp. and untreated control (Table S2). The carbon-to-nitrogen ratio, which characterizes the nitrogen supply to the plant, is shown in Figure S5. This ratio ranged from 6.2 to 8.2, and these differences were not significant, although the presence of various *Pythium* spp. may affect nitrogen use in plants. The content of photosynthetic pigments was also determined in leaf samples from experimental plants (Figure S6). The content of chlorophyll a was 11% and 28% higher in plants treated with M1 and 00X11 than in the control, respectively. The content of chlorophyll b was also higher in 00X11 and 00X42 than in other experimental groups. This corresponds to the previous assumption of positive influence of these strains on plant fitness.

In leaves, the soluble protein content varied, albeit not significantly (Figure 6a), and no differences in protein profile were detected by SDS-electrophoresis (Figure S7). However, some differences were found in the total amount of free amino acids. Plants inoculated with some *Pythium* strains showed increased total free amino acid content, whereas others showed lower content than the control (Figure 6b). More interestingly, the comparison of individual free amino acids (Figure 7) highlighted that the contribution of the first synthetized amino acid glutamine was equal in all plant groups. Conversely, the levels of some amino acids were decreased in all plant groups, e.g., aromatic amino acids, tryptophan, phenylalanine, and tyrosine. The decrease in tryptophan was particularly significant in plants treated with 00X40, 00X5, and X42 *Pythium* spp. Its concentration was under the detection limit; therefore, the tryptamine content was also measured (Figure 6c). However, tryptamine concentration was also low in plants treated with these strains, most likely because tryptamine was further metabolized to auxin. In turn, the plants inoculated with 00X30, 00X48, and 00X11 strains showed high tryptamine concentration, most likely due to slower conversion to auxin. The presence of tryptamine in control plants also documents its other uses and functions in plant metabolism. Alanine and glycine were among the more abundant free amino acids. The levels of proline, which is often synthetized in plants under stress conditions, were increased in some plant groups and unchanged or decreased in others (Figure 7).

Enhanced secondary metabolite synthesis, especially *via* phenylpropanoid and terpenoid pathways, has well-described effects on plant metabolism caused by *P. oligandrum* [3]. Surprisingly, no significant differences were found in phenolic content, although it was slightly elevated in some groups in comparison with the control (Figure 6d). The method detected only soluble phenolics and not compounds bound to the cell wall, so a significant part of polyphenols could have been incorporated as phenolic acids and especially lignin. Cell wall impregnation by lignin could significantly improve the defense against biotic stress. The soluble phenolic compounds contribute to the total antioxidative capacity; thus, this property was determined in plant extracts using two methods, DPPH (Figure 6e) and FRAP (Figure 6f). Considering the nonsignificant changes in phenolic content described above, the antioxidant capacity unsurprisingly showed no significant differences. Nevertheless, the FRAP method showed 20% enhancement of this value in plants treated with 00X5 and 00X34 strains.

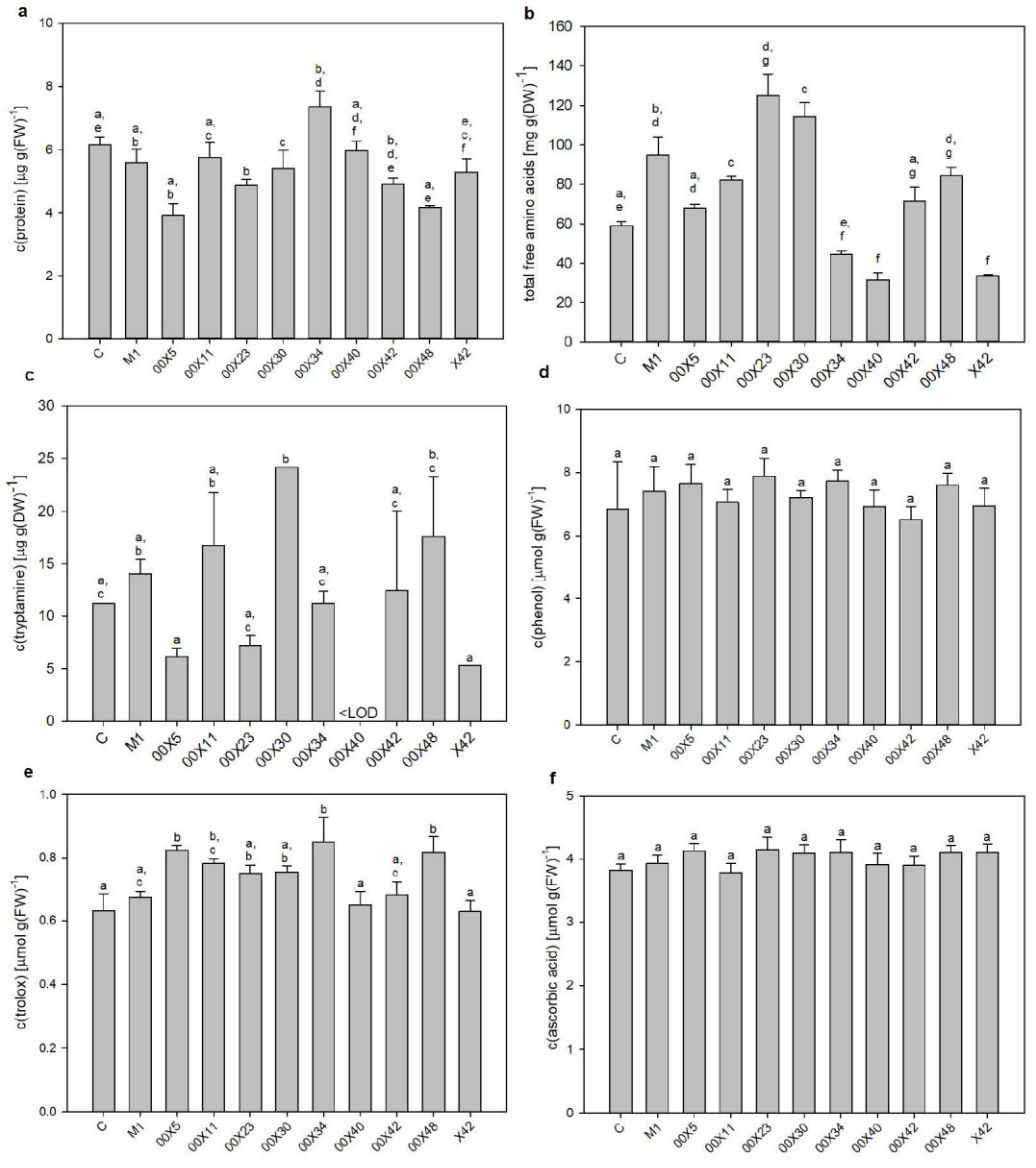


Figure 6. Characterization of the rapeseed leaves. Protein content (**a**), total free amino acids (**b**), tryptamine content (**c**), total phenolics (**d**), antioxidant capacity—2,2-diphenyl-1-picrylhydrazyl (DPPH) method (**e**), antioxidant capacity—Ferric Reducing Antioxidant Potential (FRAP) method (**f**). Each code (00X5, 00X11, 00X23, 00X30, 00X34, 00X40, 00X42, 00X48, X42, and M1) represents rapeseed plants treated with a *Pythium* strain. Control (C) was prepared as untreated rapeseed plants. The different letters above each bar denote significant differences ($p \leq 0.05$) between groups according to one-way ANOVA (Bonferroni method). Abbreviations: DW, dry weight; FW, fresh weight.

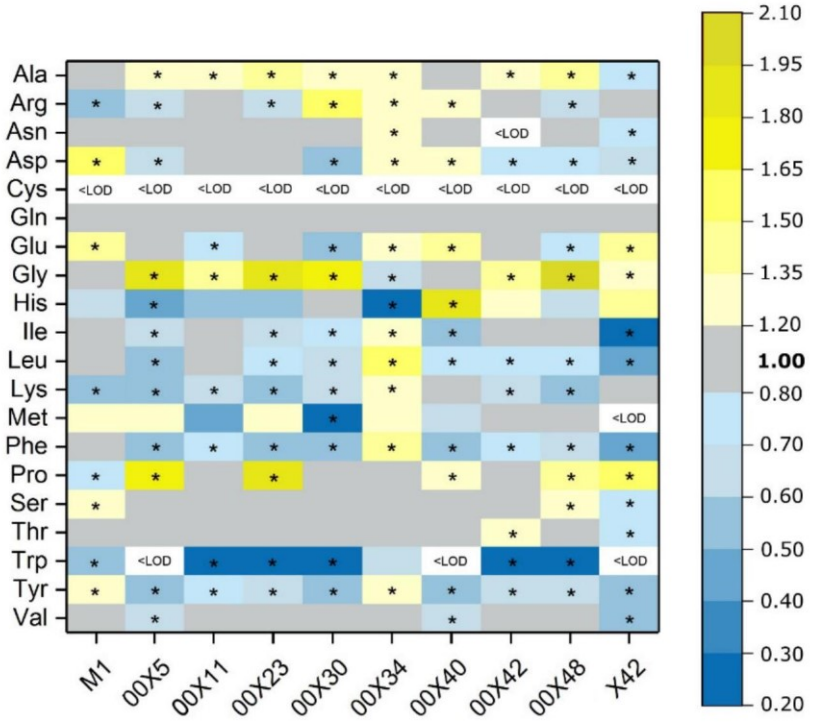


Figure 7. Free amino acid content in the rapeseed leaves. The contents of individual amino acids of all samples are expressed in % of total amount (dry weight) and compared with those of the control (untreated rapeseed plants). Each code (00X5, 00X11, 00X23, 00X30, 00X34, 00X40, 00X42, 00X48, X42, and M1) represents rapeseed plants treated with a *Pythium* strain. Asterisks denote significant differences ($p \leq 0.05$) between sample and control plants according to *t*-test. <LOD, under the limit of detection.

3.5. The Concentration of Phytohormones is Affected by Pythium spp. in the Rapeseed Plants

Plant growth and development as well as interactions with the environment are controlled by phytohormones. Accordingly, *P. oligandrum* may promote plant growth by increasing auxin concentrations. Indole-3-acetic acid (IAA), the most physiologically active auxin, may be synthetized from tryptamine provided by *P. oligandrum* [8]. Therefore, the auxin content of rapeseed plants treated with the *Pythium* strains was analyzed (Figure 8a). Considering the amount of tryptophan and tryptamine provided in their secretomes, the strains X42 and 00X11 appear to have good predispositions to increase plant growth and fitness (Table 2, Figure 2b). Indeed, the highest IAA content was found in plant leaves treated with 00X11, 00X30, X42, and M1 strains. Differences were also found in the contents of indole-3-acetamide (IAM) and indole-3-acetonitrile (IAN), which are precursors of IAA in different plant biosynthetic pathways (Figure 8b). In addition, differences were also found in the content of phenylacetic acid (PAA), a weak, evolutionarily ancient auxin. This compound was also present in higher amounts in some plants (e.g., treated with 00X11 or 00X42) than in the control (Figure 8a). These results suggest that *Pythium* likely affects auxin metabolism by multiple pathways other than just tryptamine delivery. The catabolic products of auxin metabolism were detected in all experimental groups (Figure 8b). Oxo-IAA and its glucosyl ester were the most abundant catabolites. Auxin inactivation is also performed by conjugation with amino acids, but this conjugation only occurred with aspartic acid in rapeseed plants. The highest contents of tryptamine (Figure 2c) and tryptophan (Table 2), determined in X42 medium, positively correlated with IAA level in leaves (Figure 8a). Negative correlation of tryptamine and tryptophan with the content of IAA degradation products (IAM, IAA-Asp, Ox-IAA, Ox-IAA GE) was not detected. The highest content of IAA and PAA was found in plants treated with 00X11 and 00X30 (Figure 8a).

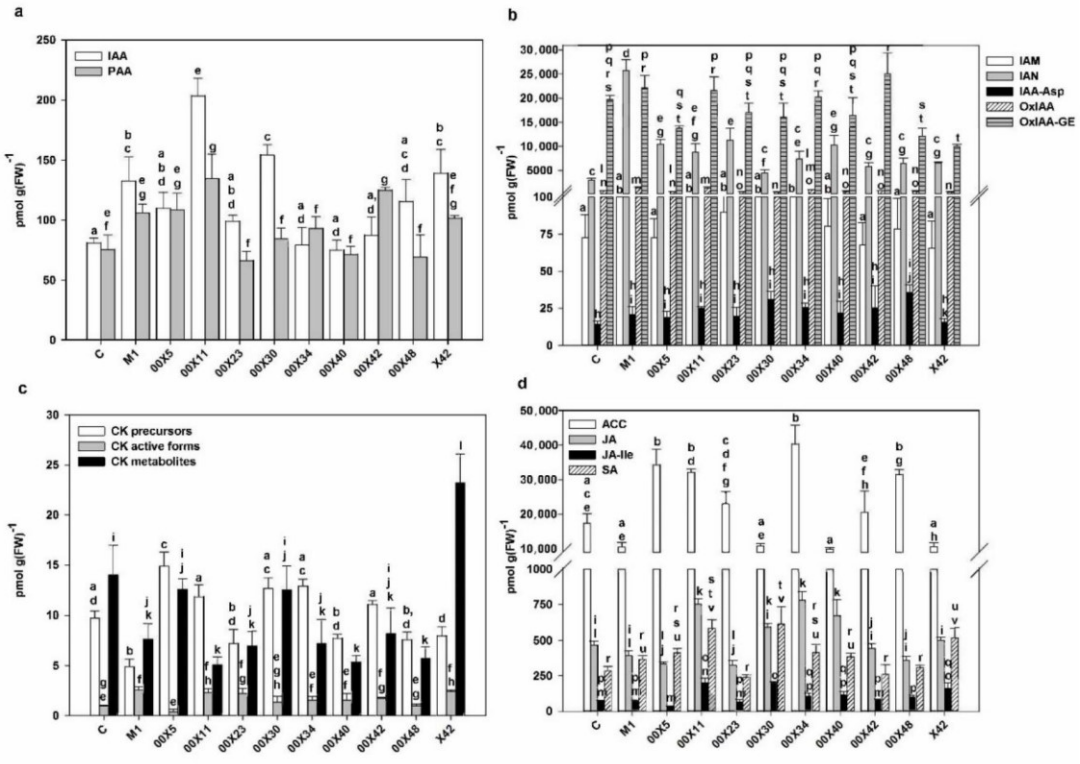


Figure 8. Phytohormone contents in the rapeseed leaves. Active auxins (**a**), precursors and deactivation products of auxins (**b**), cytokinins (**c**), aminocyclopropane-carboxylic acid, jasmonic acid; jasmonate-isoleucine, salicylic acid (**d**). Each code (00X5, 00X11, 00X23, 00X30, 00X34, 00X40, 00X42, 00X48, X42, and M1) represents rapeseed plants treated with a *Pythium* strain. Control (C) was prepared as untreated rapeseed plants. The different letters above each bar denote significant differences ($p \leq 0.05$) between groups according to one-way ANOVA (Bonferroni method). Abbreviations: FW, fresh weight; ACC, 1-aminocyclopropane-1-carboxylic acid; CK, cytokinin; IAA, indole-3-acetic acid; IAA-Asp, IAA-aspartate; IAM, indole-3-acetamide; IAN, indole-3-acetonitrile; JA, jasmonic acid; JA-Ile, JA-isoleucine; OxIAA, oxo-IAA; OxIAA-GE, oxo-IAA-glucose ester; PAA, phenylacetic acid; SA, salicylic acid.

The promotion of cell division and subsequently of plant growth requires cytokinins (CKs) as well as auxins. The active cytokinins, namely trans-zeatin and cis-zeatin, as well as their precursors, storage forms (CK O-glucosides), and degradation products (CK N-glucosides) were also determined in plants (Figure 8c). Higher concentrations of active cytokinins than in control (with the exceptions of 00X5 and 00X48) were found in all groups of rapeseed plants. High concentrations of precursors and degradation products in most experimental variants suggest intensive cytokinin metabolism.

In addition to auxins and cytokinins, hormones related to plant immunity were also monitored, particularly salicylic acid (SA) and jasmonate (JA) (Figure 8d). The treated rapeseed plants had higher SA content (except for 00X23 and 00X42) compared with the control. The highest SA concentrations were found in plants treated with 00X30 and 00X11, increasing to 216% and 205%, respectively. The contents of JA and especially of its active form JA-Ile were higher in plants treated with 00X11, 00X30, 00X34, and 00X40. SA and JA activate signaling pathways in response to biotroph or necrotroph/herbivore attack, respectively. Considering the possibility of attack by different pathogens, as well as the fact that some pathogens may change their lifestyle during infection, these hormones may enhance plant defense against a wide range of foes. The spatially separated activation of JA and SA defense pathways, which could increase the chance of successful elimination of greater pest diversity, has been described [48]. SA and JA functions are modulated by the presence of other phytohormones. Gaseous phytohormone ethylene (ET), the precursor of which is 1-aminocyclopropane-1-carboxylic acid (ACC), could modify the defense responses controlled by JA

[49]. ACC was present in all leaf samples including untreated controls. Its concentration was in six groups higher than in the control; the highest increase was observed in plants treated with 00X34 (231%). The plants treated with the 00X11 strain contained higher concentrations of all aforementioned phytohormones (Figure 8, Table S1). The higher levels of JA, JA-Ile, and ACC in treated plants are in accordance with the reported induction of JA and ET signaling pathways by *P. oligandrum* elicitins [50,51]. In turn, SA signaling including PR1 and PR5 in tomato plants has been ruled out [50], but we found higher levels of SA in rapeseed plants inoculated with some *Pythium* spp. than in control (Figure 8d). However, it is possible to assume species specificity or simply only readiness to respond faster (and to a greater extent) in the case of infection. The concentrations of individual hormones and their metabolites are shown in Table S1.

3.6. Pythium Alters the Glucosinolate Composition of Inoculated Rapeseed Plants

Brassiacaceous plants contain glucosinolates, which protect their tissues from herbivores and likely also from pathogens. The profile of glucosinolates depends on the plant species, its genotype, and growth conditions including biotic and abiotic stresses [52]. Progoitrin and gluconapine were found to be the main glucosinolates in rapeseed meal [53]. In addition, glucoraphanin, glucobrassicanapin, and glucobrassicin were found in rapeseed plants [54]. In the leaves of our experimental plants, the most abundant glucosinolates were glucobrassicin and progoitrin. Furthermore, glucoraphanin was also identified, but only in plants treated with *Pythium* strains; in the control plants and in the plants grown with 00X34, the value was below the detection limit (Table 3). *Pythium* strains can alter glucosinolate content. In the *Pythium*-treated plants, glucobrassicin content was enhanced, whereas progoitrin was rather reduced. This could be advantageous, because progoitrin is metabolized to oxazolidine-2-thione, which causes reproductive and thyroid problems when consumed by animals [55,56]. In general, glucosinolates are of crucial importance in plant defense against herbivores [57] or plant pathogens [58–60]. Tryptophan is present in *Pythium*-treated plants at very low levels or under the detection limit (Figure 7); therefore, it could be a precursor not only of auxin but also of glucobrassicin (Table 3). Methionine as a precursor of glucoraphanin and progoitrin was secreted by *Pythium* strains into the medium, but its concentration in plants depended on the *Pythium* strain (Table 2, Figure 7). It is possible that methionine is provided by *Pythium* to the plant, thus stimulating metabolic pathways originating in methionine, e.g., biosynthesis of ethylene or S-adenosylmethionine, a methyl group donor [49]. It seems that seed coating could increase plant defense at a young growth stage when plants are most vulnerable and not ready for harvest. Each step towards higher natural plant resistance leads to a reduction in the use of pesticides.

Table 3. The contents of glucosinolates in the rapeseed leaves. Each code (00X5, 00X11, 00X23, 00X30, 00X34, 00X40, 00X42, 00X48, X42, and M1) represents rapeseed plants treated with a *Pythium* strain. Control (C) was prepared as untreated rapeseed plants. The different letters in upper index denote significant differences ($p \leq 0.05$) between groups according to one-way ANOVA (Bonferroni method). Abbreviations: DW, dry weight.

	Glucobrassicin	Glucoraphanin	Progoitrin
	[mg g(DW)$^{-1}$]	[mg g(DW)$^{-1}$]	[mg g(DW)$^{-1}$]
C	0.142 ± 0.002 ^{a}	0 ± 0 ^{i}	0.196 ± 0.004 ^{l,n}
M1	0.214 ± 0.004 ^{b,c}	0.001 ± 0.000 ^{i}	0.133 ± 0.008 ^{m,p}
00X5	0.200 ± 0.004 ^{b}	0.002 ± 0.002 ^{i,j}	0.166 ± 0.005 ^{l,m}
00X11	0.230 ± 0.008 ^{c}	0.003 ± 0.000 ^{i,j}	0.139 ± 0.004 ^{m,p}
00X23	0.180 ± 0.003 ^{d}	0.009 ± 0.004 ^{j,k}	0.210 ± 0.007 ^{n,q}
00X30	0.418 ± 0.013 ^{e}	0.005 ± 0.004 ^{i,j}	0.142 ± 0.026 ^{m,p}
00X34	0.049 ± 0.005 ^{f}	0.014 ± 0.004 ^{k}	0.086 ± 0.022 ^{o}
00X40	0.097 ± 0.002 ^{g}	0.005 ± 0.001 ^{i,j}	0.120 ± 0.005 ^{o,p}
00X42	0.318 ± 0.003 ^{h}	0.003 ± 0.001 ^{i,j}	0.226 ± 0.018 ^{n}
00X48	0.179 ± 0.002 ^{d}	0.005 ± 0.002 ^{i,j}	0.175 ± 0.008 ^{l,m,q}
X42	0.148 ± 0.003 ^{a}	0 ± 0 ^{i}	0.078 ± 0.017 ^{o}

3.7. Could Pythium spp. Support the Activity of Antioxidant Enzymes in Rapeseed Plants?

The health status of a plant depends on the activity of antioxidant enzymes. The superoxide radical, one of the most dangerous reactive oxygen species, is detoxified by superoxide dismutase (SOD). SOD activity was detected in leaf extracts (Figure 9a). The individual SOD isoforms were more abundant in the plants inoculated with *Pythium* spp. than in the control plants; the highest intensity was found in 00X30 and X42 samples. The product of SOD reaction, H_2O_2, is also a reactive compound, which is degraded by catalases (CAT) (Figure S8a). CAT activity differed between plants; the highest activity was found in plants inoculated with X42, and the lowest in those treated with 00X11 and 00X42. H_2O_2 is also a substrate for peroxidases, which have broad substrate specificity. They participate in the synthesis of lignin, for example. At least two peroxidase isoforms were present. This microheterogeneity of the latter isoform could have been caused by glycosylation (Figure 9b). Another enzyme that uses H_2O_2 as a substrate is ascorbate peroxidase (Figure S8b). Its activity was higher in plants treated with *Pythium* spp. than in controls, except for 00X23 and 00X48.

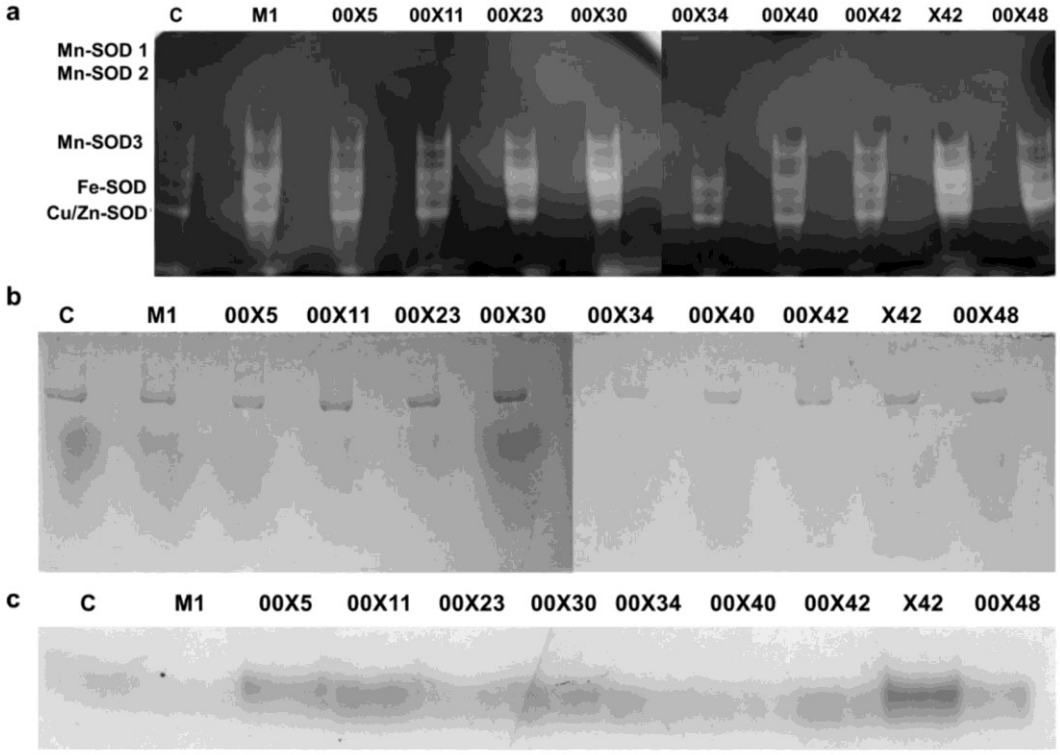


Figure 9. Detection of the activity of superoxide dismutase (SOD) isoenzymes (**a**), peroxidases (**b**), and shikimate dehydrogenase (**c**) after electrophoretic separation under native conditions. The individual SOD isoenzymes were determined in inhibition studies using H_2O_2 and KCN. Each code (00X5, 00X11, 00X23, 00X30, 00X34, 00X40, 00X42, 00X48, X42, and M1) represents rapeseed plants treated with a *Pythium* strain. Control (C) was prepared as untreated rapeseed plants.

Glutathione in its reduced form is important for the control of the reduced status of thiol groups in many proteins in plant cells. The change of glutathione from the oxidized form to the reduced one is catalyzed by glutathione reductase (GR), which uses NADPH as a coenzyme. However, the activity of GR in plants was not significantly affected by the *Pythium* spp. treatment (Figure S8c).

Plant redox state is also affected by the availability of NADPH, which is produced in chloroplasts during photosynthesis. The requirement for NADPH is enhanced under oxidative stress, and therefore other sources, such as NADPH-producing enzymes, could be used. However, the activity of the NADP-malic enzyme (NADP-ME) and of glucose-6-phosphate dehydrogenase (G6PDH) in

experimental plants showed no significant effects from *Pythium* spp. The highest activity of NADP-ME and G6PDH was in plants treated with 00X48 and 00X34, respectively (Figure S8d,e).

NADPH is used also by enzymes of the shikimate pathway, which synthetize aromatic amino acids. The shikimate dehydrogenase (SDH) activity was higher in plants inoculated with *Pythium* spp. compared to the control, and the highest activity was found in plants treated with X42 (Figure 9c). The synthesis of aromatic amino acids, especially phenylalanine and partly tyrosine, is important for plants, not only for protein synthesis but also for the production of phenylpropanoid compounds including lignin, which fortifies cell walls and thus improves plant defense.

4. Conclusions

In this study, we assess a broad number of strains for traits related to mycoparasitism as well as plant-promoting activity. The secretomes of *Pythium* spp. varied significantly in terms of the activities of enzymes capable of acting on host cell walls. Even closely related *P. oligandrum* strains differed in their properties and effects on plants. The alterations in enzyme activities and tryptamine production may indicate advantages either for mycoparasitism or plant growth promotion. Some strains showed equal prerequisites for both effects. The preferred life strategy of *Pythium* spp. has a crucial importance in the selection of new biocontrol agents. This is the first study screening seed coating with *Pythium* spp. for effects on the metabolism of rapeseed plants. In addition to differences in free amino acids and antioxidant enzyme activities, major differences in phytohormone levels were also found, showing increased concentrations of auxin and jasmonates (and salicylic acid in some strains), indicating plant growth promotion as well as readiness for effective defense.

Supplementary Materials: The following are available online at www.mdpi.com/2076-2607/8/10/1472/s1. Figure S1. The in vitro interaction between *Pythium oligandrum*—strain M1 and *Alternaria alternate*, Figure S2. The in vitro interaction between *Pythium oligandrum*—strain M1 and *Verticillium albo-atrum*, Figure S3. The in vitro interaction between *Pythium oligandrum*—strain M1 and *Alternaria brasicae*, Figure S4. The in vitro interaction between *Pythium oligandrum*—strain M1 and *Phoma lingam*, Figure S5. C/N ratio in the rapeseed leaves, Figure S6. Chlorophyll and carotenoid content in the rapeseed leaves, Figure S7. Proteins of the rapeseed leaves separated by SDS-electrophoresis, Figure S8. Enzyme activities in the rapeseed leaves: catalase (a), ascorbate peroxidase (b), glutathione reductase (c), malic enzyme (d), glucose-6-phosphate dehydrogenase (e). The different letters above each bar denote significant differences ($p \leq 0.05$) among the groups according to one way-ANOVA. Each code (00X5, 00X11, 00X23, 00X30, 00X34, 00X40, 00X42, 00X48, X42, and M1) represents rapeseed plants treated with *Pythium* strain. Control (C) was prepared as untreated rapeseed plants. Abreviations: FW, fresh weight, Table S1, Table S2. Carbon, nitrogen, sulfur, and hydrogen content in the rapeseed leaves, expressed as % of dry weight

Author Contributions: K.B. performed experiments, wrote the manuscript, and secured funding; K.V. performed experiments; T.V. took care of seed coating and plant growth; M.K. was responsible for bioinformatics; V.H. performed statistical analysis and edited the manuscript; A.Š., acquired *Pythium* isolates and performed microscopic analysis; R.V. and P.D. analyzed phytohormone content; T.K. and O.H. determined free amino acids; K.Č. and O.H. analyzed glucosinolate content; H.R. wrote the manuscript and designed and supervised the experiments. All authors have read and agreed to the published version of the manuscript.

Funding: This work was supported by Technology Agency of the Czech Republic TJ01000451 and Charles University projects GA UK No. 1304119 and SVV260427/2020.

Acknowledgments: This paper is dedicated to the memory of our inspirational colleague, teacher, and friend, Marie Stiborová, who recently passed away. We are grateful to Karel Černý, Markéta Hrabětová, and Marcela Mrázková from The Silva Tarouca Research Institute for Landscape and Ornamental Gardening (RILOG) in Průhonice (Czech Republic) for the molecular identification of the strains. We are also grateful to Martina Havelcová from the Institute of Rock Structure and Mechanics of the Czech Academy of Sciences (Czech Republic) for the elementary analysis. We would also like to thank Carlos Henrique Vieira Melo for English language editing.

Conflicts of Interest: Tomáš Vaněk and Adam Štípek are employees of the company *Biopreparáty*, which manufactures biological antifungal products based on *Pythium oligandrum*.

References

1. Gerbore, J.; Benhamou, N.; Vallance, J.; Le Floch, G.; Grizard, D.; Regnault-Roger, C.; Rey, P. Biological control of plant pathogens: Advantages and limitations seen through the case study of *Pythium oligandrum*. *Environ. Sci. Pollut. Res. Int.* **2014**, *21*, 4847–4860, doi:10.1007/s11356-013-1807-6.
2. Sivan, A.; Elad, Y.; Chet, I. Biological control effects of a new isolate of *Trichoderma harzianum* on *Pythium aphanidermatum*. *Phytopathology* **1984**, *74*, 498–501, doi:10.1094/Phyto-74-498.
3. Benhamou, N.; le Floch, G.; Vallance, J.; Gerbore, J.; Grizard, D.; Rey, P. *Pythium oligandrum*: An example of opportunistic success. *Microbiology* **2012**, *158*, 2679–2694, doi:10.1099/mic.0.061457-0.
4. Gabrielova, A.; Mencl, K.; Suchanek, M.; Klimes, R.; Hubka, V.; Kolarik, M. The oomycete *Pythium oligandrum* can suppress and kill the causative agents of dermatophytoses. *Mycopathologia* **2018**, *183*, 751–764, doi:10.1007/s11046-018-0277-2.
5. Kushwaha, S.K.; Vetukuri, R.R.; Grenville-Briggs, L.J. Draft genome sequence of the mycoparasitic oomycete *Pythium periplocum* strain CBS 532.74. *Genome Announc.* **2017**, *5*, e00057-17, doi:10.1128/genomeA.00057-17.
6. Ponchet, M.; Panabieres, F.; Milat, M.L.; Mikes, V.; Montillet, J.L.; Suty, L.; Triantaphylides, C.; Tirilly, Y.; Blein, J.P. Are elicitins cryptograms in plant-Oomycete communications? *Cell Mol. Life Sci.* **1999**, *56*, 1020–1047, doi:10.1007/s000180050491.
7. Masunaka, A.; Sekiguchi, H.; Takahashi, H.; Takenaka, S. Distribution and expression of elicitin-like protein genes of the biocontrol agent *Pythium oligandrum*. *J. Phytopathol.* **2010**, *158*, 417–426, doi:10.1111/j.1439-0434.2009.01641.x.
8. Le Floch, G.; Rey, P.; Benizri, E.; Benhamou, N.; Tirilly, Y. Impact of auxin-compounds produced by the antagonistic fungus *Pythium oligandrum* or the minor pathogen *Pythium* group F on plant growth. *Plant Soil* **2003**, *257*, 459–470, doi:10.1023/A:1027330024834.
9. Whipps, J.M. Effect of media on growth and interactions between a range of soil-born glasshouse pathogens and antagonistic fungi. *New Phytol.* **1987**, *107*, 127–142, doi:10.1111/j.1469-8137.1987.tb04887.x.
10. Vesely, D. Studies of the mycoparasitism in rhizosphere of emerging sugar-beet. *Zentralbl. Bakteriol. Naturwiss.* **1978**, *133*, 195–200, doi:10.1016/s0323-6056(78)80001-9.
11. Hyde, K.D.; Nilsson, R.H.; Alias, S.A.; Ariyawansa, H.A.; Blair, J.E.; Cai, L.; de Cock, A.W.; Dissanayake, A.J.; Glockling, S.L.; Goonasekara, I.D. One stop shop: Backbones trees for important phytopathogenic genera: I. *Fungal Divers.* **2014**, *67*, 21–125, doi:10.1007/s13225-014-0298-1.
12. Robideau, G.P.; De Cock, A.W.; Coffey, M.D.; Voglmayr, H.; Brouwer, H.; Bala, K.; Chitty, D.W.; Desaulniers, N.; Eggertson, Q.A.; Gachon, C.M.; et al. DNA barcoding of oomycetes with cytochrome c oxidase subunit I and internal transcribed spacer. *Mol. Ecol. Resour.* **2011**, *11*, 1002–1011, doi:10.1111/j.1755-0998.2011.03041.x.
13. White, T.J.; Bruns, T.; Lee, S.; Taylor, J.W. Amplification and direct sequencing of fungal ribosomal RNA genes for phylogenetics. In *PCR Protocols: A Guide to Methods and Applications*; Innis, M.A., Gelfand, D.H., Sninsky, J.J., White, T.J., Eds.; Academic Press, Inc.: New York, NY, USA, 1990; pp. 315–322.
14. Chen, J.; Lü, L.; Ye, W.; Wang, Y.-C.; Zheng, X.-B. *Pythium cedri* sp. nov. (Pythiaceae, Pythiales) from southern China based on morphological and molecular characters. *Phytotaxa* **2017**, *309*, 135–142, doi:10.11646/phytotaxa.309.2.4.
15. Faure, C.; Veyssiere, M.; Boelle, B.; San Clemente, H.; Bouchez, O.; Lopez-Roques, C.; Chaubet, A.; Martinez, Y.; Bezouska, K.; Suchanek, M.; et al. Long-read genome sequence of the sugar beet rhizosphere mycoparasite *Pythium oligandrum*. *G3 Genes Genom. Genet.* **2020**, *10*, 431–436, doi:10.1534/g3.119.400746.
16. Berger, H.; Yacoub, A.; Gerbore, J.; Grizard, D.; Rey, P.; Sessitsch, A.; Compant, S. Draft genome sequence of biocontrol agent *Pythium oligandrum* strain Po37, an Oomycota. *Genome Announc.* **2016**, *4*, e00215–00216, doi:10.1128/genomeA.00215-16.
17. Katoh, K.; Standley, D.M. MAFFT multiple sequence alignment software version 7: Improvements in performance and usability. *Mol. Biol. Evol.* **2013**, *30*, 772–780, doi:10.1093/molbev/mst010.
18. Guindon, S.; Dufayard, J.F.; Lefort, V.; Anisimova, M.; Hordijk, W.; Gascuel, O. New algorithms and methods to estimate maximum-likelihood phylogenies: Assessing the performance of PhyML 3.0. *Syst. Biol.* **2010**, *59*, 307–321, doi:10.1093/sysbio/syq010.
19. Bradford, M.M. A rapid and sensitive method for the quantitation of microgram quantities of protein utilizing the principle of protein-dye binding. *Anal. Biochem.* **1976**, *72*, 248–254, doi:10.1006/abio.1976.9999.
20. Schagger, H. Tricine-SDS-PAGE. *Nat. Protoc.* **2006**, *1*, 16–22, doi:10.1038/nprot.2006.4.

21. Laemmli, U.K. Cleavage of structural proteins during assembly of head of bacteriophage-T4. *Nature* **1970**, *227*, 680–685, doi:10.1038/227680a0.
22. Hodek, O.; Krizek, T.; Coufal, P.; Ryslava, H. Design of experiments for amino acid extraction from tobacco leaves and their subsequent determination by capillary zone electrophoresis. *Anal. Bional. Chem.* **2017**, *409*, 2383–2391, doi:10.1007/s00216-017-0184-2.
23. Dudonne, S.; Vitrac, X.; Coutiere, P.; Woillez, M.; Merillon, J.M. Comparative study of antioxidant properties and total phenolic content of 30 plant extracts of industrial interest using DPPH, ABTS, FRAP, SOD, and ORAC assays. *J. Agric. Food Chem.* **2009**, *57*, 1768–1774, doi:10.1021/jf803011r.
24. Tupec, M.; Hyskova, V.; Belonoznikova, K.; Hranicek, J.; Cerveny, V.; Ryslava, H. Characterization of some potential medicinal plants from Central Europe by their antioxidant capacity and the presence of metal elements. *Food Biosci.* **2017**, *20*, 43–50, doi:10.1016/j.fbio.2017.08.001.
25. Dobrev, P.I.; Kaminek, M. Fast and efficient separation of cytokinins from auxin and abscisic acid and their purification using mixed-mode solid-phase extraction. *J. Chromatogr. A* **2002**, *950*, 21–29, doi:10.1016/S0021-9673(02)00024-9.
26. Dobrev, P.I.; Vankova, R. Quantification of abscisic acid, cytokinin, and auxin content in salt-stressed plant tissues. *Methods Mol. Biol.* **2012**, *913*, 251–261, doi:10.1007/978-1-61779-986-0_17.
27. Prerostova, S.; Dobrev, P.I.; Konradyova, V.; Knirsch, V.; Gaudinova, A.; Kramna, B.; Kazda, J.; Ludwig-Muller, J.; Vankova, R. Hormonal responses to *Plasmodiophora brassicae* infection in *Brassica napus* cultivars differing in their pathogen resistance. *Int. J. Mol. Sci.* **2018**, *19*, 4024, doi:10.3390/ijms19124024.
28. Lechtenberg, M.; Hensel, A. Determination of glucosinolates in broccoli-based dietary supplements by cyclodextrin-mediated capillary zone electrophoresis. *J. Food Compos. Anal.* **2019**, *78*, 138–149, doi:10.1016/j.jfca.2019.02.007.
29. Hyskova, V.; Pliskova, V.; Cerveny, V.; Ryslava, H. NADP-dependent enzymes are involved in response to salt and hypoosmotic stress in cucumber plants. *Gen. Physiol. Biophys.* **2017**, *36*, 247–258, doi:10.4149/gpb_2016053.
30. Yannarelli, G.G.; Fernandez-Alvarez, A.J.; Santa-Cruz, D.M.; Tomaro, M.L. Glutathione reductase activity and isoforms in leaves and roots of wheat plants subjected to cadmium stress. *Phytochemistry* **2007**, *68*, 505–512, doi:10.1016/j.phytochem.2006.11.016.
31. Coelho, D.F.; Saturnino, T.P.; Fernandes, F.F.; Mazzola, P.G.; Silveira, E.; Tambourgi, E.B. Azocasein substrate for determination of proteolytic activity: Reexamining a traditional method using bromelain samples. *BioMed Res. Int.* **2016**, *2016*, ID8409183, doi:10.1155/2016/8409183.
32. Nakata, H.; Ishii, S. Substrate activation of trypsin and acetyltrypsin caused by -N-benzoyl-L-arginine p-nitroanilide. *J. Biochem.* **1972**, *72*, 281–290, doi:10.1093/oxfordjournals.jbchem.a129907.
33. Anthon, G.E.; Barrett, D.M. Determination of reducing sugars with 3-methyl-2-benzothiazolinonehydrazone. *Anal. Biochem.* **2002**, *305*, 287–289, doi:10.1006/abio.2002.5644.
34. Maseko, S.T.; Dakora, F.D. Rhizosphere acid and alkaline phosphatase activity as a marker of P nutrition in nodulated *Cyclopia* and *Aspalathus* species in the Cape fynbos of South Africa. *S. Afr. J. Bot.* **2013**, *89*, 289–295, doi:10.1016/j.sajb.2013.06.023.
35. Beauchamp, C.; Fridovich, I. Superoxide dismutase: Improved assays and an assay applicable to acrylamide gels. *Anal. Biochem.* **1971**, *44*, 276–287, doi:10.1016/0003-2697(71)90370-8.
36. Synkova, H.; Semoradova, S.; Schnablova, R.; Muller, K.; Pospisilova, J.; Ryslava, H.; Malbeck, J.; Cerovska, N. Effects of biotic stress caused by *Potato virus Y* on photosynthesis in *ipt* transgenic and control *Nicotiana tabacum* L. *Plant Sci.* **2006**, *171*, 607–616, doi:10.1016/j.plantsci.2006.06.002.
37. Spoustova, P.; Hyskova, V.; Muller, K.; Schnablova, R.; Ryslava, H.; Cerovska, N.; Malbeck, J.; Cvikrova, M.; Synkova, H. Tobacco susceptibility to Potato virus Y-NTN infection is affected by grafting and endogenous cytokinin content. *Plant Sci.* **2015**, *235*, 25–36, doi:10.1016/j.plantsci.2015.02.017.
38. Plaats-Niterink, A.J.v.d. Monograph of the genus *Pythium*. *Stud. Mycol.* **1981**, *21*, 1–244.
39. McGowan, J.; Fitzpatrick, D.A. Genomic, network, and phylogenetic analysis of the oomycete effector arsenal. *MSphere* **2017**, *2*, e00408-17, doi:10.1128/mSphere.00408-17.
40. Judelson, H.S. Metabolic diversity and novelties in the oomycetes. *Annu. Rev. Microbiol.* **2017**, *71*, 21–39, doi:10.1146/annurev-micro-090816-093609.
41. Brunner, F.; Wirtz, W.; Rose, J.K.; Darvill, A.G.; Govers, F.; Scheel, D.; Nurnberger, T. A beta-glucosidase/xylosidase from the phytopathogenic oomycete, *Phytophthora infestans*. *Phytochemistry* **2002**, *59*, 689–696, doi:10.1016/s0031-9422(02)00045-6.

42. Bowyer, P.; Clarke, B.R.; Lunness, P.; Daniels, M.J.; Osbourn, A.E. Host range of a plant pathogenic fungus determined by a saponin detoxifying enzyme. *Science* **1995**, *267*, 371–374, doi:10.1126/science.7824933.
43. Crombie, W.M.L.; Crombie, L.; Green, J.B.; Lucas, J.A. Pathogenicity of 'take-all' fungus to oats: Its relationship to the concentration and detoxification of the four avenacins. *Phytochemistry* **1986**, *25*, 2075–2083, doi:10.1016/0031-9422(86)80069-3.
44. Ivanov, D.A.; Bernards, M.A. Ginsenosidases and the pathogenicity of *Pythium irregulare*. *Phytochemistry* **2012**, *78*, 44–53, doi:10.1016/j.phytochem.2012.02.024.
45. Brzobohaty, B.; Moore, I.; Kristoffersen, P.; Bako, L.; Campos, N.; Schell, J.; Palme, K. Release of active cytokinin by a beta-glucosidase localized to the maize root meristem. *Science* **1993**, *262*, 1051–1054, doi:10.1126/science.8235622.
46. Le Roy, J.; Huss, B.; Creach, A.; Hawkins, S.; Neutelings, G. Glycosylation is a major regulator of phenylpropanoid availability and biological activity in plants. *Front. Plant Sci.* **2016**, *7*, 735, doi:10.3389/fpls.2016.00735.
47. Ma, Y. Seed coating with beneficial microorganisms for precision agriculture. *Biotechnol. Adv.* **2019**, *37*, 1–11, doi:10.1016/j.biotechadv.2019.107423.
48. Tsuda, K. Division of Tasks: Defense by the Spatial Separation of Antagonistic Hormone Activities. *Plant Cell Physiol.* **2017**, *54*, 3–4, doi:10.1093/pcp/pcx208.
49. Pieterse, C.M.; Van der Does, D.; Zamioudis, C.; Leon-Reyes, A.; Van Wees, S.C. Hormonal modulation of plant immunity. *Annu. Rev. Cell Dev. Biol.* **2012**, *28*, 489–521, doi:10.1146/annurev-cellbio-092910-154055.
50. Kawamura, Y.; Takenaka, S.; Hase, S.; Kubota, M.; Ichinose, Y.; Kanayama, Y.; Nakaho, K.; Klessig, D.F.; Takahashi, H. Enhanced defense responses in Arabidopsis induced by the cell wall protein fractions from *Pythium oligandrum* require SGT1, RAR1, NPR1 and JAR1. *Plant Cell Physiol.* **2009**, *50*, 924–934, doi:10.1093/pcp/pcp044.
51. Takenaka, S.; Yamaguchi, K.; Masunaka, A.; Hase, S.; Inoue, T.; Takahashi, H. Implications of oligomeric forms of POD-1 and POD-2 proteins isolated from cell walls of the biocontrol agent *Pythium oligandrum* in relation to their ability to induce defense reactions in tomato. *J. Plant Physiol.* **2011**, *168*, 1972–1979, doi:10.1016/j.jplph.2011.05.011.
52. Bjorkman, M.; Klingen, I.; Birch, A.N.; Bones, A.M.; Bruce, T.J.; Johansen, T.J.; Meadow, R.; Molmann, J.; Seljasen, R.; Smart, L.E.; et al. Phytochemicals of Brassicaceae in plant protection and human health-influences of climate, environment and agronomic practice. *Phytochemistry* **2011**, *72*, 538–556, doi:10.1016/j.phytochem.2011.01.014.
53. Ishikawa, S.; Maruyama, A.; Yamamoto, Y.; Hara, S. Extraction and characterization of glucosinolates and isothiocyanates from rape seed meal. *J. Oleo Sci.* **2014**, *63*, 303–308, doi:10.5650/jos.ess13170.
54. Schaefer, H.L.; Brandes, H.; Ulber, B.; Becker, H.C.; Vidal, S. Evaluation of nine genotypes of oilseed rape (*Brassica napus* L.) for larval infestation and performance of rape stem weevil (*Ceutorhynchus napi* Gyll.). *PLoS ONE* **2017**, *12*, e0180807, doi:10.1371/journal.pone.0180807.
55. Angelino, D.; Dosz, E.B.; Sun, J.; Hoeflinger, J.L.; Van Tassell, M.L.; Chen, P.; Harnly, J.M.; Miller, M.J.; Jeffery, E.H. Myrosinase-dependent and -independent formation and control of isothiocyanate products of glucosinolate hydrolysis. *Front. Plant Sci.* **2015**, *6*, 831, doi:10.3389/fpls.2015.00831.
56. Halkier, B.A.; Gershenzon, J. Biology and biochemistry of glucosinolates. *Annu. Rev. Plant Biol.* **2006**, *57*, 303–333, doi:10.1146/annurev.arplant.57.032905.105228.
57. Wittstock, U.; Kliebenstein, D.J.; Lambrix, V.; Reichelt, M.; Gershenzon, J. Chapter five Glucosinolate hydrolysis and its impact on generalist and specialist insect herbivores. *Recent Adv. Phytochem.* **2003**, *37*, 101–125, doi:10.1016/S0079-9920(03)80020-5.
58. Brader, G.; Mikkelsen, M.D.; Halkier, B.A.; Tapio Palva, E. Altering glucosinolate profiles modulates disease resistance in plants. *Plant J.* **2006**, *46*, 758–767, doi:10.1111/j.1365-313X.2006.02743.x.

59. Giamoustaris, A.; Mithen, R. Glucosinolates and disease resistance in oilseed rape (*Brassica napus* ssp. oleifera). *Plant Pathol.* **1997**, *46*, 271–275, doi:10.1046/j.1365-3059.1997.d01-222.x.
60. Schlaeppi, K.; Abou-Mansour, E.; Buchala, A.; Mauch, F. Disease resistance of Arabidopsis to *Phytophthora brassicae* is established by the sequential action of indole glucosinolates and camalexin. *Plant J.* **2010**, *62*, 840–851, doi:10.1111/j.1365-313X.2010.04197.x.



© 2020 by the authors. Licensee MDPI, Basel, Switzerland. This article is an open access article distributed under the terms and conditions of the Creative Commons Attribution (CC BY) license (http://creativecommons.org/licenses/by/4.0/).

3.2.2 Effects of heat treatment on metabolism of tobacco plants infected with *Potato virus Y*

Our laboratory enjoys a long-time and friendly co-operation with the Laboratory of Virology at the Institute of Experimental Botany of the Czech Academy of Sciences. Various factors affect virus propagation and plant defense responses. One of the most discussed abiotic stress factors is the increasing temperature. Therefore, we focused on how a heat-shock could influence the viral propagation. We followed the course of potyviral (PVY^{NTN}) infection in *Nicotiana tabacum* plants if treated before or after viral inoculation with a two-hour long heat shock of 42°C. The overview of the publication is summarized in the graphical abstract (Fig. 14).

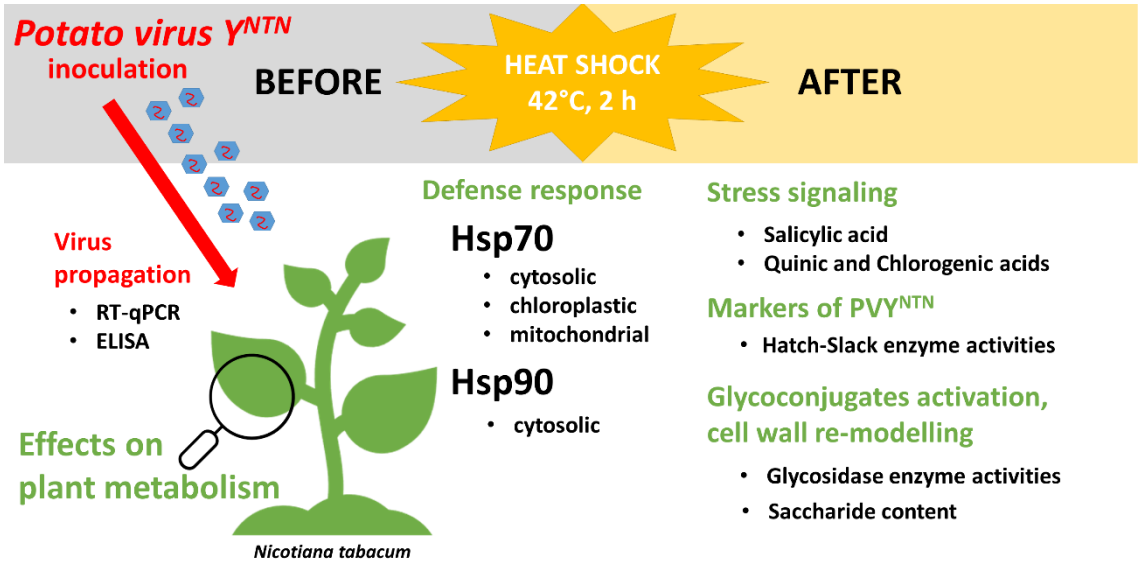


Fig. 14: Graphical abstract of the publication about the impact of heat shock on the course of *Potato virus Y* infection (Hýsková et al 2021b). We thoroughly analyzed five different experimental groups. C20 - non-inoculated control plants grown without experiencing heat shock, C42 - non-inoculated control plants with experiencing heat shock, 42Y - plants that experienced heat shock before potyviral infection, Y42 - plants that experienced heat shock after potyviral inoculation, Y20 - inoculated plants without experiencing heat shock. The mechanical wounding during PVY^{NTN} inoculation could represent another form of stress. Therefore, we also studied mock (M) inoculated plants in the first week of the experiment (M, M42, 42M).

Heat shock and almost all types of stress are associated with the expression of heat shock proteins (Hsps) which are involved in refolding of denaturated proteins or directing them for degradation. However, Hsps play an ambiguous role

during the viral propagation. Viruses usually can recruit Hsp70 which then may promote viral genome replication, translation, and virus propagation from cell to cell (Hýsková et al 2021a, Hýsková et al 2021b). We analyzed the impact of potyviral infection and heat shock for 28 days long plant growth. The plants were inoculated with PVY^{NTN} either before or after heat shock. The leaf samples were collected after one hour, one day and then each week. Firstly, we observed that heat shock accelerated PVY^{NTN} propagation since the plants with both stress factors had showed earlier onset of viral infection (Fig. 1 in Hýsková et al 2021b). The amounts of Hsp70 and Hsp90 were increased during the first 24 hours of the experiment. Considering the mock-inoculation and viral content analysis, we concluded that this early increase of Hsps could be more related to the mechanical wounding than the viral factor (Fig. 1, Fig. S2 in Hýsková et al 2021b). In the Western blot analysis, we also observed that Hsp70 cytosolic and mitochondrial isoforms (~50-75 kDa) that persisted during the developed viral infection (Fig. 2, Fig. 3 in Hýsková et al 2021b). In *Nicotiana tabacum* plants, there are a total of 61 genes (20 cytosolic, 6 mitochondrial, 4 chloroplast isoforms, and others from the endoplasmic reticulum) for Hsp70 with a large dispersion of relative molecular weights, the transcription of which is induced by a number of factors such as heat shock, mechanical damage and salicylic acid (Song et al 2019). Thus, we believe that PVY^{NTN} infection induced the NtHsp70-23 and NtHsp70-35 isoforms (Fig. 1a,b, Fig. 2a, Fig. 4a in Hýsková et al 2021b).

Viral infection as a stress factor results in the plant metabolism alteration. In our previous studies, we observed its impact on photosynthesis, carbohydrate pathways, antioxidant system and Hatch-Slack enzymes (Doubnerová et al 2007, Muller et al 2009, Ryšlavá et al 2003, Spoustová et al 2015, Synková et al 2006). In this project, we introduced and began to optimize a method for phenolic compounds detection by LC-MS in our laboratory. Therefore, we could follow the alteration of SA, chlorogenic acid (CGA), quinic acid (QA) and ferulic acid contents in the leaves. SA and CGA increased in a positive correlation with potyviral infection. While QA decreased in time in probable relation to CGA production, being its precursor. Also, we detected a high content of ferulic acid in all the potyviral infected groups on the 21st, and 28th day (Fig. S3 in Hýsková et al 2021b).

All these phenolic compounds could be related to defense responses, CGA and ferulic acid could also be engaged in lignin biosynthesis and thus plant cell wall fortification. The Hatch-Slack enzymes were already shown to be markers of potyviral infection in tobacco plants (Doubnerová et al 2007, Doubnerová & Ryšlavá 2011, Ryšlavá et al 2003, Spoustová et al 2015). In accordance, phosphoenolpyruvate carboxylase (EC 4.1.1.31), NADP-malic enzyme (EC 1.1.1.40), and pyruvate, phosphate dikinase (EC 2.7.9.1) activities were increased in the potyviral infected plants during the 14th-28th day period (Fig. 5 in Hýsková et al 2021b). However, their activities were not further enhanced with heat shock. Plant cell walls represent the front line for pathogen attacks, and consist of carbohydrate polymers, lignin, and structural proteins in variable amounts (Tenhaken 2015). The cell wall dynamics is not easy to follow. We analyzed various glycosidases that are involved in cell wall remodeling, hydrolysis of glycoconjugates, such as phenolic compounds, including flavonoids and phytohormones (Ludwig-Muller 2011, Slámová et al 2018). Shortly after heat shock (1 hour), ß-glucosidase and α-mannosidase activities were increased. We suggested that ß-glucosidase could be involved in the de-glucosylation of various phenolic compounds, degradation of glucosylated phytohormones, resulting in their fast activation and signal transmission. α-Mannosidase may have modulated various glycoproteins (oligosaccharide chains) which also may play a role in plant signaling of heat shock and viral infection (Strasser 2016). In the stage of maximal viral content (14th-28th day), PVY^{NTN} infection induced α-galactosidase, α-mannosidase, ß-N-acetylhexosaminidase and α-glucosidase. Our previous studies concerned the kinetic properties of ß-N-acetylhexosaminidase in tobacco leaves (Ryšlavá et al 2014). However, its function and natural substrates are still rather unclear. Generally, ß-N-acetylhexosaminidase cleaves N-acetylglucosamine or N-acetylgalactosamine from non-reducing end of oligosaccharides, glycoproteins, glycolipids, and other glycoconjugates. In connection with viral infection, considering, its chinolytic activity ß-N-acetylhexosaminidase could participate in defense responses similarly as PR proteins such as chitinases (Hýsková & Ryšlavá 2015). Various stress factors as well as viruses are linked to the ROS formation and together with the elevated

action of peroxidases, their interaction can result in cross-linking of cell wall components to strengthen the wall mechanical properties (Tenhaken 2015). Although we have not published the data yet, due to viral infection, the activity and number of peroxidase isoforms increased as seen in native electrophoresis. The uninfected plants as well as mock-inoculated showed three isoforms while the potyviral infected ones showed at least six isoforms, persisting throughout the whole experiment.

My contribution:

I extracted RNA and detected PVY^{NTN} by RT-qPCR. I analyzed the Hsp70 (cytosolic, chloroplastic and mitochondrial) and Hsp90 contents by Western blotting. I prepared the plant extracts for phenolic acid determination by LC-MS and analyzed the data. I also measured the total saccharide content. I prepared the resulting figures for the publication.

plant biology

Plant Biology ISSN 1435-8603

RESEARCH PAPER

Effects of heat treatment on metabolism of tobacco plants infected with *Potato virus Y*

V. Hýsková[1], K. Bělonožníková[1], V. Doričová[1], D. Kavan[1], S. Gillarová[2], S. Henke[2], H. Synková[3], H. Ryšlavá[1] & N. Čeřovská[3]

1 Department of Biochemistry, Faculty of Science, Charles University, Prague 2, Czech Republic
2 Department of Carbohydrates and Cereals, University of Chemistry and Technology, Prague 6, Czech Republic
3 Institute of Experimental Botany, Academy of Sciences of the CR, Praha 6, Czech Republic

Keywords
heat shock; Hsp70; Hsp90; phenolic acids; Potato virus Y; Hatch–Slack cycle; glycosidases.

Correspondence
H. Ryšlavá, Department of Biochemistry, Faculty of Science, Charles University, Hlavova 2030, Prague 2, 128 40, Czech Republic.
E-mail: helena.ryslava@natur.cuni.cz

Editor
Y. Hu

Received: 26 October 2020; Accepted: 5 January 2021

doi:10.1111/plb.13234

ABSTRACT

- Many factors affect successful virus propagation and plant defence responses. Heat shock protein (Hsp) expression after heat shock plays an ambiguous role in viral infection. On the one hand, Hsp70 participates in plant defence response; on the other hand, Hsp70 could interact with viral proteins and facilitate virus propagation.
- Here, we studied metabolic adaptations of *Nicotiana tabacum* L. subjected to heat shock (42 °C, 2 h) before or after inoculating the plants with *Potato virus Y* (potyvirus).
  RT-qPCR and ELISA were used for potyvirus quantification. Hsp70 and Hsp90 isoforms were analysed by Western blotting. Salicylic, quinic and chlorogenic acid content was determined by LC-MS. The activity of Hatch–Slack enzymes (as markers of potyviral infection in tobacco) and glycosidases was assayed.
- Application of heat shock before or after inoculation showed accelerated potyviral propagation in comparison with only inoculated plants. Plants exposed to heat shock and concurrently inoculated showed higher potyviral content, higher amount of Hsp70, together with late decline of quinic acid content and low chlorogenic acid content. Spread of potyviral infection correlated with enhanced salicylic acid content and activities of enzymes of the Hatch–Slack cycle, α- and β-galactosidase, α-mannosidase, α-glucosidase and β-N-acetylhexosaminidase.
- Heat shock proteins accelerate potyviral propagation. The lower weight cytosolic and mitochondrial Hsp70 (~50-75 kDa) persist throughout the viral infection. Also, the plant defense response results in increase of salicylic and chlorogenic acids but decrease of quinic acid content.

INTRODUCTION

Heat shock proteins (Hsp) are ubiquitous constitutive and stress-induced proteins, primarily participating in maintenance of cell protein quality. Hsp are divided into six groups according to their relative molecular weight and primary structure homology (Wang *et al.* 2004; Park & Seo 2015). In particular, the Hsp70 class arguably belongs to the most conserved proteins among all organisms, from bacteria to plants and animals. Hsp70 and Hsp90 act as chaperones, stabilizing nascent proteins during protein folding, assembling or disassembling multi-protein complexes, preventing protein aggregation, repairing misfolded proteins or targeting irreparable proteins for degradation by the ubiquitin-proteasome system and transporting and sorting organelle-specific proteins (Doubnerova & Ryslava 2014; Anaraki *et al.* 2018; Kozeko 2019). In addition, Hsp90 determines functioning of several complicated protein complexes, including 26S proteasome, ribosomal subunit 40S, RNA-induced silencing complex, etc. (Kozeko 2019).

Expression of Hsp70 is induced not only by heat shock but also by almost all types of plant stress (Park & Seo 2015; Usman *et al.* 2017). Hsp70 overexpression in plants positively correlates with the acquisition of thermotolerance and results in enhanced tolerance to abiotic stress treatments (Wang *et al.* 2004; Su & Li 2008), whereas Hsp70 downregulation reduces tolerance to abiotic stresses (Su & Li 2008). Thus, the Hsp70 system plays a key role in plants recovering from various stresses (Usman *et al.* 2017; Anaraki *et al.* 2018).

The Hsp70 comprises a highly conserved protein family of cellular chaperones, which can be divided according to sequence homology into six subfamilies. There are at least 18 genes for Hsp70 in *Arabidopsis thaliana*, 32 genes in rice and 61 genes have been even identified in tobacco plants (Lin *et al.* 2001; Sarkar *et al.* 2013; Song *et al.* 2019). Members of the Hsp70 family in tobacco plants consist of 118 to 904 amino acids, their molecular weight ranges from 12.58 to 99.88 kDa. Most Hsp70 are located in the endoplasmic reticulum and cytoplasm, 25 and 20, respectively. Four chloroplastic Hsp70 isoforms maintain normal operation of photosystem II, participate in formation of thylakoid membranes and assist in protein transport. In addition, six Hsp70 isoforms in mitochondria have been identified (Song *et al.* 2019).

Upon infection, virus activates a stress response in host cells. However, the interaction between viral infection and Hsp70 is

highly complex and ambiguous. Hsp70 are involved in all steps of the virus life cycle (Nagy *et al.* 2011; Verchot 2012; Jiang *et al.* 2014). Systemic invasion of plants by viruses depends on compatible interactions between host and virus-encoded factors, which facilitate genome replication, cell-to-cell movement *via* plasmodesmata and long-distance transport through vascular tissues (Carrington *et al.* 1996; Heinlein 2015). In this context, the main plant defence system against viral infection is RNA silencing, which is also affected by temperature (Szittya *et al.* 2003; Gaffar & Koch 2019). Lack of Hsp70 prevents efficient viral infection (Hofius *et al.* 2007; Dufresne *et al.* 2008; Chen *et al.* 2008; Hafren *et al.* 2010; Jungkunz *et al.* 2011; Mine *et al.* 2012; Jiang *et al.* 2014; Gorovits & Czosnek 2017). Conversely, temperature increase inhibits virus development in some host and virus systems, and the success of thermotherapy depends not only on the temperature and treatment period or duration but also on the plant species and virus strain (Tan *et al.* 2010; Kwon *et al.* 2012; Achachi *et al.* 2014).

Potyviral infection upregulates Hsp70 through cytosolic unfolded protein response (Sugio *et al.* 2009), thus indicating that PVY triggers Hsp70-dependent plant defence mechanisms. In PVY-infected tobacco plants, defence responses involve the synthesis of salicylic acid (SA), pathogenesis-related proteins, phenolic compounds and lignin (Schnablova *et al.* 2006; Spoustova *et al.* 2015). Phosphoenolpyruvate carboxylase (PEPC, EC 4.1.1.31), NADP-malic enzyme (NADP-ME, EC 1.1.1.40) and pyruvate, phosphate dikinase (PPDK, EC 2.7.9.1) participate in the process of concentrating CO_2 in C_4 photosynthesis, whereas the non-photosynthetic counterparts of these enzymes are involved in plant responses to stress (Doubnerova & Ryslava 2011; Ryslava *et al.* 2015). PEPC, NADP-ME and PPDK activities were increased during potyviral infection (Ryslava *et al.* 2003) as a function of virulence (Doubnerova *et al.* 2009; Muller *et al.* 2009).

The Hsp70 substrate binding and release cycle is exclusively regulated by ATP (Mayer & Bukau 2005; Doubnerova & Ryslava 2014). Saccharides may also be hydrolysed from glycoconjugates by glycosidases, which could respond to viral infection (Ryslava *et al.* 2009).

Among other functions, glycosidases participate in the formation of correct oligosaccharide chains in glycoproteins (Strasser 2016). Glycosidases are also involved in cell wall remodelling and in the hydrolysis of glycoconjugates, such as phenolic compounds, including flavonoids and phytohormones (Ludwig-Muller 2011; Slamova *et al.* 2018).

The aim of this study was to investigate if Hsp induced by heat shock in tobacco plants could alter virus propagation and/or modify the defence reactions of the plant. Therefore, we have applied heat shock (before or after PVY^{NTN} inoculation) to tobacco plants and monitored the contents of virus, cytosolic, chloroplastic, mitochondrial Hsp70 isoforms and cytosolic Hsp90.1. Plant defence reactions were characterized by SA and other phenolics content and activities of key metabolic enzymes.

MATERIAL AND METHODS

Plant material

Nicotiana tabacum L., cv. Petit Havana SR1 seeds were sown in pots containing soil and sand (ratio 3:1), transferring the seedlings to soil 3 weeks after sowing. Plants were grown in a growth chamber under a 16-h/8-h light/dark period, ca. 150 μmol (photon)·m^{-2}·s^{-1} irradiance, at 20 °C and 75% relative humidity. After 7 weeks, approximately 100 plants were divided into five experimental groups. The first group (C20) remained at 20 °C throughout the experiment. The second group (C42) was exposed to heat shock (42 °C) for 2 h. The following groups involved mechanical inoculation of plants on the adaxial surface of leaves with *Potato virus Y*, strain NTN (PVY^{NTN}) provided by Dr. Dědič (Potato Research Institute, Havlíčkův Brod, Czech Republic). Infected tobacco leaves with a positively detected PVY^{NTN}, extracted in ten-fold 0.05 M phosphate buffer, pH 8, were used for inoculation with carborundum powder.

The third group (42Y) consisted of plants first exposed to heat shock (2 h at 42 °C) and then inoculated with PVY^{NTN}, while the fourth group (Y42) contained plants first inoculated with PVY^{NTN} and then exposed to heat shock (2 h at 42 °C). Subsequently, all plants were returned to the growth chamber and grown at 20 °C under the aforementioned conditions. The fifth group represented PVY^{NTN} inoculated plants without heat shock (Y20).

The mixed leaf samples collected 1 h, 1 day, 1, 2 and 3 weeks after heat shock exposure and inoculation contained the four to five first fully developed leaves without the midrib. The 0.5 g samples were immediately frozen in liquid nitrogen and stored at −80 °C. The experiment was terminated 28 days after inoculation. Since virus inoculation is accompanied by mechanical stress, mock-inoculated plants were processed over 1 week. The M20 group consisted of mock-inoculated plants (with carborundum powder and 0.05 M phosphate buffer, pH 8). The M42 group included plants first exposed to heat shock (2 h at 42 °C) and then mock-inoculated, whereas the 42M group contained plants first mock-inoculated and then exposed to heat shock (2 h at 42 °C).

Extraction of RNA and detection of PVY^{NTN} by RT-qPCR

Total mRNA was isolated from 100 mg leaf sample using the RNeasy kit (Qiagen, Hilden, Germany). Any contaminated genomic DNA was removed by treatment with DNase Max (Qiagen).

Approximately 0.5 μg RNA was transcribed using the PrimeScript™ RT Reagent Kit (Perfect Real Time; TaKaRa, Kyoto, Japan). Quantitative real-time PCR was performed on a CFX Connect Real-Time Detection System (Bio-Rad, Hercules, CA, USA) using SsoAdvanced Universal SYBR® Green Supermix (Bio-Rad). Conditions for the amplification were: 30 s at 95 °C and 40 cycles, each cycle at 95 °C for 5 s, and 60 °C for 30 s. The primer pairs for RT-qPCR were PVY (Fageria *et al.* 2013) and reference genes *Actin (Tac9)*, *L25 ribosomal protein, Ubiquitin-conjugating enzyme E2 (Ntubc2)* (Schmidt & Delaney, 2010). Primers are listed in Table S1.

Immunochemical methods

The amount of PVY^{NTN} virus (viral coat protein) in leaves was determined by indirect ELISA using a specific rabbit polyclonal primary antibody (1 μg·ml^{-1}) prepared in our laboratory (Cerovska 1998). Hsp70 and Hsp90.1 were also detected by indirect ELISA using rabbit primary antibody against polyclonal

cytoplasmic Hsp70 and Hsp90.1 (Agrisera, Vännäs, Sweden) product numbers AS08371 and AS08346) diluted 1:3000. Secondary polyclonal goat antibody against rabbit antibody conjugated with alkaline phosphatase (Sigma-Aldrich, St. Louis, MO, USA) was in both cases and diluted to 1:30,000. Hsp70 and Hsp90.1 isoforms were also immunochemically detected on nitrocellulose membranes (0.45 μm; Schleicher & Schuell, Dassel, Germany) after protein transfer from 12% gel following SDS electrophoresis (Laemmli 1970), loading 10 μg protein and visualized as described previously (Hyskova *et al.* 2017). In addition to antibody against cytoplasmic Hsp70, also the polyclonal chloroplastic (Agrisera; product no. AS08348), polyclonal mitochondrial (Agrisera; product no. AS08347) or against Hsp90.1, diluted according to the manufacturer's instructions, were used.

Analysis of phenolic acids

Salicylic acid, quinic acid (QA), chlorogenic acid (CGA) and ferulic acid were analysed by reversed-phase liquid chromatography coupled to electrospray mass spectrometry (LC-MS) (Agut *et al.* 2014). Briefly, 20 mg freeze-dried leaf sample were extracted with 1 ml 10% methanol containing 0.01% formic acid. The homogenate was shaken continuously for 1 h at room temperature, then centrifuged at 20,000 *g* for 30 min at 4 °C. The resulting supernatant was assayed with a LC system 1290 Infinity II (Agilent, Santa Clara, CA, USA) interfaced to Q-TOF maXis II (Bruker, Billerica, MA, USA). A Zorbax C18 reverse-phase silica-based column was used for separation (150 × 2.1 mm, 3.5 μm; Agilent). The compound quantities were compared with their respective standard curves. The standards were purchased from Sigma-Aldrich and Carl Roth (Karlsruhe, Germany).

Enzyme activity assays

For enzyme activity assays, plant tissue was homogenized in 100 mM Tris-HCl buffer (pH 7.8) containing 1 mM dithiothreitol, 1 mM EDTA and 5 mM $MgCl_2$. Then 0.02 $g \cdot ml^{-1}$ of PVP was added, and the homogenate centrifuged at 23,000 *g* for 15 min at 4 °C.

Phosphoenolpyruvate carboxylase (PEPC), NADP-ME and PPDK were determined according to our previous study (Ryslava *et al.* 2003). The activity of glycosidases (α-glucosidase, β-glucosidase, α-galactosidase, β-galactosidase, α-mannosidase and β-N-acetylhexosaminidase) was determined according to Belonoznikova *et al.* (2020). Soluble proteins were determined using the Bradford method (Bradford 1976).

Determination of total saccharide content

Leaf samples were ground in liquid N_2 and then in 50 mM Tris-HCl, 1 mM EDTA, 0.02 $g \cdot ml^{-1}$ PVP, pH 7.0. The homogenate was centrifuged at 20,000 *g* for 15 min at 4 °C. The resulting supernatant was used for total soluble saccharide content measurement. The pellet was resuspended in the extraction buffer and centrifuged under the same conditions. The supernatant was removed, and the resulting pellet was resuspended in the extraction buffer with 1 M NaCl. The suspension was centrifuged again, and the resulting supernatant was used for the measurement of membrane (ionically bound) saccharides.

The total saccharide content was measured according to the original method (Dubois *et al.* 1951).

Statistical analysis

Three biological replicates (100 plants each replicate, *i.e.* 20 per group) were performed. Leaf samples from the infected plants were taken at intervals of 1 h, 1 day, 7 days, 14 days, 21 and 28 days after the inoculation from the most developed leaves (upper leaves) in which symptoms of the systemic infection were emerging. Samples from the healthy plants were taken at the same time at the same leaf insertion level. All measurements were performed in triplicate, calculating standard deviations. Data were analysed by ANOVA (Holm-Sidak method) in SigmaPlot (San Jose, CA, USA) version 12, and differences were considered significant at $P \leq 0.05$. Different letters above each bar denote significant differences ($P \leq 0.05$) between plant groups according to one-way ANOVA. The same letters above a bar indicate that no significant differences were found between groups. Asterisks denote significant differences between individual groups subjected to stress treatment and the control group (C20): $***P \leq 0.001$, $**P \leq 0.01$, $*P \leq 0.05$.

RESULTS

Heat shock enhanced PVY^{NTN} amount and accelerated virus propagation

The consequences of heat shock and potyviral infection were compared for 28 days. The tobacco plants inoculated with PVY^{NTN} had necrotic middle veins and chlorotic, crinkled leaves with mosaic (Figure S1). Heat shock (2 h at 42 °C) was applied either before (42Y group) or after (Y42 group) PVY^{NTN} inoculation in comparison with inoculated plants without heat shock (Y20). The propagation of PVY^{NTN} was evaluated by quantification of viral RNA using RT-qPCR (Fig. 1A), which correlated with viral coat protein detected immunochemically with ELISA (Fig. 1B). During the first week, the relative virus content was low in all infected groups (42Y, Y42 and Y20). The onset of viral infection began on day 14, with 42Y significantly exceeding Y42 and Y20, which had twice and 2.4 times higher RNA content and 5.5 and 4.0 times higher coat protein, respectively. On day 21, the virus content peaked in Y42, where it was significantly higher than in Y20. Y20 plants exhibited the slowest viral development. Both groups treated with heat shock (42Y and Y42) showed earlier onset of viral infection. However, it seems that the order of heat shock application and viral inoculation did not play a crucial role (Fig. 1).

The content of cytosolic Hsp70 and stress induced Hsp90.1 was monitored using the ELISA test. Heat shock significantly increased cytosolic Hsp70 expression, especially in 42Y and C42 plants in the first week. One day after heat shock, the Hsp70 content was 5.8- and 5.9-fold higher in 42Y and C42 plants, respectively, than in C20 plants (Fig. 1C); while Y42 and Y20 plants showed 3.5- and 3.4-times higher Hsp70 content, respectively, than C20 plants 1 day after inoculation. Plant wounding during inoculation also plays a role in Hsp70 expression, as shown by the results of mock inoculation (Figure S2). C20 plants showed no change in Hsp70 content for 28 days, albeit sharply declining in all treated plants (Fig. 1C). Hsp90 was also increased by heat shock and virus application,

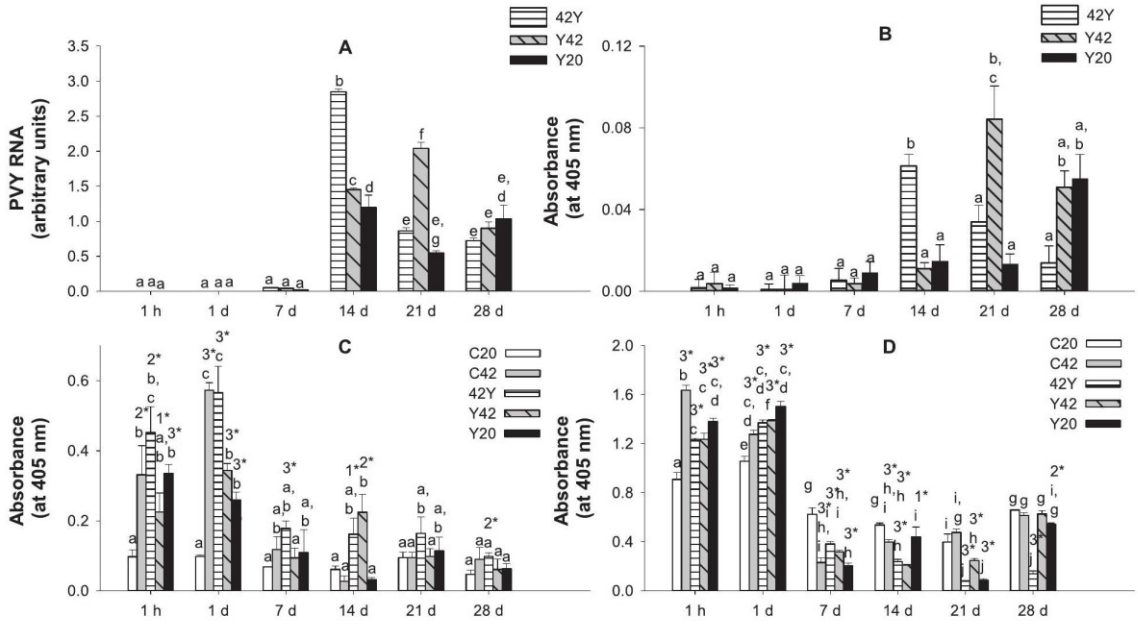


Fig. 1. Time course of relative content of PVY^{NTN} determined by RT-qPCR (A) and ELISA (B), content of cytosolic Hsp70 (C) and of Hsp90 (D) determined with ELISA. The relative content was determined in leaves of tobacco plants exposed to heat shock at 42 °C (C42), to combined stress induced by heat shock followed by PVY^{NTN} inoculation (42Y), to combined stress induced by PVY^{NTN} inoculation followed by heat shock at 42 °C (Y42), and to single stress induced by PVY^{NTN} (Y20) in comparison with non-inoculated controls grown at 20 °C (C20). Different letters above each bar denote significant differences ($P \leq 0.05$) between plant groups according to one-way ANOVA. The same letters above a bar indicate that no significant differences between groups. Asterisks denote significant differences between individual groups subjected to stress and the control group (C20): ***$P \leq 0.001$ (3*), **$P \leq 0.01$ (2*), *$P \leq 0.05$ (1*).

especially 1 h after stress: the relative content of Hsp90 in C42, 42Y, Y42 and Y20 plants was 1.8-,1.4-,1.4-, and 1.5-fold higher, respectively, than in C20 (Fig. 1D).

In order to provide detailed study of the presence of Hsp isoforms, Western blot detection was performed with antibodies against cytosolic, chloroplastic and mitochondrial Hsp70 and also Hsp90 (Figs 2 and 3 and Figure S2). The cytosolic Hsp70 antibody had one double band with molecular mass between ~75–100 kDa and also another double band corresponding to ~50–75 kDa. Whereas the ~75–100 kDa protein was most evident in plants exposed to heat shock, virus and mock inoculation (C42, 42Y, Y42, Y20, M42, 42M, C42) after 1 h and 1 day, and then disappeared after 7 days, the ~50–75 kDa protein was most visible after 28 days and also after 21 days (Fig. 2A, Figure S2). Moreover, the antibody against Hsp90 reacted with two protein forms: one ~90 kDa was most evident after 1 h and 1 day in all stressed plants, and the other ~150 kDa form was intense after 1 h and 1 day and then became weaker, but still present, until day 28 (Fig. 2B, Figure S2).

Chloroplastic isoforms of Hsp70 showed significant double bands in the range of 70 to 75 kDa, which were intense in plants treated with heat shock (C42, 42Y, Y42) and by mechanical wounding (application of PVY in 42Y, Y42, Y20; mock inoculation of 42M, M42, M20). After 7 days, these bands were visible only in plants C42 and partly in 42Y. In addition to these bands, lower molecular weight bands were also apparent, which are likely to be degradation products of chloroplast Hsp70 (Fig. 3A, Figure S2).

Mitochondrial isoforms of Hsp70 were detected in control plants as constitutively expressed, with molecular weights of ~100 and ~50 kDa. Both bands were more pronounced in plants treated with heat shock and mechanical wounding; in addition, bands with a molecular weight of about 70 kDa newly appeared. During viral infection, the proportion of ~100 kDa isoforms decreased and the proportion of ~50 kDa isoforms increased (Fig. 3B, Figure S2).

Virus caused a dramatic increase of SA and a decrease of QA

In all virus-infected plants, the signal molecule SA was significantly increased from day 7, reaching a maximum on day 14 and remaining high until day 28 of the experiment (up to 60-fold in Y42 plants compared to C20). Heat shock had no effect on SA induction (Fig. 4A). On the contrary, QA content decreased. Whereas in Y42 and Y20 plants the decline of QA content was apparent from day 1 and statistically significant from day 7 after inoculation, in 42Y plants the decrease of QA began later, from day 14 after inoculation. After 21 days in 42Y, Y42 and Y20 plants there was a decline in QA of 3.9-, 5.9- and 3.8-fold, respectively, compared to C20. QA contents in non-inoculated controls (C20 and C42) were similar and increased over time (Fig. 4B). Also, CGA content decreased dramatically, in this case from 1 h after stress application, and in response to both viral infection and heat shock. On most experimental days, CGA content was lowest in 42Y plants (Fig. 4C). According to two-way ANOVA, on days 14 to 28 of

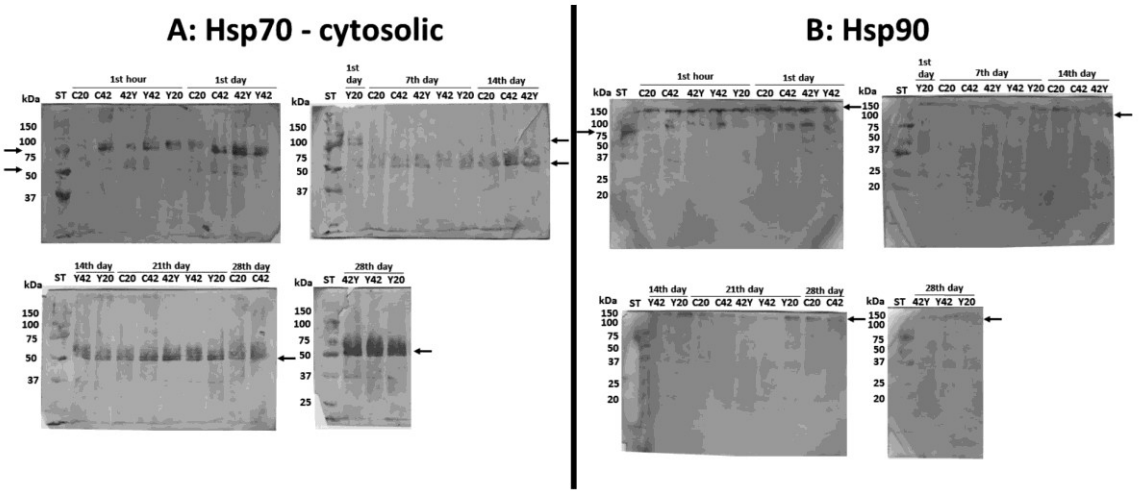


Fig. 2. Relative content of cytosolic Hsp70 (A) and Hsp90 (B) determined by immunoblot after SDS electrophoresis. The relative contents were determined in leaves of tobacco plants exposed to heat shock at 42 °C (C42), to combined stress induced by heat shock followed by PVY^{NTN} inoculation (42Y), to combined stress induced by PVY^{NTN} inoculation followed by heat shock at 42 °C (Y42), and to single stress induced by PVY^{NTN} (Y20) in comparison with non-inoculated controls grown at 20°C (C20). Mock-inoculated leaves (M) were also tested over 7 days (Figure S2). Arrows indicate main isoforms discussed.

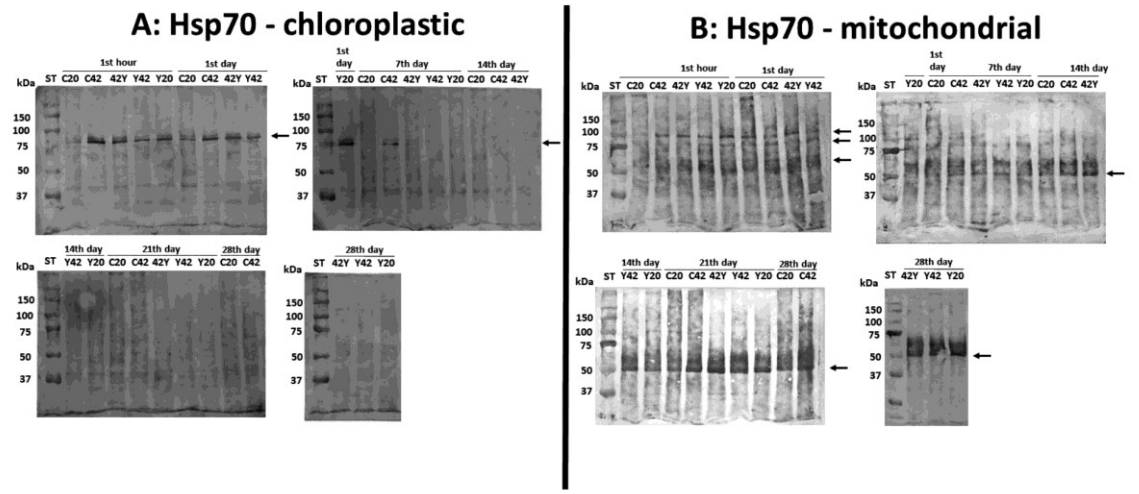


Fig. 3. Relative content of chloroplastic Hsp70 (A) and mitochondrial Hsp70 (B) determined by immunoblot after SDS electrophoresis. The relative contents were determined in leaves of tobacco plants exposed to heat shock at 42 °C (C42), to combined stress induced by heat shock followed by PVY^{NTN} inoculation (42Y), to combined stress induced by PVY^{NTN} inoculation followed by heat shock at 42 °C (Y42), and to single stress induced by PVY^{NTN} (Y20) in comparison with non-inoculated controls grown at 20 °C (C20). Mock-inoculated leaves (M) were also tested over 7 days (Figure S2). Arrows indicate main isoforms discussed.

the experiment, the statistical factor 'infection' affected the content of all three acids (SA, QA, CGA). In the case of CGA, the statistical factor 'heat shock' also applied and initially could interact with the factor 'infection' (Table S2). Interestingly, the content of ferulic acid was not detectable in C20 plants but was induced by both heat and viral stress. However, in C42 plants ferulic acid returned to a non-detectable concentration after 1 day; its content in viral-infected groups remained high at the same level to the end of experiment (day 28) (Figure S3).

Viral infection increased the activity of enzymes of the Hatch–Slack cycle

The activity of Hatch–Slack enzymes was enhanced in the period 14–28 days of the virus propagation (Figs 1 and 5, Table S2). The activity of NADP-ME was 8.6-, 5.8- and 4.9-fold higher in Y42, Y20 and 42Y plants, respectively, than in the control plants C42 and C20. Other Hatch–Slack enzymes, PEPC and PPDK, were also significantly induced; PEPC activity was 3.2-, 2.8- and 2.5-fold higher in 42Y, Y42 and Y20

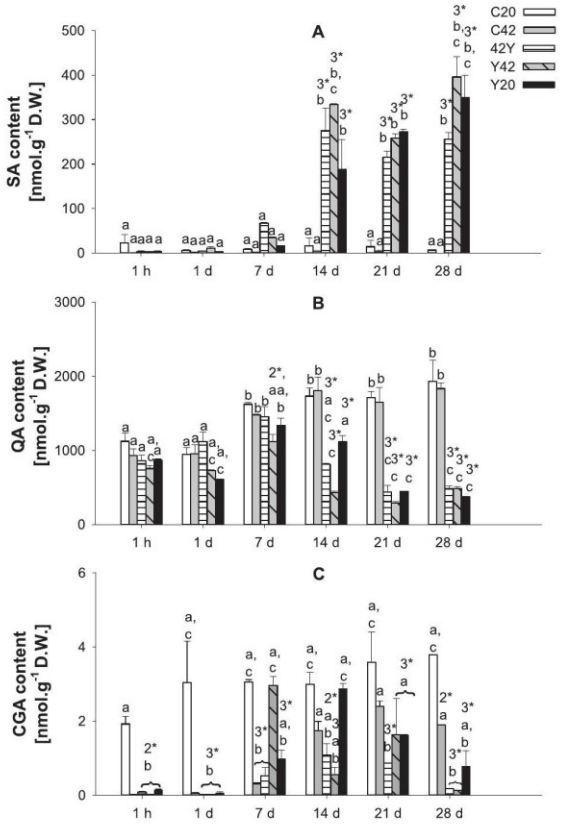


Fig. 4. Content of SA (A), QA (B) and CGA (C) in leaves of tobacco plants exposed to heat shock at 42 °C (C42), to combined stress induced by heat shock followed by PVY^{NTN} inoculation (42Y), to combined stress induced by PVY^{NTN} inoculation followed by heat shock at 42 °C (Y42), and to single stress induced by PVY^{NTN} (Y20) in comparison with non-inoculated controls grown at 20 °C (C20). Statistical symbols are explained in Fig. 1.

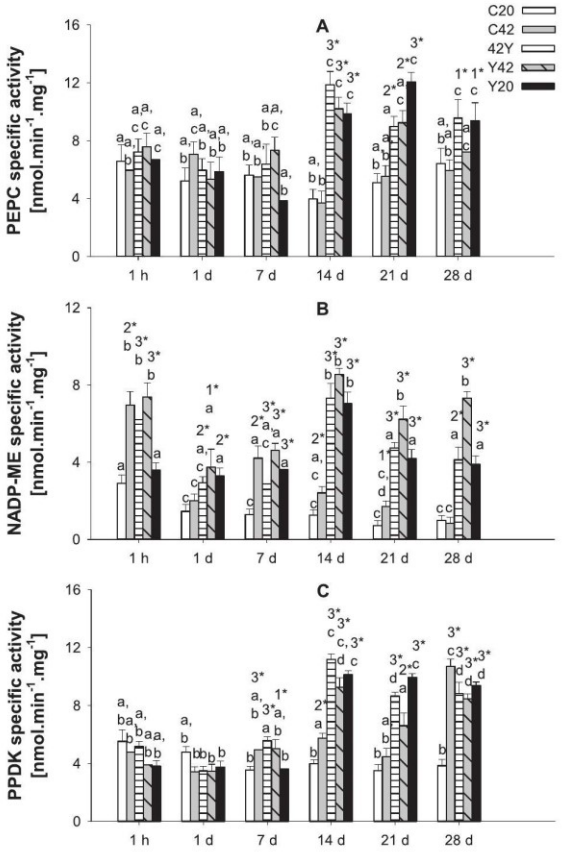


Fig. 5. Activity of enzymes of the Hatch–Slack cycle. PEPC (A), NADP-ME (B) and PPDK (C) activity in leaves of tobacco plants exposed to heat shock at 42 °C (C42), to combined stress induced by heat shock followed by PVY^{NTN} inoculation (42Y), to combined stress induced by PVY^{NTN} inoculation followed by heat shock at 42 °C (Y42), and to single stress induced by PVY^{NTN} (Y20) in comparison with non-inoculated controls grown at 20 °C (C20). Statistical symbols are explained in Fig. 1.

leaves, respectively, and PPDK activity was 2.8-, 2.0- and 1.6-fold higher in Y20, 42Y and Y42 plants, respectively, than in the control plants C42 and C20 (Fig. 5, Table S2).

Heat shock and viral infection induced activity of some glycosidases

Statistical analysis showed that the factor 'heat shock' at the beginning of the experiment significantly induced the activity of three enzymes in leaves, namely β-glucosidase, α-mannosidase and β-N-acetylhexosaminidase (Fig. 6B,E,F), whereas the factor 'infection' only significantly induced activity of β-glucosidase (Table S2). Heat shock caused a 3.6–4.6-fold increase in β-glucosidase activity 1 h after the treatment, and viral infection caused a 2.3-fold increase in comparison with control C20 plants (Fig. 6B). This increase may be due to mechanical stress; activity of β-glucosidase (and α-mannosidase) was also induced in mock inoculated plants, but only after 1h, after which the activities were similar to C20 plants (data not shown). Activity of α- and β-galactosidase and β-N-acetylhexosaminidase was not affected by mock inoculation. The heat shock-induced increase of α-mannosidase and β-N-acetylhexosaminidase activity in the treated plants was 1.7–2.0-fold higher than that in C20 plants, depending on the plant group (C42, 42Y, Y42) (Fig. 6E,F).

Furthermore, in 42Y and Y42, the activity of β-glucosidase and β-galactosidase was significantly stimulated on days 14 and 28. After 28 days, β-glucosidase activity was 7.2-, 7.0-, and 1.4-fold higher in 42Y, Y42, and Y20 plants, respectively, than in the control plants C42 and C20 (Fig. 6, Table S2). On day 14, Y20 plants exhibited the highest α-glucosidase activity, which was 4.2-fold higher in these plants than in C20 controls. In 42Y and Y42 plants, α-glucosidase activity increased 3.2- and 2.8-fold, respectively, in comparison with C42 controls. Moreover, β-N-acetylhexosaminidase and α-mannosidase showed the highest increase in activity in Y42 plants (3.3-fold increase compared to C20). In turn, α-galactosidase showed a similar increase in activity in Y42, 42Y and Y20 plants (3.9-, 3-, 2.8-fold, respectively) in comparison with the relevant controls (Fig. 6, Table S2).

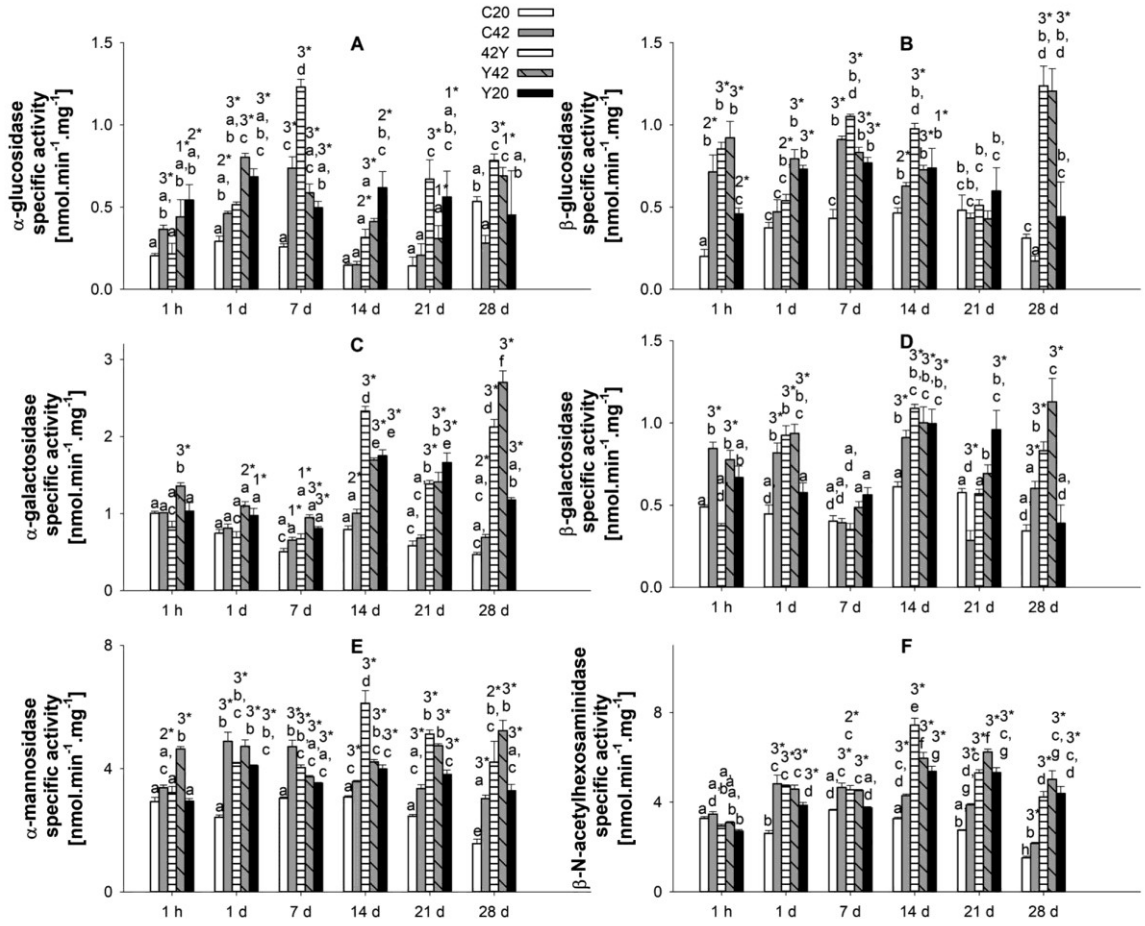


Fig. 6. Activity of glycosidases in leaves of tobacco plants exposed to heat shock at 42 °C (C42), to combined stress induced by heat shock followed by PVY^{NTN} inoculation (42Y), to combined stress induced by PVY^{NTN} inoculation followed by heat shock at 42 °C (Y42), and to single stress induced by PVY^{NTN} (Y20) in comparison with non-inoculated controls grown at 20°C (C20). Statistical symbols are explained in Fig. 1.

Saccharide content in treated plants

Total saccharide content determined with the Dubois method showed that all plant groups increased the content of soluble saccharides during the 28 days of the experiments (C20 plants up to 2.5-fold). On any particular experimental day, stressed plants were mostly comparable. The highest content of soluble saccharides was determined in the 42Y group on day 21 (Fig. 7A). Similarly, the highest content of insoluble, membrane-bound saccharides was in 42Y, namely on days 14 and 21 (Fig. 7B).

DISCUSSION

Many factors affect virus multiplication and penetration of plant cells, and the ability of plants to activate defence reactions and to prevent virus propagation. The balance between the success of a virus and that of a plant depends on the plant species, its health and developmental stage, on the virus species and strain and on abiotic factors, including temperature.

Whereas Hsp70 synthesis under abiotic stress conditions is associated with positive effects on plants, in virus-infected plants Hsp70 can have negative effects because viruses usually recruit host Hsp70 for almost all steps of the viral cycle, *e.g.* for RNA-dependent RNA polymerase (Dufresne *et al.* 2008; Mine *et al.* 2012; Pogany & Nagy 2015; Yang *et al.* 2017). In turn, an increase in temperature boosts the defence response (RNA silencing) in *Nicotiana benthamiana* plants infected with *Tobacco ringspot virus* (Szittya *et al.* 2003).

Proposed functions of Hsp70 and Hsp90 in potyviral propagation in tobacco plants

In this study, we assessed the effect of heat shock both before and after inoculating tobacco plants with PVY^{NTN}. After 21 days of the experiment, PVY^{NTN} amount was higher in plants exposed to heat shock (42Y and Y42) than in Y20 grown at a constant temperature (Fig. 1A,B). Thus, Hsp70 protein could facilitate the propagation of viral particles

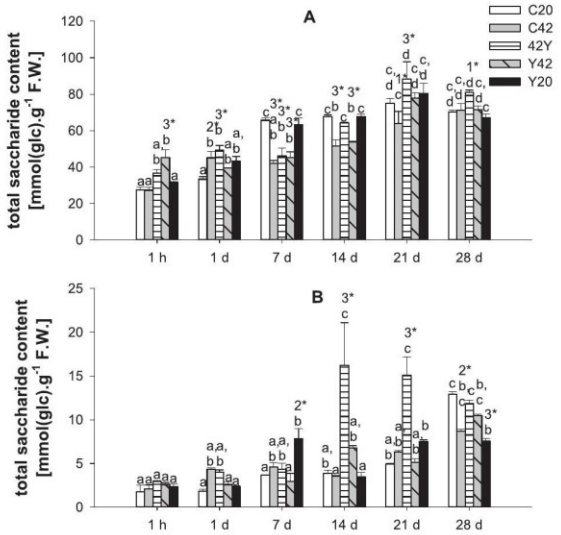


Fig. 7. Total saccharide content in leaves of tobacco plants exposed to heat shock at 42 °C (C42), to combined stress induced by heat shock followed by PVY^{NTN} inoculation (42Y), to combined stress induced by PVY^{NTN} inoculation followed by heat shock at 42 °C (Y42), and to single stress induced by PVY^{NTN} (Y20) in comparison with noninoculated controls grown at 20 °C (C20). The total soluble saccharide (A) and membrane (ionically bound) saccharide contents (B) were measured. Symbols of statistical analysis are explained in Fig. 1.

(Fig. 1), as found in other model systems mentioned above. The heat shock applied to plants both before and after PVY^{NTN} inoculation increased the amount of Hsp70 and Hsp90 proteins, namely within the first 24 h of the experiment. In addition to heat shock alone, mock inoculation increased the amount of Hsp70 and Hsp90 proteins in plants, primarily after 1 h and 1 day. Therefore, the expression of Hsp at the beginning of experiment is rather related to mechanical than viral stress (Fig. 1, Figure S2). In plants exposed to combined stress, the increase in Hsp70 due to heat shock may help to accelerate the propagation of viral particles (Figs 1–3 and Figure S2). In particular, Hsp70 may be involved in the synthesis of viral particles and in their propagation in plants. In *Arabidopsis*, it was found out that under normal conditions heat shock transcription factors (HSF) are associated with the Hsp90/Hsp70 complex. During the stress, the chaperones switch to the binding of damaged proteins and release HSF, which trigger gene expression of Hsp and several HSF (Kozeko 2019). In our experiment, intense ~150 kDa protein apparent in all plant groups mainly at 1 h and 1 day could correspond to Hsp90/Hp70 complex. Its loss in the following days in infected plants could indicate that the dimer complex is dissociated, and plants encounter stress (Fig. 2B). In addition, Hsp70 cytosolic, chloroplastic and mitochondrial isoforms and stress-induced Hsp90-1 were significantly increased due to heat shock immediately after inoculation, and then declined. But cytosolic and mitochondrial isoforms with lower molecular weight (~50–75 kDa) persist throughout the viral infection (Figs 2 and 3).

Interpretation of Hsp70 immunochemical detection in the genomic context

Genome analysis of *N. tabacum* revealed 61 members with molecular weight ranging from 12.58 to 99.88 kDa (Song *et al.* 2019). It is still difficult to determine which of the genes are involved in the various Hsp functions. Many factors control the transcription of individual Hsp. In the promoter region of tobacco Hsp70, at least 16 *cis* regulatory elements, including SA response elements, stress-induced component and light control elements, were identified (Song *et al.* 2019). The level of SA increases during viral infection, including PVY^{NTN} infection (Fig. 4A). Thus, proteins in the 60–75 kDa region of cytosolic Hsp70 at the time of fully developed viral infection may be NtHsp70-23 and NtHsp70-35 (Fig. 2A).

According to Song *et al.* (2019), heat shock induces transcription of seven genes, in addition to NtHsp70-35 also induced by SA, this includes the NtHsp70-30 gene and other genes from group I with higher molecular weights (84–94 kDa). At the beginning of the experiment, when the virus is applied, it is wounding that is associated with the two Hsp70 genes located in the endoplasmic reticulum and the NtHsp70-56 gene, which is also associated with heat shock (Song *et al.* 2019).

Chloroplastic Hsp70 are encoded by four genes, NtHsp70 46 to 49, which serve primarily as a protection for the photosynthetic apparatus Song *et al.* (2019). Isoforms of Hsp70 located in chloroplasts were induced in our experiments by heat shock and/or by mechanical wounding caused by virus application (Fig. 3A, Figure S2). The mitochondrial isoforms are encoded by six genes with a molecular weight of 12–73 kDa. The molecular weights of mitochondrial Hsp70 detected in control plants were around ~100 kDa and ~50 kDa, which could correspond to NtHsp70-42, –43 or a degradation product of 73 kDa molecules. The higher molecular weight may be complexed with some Hsp70 isoforms (Fig. 3B, Figure S2).

Possible interaction between depletion of QA and CGA as defence compounds and the viral spread

Generally, under stress conditions, plants adjust their metabolism. From our previous work, it was concluded that tobacco systemic response during PVY^{NTN} infection involved the induction of SA, accumulation of H_2O_2 and that viral infection affected plant photosynthesis, carbohydrate metabolism and the synthesis of anti-oxidative stress agents, as well as other metabolic pathways, such as the Hatch–Slack cycle (Ryslava *et al.* 2003; Synkova *et al.* 2006; Doubnerova *et al.* 2007; Muller *et al.* 2009; Spoustova *et al.* 2015). Primary metabolism, phenylpropanoids and antioxidant pathways in PVY-infected potato plants have also been studied (Kogovsek *et al.* 2016). Interestingly, the potato cultivar resistant to PVY was also thermotolerant, and Hsp70 increased only at elevated temperature and not due to viral infection. The expression of Hsp90 correlates with different sensitivities to heat stress (Makarova *et al.* 2018).

Salicylic acid (SA) functions as a natural induction signal that affects pathogenesis-related proteins upon infection. Resistant cultivars have many times higher SA concentrations than susceptible cultivars, as in the case of tobacco infected with PVY or *tobacco mosaic virus* (Malamy *et al.* 1990; Spoustova *et al.* 2015). In PVY^{NTN}-infected tobacco there was no difference in the SA level due to application

of heat shock but there was a positive correlation with infection (Fig. 4A, Table S2). CGA are powerful antioxidants synthesized *in planta via* the phenylpropanoid pathway and by esterification of dihydroxycinnamic acid (*e.g.* caffeic acid, ferulic acid) with QA. The amounts of phenolic acids seem to correlate with their function in defence. Metabolism of CGA is related to biosynthesis of lignans, and lignin and acyl-quinic acids may have possible links to phytohormone-activating defence signalling networks and might act as defence metabolites (Clifford *et al.* 2017). Transgenic tobacco plants with inhibited acyl-quinic biosynthesis were more susceptible to oxidative damage and had accelerated cell death (Tamagnone *et al.* 1998; Clifford *et al.* 2017). In this study, depletion of QA and CGA (Fig. 4B,C, Table S2) and, on the contrary, induction of ferulic acid (Figure S3) indicates the impact of viral infection (alone or combined with heat shock) on metabolism of CGA as defence compounds. In the case of CGA, we found an interaction between heat shock and infection (Table S2A). Interestingly, the lowest concentrations of CGA during most experimental days were in 42Y, the plant group with the highest PVY^{NTN} and high Hsp70 (Figs 1 and 4C). It is possible, that the early depletion of QA in Y20 and Y42 (Fig. 4B) is related to the synthesis of CGA as defence compounds against PVY^{NTN} in the period between 7 and 21 days. The long-term increased concentration of ferulic acid in the viral-infected group, in contrast to the C42 group, which after 1 day returned to non-detectable value as in C20 controls, may indicate its function as a lignin precursor (Figure S3). Higher content of lignin in PVY^{NTN}-infected tobacco plants than in non-inoculated controls have been found previously (Spoustova *et al.* 2015).

Activities of Hatch–Slack enzymes as markers of potyviral infection were not further increased by heat shock

As previously confirmed, enzymes of the Hatch–Slack cycle are markers of PVY^{NTN} infection in *N. tabacum* (Ryslava *et al.* 2003; Doubnerova *et al.* 2007; Doubnerova & Ryslava 2011; Spoustova *et al.* 2015). As a result of viral infection in tobacco plants, the enzyme activity of PEPC, NADP-ME and PPDK increased in all groups of infected plants (Y42, 42Y and Y20), especially 14–28 days after inoculation (Fig. 5). The results show a significant increase in both combined (Y42, 42Y) and single (Y20) stress groups. However, there was no apparent synergistic effect of combined stress as similar enzyme activities were found in all infected plants (Fig. 5, Table S2). In tobacco plants under stress induced by PVY^{NTN}, NADP-ME is regulated at the *de novo* synthesis level, whereas PEPC and PPDK are regulated *via* phosphorylation by specific kinases (Chastain *et al.* 2008; Doubnerova *et al.* 2009; Muller *et al.* 2009); however, their involvement in signalling cascades of defence reactions remains unknown. Heat shock alone increased NADP-ME activity in tobacco plants 1 h and 1 week after the treatment (Fig. 5B).

Carbohydrate metabolism in plants is a very dynamic process. Carbohydrates are synthesized by photosynthesis, transported to other parts of the plant (sink), converted into intermediates for the synthesis of many other compounds, and degraded from storage polysaccharides and other glycoconjugates. It seems that a high content of virus corresponds to a high saccharide content, especially in 42Y group (Figs 1 and 7).

Suggested roles of glycosidases during heat shock and viral stress

Glycosidases contribute to the saccharide pool *via* glycoconjugate degradation. The results of our experiments indicate that both viral infection and heat shock increased some glycosidase activity in tobacco leaves (Fig. 6, Table S2). Both α- and β-glucosidases contribute to the levels of free glucose through degradation of starch, maltose and cellulose and β-glucan, respectively. On days 1 and 7, their activities increased in all treatment groups. β-Glucosidase could affect cell wall metabolism and/or degradation of glucosylated phytohormones, which could be quickly activated. Phenolic compounds, including flavonoids, are important antioxidants involved in defence responses and can be de-glucosylated. α-Galactosidase can hydrolyse terminal galactose from glycoproteins and oligosaccharides of the raffinose family (Sengupta *et al.* 2015). Our results also showed enhanced α-galactosidase, α-mannosidase, β-N-acetylhexosaminidase and α-glucosidase activity when viral proteins accumulated in the plants (Fig. 6, Table S2). β-Galactosidase can participate in cell wall remodelling, hydrolysing galactoglucans. The role of α-mannosidase is particularly important for oligosaccharide chain processing in glycoproteins (Strasser 2016); both heat shock and viral infection could also affect this process. Although β-N-acetylhexosaminidase shows relatively high activity in tobacco leaves, its function, and hence its substrates, in plants are not entirely clear (Ryslava *et al.* 2014). Chitooligosaccharides do not occur in plant metabolism, but chitinases are important for pathogenesis-related proteins synthesized in response to biotic stress. Even application of chitosan alone can induce defence responses in plants. Chitinases protect plants primarily from fungal pathogens, but they are also synthesized during infections associated with SA signalling (Ali *et al.* 2018). Thus, increased β-N-acetylhexosaminidase activity during a viral infection could have a similar function to that of a pathogenesis-related protein, although N-acetylglucosamine hydrolysis in glycoproteins and synthesis of paucimannosidic oligosaccharides may also be related to viral infection.

CONCLUSIONS

- Heat shock before or after inoculation of tobacco plants with PVY^{NTN} accelerated the propagation of infection. The virus content was positively correlated with SA and CGA but was negatively correlated with QA.
- Cytosolic, chloroplastic and mitochondrial Hsp70 and Hsp90.1 isoforms were induced during the first week after heat shock and virus inoculation. The lower weight cytosolic and mitochondrial Hsp70 (~50–75 kDa) persist throughout the viral infection.
- Viral infection increased the SA content and activity of Hatch–Slack enzymes, but there was no synergistic reaction with heat shock.
- Shortly after heat shock, β-glucosidase, α-mannosidase and β-N-acetylhexosaminidase activities were induced. In the viral phase (14–28 days), PVY^{NTN} infection induced α-galactosidase, α-mannosidase, β-N-acetylhexosaminidase and α-glucosidase activities.

AUTHORS CONTRIBUTIONS

VH collected and plotted the data, performed statistical analysis, and wrote the manuscript. VD, KB, DK, SG and SH performed experiments. HS, HR and NČ conceived, designed and supervised the study, provided the materials and wrote and edited the manuscript.

FUNDING

This work was supported by the Charles University, projects SVV260427/2020 and GA UK No. 1304119. This work was further supported by the Ministry of Education, Youth and Sports of CR through the European Regional Development Fund Project "Centre for Experimental Plant Biology": No. CZ.02.1.01/0.0/0.0/16_019/0000738.

ACKNOWLEDGEMENT

The authors thank to Dr. Carlos V. Melo for English proof reading.

CONFLICT OF INTEREST

The authors declare no conflict of interest.

SUPPORTING INFORMATION

Additional supporting information may be found online in the Supporting Information section at the end of the article.

Figure S1. The tobacco plants after 14 days of cultivation. Control (A) and PVY^{NTN} inoculated (B) plants.

Figure S2. Relative content of cytosolic Hsp70 (A), Hsp90 (B), chloroplastic Hsp70 (C), and mitochondrial Hsp70 (D) determined by immunoblot after SDS-electrophoresis. The relative contents were determined in leaves of mock-inoculated tobacco plants exposed to combined stress induced by mock-inoculation followed by heat shock at 42 °C (M42), to combined stress induced by heat shock followed by mock-inoculation (42M), and to single stress induced by mock-inoculation (M) in comparison with controls exposed to heat shock (C42). Arrows indicated main isoforms, which are discussed.

Figure S3. The content of ferulic acid in leaves of tobacco plants exposed to heat shock at 42 °C (C42), to combined stress induced by heat shock followed by PVY^{NTN} inoculation (42Y), and to combined stress induced by PVY^{NTN} inoculation followed by heat shock at 42 °C (Y42) in comparison with non-inoculated controls grown at 20 °C (C20). Different letters above each bar denote significant differences ($P \leq 0.05$) between plant groups according to one way-ANOVA. The same letters above a bar indicate that no significant differences were found between groups. Asterisks denote significant differences between individual groups subjected to stress and the control group (C20), 3*, 2*,1* stands for $P \leq 0.001$, $P \leq 0.01$, and $P \leq 0.05$, respectively.

Table S1. The primer pairs for RT-qPCR were PVY, and reference genes Actin (Tac9), L25 ribosomal protein, Ubiquitin-conjugating enzyme E2 (Ntubc2).

Table S2. (A) Two way-ANOVA statistical analysis of the results 1 h–7 days. (B) Two way-ANOVA statistical analysis of the results 14–28 days.

REFERENCES

Achachi A., Ait Barka E., Ibriz M. (2014) Recent advances in *Citrus psorosis* virus. *VirusDisease*, **25**, 261–276.

Agut B., Gamir J., Jacas J.A., Hurtado M., Flors V. (2014) Different metabolic and genetic responses in citrus may explain relative susceptibility to *Tetranychus urticae*. *Pest Management Science*, **70**, 1728–1741.

Ali S., Ganai B.A., Kamili A.N., Bhat A.A., Mir Z.A., Bhat J.A., Tyagi A., Islam S.T., Mushtaq M., Yadav P., Rawat S., Grover A. (2018) Pathogenesis-related proteins and peptides as promising tools for engineering plants with multiple stress tolerance. *Microbiological Research*, **212–213**, 29–37.

Anaraki Z.E., Tafreshi S.A.H., Shariati M. (2018) Transient silencing of heat shock proteins showed remarkable roles for HSP70 during adaptation to stress in plants. *Environmental and Experimental Botany*, **155**, 142–157.

Belonoznikova K., Vaverova K., Vanek T., Kolarik M., Hyskova V., Vankova R., Dobrev P., Krizek T., Hodek O., Cokrtova K., Stipek A., Ryslava H. (2020) Novel insights into the effect of *Pythium* strains on rapeseed metabolism. *Microorganisms*, **8**, 1472.

Bradford M.M. (1976) A rapid and sensitive method for the quantitation of microgram quantities of protein utilizing the principle of protein–dye binding. *Analytical Biochemistry*, **72**, 248–254.

Carrington J.C., Kasschau K.D., Mahajan S.K., Schaad M.C. (1996) Cell-to-cell and long-distance transport of viruses in plants. *The Plant Cell*, **8**, 1669–1681.

Cerovska N. (1998) Production of monoclonal antibodies to potato virus YNTN strain and their use for strain differentiation. *Plant Pathology*, **47**, 505–509.

Chastain C.J., Xu W., Parsley K., Sarath G., Hibberd J.M., Chollet R. (2008) The pyruvate, orthophosphate dikinase regulatory proteins of Arabidopsis possess a novel, unprecedented Ser/Thr protein kinase primary structure. *The Plant Journal*, **53**, 854–863.

Chen Z., Zhou T., Wu X., Hong Y., Fan Z., Li H. (2008) Influence of cytoplasmic heat shock protein 70 on viral infection of *Nicotiana benthamiana*. *Molecular Plant Pathology*, **9**, 809–817.

Clifford M.N., Jaganath I.B., Ludwig I.A., Crozier A. (2017) Chlorogenic acids and the acyl-quinic acids: discovery, biosynthesis, bioavailability and bioactivity. *Natural Product Reports*, **34**, 1391–1421.

Doubnerova V., Janoskova M., Synkova H., Subr Z., Cerovska N., Ryslava H. (2007) Effect of *Potato virus Y* on activities of antioxidant and anapleurotic enzymes in transgenic *Nicotiana tabacum* L. plants with the gene for P_3 protein *General and Applied. Plant Physiology*, **33**, 123–140.

Doubnerova V., Muller K., Cerovska N., Synkova H., Spoustova P., Ryslava H. (2009) Effect of *Potato Virus Y* on the NADP-malic enzyme from *Nicotiana tabacum* L.: mRNA, expressed protein and activity. *International Journal of Molecular Science*, **10**, 3583–3598.

Doubnerova V., Ryslava H. (2011) What can enzymes of C_4 photosynthesis do for C_3 plants under stress? *Plant Science*, **180**, 575–583.

Doubnerova V., Ryslava H. (2014) Roles of Hsp70 in plant abiotic stress. In: Gaur R.K., Sharma P. (Eds), *Molecular approaches in plant abiotic stress*. CRC Press, Boca Raton, FL, USA, pp 44–66.

Dubois M., Gilles K., Hamilton J.K., Rebers P.A., Smith F. (1951) A colorimetric method for the determination of sugars. *Nature*, **168**, 167.

Dufresne P.J., Thivierge K., Cotton S., Beauchemin C., Ide C., Ubalijoro E., Laliberte J.F., Fortin M.G. (2008) Heat shock 70 protein interaction with *Turnip mosaic virus* RNA-dependent RNA polymerase within virus-induced membrane vesicles. *Virology*, **374**, 217–227.

Fageria M.S., Singh M., Nanayakkara U., Pelletier Y., Nie X., Wattie D. (2013) Monitoring current-season spread of *Potato virus Y* in potato fields using ELISA and Real-Time RT-PCR. *Plant Disease*, **97**, 641–644.

Gaffar F.Y., Koch A. (2019) Catch me if you can! RNA silencing-based improvement of antiviral plant immunity. *Viruses*, **11**, 673.

Gorovits R., Czosnek H. (2017) The involvement of heat shock proteins in the establishment of *Tomato yellow leaf curl virus* infection. *Frontiers in Plant Science*, **8**, 355.

Hafren A., Hofius D., Ronnholm G., Sonnewald U., Makinen K. (2010) HSP70 and its cochaperone CPIP

promote *Potyvirus* infection in *Nicotiana benthamiana* by regulating viral coat protein functions. *The Plant Cell*, **22**, 523–535.

Heinlein M. (2015) Plasmodesmata: channels for viruses on the move. *Methods in Molecular Biology*, **1217**, 25–52.

Hofius D., Maier A.T., Dietrich C., Jungkunz I., Bornke F., Maiss E., Sonnewald U. (2007) Capsid protein-mediated recruitment of host DnaJ-Like proteins is required for *Potato virus Y* infection in tobacco plants. *Journal of Virology*, **81**, 11870–11880.

Hyskova V., Pliskova V., Cerveny V., Ryslava H. (2017) NADP-dependent enzymes are involved in response to salt and hypoosmotic stress in cucumber plants. *General Physiology and Biophysics*, **36**, 247–258.

Jiang S., Lu Y., Li K., Lin L., Zheng H., Yan F., Chen J. (2014) Heat shock protein 70 is necessary for *Rice stripe virus* infection in plants. *Molecular Plant Pathology*, **15**, 907–917.

Jungkunz I., Link K., Vogel F., Voll L.M., Sonnewald S., Sonnewald U. (2011) AtHsp70-15-deficient *Arabidopsis* plants are characterized by reduced growth, a constitutive cytosolic protein response and enhanced resistance to TuMV. *The Plant Journal*, **66**, 983–995.

Kogovsek P., Pompe-Novak M., Petek M., Fragner L., Weckwerth W., Gruden K. (2016) Primary metabolism, phenylpropanoids and antioxidant pathways are regulated in potato as a response to *Potato virus Y* infection. *PLOS One*, **11**, e0146135.

Kozeko L.Y. (2019) The role of HSP90 chaperones in stability and plasticity of ontogenesis of plants under normal and stressful conditions (*Arabidopsis thaliana*). *Cytology and Genetics*, **53**, 143–161.

Kwon Y., Kabir M.A., Wang H.W., Karuppanapandian T., Monn J.-C., Ryu K.H., Lee G.P., Kim W. (2012) Elimination of *Pepper mild mottle virus* from infected tobacco (*Nicotiana benthamiana* L.) plants by callus culture and the sieving technique. *Vitro Cellular & Developmental Biology - Plant*, **48**, 595–599.

Laemmli U.K. (1970) Cleavage of structural proteins during assembly of head of bacteriophage-T4. *Nature*, **227**, 680–685.

Lin B.L., Wang J.S., Liu H.C., Chen R.W., Meyer Y., Barakat A., Delseny M. (2001) Genomic analysis of the Hsp70 superfamily in *Arabidopsis thaliana*. *Cell Stress and Chaperones*, **6**, 201–208.

Ludwig-Muller J. (2011) Auxin conjugates: their role for plant development and in the evolution of land plants. *Journal of Experimental Botany*, **62**, 1757–1773.

Makarova S., Makhotenko A., Spechenkova N., Love A.J., Kalinina N.O., Taliansky M. (2018) Interactive responses of potato (*Solanum tuberosum* L.) plants to heat stress and infection with *Potato Virus Y*. *Frontiers in Microbiology*, **9**, 2582.

Malamy J., Carr J.P., Klessig D.F., Raskin I. (1990) Salicylic acid: a likely endogenous signal in the resistance response of tobacco to viral infection. *Science*, **250**, 1002–1004.

Mayer M.P., Bukau B. (2005) Hsp70 chaperones: cellular functions and molecular mechanism. *Cellular and Molecular Life Sciences*, **62**, 670–684.

Mine A., Hyodo K., Tajima Y., Kusumanegara K., Taniguchi T., Kaido M., Mise K., Taniguchi H., Okuno T. (2012) Differential roles of Hsp70 and Hsp90 in the assembly of the replicase complex of a positive-strand RNA plant virus. *Journal of Virology*, **86**, 12091–12104.

Muller K., Doubnerova V., Synkova H., Cerovska N., Ryslava H. (2009) Regulation of phosphoenolpyruvate carboxylase in PVY^{NTN}-infected tobacco plants. *Biological Chemistry*, **390**, 245–251.

Nagy P.D., Wang R.Y., Pogany J., Hafren A., Makinen K. (2011) Emerging picture of host chaperone and cyclophilin roles in RNA virus replication. *Virology*, **411**, 374–382.

Park C.J., Seo Y.S. (2015) Heat shock proteins: a review of the molecular chaperones for plant immunity. *The Plant Pathology Journal*, **31**, 323–333.

Pogany J., Nagy P.D. (2015) Activation of *Tomato bushy stunt virus* RNA-dependent RNA polymerase by cellular heat shock protein 70 is enhanced by phospholipids *in vitro*. *Journal of Virology*, **89**, 5714–5723.

Ryslava H., Holakovská B., Trefancová J., Doubnerova V., Spoustova P., Synkova H., Cerovska N. (2009) The activity of glycosidases in tobacco leaves under stress conditions, 34th Congress of the Federation-of-European-Biochemical-Societies. Prague. *FEBS Journal*, **276**, 24.

Ryslava H., Muller K., Semoradova S., Synkova H., Cerovska N. (2003) Photosynthesis and activity of phosphoenolpyruvate carboxylase in *Nicotiana tabacum* L. leaves infected by *Potato virus A* and *Potato virus Y*. *Photosynthetica*, **41**, 357–363.

Ryslava H., Pomeislova A., Psondrova S., Hyskova V., Smrcek S. (2015) Phytoremediation of carbamazepine and its metabolite 10,11-epoxycarbamazepine by C_3 and C_4 plants. *Environmental Science and Pollution Research*, **22**, 20271–20282.

Ryslava H., Valenta R., Hyskova V., Krizek T., Liberda J., Coufal P. (2014) Purification and enzymatic characterization of tobacco leaf beta-N-acetylhexosaminidase. *Biochimie*, **107**, 263–269.

Sarkar N.K., Kundnani P., Grover A. (2013) Functional analysis of Hsp70 superfamily proteins of rice (*Oryza sativa*). *Cell Stress and Chaperones*, **18**, 427–437.

Schmidt G.W., Delaney S.K. (2010) Stable internal reference genes for normalization of real-time RT-PCR in tobacco (*Nicotiana tabacum*) during development and abiotic stress. *Molecular Genetics and Genomics*, **283**, 233–241.

Schnablova R., Synkova H., Vicankova A., Burketova L., Eder J., Cvikrova M. (2006) Transgenic *ipt* tobacco overproducing cytokinins overaccumulates phenolic compounds during *in vitro* growth. *Plant Physiology and Biochemistry*, **44**, 526–534.

Sengupta S., Mukherjee S., Basak P., Majumder A.L. (2015) Significance of galactinol and raffinose family oligosaccharide synthesis in plants. *Frontiers in Plant Science*, **6**, 656.

Slamova K., Kapesova J., Valentova K. (2018) "Sweet flavonoids": glycosidase-catalyzed modifications. *International Journal of Molecular Sciences*, **19**, 2126.

Song Z., Pan F., Lou X., Wang D., Yang C., Zhang B., Zhang H. (2019) Genome-wide identification and characterization of Hsp70 gene family in *Nicotiana tabacum*. *Molecular Biology Reports*, **46**, 1941–1954.

Spoustova P., Hyskova V., Muller K., Schnablova R., Ryslava H., Cerovska N., Malbeck J., Cvikrova M., Synkova H. (2015) Tobacco susceptibility to *Potato virus Y*-NTN infection is affected by grafting and endogenous cytokinin content. *Plant Science*, **235**, 25–36.

Strasser R. (2016) Plant protein glycosylation. *Glycobiology*, **26**, 926–939.

Su P.H., Li H.M. (2008) Arabidopsis stromal 70-kD heat shock proteins are essential for plant development and important for thermotolerance of germinating seeds. *Plant Physiology*, **146**, 1231–1241.

Sugio A., Dreos R., Aparicio F., Maule A.J. (2009) The cytosolic protein response as a subcomponent of the wider heat shock response in Arabidopsis. *The Plant Cell*, **21**, 642–654.

Synkova H., Semoradova S., Schnablova R., Muller K., Pospisilova J., Ryslava H., Malbeck J., Cerovska N. (2006) Effects of biotic stress caused by *Potato virus Y* on photosynthesis in *ipt* transgenic and control *Nicotiana tabacum* L. *Plant Science*, **171**, 607–616.

Szittya G., Silhavy D., Molnar A., Havelda Z., Lovas A., Lakatos L., Banfalvi Z., Burgyan J. (2003) Low temperature inhibits RNA silencing-mediated defence by the control of siRNA generation. *EMBO Journal*, **22**, 633–640.

Tamagnone L., Merida A., Stacey N., Plaskitt K., Parr A., Chang C.F., Lynn D., Dow J.M., Roberts K., Martin C. (1998) Inhibition of phenolic acid metabolism results in precocious cell death and altered cell morphology in leaves of transgenic tobacco plants. *The Plant Cell*, **10**, 1801–1816.

Tan R., Wang L., Hong N., Wang G. (2010) Enhanced efficiency of virus eradication following thermotherapy of shoot-tip cultures of pear. *Plant, Cell, Tissue and Organ Culture*, **101**, 229–235.

Usman M.G., Rafii M.Y., Martini M.Y., Yusuff O.A., Ismail M.R., Miah G. (2017) Molecular analysis of Hsp70 mechanisms in plants and their function in response to stress. *Biotechnology & Genetic Engineering Reviews*, **33**, 26–39.

Verchot J. (2012) Cellular chaperones and folding enzymes are vital contributors to membrane bound replication and movement complexes during plant RNA virus infection. *Frontiers in Plant Science*, **3**, 275.

Wang W., Vinocur B., Shoseyov O., Altman A. (2004) Role of plant heat-shock proteins and molecular chaperones in the abiotic stress response. *Trends in Plant Science*, **9**, 244–252.

Yang J., Zhang F., Cai N.J., Wu N., Chen X., Li J., Meng X.F., Zhu T.Q., Chen J.P., Zhang H.M. (2017) A furoviral replicase recruits host HSP70 to membranes for viral RNA replication. *Scientific Reports*, **7**, 45590.

3.2.3 Hsp70 plays an ambiguous role during viral infections in plants (Review)

During the project about effects of heat treatment on metabolism of tobacco plants infected with *Potato virus Y*, we had to perform quite an extensive research about Hsps. Therefore, we decided to write a short review about the ambiguous role of Hsp70 during viral propagation in plants. The interaction between viral infection and Hsp70 is highly complex and ambiguous (Fig. 1 in Hýsková et al 2021a). In contrast with eukaryotes and bacteria, viruses lack Hsps and rely on host Hsps for protein folding (Bolhassani & Agi 2019). It seems that viruses do not encode a specific inducer for Hsp70. The initiation of chaperons' response is related to the production of virus-specific proteins, a likely analogous way to the unfolded protein response in the endoplasmic reticulum as shown for *Turnip mosaic virus* and *Turnip crinkle virus* (Aparicio et al 2005). The content of the insoluble coat protein of *Tobacco mosaic virus* was also shown to be in correlation with the increase of Hsp70 content (Jockusch et al 2001).

High temperatures lead to Hsp synthesis and its expression aids the plant cell in maintaining homeostasis and proteostasis as well as the virus in viral nucleic acid replication, protein synthesis, and propagation *in planta* (Hýsková et al 2021a). Many viral proteins are folded by plant Hsp molecular chaperones (Milani et al 2016). For *Tomato bushy stunt tombusvirus,* its RNA-dependent RNA polymerase was found in replicase complex with host proteins including Hsp70 (Pogany & Nagy 2015). In some studies, Hsp70 affected viral coat protein movement from cell to cell or a long-distance transport (Table 2 in Hýsková et al 2021a).

Therefore, Hsp70 silencing, or inhibition prevented viral infection for a variety of plant viruses such as *Rice stripe virus* (Jiang et al 2014), *Turnip mosaic virus* (Jungkunz et al 2011) and *Tomato yellow leaf curl virus* (Gorovits & Czosnek 2017) and many more (Hýsková et al 2021a).

However, temperature can also help the plant to affect the course of viral infection (Table 1 in Hýsková et al 2021a). For example, the increase in temperature supported RNA silencing in *Nicotiana benthamiana* infected with

Tobacco ringspot virus (Szittya et al 2003). An extensive summary of discovered function of Hsp 70 during various viral infections can be found in Table 2 in Hýsková et al 2021a. Heat treatment may not eliminate virus completely but help to reduce the viral multiplication and propagation in plants (Kwon et al 2012). These findings are advantageously used in a process called thermotherapy. The viral infections that were successfully treated with thermotherapy are summarized in Table 1 in Hýsková et al 2021a.

However, many factors and conditions (such as plant species, susceptibility, virulence etc.) crucially influence the role of Hsp70 as shown in Fig. 2 in Hýsková et al 2021a.

My contribution:

I participated in both literary research and writing the text of the manuscript as well as in critical reading.

biologia plantarum
an international journal for experimental botany

BIOLOGIA PLANTARUM (2021) 65: 68-79 DOI: 10.32615/bp.2021.001
REVIEW

HSP70 plays an ambiguous role during viral infections in plants

V. HÝSKOVÁ[1], K. BĚLONOŽNÍKOVÁ[1], N. ČEŘOVSKÁ[2], and H. RYŠLAVÁ[1,*]

[1] *Department of Biochemistry, Faculty of Science, Charles University, CZ-12843 Prague 2, Czech Republic*
[2] *Institute of Experimental Botany of the Czech Academy of Sciences, CZ-16500 Prague 6, Czech Republic*

[*]Corresponding author: E-mail: helena.ryslava@natur.cuni.cz

Abstract

Heat shock and almost all types of stresses associated with oxidative stress are accompanied by heat shock protein (HSP) expression. HSPs are involved in refolding denatured proteins and directing unrepairable proteins for degradation. Thus, under stress conditions, HSPs help to restore cellular balance. However, in virus-infected plants, HSP70 can have both positive and negative effects because viruses usually recruit HSP70. HSP70 can promote the replication and translation of the viral genome, the formation of viral replication complexes, and the propagation of viral particles from cell to cell and throughout the plant. *HSP* gene silencing in various virus-host plants systems and the comparison of susceptible and resistant species have shown that HSPs70 accelerate the development of infection. Conversely, during the process known as thermotherapy, the temperature increase inhibits viral replication in some host and virus systems. The success of thermotherapy depends not only on the temperature and treatment period or duration but also on the plant species and viral strain. In this review, we discuss the ambiguous role that HSPs70 play during viral infections in plants towards weighing the balance between their positive and negative functions.

Keywords: acquired tolerance, heat shock, host factor, plant viruses, thermotherapy, virus propagation.

Introduction

Heat shock proteins (HSPs) are a family of mainly stress-induced proteins whose primary function is to refold denatured proteins. HSPs are divided into six groups according to their relative molecular mass and primary structure homology (Wang *et al.* 2004, Park and Seo 2015). The genes that encode HSPs are found in different cell compartments, and HSP expression is controlled by transcriptional factors known as heat shock factors (HSFs) (Haq *et al.* 2019).

In particular, HSP70 is arguably the most conserved protein family among all the organisms, from bacteria to plants and animals. The number of members in different HSP70 families ranges from 18 in *Arabidopsis thaliana* and 20 in *Solanum tuberosum*, through 30 in *Oryza sativa* to 61 in *Nicotiana tabacum* (Liu *et al.* 2018, Song *et al.* 2019). HSP70 are crucial for cells as constitutive and ubiquitously expressed proteins, but HSP70 expression is also induced, not only by heat shock (HS), but by almost all types of plant stresses as well (Park and Seo 2015, Usman *et al.* 2017).

In the classical model for stress activation of HSPs, the presence of stress-induced unfolded proteins in the cell causes the release of HSPs from their constitutive inhibitory association with HSF monomers, although this model could involve more pathways, especially at temperatures that do not unfold proteins. The unfolded

Received 2 October 2020, *last revision* 14 December 2020, *accepted* 7 January 2021.
Abbreviations: CP - coat protein; HS - heat shock; HSC70 - heat shock cognate 70; HSF(s) - heat shock factor(s); HSP(s) - heat shock protein(s); RdRp - viral coded RNA-dependent RNA polymerase; ROS - reactive oxygen species; UPR - unfolded protein response; VRC - viral replicase complex.
Acknowledgements: We sincerely apologize to colleagues whose publications could not be cited here owing to space constrains. The authors thank Dr. Carlos V. Melo for English proofreading this review. This work was supported by the Charles University, projects SVV260427/2020 and GA UK No. 1304119 and the Ministry of Education, Youth and Sports of CR from European Regional Development Fund-Project "Centre for Experimental Plant Biology" (grant number CZ.02.1.01/0.0/0.0/16_019/0000738).
Conflict of interest: The authors declare that they have no conflict of interest.

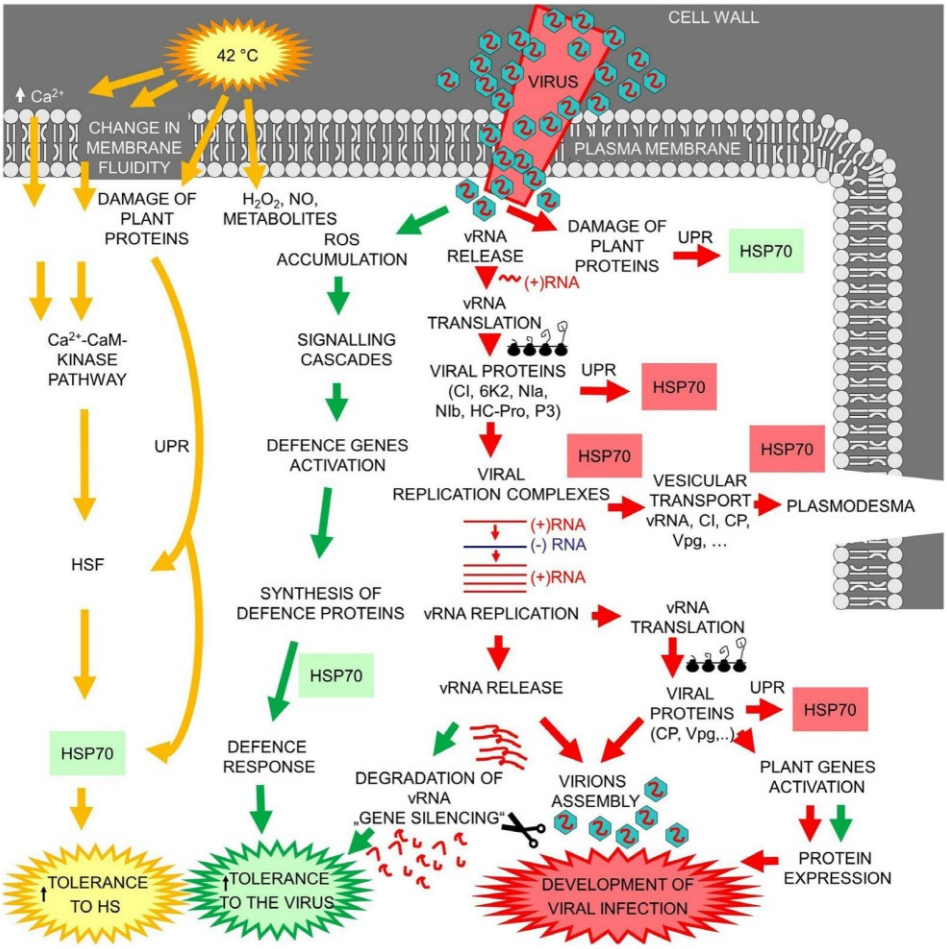


Fig. 1. The main events in the potyviral infection cycle (red) and during HS response (yellow). Heat shock proteins (HSP70) are formed to help plants respond to both stressors (green), but HSP70 can also be misused by viral particles to facilitate their propagation (red). The scheme represents the complexity of HSP70 involvement in the stress situation. Abbreviations: CI - cytoplasmic inclusion, CP - coat protein, HS - heat shock, HSF - heat shock factor, NIa - nuclear inclusion type a with proteolytic activity, NIb - potyviral RNA-dependent RNA polymerase, 6K2 - membrane associated protein, UPR - unfolded protein response, VPg - viral genome linked protein. The viral replication scheme was modified from Ivanov *et al.* 2014.

protein response (UPR) is a signaling pathway activated in cells in response to stresses that impair protein stability. Changes in ambient temperatures are sensed *via* a complex network of molecular sensors located in different cell compartments: the plasma membrane sensing mechanism, which triggers a specific inward calcium flux, UPR sensors in endoplasmic reticulum and cytosol and histone decreased occupancy in the nuclei. These signals generated by different sensors are integrated by a signal transduction network that involves calcium fluxes, calmodulin, protein kinases, phosphatases, and transcriptional regulators, such as HSFs (Mittler *et al.* 2012).

In response to heat stress, HSP70 is activated as shown in Fig. 1. Pre-treatment of a plant with a moderately elevated temperature can enhance heat stress tolerance and accelerate recovery after stress (Prerostova *et al.* 2020). During this process (acquired thermotolerance), plants sense an elevation in ambient temperature and initiate signal transduction networks, which regulate the expression of several genes, including those encoding HSPs and reactive oxygen species (ROS)-scavenging enzymes, to increase their thermotolerance. The integration of hormone and radiation signaling, circadian clock, and high ambient temperature regulates plant thermoresponsive growth (Li *et al.* 2018). In the absence of heat stress, some HSP family members are nevertheless constitutively expressed, and these family members are known as heat-shock cognate proteins HSC70 (Duck and Folk 1994).

HSPs70 have a highly conserved primary and 3D structure. The protein consists of two domains. The N-terminal domain binds ATP, Mg^{2+}, and K^{+} ions and has ATPase activity, whereas the β strands and loops of the C-terminal domain form the substrate-binding pocket (Frydman 2001, Hartl *et al.* 2011). The HSP70 substrate binding and release cycle is exclusively regulated by ATP binding and hydrolysis, whereby HSP70 switches between

(ATP-bound) low- and (ADP-bound) high-affinity states. The former is the open form, which can bind to the substrate protein. Another molecular chaperone, HSP40, is also required for initial protein binding in this cycle (Mayer and Bukau 2005, Doubnerova and Ryslava 2014).

HSPs70 act as chaperones, stabilizing nascent proteins during protein folding, assembling or disassembling multi-protein complexes, assisting protein unfolding, transporting, and sorting organelle-specific and secretory proteins into subcellular compartments or the extracellular space, respectively (Doubnerova and Ryslava 2014, Asea *et al.* 2016, Anaraki *et al.* 2018). HSPs70 are also involved in preventing protein aggregation, repairing misfolded proteins or targeting irreparable proteins for degradation by the ubiquitin-proteasome system. Furthermore, HSP70 overexpression in plants positively correlates with acquired thermotolerance and results in enhanced tolerance to abiotic stress treatments (Wang *et al.* 2004, Su and Li 2008), whereas HSP70 downregulation reduces tolerance to abiotic stresses (Lee and Schoffl 1996, Su and Li 2008). Thus, the HSP70 system plays a key role in plants recovering from various biotic and abiotic stresses (Usman *et al.* 2017, Anaraki *et al.* 2018).

To respond to biotic stresses (viruses, bacteria, fungi, and nematodes), plants have evolved different strategies, signal perception, transduction, and activation of the immune system, including stress-related HSPs (Haq *et al.* 2019). Pathogen-derived homologs of HSP70 may be involved in pathogenesis (*e.g.*, facilitation of colonization) (Ghazaei 2017), but plant HSPs70 expressed in response to stress caused by pathogens with their own HSPs is mostly associated with beneficial effects. For example, HSPs play a key role in defense against virulent bacterial strains, and along with PR proteins, HSPs are more effective against fungal pathogen or work in cooperation with antioxidant-related enzymes to develop resistance against nematodes (for more examples, please refer to the review by Haq *et al.* 2019). However, the interaction between viral infection and HSP70 is highly complex and ambiguous. Unlike eukaryotes and bacteria, viruses lack HSPs and rely on host HSPs for protein folding (Bolhassani and Agi 2019). It seems that viruses do not encode a specific inducer of HSP70. The initiation of chaperons' response was associated with production of virus-specific proteins and the process could be analogous to the UPR in the endoplasmic reticulum as shown for *Turnip mosaic virus* and *Turnip crinkle virus* (Aparicio *et al.* 2005). The concentration of the insoluble viral coat protein of *Tobacco mosaic virus* was in correlation with the induction of HSP70 (Jockusch *et al.* 2001). Nascent viral protein or misfolded cellular proteins compete with HSF for HSP70 binding, which results in an increased amount of free and active HSF (Morimoto *et al.* 1994, Kim and Oglesbee 2012).

How does temperature affect the course of viral infections?

Elevated temperatures lead to HSP synthesis. On the one hand, HSP expression can help maintain homeostasis and proteostasis in the plant cell, even under stress conditions. On the other hand, it can help viral nucleic acid replication, protein synthesis and particle assembly, as well as virus spread to other cells (Nagy *et al.* 2011, Verchot 2012, Jiang *et al.* 2014, Heinlein 2015). Accordingly, HSP70 silencing or inhibition prevents efficient viral infection. This effect has been shown in plants infected with *Rice stripe virus* (Jiang *et al.* 2014), *Turnip mosaic virus* (Dufresne *et al.* 2008, Jungkunz *et al.* 2011), *Tomato yellow leaf curl virus* (Gorovits and Czosnek 2017), *Red clover necrotic mosaic virus* (Mine *et al.* 2012), *Tomato bushy stunt tombusvirus* (Wang *et al.* 2009a), *Abutilon mosaic virus* (Krenz *et al.* 2010), *Pepino mosaic virus* (Mathioudakis *et al.* 2012), and *Potato virus A*, *X,* and *Y* (Hofius *et al.* 2007, Chen *et al.* 2008, Hafren *et al.* 2010). However, elevated temperatures may aid in defensive reactions against viruses, as demonstrated in thermotherapy experiments. Thermotherapy usually involves subjecting plants to a slightly elevated temperature for a long time until HSP synthesis stops increasing and is hindered by other mechanisms. The success of thermotherapy depends not only on the temperature and treatment period or duration but also on the plant species and virus strain (Tan *et al.* 2010, Kwon *et al.* 2012, Achachi *et al.* 2014).

The balance between the success of a virus and that of a plant depends on the plant species, its health and developmental stage, on the virus species and strain, and on abiotic factors, including temperature. In this context, the role of HSP70 may vary from supportive to deleterious, depending on the nature of the infectious agent and possibly on the host itself (Asea *et al.* 2016).

When the elevated temperature helps the plant

In general, HSP70 synthesis under abiotic stress conditions is associated with positive effects on plants (Haq *et al.* 2019). Many factors affect the ability of a virus to multiply and penetrate plants and their ability to activate defense reactions and to prevent virus propagation. In addition to their antiviral innate immunity based on pathogen-associated molecular pattern (PAMP)-triggered immunity (PTI) and effector-triggered immunity (ETI), plants degrade viral nucleic acids *via* gene silencing. However, viral pathogens continuously develop new strategies to overcome host defenses (Gouveia *et al.* 2017, Carr *et al.* 2019, Gaffar and Koch 2019).

HSPs90 regulate stomatal development under acute heat stress in *Arabidopsis*. Acute stress suppresses stomatal development in a HSP90-dependent manner (Samakovli *et al.* 2020). Temperature strongly affects plant-virus interactions. The increase in temperature boost the defense response (RNA silencing) in *Nicotiana benthamiana* plants infected with *Tobacco ringspot virus*. In contrast, in the cold, the amount of central molecules

of RNA silencing (siRNAs) rapidly decreases, and plants become more susceptible to viruses (Szittya *et al.* 2003).

A number of recent studies have provided evidence for connections between HSFs, HSPs, ROS, and ROS scavengers upon heat stress. In a recently proposed model, HS induced a short-term positive and a long-term negative feedback loop in the HSF signaling pathway (Driedonks *et al.* 2015). Overexpression of small HSPs in *Arabidopsis* and tobacco enhanced the activity of antioxidant enzymes (Jiang *et al.* 2009, Sun *et al.* 2012). Accordingly, HSPs may decrease the concentration of ROS by protecting the conformation of ROS scavenging proteins. This model for interactions between HSFs, HSPs, ROS, and ROS scavengers also seems applicable to stresses other than heat and may explain the phenomenon of cross-acclimation (Driedonks *et al.* 2015). Plants likely show defense signaling crosstalk and take advantage of HSP70 acquired by abiotic stress for protection against biotic stress. However, the mechanism of this process remains unknown, and the response to prolonged exposure to elevated temperatures likely differs from acute exposure to HS. Heat treatment may not eliminate viruses at all, but it reduces virus multiplication and translocation in plants, and virus elimination requires long treatment periods (Kwon *et al.* 2012).

Thermotherapy

Outbreaks of virus disease are often associated with low temperature, whereas high temperature is frequently associated with attenuated symptoms ("heat masking") and with low virus content in virus-infected plants (Szittya *et al.* 2003). Thermotherapy is the most common method for virus eradication because virus content can be reduced when plants are heat-treated. Thermotherapy temperature and time application depend on the virus present and plant cultivar sensitivity to heat (Aguilar-Camacho *et al.* 2016). In general, the higher the temperature and the longer the exposure are, the higher the virus eradication will be. Often, thermotherapy 35 - 42 °C for 4 - 6 weeks is applied to the target plants, albeit depending on the specific virus-plant system (Wang *et al.* 2018). Some examples of effective thermotherapy schemes for virus eradication are outlined in Table 1. Thermotherapy using alternating day/night temperatures was found to alleviate the negative effects of a high constant temperature (Lizárraga *et al.* 2017, Wang *et al.* 2018). Thermotherapy could be applied as both hot-air and hot-water (37 °C) treatments, which are suitable for example for eliminating *Potato leaf roll virus* from potato tubers (Abbas *et al.* 2016). Recently, the effect of thermotherapy has been amplified by combining cryotherapy with chemotherapy (Mathew *et al.* 2021). Salicylic acid- and H_2O_2-induced thermotolerance and their long-time effects significantly increased post-thermotherapy survival in *Potato virus X*-infected microplants (Aguilar-Camacho *et al.* 2016). Therefore, studies on oxidative stress physiology and on the fate of HSPs during thermotherapy could elucidate the balance between the positive and negative functions of HSPs in viral propagation.

When the elevated temperature helps the virus

In addition to positive effects, HSP70 expression can have negative effects on virus-infected plants because viruses usually recruit HSP70. The possible involvement of HSP70 in viral infection is shown in Fig. 1. Generally, during viral infections, many viral proteins are folded by plant HSP molecular chaperones (Milani *et al.* 2016). HSP70, HSC70, the J-domain chaperons, and HSP90 were associated with some plant viruses (Table 2). As shown in Table 2, HSPs70 are an infection factor for many plant viruses.

The replication and translation of the viral genome, the formation of viral replication complexes, and the propagation of viral particles from cell to cell and throughout the plant can all be promoted by HSP70 (Mayer and Bukau 2005, Hafren *et al.* 2010, Nagy *et al.* 2011, Jiang *et al.* 2014, Lohmus *et al.* 2017, Yang *et al.* 2017). The identification of host factors recruited to the replicase complex helps to elucidate virus-cell interactions and to reveal mechanistic components required for viral nucleic acid replication (Dufresne *et al.* 2008). The viral-coded RNA-dependent RNA polymerase (RdRp) is responsible for synthesizing viral progeny in infected cells by positive strand RNA viruses (Pogany and Nagy 2015). Host HSP70 are required for RdRp within virus-induced membrane vesicles or replication complexes on intracellular membrane systems (Dufresne *et al.* 2008, Mine *et al.* 2012, Pogany and Nagy 2015, Yang *et al.* 2017). Furthermore, the RdRp of several positive-strand RNA viruses is initially inactive to avoid viral synthesis in cytosol, which would rapidly induce cellular antiviral responses. Pogany and Nagy (2015) identified co-opted cellular HSP70 and neutral phospholipids as activators of *Tomato bushy stunt tombusvirus* RdRp *in vitro*. In addition, these authors found that the membrane-bound tombusvirus replicase complex (VRC) consist of RdRp, the viral p33 RNA chaperone and several co-opted host proteins, one of which is HSP70. HSP70 and HSP90 were identified as host factors required for *Red clover necrotic mosaic virus* RNA replication. These chaperones promote VRC assembly by binding to p27, a virus-encoded component of the replicase complex (Mine *et al.* 2012). Furthermore, the furoviral replicase of the *Chinese wheat mosaic virus* recruits both *Triticum aestivum* L. HSP70 and *Nicotiana benthamiana* HSP70 from the cytoplasm or nucleus to the inclusion-like structures, suggesting that both HSPs70 may be recruited into VRC and promote furoviral infection (Yang *et al.* 2017). In addition, Yang *et al.* (2017) identified that the amino acid region 167-333 of the replicase is responsible for this interaction. DNA viruses such as gemniviruses do not encode their own DNA-polymerase; instead, they utilize the host nuclear DNA replication machinery and reprogram the expression of many plant genes. To ensure a successful long-term infection, these viruses restrain their destructive effect on host cells, delaying or preventing cell death by interfering with the plant cell death pathway

Table 1. Successful thermotherapy applied to various plant viruses (* - thermotherapy was also combined with cryotherapy or chemotherapy; ** - temperature gradient with the posterior isolation and culture of apical meristems; *** - symptoms that were not mentioned in the selected reference, were derived from an online database by Brunt *et al.* 1996). Several examples, which are alphabetically ordered are shown.

Virus	Plant	Symptoms	Reference
**Apple chlorotic leaf spot virus* (ACLSV) **Apple necrosis mosaic virus* (ApNMV) **Apple stem pitting virus* (ASPV) **Apple stem grooving virus* (ASGV)	*Malus domestica* (4 different cultivars)	apple mosaic disease: bright yellow patterning on leaves	(Hu *et al.* 2019)
Apple chlorotic leaf spot virus (ACLSV) *Apple stem grooving virus* (ASGV) *Apple stem pitting virus* (ASPV)	*Pyrus pyrifolia* cv. Fengshui	ACLSV: plum pseudo pox ASGV: tatter leaf symptoms in citrus ASPV: pear vein yellowing, leaf necrotic spot and fruit stone pitting	(Tan *et al.* 2010)
***Apple chlorotic leaf spot virus* (ACLSV) ***Apple mosaic virus* (ApMV)	*Malus domestica* (6 cultivars) *Pyrus communis* (2 cultivars)	growth retardation and loss of productivity	(Lizárraga *et al.* 2017)
Apple chlorotic leaf spot virus (ACLSV) *Apple stem grooving virus* (ASGV)	*Pyrus pyrifolia*	Generally asymptomatic in most cultivars. ACLSV can cause leaf malformation and chlorotic rings or line patterns in some pear cultivars, ASGV: pear black necrotic leaf spot	(Hu *et al.* 2012)
**Apple stem grooving virus* (ASGV)	I*n vitro*-cultured apple shoots *Malus domestica*	latent virus causing graft incompatibility, reduced growth vigor and decreased fruit yield	(Zhao *et al.* 2018)
Grapevine leafroll-associated virus Pr (GLRaV-Pr) *Grapevine rupestris stem pitting associated virus* (GRSPaV)	*Vitis vinifera*	GRSPaV-rugose wood syndrome of grapevine	(Maliogka *et al.* 2009)
**Grapevine leafroll-associated virus* 3 (GLRaV-3)	*Vitis champini*	grapevine leafroll disease: apparent downward curling and rolling of leaves. Virus can minimize shoot vigor and fruit yield and quality	(Hu *et al.* 2020)
Lily symptomless virus (LSV)	*Lilium* × *elegans*	LSV decreases plant vigor and production despite an apparent symptomless behavior	(Nesi *et al.* 2009)
Onion yellow dwarf virus (OYDV)	*Allium sativum*	leaf striping and curling, stunting***	(Robert *et al.* 1998)
Plum pox virus (PPV) *Prunus necrotic ringspot virus* (PNRSV)	*Prunus persica* var. *nectarina*	poor fruit quality, reduction of productivity and shortening of tree life	(Manganaris *et al.* 2003)
Potato leaf roll virus (PLRV)	*Solanum tuberosum*	upward curling of leaves and vein swelling on young plants***	(Abbas *et al.* 2016)
Potato virus Y (PVY)	*Solanum tuberosum*	mild to severe leaf mottling or streak or 'leaf-drop streak' with vein necrosis***	(AlMaarri *et al.* 2012)
**Raspberry bushy dwarf virus* (RBDV)	*Rubus idaeus*	lower fruit mass and drupelet number per fruit, crumbly fruit, leaf yellowing and reduced cane growth	(Mathew *et al.* 2021)
Raspberry bushy dwarf virus (RBDV)	*Rubus idaeus*	small or crumbly berries, yellow ring spots on leaves that soon disappear***	(Wang *et al.* 2008)
Tomato spotted wilt tospovirus (TSWV)	*Nicotiana benthamiana*	firstly, chlorotic spots on apical leaves, rapidly turning to bronze and dark-brown (necrosis) in tomato and pepper (Vaira *et al.* 1995)	(Roggero and Pennazio 1997)

Table 2. Function of HSP70 as host factors during viral infections in plants. Studies targeting both upregulation (overexpression) or down regulation (loss of function mutants or silencing) of a protein have been used to confirm the function of HSP70 as a host factor. If HSP mutant plants have not been studied, N.A. (not applied) is indicated. Symptoms were derived from an online database by Brunt *et al.* 1996, Chl - chloroplastic, Mit - mitochondrial.

Virus	Symptoms	Factor	Up- (↑) or down- (↓) regulation	Nucleic acid	Plant	Function
Red clover necrotic mosaic virus (Mine *et al.* 2012)	necrotic local lesions, mosaics, leaf deformation	HSP70 HSP90	↓	(+) ssRNA	*Nicotiana benthamiana*	HSP70 and HSP90 promote the assembly of the VRC through interactions with viral p27
Tomato bushy stunt tombusvirus (Pogany and Nagy 2015)	stunting, mottling, deformed fruit,	HSP70	N.A.	(+) ssRNA	recombinant *RdRp*	HSP70 is host factor required for the activation on N-terminal truncated recombinant TBSV RdRp. interaction with viral p33 in VRC
Chinese wheat mosaic virus (Yang *et al.* 2017)	chlorotic and necrotic spots or netting	NbHSP70 TaHSP70	↑	(+) ssRNA	*Nicotiana benthamina* (silenced HSP70) T*riticum aestivum* (transiently overexpressed HSP70	interaction with the region aa 167-333 of replicase. Both HSP70 are very probably recruited into VRC to promote furoviral replication.
Rice stripe virus (Jiang *et al.* 2014)	systemic necrotic or chlorotic spots and streaking	HSP70	↓	(-) ssRNA	*Oryza sativa* N*icotiana benthamiana* (silenced HSP70)	HSP70 plays a role in viral replication and probably in interaction with RdRp
Turnip mosaic virus (Dufresne *et al.* 2008)	chlorotic local lesions, mosaic, mottling, puckering or rugosity	HSC70-3	N.A.	(+) ssRNA	*Arabidopsis thaliana*	HSC70-3 is potentially integral compartment of the replicase complex and could has important roles to play in the regulation of RdRp functions.
Turnip mosaic virus (Jungkunz *et al.* 2011)		HSP70	↓	(+) ssRNA	*Arabidopsis thaliana* (*AtHSP70-15* deficient)	key factor in proper folding of cytosolic proteins
Beet yellows virus (Peremyslov *et al.* 1999, Alzhanova *et al.* 2001, Prokhnevsky *et al.* 2002)	vein clearing, then leaves become thick, brittle, yellow with necrotic spots	HSP70h (viral homolog)	N.A.	(+) ssRNA	the mutant and wild type full length cDNA viral clones transcribed into tobacco protoplasts	HSP70 functions in intercellular translocation, viral tail (special device to cell-to cell movement) assembly and transport and severs as molecular link between local and systemic spread of a plant virus by docking a long-distance transport protein (viral p20) to virions.
Tomato bushy stunt virus (Wang *et al.* 2009a)	stunting, mottling, deformed fruit	HSP70	↓	(+) ssRNA	*Nicotiana benthamiana*	part of virus replicase complex. HSP70 affects the subcellular localization and membrane insertion of the viral replication proteins as well as assembly of the viral replicase
Potato virus A, *X,* and *Y* (Hafren *et al.* 2010)	PVA: mild mosaic, leaf surface rough with wavy margins, or symptomless PVX: symptoms vary, some strains symptomless, others induce necrotic streaks PVY: mild to severe leaf mottling or streak or `leaf-drop streak' with vein necrosis	HSP70	↓	(+) ssRNA	*Nicotiana benthamiana* (downregulated HSP70)	HSP70 together with its cochaperone CPIP regulates the function of a potyviral CP during replication-associated translation. HSP70 as a crucial component of a distinct translational activity that is associated with potyvirus replication

Virus	Symptoms	Factor	Up- (↑) or down- (↓) regulation	Nucleic acid	Plant	Function
Tomato yellow leaf curl virus (Gorovits and Czosnek 2017)	plants stunted with small chlorotic puckered leaves; fruit yield much decreased	HSP70, not HSP90	↓	DNA	*Solanum lycopersicum*	HSP70 participates in the translocation of CP from the cytoplasm into the nucleus
Tomato yellow leaf curl virus (Moshe *et al.* 2016)	plants stunted with small chlorotic puckered leaves; fruit yield much decreased	HSP90	↓	DNA	*Solanum lycopersicum*	the suppression effect on cell death is induced by the inhibition effect of HSP90 and its co-chaperone SGT1.
Tomato yellow leaf curl virus (Anfoka *et al.* 2016)	plants stunted with small chlorotic puckered leaves; fruit yield much decreased	HSP90, HSP17	↓	DNA	*Solanum lycopersicum* (with downregulated HSF and thus HSP90)	combined heat and viral stresses induce the aggregation of HSP90 and HSP70. The maintenance of cellular chaperones in the aggregated state prevents the circulation of free soluble forms causing an additional decrease in stress response efficiency.
Abutilon mosaic virus (Krenz *et al.* 2010)	Yellow mosaic	cpHSC70-1	↓	ssDNA	*Nicotiana benthamiana* silenced cpHSC70	functional relevance of viral movement protein-chaperone interaction for viral transport and symptom induction
Pepino mosaic virus (Mathioudakis *et al.* 2012)	mosaic, dark green enations on the abaxial surfaces	HSC70	N.A.	(+) ssRNA	*Solanum lycopersicum*	interaction with PepMV CP during infection
Potato virus Y (Hofius *et al.* 2007)	mild to severe leaf mottling or streak or 'leaf-drop streak' with vein necrosis	Dna-J like proteins, designated Nt CPIPs	↑	(+) ssRNA	*Nicotiana tabacum*	*in vivo* confirmation for the essential role of plant chaperones in virus movement.
Tobacco mosaic virus (Chen *et al.* 2008)	leaf mosaic, severe crop losses	HSP70	↓,↑	(+) ssRNA	*Nicotiana benthamiana*	enhancement of *N. benthamiana* viral infection by diverse viruses
Potato virus X (Chen *et al.* 2008)	symptoms vary, some strains symptomless, others induce necrotic streaks	HSP70	↓,↑	(+) ssRNA	*Nicotiana benthamiana*	enhancement of *N. benthamiana* viral infection by diverse viruses
Watermelon mosaic virus (Chen *et al.* 2008)	mosaic, mottling, leaves and fruit malformed	HSP70	↓,↑	(+) ssRNA	*Nicotiana benthamiana*	enhancement of *N. benthamiana* viral infection by diverse viruses
Cucumber mosaic virus (Chen *et al.* 2008)	mosaics and stunting, reduced fruit yield	HSP70	↓,↑	(+) ssRNA	*Nicotiana benthamiana*	enhancement of *N. benthamiana* viral infection by diverse viruses
Tobacco mosaic virus (Jockusch *et al.* 2001)	leaf mosaic, severe crop losses	HSP18, HSP70	N.A.	(+) ssRNA	*Nicotiana tabacum* temperature sensitive CP mutants	the induction of HSPs paralleled the amount of insoluble CP in leaf extracts.
Potato virus Y (Makarova *et al.* 2018)	mild to severe leaf mottling or streak or 'leaf-drop streak' with vein necrosis	HSP70 HSP90	N.A.	(+) ssRNA	*Solanum tuberosum* thermosensitive and thermoresistant cultivar	response to heat stress and PVY in cultivar-specific manner.

Virus	Symptoms	Factor	Up- (↑) or down- (↓) regulation	Nucleic acid	Plant	Function
Potato virus Y, strain *NTN*, (Hyskova *et al.* 2021)	necrotic middle veins and chlorotic, crincled leaves with mosaic	cytosolic HSP70, Chl. HSP70, Mit. HSP70, HSP90-1	N.A.	(+) ssRNA	*Nicotiana tabacum*	the order of HS application and inoculation affect the virus propagation. In the beginning HSPs help the virus, but at a later stage specific isoforms could be also part of the plant's defense.

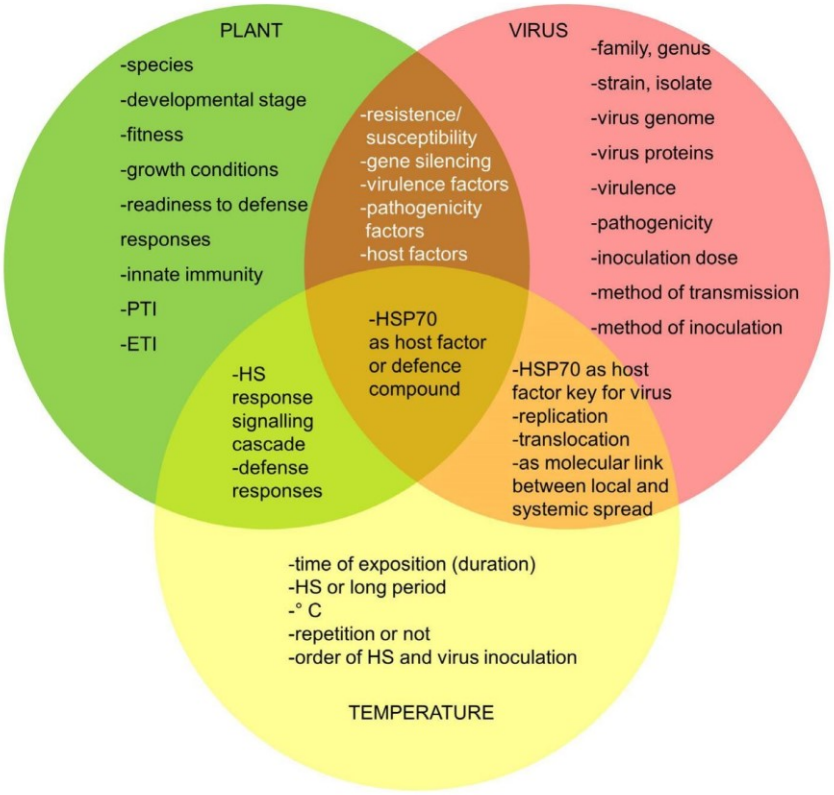


Fig. 2. Factors and conditions that determine whether HSP70 will act as host factor accelerating virus replication and spread or as a defense compound.

(Anfoka *et al.* 2016, Moshe *et al.* 2016). *Tomato yellow leaf curl viruses* suppress cell death induced by the inhibition of HSP90 (Moshe *et al.* 2016).

Viral coat proteins (CP) act as multifunctional proteins involved in almost every stage of the viral infection cycle. Their versatility is achieved *via* specific CP interactions with viral and host components in the infected cell (Ivanov and Makinen 2012). Hafren *et al.* (2010) found that the function of a potyviral CP (which can interfere with viral gene expression) is regulated by HSP70 together with its co-chaperone capsid protein interacting protein (CPIP). Other studies also suggest that HSP70 affects viral CP local movement from cell to cell or long-distance transport through the vascular system (Table 2). Some viruses (Closteroviruses) even form viral HSP70 homologs, which enable their translocation (Karasev 2000, Alzhanova *et al.* 2001). Thus, Closteroviruses, for example, need a specialized movement device with HSP70h most likely because they are exceptionally long (Alzhanova *et al.* 2001). Similarly, a subsequent study highlighted a new function of the HSP70 viral homolog as a molecular link between the local and systemic spread of *Beet yellows virus* by docking the long-distance transport factor p20 to virions (Prokhnevsky *et al.* 2002).

Cytoplasmic HSP70 enhances *Nicotiana benthamiana* infection with *Tobacco mosaic virus, Potato virus X*, and *Watermelon mosaic virus* (Chen *et al.* 2008). Heat stress inhibits the tobacco and potato hypersensitive response to *Tobacco mosaic virus* and *Potato virus X* (Kiraly *et al.* 2008, Wang *et al.* 2009b). For example, in plants, HSP70 silencing by RNAi technology or chemical inhibition of HSP70 expression impairs a number of positive sense,

single-stranded RNA viruses (Wang 2015). Mutant HSP70-deficient plants exhibit reduced virus content and delayed infection onset (Hafren *et al.* 2010, Jiang *et al.* 2014, Gorovits and Czosnek 2017, Huang *et al.* 2017). Furthermore, HSP-deficient *Arabidopsis* plants are more tolerant to *Turnip mosaic virus* (Jungkunz *et al.* 2011), and HSP70 overexpression has been correlated with the accumulation of furoviral genomic RNAs (Yang *et al.* 2017). Interestingly, the potato cultivar resistant to *Potato virus Y* is also thermotolerant, with HSP70 increasing only at elevated temperature and not due to viral infection. Conversely, the *Potato virus Y* and thermosensitive potato cultivar also shows increased HSP70 synthesis in response to viral infection (Makarova *et al.* 2018).

The order of HS application and inoculation affects the virus propagation. HSP70 cytosolic, chloroplastic, and mitochondrial isoforms and stress-induced Hsp90-1 were significantly increased due to HS immediately after inoculation and then declined. On the other hand, cytosolic and mitochondrial Hsp70 with lower molecular mass were enhanced simultaneously with viral propagation and increase of salicylic acid content.

Hatch-Slack cycle enzymes that serve as markers of *Potato virus Y* infection do not respond to HS, so the activity of phosphoenolpyruvate carboxylase, NADP-malic enzyme, and pyruvate, phosphate dikinase corresponds to infection, regardless of previous HS treatment (Hýsková *et al*. unpublished results).

During human diseases as well, several HSPs70 are associated with viral particles, e.g., *rabies virus*, *hepatitis C virus*, *adenovirus*, *the human immunodeficiency virus type 1*, and *Zika virus*. In such infections, HSPs70 usually act as an infection factor promoting viral transcriptional activity and spread (Milani *et al*. 2016, Bolhassani and Agi 2019). HSP70 even serves as a biomarker and drugs targeting HSP70 (HSP70 inhibitors) are attractive candidates for therapeutics targeting various viruses, such as the *Zika virus*, which is intensively studied in connection with HSP70 inhibitors (Taguwa *et al.* 2019).

Conclusions

Many factors, conditions, and circumstances determine whether elevated temperature or HS inducing HSP70 promote or inhibit viral replication and propagation in plants (Fig. 2). In addition to predetermined factors (Fig. 2), such as plant species, innate immunity, or virus pathogenicity, the combination in time and space of plant predispositions, HSP70 content and viral infection affect the resulting function of HSP70 in the plant during a viral infection. Crosslinking individual signaling pathways (UPR, HSF, ROS, ROS scavengers and hypersensitive response, gene silencing) temporally and spatially determines the role of HSP70 in a virus-infected plant. Furthermore, the process known as acquired thermo-tolerance can interfere with plant defense responses.

References

Abbas, A., Arif, M., Ali, A.: Use of hot water-thermotherapy to free potato tubers of *Potato leaf roll virus* (PLRV). - Int. J. Life Sci. sci. Res. **2**: 155-162, 2016.

Achachi, A., Ait Barka, E., Ibriz, M.: Recent advances in *Citrus psorosis virus*. - Virus Disease **25**: 261-276, 2014.

Aguilar-Camacho, M., Mora-Herrera, M.E., López-Delgado, H.A.: *Potato virus X* (PVX) elimination as short and long term effects of hydrogen peroxide and salicylic acid is differentially mediated by oxidative stress in synergism with thermotherapy. - Amer. J. Potato Res. **93**: 360-367, 2016.

AlMaarri, K., Massa, R., AlBiski, F.: Evaluation of some therapies and meristem culture to eliminate *Potato Y potyvirus* from infected potato plants. - Plant Biotechnol. **29**: 237-243, 2012.

Alzhanova, D.V., Napuli, A.J., Creamer, R., Dolja, V.V.: Cell-to-cell movement and assembly of a plant closterovirus: roles for the capsid proteins and Hsp70 homolog. - EMBO J. **20**: 6997-7007, 2001.

Anaraki, Z.E., Tafreshi, S.A.H., Shariati, M.: Transient silencing of heat shock proteins showed remarkable roles for *HSP70* during adaptation to stress in plants. - Environ. exp. Bot. **155**: 142-157, 2018.

Anfoka, G., Moshe, A., Fridman, L., Amrani, L., Rotem, O., Kolot, M., Zeidan, M., Czosnek, H., Gorovits, R.: *Tomato yellow leaf curl virus* infection mitigates the heat stress response of plants grown at high temperatures. - Sci. Rep. **6**: 19715, 2016.

Aparicio, F., Thomas, C.L., Lederer, C., Niu, Y., Wang, D., Maule, A.J.: Virus induction of heat shock protein 70 reflects a general response to protein accumulation in the plant cytosol. - Plant Physiol. **138**: 529-536, 2005.

Asea, A.A.A., Calderwood, S.K., Kaur, P (ed.): Heat Shock Proteins and Plants - Springer, Switzerland, 2016.

Bolhassani, A., Agi, E.: Heat shock proteins in infection. - Clin. chim. Acta **498**: 90-100, 2019.

Brunt, A.A., Crabtree, K., Dallwitz, M.J., Gibbs, A.J., Watson, L., Zurcher, E.J. (ed.): Descriptions and Lists from the VIDE Database, CAB International, Wallingford, UK, 1990, ISBN : 9780851986630.

Carr, J.P., Murphy, A.M., Tungadi, T., Yoon, J.Y.: Plant defense signals: players and pawns in plant-virus-vector interactions. - Plant Sci. **279**: 87-95, 2019.

Chen, Z., Zhou, T., Wu, X., Hong, Y., Fan, Z., Li, H.: Influence of cytoplasmic heat shock protein 70 on viral infection of *Nicotiana benthamiana*. - Mol. Plant Pathol. **9**: 809-817, 2008.

Doubnerova, V., Ryslava, H.: Roles of Hsp70 in plant abiotic stress. - In: Gaur, R.K., Sharma, P. (ed.): Molecular Approaches in Plant Abiotic Stress, Pp. 44-66. CRC Press, Boca Raton - London - New York 2014.

Driedonks, N., Xu, J., Peters, J.L., Park, S., Rieu, I.: Multi-level interactions between heat shock factors, heat shock proteins, and the redox system regulate acclimation to heat. - Front Plant Sci. **6**: 999, 2015.

Duck, N.B., Folk, W.R.: Hsp70 heat shock protein cognate is expressed and stored in developing tomato pollen. - Plant mol. Biol. **26**: 1031-1039, 1994.

Dufresne, P.J., Thivierge, K., Cotton, S., Beauchemin, C., Ide, C., Ubalijoro, E., Laliberté, J.F., Fortin, M.G.: Heat shock 70 protein interaction with *Turnip mosaic virus* RNA-dependent RNA polymerase within virus-induced membrane vesicles. - Virology **374**: 217-227, 2008.

Frydman, J.: Folding of newly translated proteins *in vivo*: the role of molecular chaperones. - Annu. Rev. Biochem. **70**: 603-647,

2001.
Gaffar, F.Y., Koch, A.: Catch me if you can! RNA silencing-based improvement of antiviral plant immunity. - Viruses **11**: 673, 2019.
Ghazaei, C.: Role and mechanism of the Hsp70 molecular chaperone machines in bacterial pathogens. - J. Med. Microbiol. **66**: 259-265, 2017.
Gorovits, R., Czosnek, H.: The involvement of heat shock proteins in the establishment of *Tomato yellow leaf curl virus* infection. - Front. Plant Sci. **8**: 355, 2017.
Gouveia, B.C., Calil, I.P., Machado, J.P., Santos, A.A., Fontes, E.P.: Immune receptors and co-receptors in antiviral innate immunity in plants. - Front. Microbiol. **7**: 2139, 2017.
Hafrén, A., Hofius, D., Ronnholm, G., Sonnewald, U., Makinen, K.: HSP70 and its cochaperone CPIP promote Potyvirus infection in *Nicotiana benthamiana* by regulating viral coat protein functions. - Plant Cell **22**: 523-535, 2010.
Haq, S.u., Khan, A., Ali, M., Khattak, A.M., Gai, W.-X., Zhang, H.-X., Wei, A.-M., Gong, Z.-H.: Heat shock proteins: dynamic biomolecules to counter plant biotic and abiotic stresses. - Int. J. Mol. Sci. **20**: 5321, 2019.
Hartl, F.U., Bracher, A., Hayer-Hartl, M.: Molecular chaperones in protein folding and proteostasis. - Nature **475**: 324-332, 2011.
Heinlein, M.: Plasmodesmata: channels for viruses on the move. - Methods mol. Biol. **1217**: 25-52, 2015.
Hofius, D., Maier, A.T., Dietrich, C., Jungkunz, I., Bornke, F., Maiss, E., Sonnewald, U.: Capsid protein-mediated recruitment of host DnaJ-like proteins is required for *Potato virus Y* infection in tobacco plants. - J. Virol. **81**: 11870-11880, 2007.
Hu, G., Dong, Y., Zhang, Z., Fan, X., Ren, F.: Elimination of apple necrosis mosaic virus from potted apple plants by thermotherapy combined with shoot-tip grafting. - Sci. Hort. **252**: 310-315, 2019.
Hu, G., Dong, Y., Zhang, Z., Fan, X., Ren, F.: Efficiency of chemotherapy combined with thermotherapy for eliminating *grapevine leafroll-associated virus* 3 (GLRaV-3). - Sci. Hort. **271**: 109462, 2020.
Hu, G.J., Hong, N., Wang, L.P., Hu, H.J., Wang, G.P.: Efficacy of virus elimination from *in vitro*-cultured sand pear (*Pyrus pyrifolia*) by chemotherapy combined with thermotherapy. - Crop Protect. **37**: 20-25, 2012.
Huang, Y.W., Hu, C.C., Tsai, C.H., Lin, N.S., Hsu, Y.H.: Chloroplast Hsp70 isoform is required for age-dependent tissue preference of *Bamboo mosaic virus* in mature *Nicotiana benthamiana* leaves. - Mol. Plant Microbe Interact. **30**: 631-645, 2017.
Hyskova, V., Belonoznikova, K., Doricova, V., Kavan, D., Gillarova, S., Henke, S., Synkova, H., Ryslava, H., Cerovska, N. Effects of heat treatment on metabolism of tobacco plants infected with Potato virus Y. - Plant Biol. 2021 Epub ahead of print. PMID: 33417742.
Ivanov, K.I., Eskelin, K., Lohmus, A., Makinen, K.: Molecular and cellular mechanisms underlying potyvirus infection. - J. gen. Virol. **95**: 1415-1429, 2014.
Ivanov, K.I., Makinen, K.: Coat proteins, host factors and plant viral replication. - Curr. Opin. Virol. **2**: 712-718, 2012.
Jiang, C., Xu, J., Zhang, H., Zhang, X., Shi, J., Li, M., Ming, F.: A cytosolic class I small heat shock protein, RcHSP17.8, of *Rosa chinensis* confers resistance to a variety of stresses to *Escherichia coli*, yeast and *Arabidopsis thaliana*. - Plant Cell Environ. **32**: 1046-1059, 2009.
Jiang, S., Lu, Y., Li, K., Lin, L., Zheng, H., Yan, F., Chen, J.: Heat shock protein 70 is necessary for *Rice stripe virus* infection in plants. - Mol. Plant Pathol. **15**: 907-917, 2014.
Jockusch, H., Wiegand, C., Mersch, B., Rajes, D.: Mutants of *Tobacco mosaic virus* with temperature-sensitive coat proteins induce heat shock response in tobacco leaves. - Mol. Plant Microbe Interact. **7**: 914-917, 2001.
Jungkunz, I., Link, K., Vogel, F., Voll, L.M., Sonnewald, S., Sonnewald, U.: AtHsp70-15-deficient *Arabidopsis* plants are characterized by reduced growth, a constitutive cytosolic protein response and enhanced resistance to TuMV. - Plant J. **66**: 983-995, 2011.
Karasev, A.V.: Genetic diversity and evolution of *Closteroviruses*. - Annu. Rev. Phytopathol. **38**: 293-324, 2000.
Kim, M.Y., Oglesbee M.: Virus-heat shock protein interaction and a novel axis for innate antiviral immunity. - Cells **1**: 646-666, 2012.
Király, L., Hafez, Y.M., Fodor, J., Király, Z.: Suppression of tobacco mosaic virus-induced hypersensitive-type necrotization in tobacco at high temperature is associated with downregulation of NADPH oxidase and superoxide and stimulation of dehydroascorbate reductase. - J. gen. Virol. **89**: 799-808, 2008.
Krenz, B., Windeisen, V., Wege, C., Jeske, H., Kleinow, T.: A plastid-targeted heat shock cognate 70 kDa protein interacts with the *Abutilon mosaic virus* movement protein. - Virology **401**: 6-17, 2010.
Kwon, Y., Kabir, M.A., Wang, H.W., Karuppanapandian, T., Moon, J.-C., Ryu, K.H., Lee, G.P., Kim, W.: Elimination of *pepper mild mottle virus* from infected tobacco (*Nicotiana benthamiana* L.) plants by callus culture and the sieving technique. - *In Vitro* cell. dev. Biol. Plant **48**: 595-599, 2012.
Lee, J.H., Schoffl, F.: An Hsp70 antisense gene affects the expression of HSP70/HSC70, the regulation of HSF, and the acquisition of thermotolerance in transgenic *Arabidopsis thaliana*. - Mol. gen. Genet. **252**: 11-19, 1996.
Li, B., Gao, K., Ren, H., Tang, W.: Molecular mechanisms governing plant responses to high temperatures. - J. integr. Plant Biol. **60**: 757-779, 2018.
Liu, J., Pang, X., Cheng, Y., Yin, Y., Zhang, Q., Su, W., Hu, B., Guo, Q., Ha, S., Zhang, J., Wan, H.: The Hsp70 gene family in *Solanum tuberosum*: genome-wide identification, phylogeny, and expression patterns. - Sci Rep. **8**: 16628, 2018.
Lizárraga, A., Ascasíbar, J., González, M.L.: Fast and effective thermotherapy treatment for *in vitro* virus eradication in apple and pear trees. - Amer. J. Plant Sci. **8:** 2474-2482, 2017.
Lohmus, A., Hafrén, A., Makinen, K.: Coat protein regulation by CK2, CPIP, HSP70, and CHIP is required for *Potato Virus A* replication and coat protein accumulation. - J. Virol. **91**: e01316-16, 2017.
Makarova, S., Makhotenko, A., Spechenkova, N., Love, A.J., Kalinina, N.O., Taliansky, M.: Interactive responses of potato (*Solanum tuberosum* L.) plants to heat stress and infection with *Potato virus Y*. - Front. Microbiol. **9**: 2582, 2018.
Maliogka, V.I., Skiada, F.G., Eleftheriou, E.P., Katis, N.I.: Elimination of a new *ampelovirus* (GLRaV-Pr) and *Grapevine rupestris stem pitting associated virus* (GRSPaV) from two *Vitis vinifera* cultivars combining *in vitro* thermotherapy with shoot tip culture. - Sci. Hort. **123**: 280-282, 2009.
Manganaris, G.A., Economou, A.S., Boubourakas, I.N., Katis, N.I.: Elimination of PPV and PNRSV through thermotherapy and meristem-tip culture in nectarine. - Plant Cell Rep. **22**: 195-200, 2003.
Mathew, L., Tiffin, H., Erridge, Z., McLachlan, A., Hunter, D., Pathirana, R.: Efficiency of eradication of Raspberry bushy dwarf virus from infected raspberry (Rubus idaeus) by in vitro chemotherapy, thermotherapy and cryotherapy and their combinations. - Plant Cell Tissue Organ Cult. **144**: 133-141, 2021.

Mathioudakis, M.M., Veiga, R., Ghita, M., Tsikou, D., Medina, V., Canto, T., Makris, A.M., Livieratos, I.C.: *Pepino mosaic virus* capsid protein interacts with a tomato heat shock protein cognate 70. - Virus Res. **163**: 28-39, 2012.

Mayer, M.P., Bukau, B.: Hsp70 chaperones: cellular functions and molecular mechanism. - Cell Mol. Life Sci. **62**: 670-684, 2005.

Milani, A., Basirnejad, M., Shahbazi, S., Bolhassani, A.: HSP roles as biomarkers and antigens in bacterial and viral infections. - J. Med. Microbiol. Infect. Dis. **4**: 1-7, 2016.

Mine, A., Hyodo, K., Tajima, Y., Kusumanegara, K., Taniguchi, T., Kaido, M., Mise, K., Taniguchi, H., Okuno, T.: Differential roles of Hsp70 and Hsp90 in the assembly of the replicase complex of a positive-strand RNA plant virus. - J. Virol. **86**: 12091-12104, 2012.

Mittler, R., Finka, A., Goloubinoff, P.: How do plants feel the heat? - Trends Biochem. Sci. **37**: 118-125, 2012.

Morimoto, R.I., Jurivich, D.A., Kroeger, P.E., Mathur, S.K., Murphy, S.P., Nakai, A., Sarge, K., Abravaya, K., Sistonen, L.T.: Regulation of heat shock gene transcription by a family of heat shock transcription factors. - In: Morimoto, R.I., Tissieres, A., Georgopoulos, C. (eds.): The Biology of Heat Shock Proteins and Molecular Chaperones. Cold Spring Harbor Laboratory Press, Cold Spring Harbor, NY, Pp. 417-455, 1994, ISBN: 0879694270.

Moshe, A., Gorovits, R., Liu, Y., Czosnek, H.: Tomato plant cell death induced by inhibition of HSP90 is alleviated by *Tomato yellow leaf curl virus* infection. - Mol. Plant Pathol. **17**: 247-260, 2016.

Nagy, P.D., Wang, R.Y., Pogany, J., Hafren, A., Makinen, K.: Emerging picture of host chaperone and cyclophilin roles in RNA virus replication. - Virology **411**: 374-382, 2011.

Nesi, B., Trinchello, D., Lazzereschi, S., Grassotti, A., Ruffoni, B.: Production of lily symptomless virus-free plants by shoot meristem tip culture and *in vitro* thermotherapy. - Hort. Sci. **44**: 217-219, 2009.

Park, C.J., Seo, Y.S.: Heat shock proteins: a review of the molecular chaperones for plant immunity. - Plant Pathol. J. **31**: 323-333, 2015.

Peremyslov, V.V., Hagiwara, Y., Dolja, V.V.: HSP70 homolog functions in cell-to-cell movement of a plant virus. - Proc. nat. Acad. Sci. USA **96**: 14771-14776, 1999.

Pogany, J., Nagy, P.D.: Activation of *Tomato bushy stunt virus* RNA-dependent RNA polymerase by cellular heat shock protein 70 is enhanced by phospholipids *in vitro*. - J. Virol. **89**: 5714-5723, 2015.

Prerostova, S., Dobrev, P.I., Kramna, B., Gaudinova, A., Knirsch, V., Spichal, L., Zatloukal, M., Vankova, R.: Heat acclimation and inhibition of cytokinin degradation positively affect heat stress tolerance of *Arabidopsis*. - Front. Plant Sci. **11**: 87, 2020.

Prokhnevsky, A.I., Peremyslov, V.V., Napuli, A.J., Dolja, V.V.: Interaction between long-distance transport factor and Hsp70-related movement protein of *Beet yellows virus*. - J. Virol. **76**: 11003-11011, 2002.

Robert, U., Žel, J., Ravnikar, M.: Thermotherapy in virus elimination from garlic: influences on shoot multiplication from meristems and bulb formation *in vitro*. - Sci. Hort. **73**: 193-202, 1998.

Roggero, P., Pennazio, S.: Thermal inactivation of *tomato spotted wilt tospovirus in vivo*. - Physiol. mol. Plant Pathol. **51**: 35-40, 1997.

Samakovli, D., Ticha, T., Vavrdova, T., Ovecka, M., Luptovciak, I., Zapletalova, V., Kucharova, A., Krenek, P., Krasylenko, Y., Margaritopoulou, T., Roka, L., Milioni, D., Komis, G., Hatzopoulos, P., Samaj, J.: YODA-HSP90 module regulates phosphorylation-dependent inactivation of SPEECHLESS to control stomatal development under acute heat stress in *Arabidopsis*. - Mol. Plant **13**: 612-633, 2020.

Song, Z., Pan, F., Lou, X., Wang, D., Yang, C., Zhang, B., Zhang, H.: Genome-wide identification and characterization of Hsp70 gene family in *Nicotiana tabacum*. - Mol. Biol. Rep. **46**: 1941-1954, 2019.

Su, P.H., Li, H.M.: *Arabidopsis* stromal 70-kD heat shock proteins are essential for plant development and important for thermotolerance of germinating seeds. - Plant Physiol. **146**: 1231-1241, 2008.

Sun, L., Liu, Y., Kong, X., Zhang, D., Pan, J., Zhou, Y., Wang, L., Li, D., Yang, X.: ZmHSP16.9, a cytosolic class I small heat shock protein in maize (*Zea mays*), confers heat tolerance in transgenic tobacco. - Plant Cell Rep. **31**: 1473-1484, 2012.

Szittya, G., Silhavy, D., Molnar, A., Havelda, Z., Lovas, A., Lakatos, L., Banfalvi, Z., Burgyan, J.: Low temperature inhibits RNA silencing-mediated defence by the control of siRNA generation. - EMBO J. **22**: 633-640, 2003.

Taguwa, S., Yeh, M.T., Rainbolt, T.K., Nayak, A., Shao, H., Gestwicki, J.E., Andino, R., Frydman, J.: Zika virus dependence on host Hsp70 provides a protective strategy against infection and disease. - Cell Rep. **26**: 906-920, 2019.

Tan, R., Wang, L., Hong, N., Wang, G.: Enhanced efficiency of virus eradication following thermotherapy of shoot-tip cultures of pear. - Plant Cell Tissue Organ Cult. **101**: 229-235, 2010.

Usman, M.G., Rafii, M.Y., Martini, M.Y., Yusuff, O.A., Ismail, M.R., Miah, G.: Molecular analysis of Hsp70 mechanisms in plants and their function in response to stress. - Biotechnol. Genet. Eng. Rev. **33**: 26-39, 2017.

Vaira, A.M., Semeria, L., Crespi, S., Lisa, V., Allavena, A., Accotto, G.P.: Resistance to tospoviruses in *Nicotiana benthamiana* transformed with the N gene of tomato spotted wilt virus: correlation between transgene expression and protection in primary transformants. - Mol. Plant Microbe Interact. **8**: 66-73, 1995.

Verchot, J.: Cellular chaperones and folding enzymes are vital contributors to membrane bound replication and movement complexes during plant RNA virus infection. - Front. Plant Sci. **3**: 275, 2012.

Wang, A.: Dissecting the molecular network of virus-plant interactions: the complex roles of host factors. - Annu. Rev. Phytopathol. **53**: 45-66, 2015.

Wang, M.R., Cui, Z.H., Li, J.W., Hao, X.Y., Zhao, L., Wang, Q.C.: *In vitro* thermotherapy-based methods for plant virus eradication. - Plant Methods **14**: 87, 2018.

Wang, Q., Cuellar, W.J., Rajamaki, M.L., Hirata, Y., Valkonen, J.P.: Combined thermotherapy and cryotherapy for efficient virus eradication: relation of virus distribution, subcellular changes, cell survival and viral RNA degradation in shoot tips. - Mol. Plant Pathol. **9**: 237-250, 2008.

Wang, R.Y., Stork, J., Pogany, J., Nagy, P.D.: A temperature sensitive mutant of heat shock protein 70 reveals an essential role during the early steps of tombusvirus replication. - Virology **394**: 28-38, 2009a.

Wang, Y., Bao, Z., Zhu, Y., Hua, J.: Analysis of temperature modulation of plant defense against biotrophic microbes. - Mol. Plant Microbe Interact. **22**: 498-506, 2009b.

Wang, W., Vinocur, B., Shoseyov, O., Altman, A.: Role of plant heat-shock proteins and molecular chaperones in the abiotic stress response. - Trends Plant Sci. **9**: 244-252, 2004.

Yang, J., Zhang, F., Cai, N.J., Wu, N., Chen, X., Li, J., Meng, X.F., Zhu, T.Q., Chen, J.P., Zhang, H.M.: A furoviral replicase recruits host HSP70 to membranes for viral RNA replication. - Sci. Rep. **7**: 45590, 2017.

Zhao, L., Wang, M.R., Cui, Z.H., Chen, L., Volk, G.M., Wang, Q.C.: Combining thermotherapy with cryotherapy for efficient eradication of *apple stem grooving virus* from infected *in-vitro*-cultured apple shoots. - Plant Dis. **102**: 1574-1580, 2018.

© *The authors. This is an open access article distributed under the terms of the Creative Commons BY-NC-ND Licence.*

3.2.4 How is the activity of shikimate dehydrogenase from parsley root regulated and which side reactions are catalyzed?

In 2021, we concluded our study about shikimate dehydrogenase (SDH - EC 1.1.1.25) from *Petroselinum crispum* (parsley) roots. SDH is one of the key enzymes of the shikimate pathway which is absent in human and animal metabolism. In plants, SDH is a bifunctional enzyme which N-terminal domain functions as 3-dehydroquinatedehydratase (DHD - EC 4.2.1.10) and the C-terminal domain catalyzes the reduction of 3-dehydroshikimate (DHS) to shikimate (SKA) in the presence of NADPH. The main aims of our study were to elucidate SDH kinetic mechanism, to determine all the possible reaction by-products and to test various phenylpropanoids as SDH inhibitors (Fig. 15).

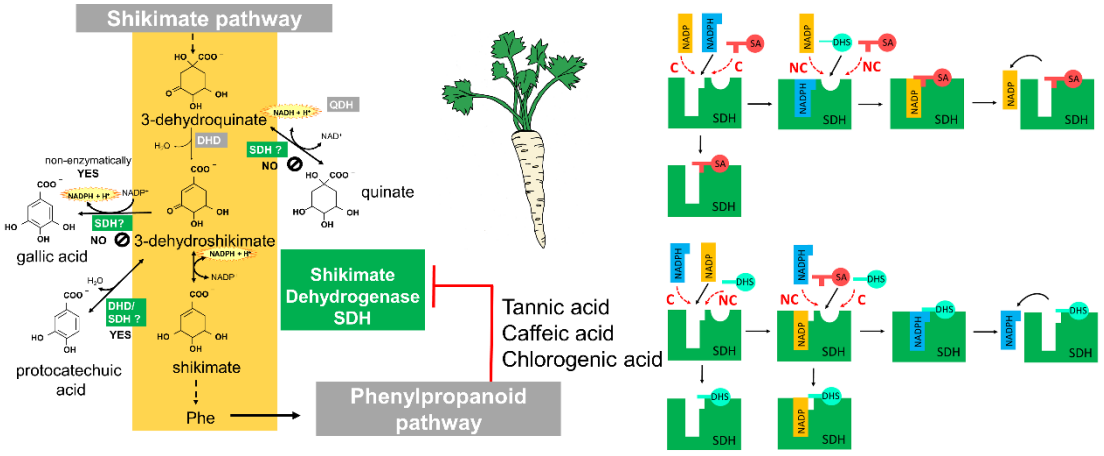


Fig. 15: Graphical abstract (Hýsková et al 2021c). We followed the SDH reactions by mass spectrometry to identify which side-reactions take place in the shikimate pathway in the parsley roots. Tannic acid, caffeic acid and chlorogenic acid were the most effective inhibitors of SDH. The product inhibition analysis showed formation of three dead end complexes. *Abbreviations: NC - non-competitive, C - competitive.*

The research of non-photosynthetic tissues like roots is challenging because the stiff and lignified cell walls render the isolation of enzyme proteins, and high contents of phenolics and other tanning products often inactivate the enzymes during extraction (Schmidt et al 1991). From a wide variety of root vegetables, we selected parsley as a source of high SDH activity and low content of phenolic compounds (Fig. 1 in Hýsková et al 2021c). SDH was purified by ion exchange and gel chromatography to a final specific activity 470 ± 18 nmol.min^{-1}.mg^{-1}, with

determined molecular weight 63 kDa, and isoelectric point 4.5 (Fig. 2 in Hýsková et al 2021c). We determined the kinetic parameters in both physiological NADPH + DHS → SKA + NADP and reverse SKA + NADP → DHS + NADPH directions based on kinetics of bi-substrate reaction and product inhibition analysis (Fig. 3, Fig. 4 in Hýsková et al 2021c). Dehydrogenases usually follow a typical sequential mechanism. However, during the kinetic analysis of SDH, we observed its untypical behavior in the product inhibition study, resulting in proposing an ordered mechanism in both directions but with three dead-end complexes (enzyme-DHS, enzyme-SKA, and enzyme-NADP-DHS, Table 2, Fig. 5 in Hýsková et al 2021c).

Juglans regia, Eucalyptus camaldulensis and *Vitis vinifera* contain SDH enzymes that oxidize DHS to gallic acid (Bontpart et al 2016, Muir et al 2011, Tahara et al 2021), which may then *via* conjugations lead to the accumulation of polyphenols like hydrolysable tannins (gallotannins and ellagitannins), condensed tannins (galloylated proanthocyanidins) or galloylated catechins (Tahara et al 2021). However, for parsley roots we could confirm only non-enzymatic spontaneous formation of gallic acid (Table 3, Fig. 6 in Hýsková et al 2021c) as also observed in the *in vitro* studies of *Camellia sinensis* as well as *Vitis vinifera* (Bontpart et al 2016, Huang et al 2019). For *Populus trichocarpa, Eucalyptus camaldulensis*, and *Vitis vinifera* some SDH isoenzymes showed high quinate dehydrogenase (QDH) activity catalyzing reversible reduction of 3-dehydroquinate to quinate, classifying them rather to NAD-dependent QDHs (Bontpart et al 2016, Guo et al 2014, Tahara et al 2021). This reaction may represent a link to the synthesis of chlorogenate (caffeoyl ester of quinate) (Tahara et al 2021). For parsley roots, we detected no such activity for SDH (Table 3, Fig. 6 in Hýsková et al 2021c), which thus belongs to the *bona fide* SDH group, that uses exclusively NADP and SKA; NADPH and DHS. The only found by-product produced in parsley roots was protocatechuic acid, resulting from the dehydration of DHS (Table 3, Fig. 6 in Hýsková et al 2021c).

Since the lack of the shikimate pathway in the animal and human metabolism, its inhibitors are widely used as herbicides, antiparasitic agents and

antimicrobials. We screened various products of the shikimate pathway i.e., aromatic amino acids (phenylalanine, tyrosine, and tryptophan), and phenylpropanoids (Fig.7 in Hýsková et al 2021c). We observed that the higher the hydroxyl number the higher the inhibition impact on SDH. The most effective inhibitors were tannic acid, caffeic acid and chlorogenic acid (Fig. 7 in Hýsková et al 2021c). The aromatic amino acids did not show any effect on SDH activity.

My contribution:

I isolated SDH from *Petroselinum crispum* (parsley). I measured the inhibition effect of various phenylpropanoids on SDH activity and performed some of the product inhibition analysis. I prepared the samples for LC-MS detection and analyzed the data. I edited the manuscript.

Research article

How is the activity of shikimate dehydrogenase from parsley root regulated and which side reactions are catalyzed?

Veronika Hýsková[a*], Kateřina Bělonožníková[a], Ingrida Šmeringaiová[a], Daniel Kavan[a], Marek Ingr[a,b] Helena Ryšlavá[a]

[a]*Department of Biochemistry, Faculty of Science, Charles University, Hlavova 2030, Prague 2, 128 40, Czech Republic*

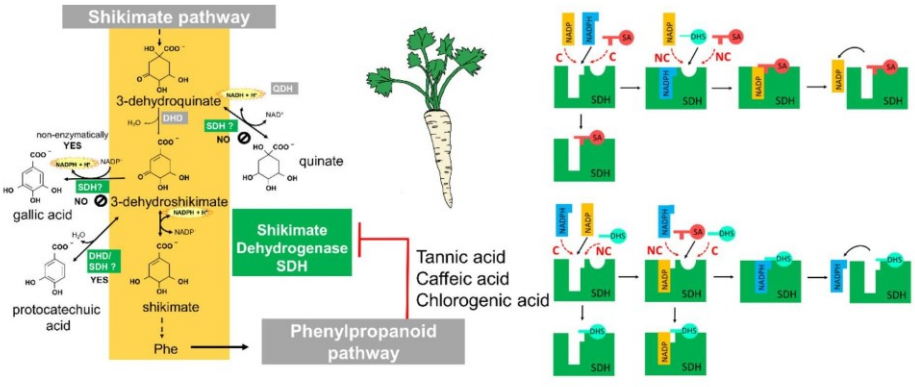
[b]*Tomas Bata University in Zlín, Faculty of Technology, Department of Physics and Materials Engineering, Nám. T.G. Masaryka 5555, 760 01 Zlín, Czech Republic*

[*]Corresponding author at: Charles University, Hlavova 2030, Prague 2, 128 40, Czech Republic

E-mail addresses: veronika.hyskova@natur.cuni.cz (V. Hyskova) katerina.belonoznikova@natur.cuni.cz (K. Belonoznikova), smer.inga@gmail.com (I. Smeringaiova), daniel.kavan@natur.cuni.cz (D. Kavan), marek.ingr@natur.cuni.cz (M. Ingr), helena.ryslava@natur.cuni.cz (H. Ryslava)

Tel: +420 221 951 282; fax: +420 221 951 283

Graphical Abstract:



Highlights

- Parsley SDH follows an ordered reaction mechanism with three dead-end complexes.
- Gallic acid and quinate are not direct bypass products of parsley SDH.
- Tannic acid, chlorogenic acid, and caffeic acid effectively inhibit SDH.
- Parsley SDH also forms protocatechuic acid in an irreversible reaction.

Abstract

Inhibitors of the shikimate pathway are widely used as herbicides, antibiotics, and anti-infectious drugs. However, the regulation of the shikimic pathway is complex, and little is known about the feedback regulation of the shikimate dehydrogenase (SDH, EC 1.1.1.25) in plants. Thus, the aim of this study was to elucidate the kinetic mechanism of SDH purified from non-photosynthetic tissue: parsley root (*Petroselinum crispum*), to determine all possible reaction products and to identify phenylpropanoid compounds that affect its activity. Our results showed that the bisubstrate reaction catalyzed by parsley SDH follows a sequential ordered mechanism, except for three dead-end complexes. The main and lateral reactions of SDH were monitored by mass spectrometry, thereby detecting protocatechuic acid as a byproduct. Gallic acid was formed non-enzymatically, whereas quinate was not detected. Several polyphenolic compounds inhibited SDH activity, especially tannic, caffeic and chlorogenic acids, with IC_{50} 0.014 mM, 0.15 mM, and 0.19 mM, respectively. The number of hydroxyl groups influenced their inhibition effect on SDH, and *p*-coumaric, *t*-ferulic, sinapic, syringic and salicylic acids were less effective SDH inhibitors. Nevertheless, one branch of the phenylpropanoid pathway may affect SDH activity through feedback regulation.

Keywords: chlorogenic acid; dehydroshikimate; gallic acid; hydroxycinnamic acids; simple phenols; tannic acid.

Abbreviations: AMP, 2-amino-2-methyl-1-propanol; DHD, 3-dehydroquinate dehydratase DHS, 3-dehydroshikimate; DHQ, 3-dehydroquinate; GA, gallic acid; PCA, protocatechuic acid; SA, shikimic acid; SDH, shikimate dehydrogenase; QA, quinate.

1. Introduction

The shikimate pathway is well known for the synthesis of aromatic amino acids in bacteria, fungi, apicomplexan parasites, and plants. In turn, this pathway is absent in animals. For this reason, inhibitors of individual enzymes were identified as antimicrobial agents and herbicides (Carrington et al., 2018; Deng and Lu, 2017; Tzin and Galili, 2010). The key enzyme of the shikimate pathway is shikimate dehydrogenase (SDH, EC 1.1.1.25). In plants, SDH is a bifunctional enzyme that catalyzes steps three and four. The N-terminal domain functions as 3-dehydroquinate dehydratase (DHD, EC 4.2.1.10), the C- terminal domain catalyzes the reduction of 3-dehydroshikimate (DHS) to shikimate (SA) in the presence of NADPH. The regulation of the shikimate pathway in plants is more complex than in bacteria and yeast (Carrington et al., 2018; Deng and Lu, 2017; Heldt et al., 2011; Tzin and Galili, 2010). The products of the shikimate pathway include not only phenylalanine, tyrosine, and tryptophan but also a wide range of polyphenolic compounds, such as phenolic acids, lignans, lignin, flavonoids, stilbenes and tannins. These compounds can protect plants against oxidative stress and UV radiation, impregnate cell walls and have antimicrobial properties. Thus, secondary metabolites are often synthetized and accumulated in plants in response to various stress conditions and can be associated with increased SDH activity (Belonoznikova et al., 2020; Cabane et al., 2004; Hyskova et al., 2017; Kovacik et al., 2009; Moura et al., 2010).

Another reaction catalyzed by SDH was proposed in walnut (*Juglans regia*) and *Escherichia coli*, in which 3-DHS was identified as the substrate of SDH in the presence of NADP. In the proposed SDH reaction mechanism, 3-DHS is oxidized to 3,5-didehydroshikimate, and gallic acid is formed after enolization, thereby continuously generating both shikimate and gallic acid (Muir et al., 2011). Therefore, this reaction is important for plants such as grapevine

(*Vitis vinifera*) that produce derivates of gallic acid, epicatechin 3-gallate and β-glucogallin, (Bontpart et al., 2016).

Guo *et al.* (2014) and Tahara *et al.* (2021) also described the synthesis of quinate (QA) from 3-dehydroquinate (DHQ) by DHD/SDH from poplar (*Populus trichocarpa*), and from *Eucalyptus camaldulensis*, respectively. However, only some members of the gene family catalyzed this reaction in which NADH is used for reduction instead of NADPH (Guo et al., 2014; Tahara et al., 2021). These reactions were described in plants with more than one gene for DHD/SDH, which could be separated into groups with "classical" SDH activity and groups that produce quinic acids (Bontpart et al., 2016; Guo et al., 2014; Muir et al., 2011). Moreover, another SDH side reaction – DHS dehydration to protocatechuic acid (PCA) – is also considered (Bontpart et al., 2016; Muir et al., 2011).

Similarly, to other enzymes of the shikimate and phenylpropanoid pathways, SDH is localized in chloroplasts where the reducing equivalents of NADPH and ATP from photosynthesis are available. On the other hand, in non-photosynthetic plastids, the reducing equivalents of NADPH required for synthetic pathways are provided by the oxidative pentose phosphate cycle, i.e., glucose-6-phosphate dehydrogenase and 6-phosphogluconate dehydrogenase (Esposito et al., 2003). Although the shikimate pathway is a very important metabolic flow in plants, the regulation of its key enzyme (SDH) by phenylpropanoid compounds and possible SDH products are less studied, especially in non-photosynthetic tissues.

Considering the above, this study aimed to find a plant source with naturally high SDH activity and to study the kinetic properties of SDH from non-photosynthetic tissue. The mechanism of reaction was characterized in both directions, thus gaining insights into dead-end complexes involved in the regulation of parsley SDH activity. The effect of phenolic compounds as potential inhibitors was tested, and the results show that not only tannic acid but also caffeic acid and chlorogenic acid function as SDH strong inhibitors.

2. Results

2.1. Characterization of parsley root SDH: typical high pH optimum and 61.5 kDa molecular weight

SDH activity was screened in crude extracts from 8 different vegetables. Onion and broccoli crude extracts had low SDH activity, whereas crude extracts from parsley root and zucchini were identified as the richest sources of SDH among all plants tested. A high SDH activity per gram of fresh weight correlates with a low total phenolics content and *vice versa* (Fig.1). SDH was purified by ion exchange and gel chromatography from parsley (*Petroselinum crispum*) root to a final specific activity of 470 ± 18 nmol.min^{-1}.mg^{-1}.

SDH activity was pH-dependent, with a pH optimum between 7-8.5 and 9.5- 10 in the physiological and reverse reactions, respectively (Table 1). The molecular weight was 63 kDa when determined by red native electrophoresis (Fig. 2A) and 60 kDa when assessed by gel chromatography (Fig. 2B). The isoelectric point of parsley SDH was 4.5 (Fig. 2C). Only one protein band with SDH activity was detected after native red electrophoresis and isoelectric focusing. During gel chromatography, SDH was eluted as a single peak. Thus, only one isoform of SDH is present in parsley root.

2.2. The kinetic properties of parsley SDH differ from those of other dehydrogenases

The kinetic parameters of the reaction catalyzed by parsley SDH were studied in both directions, i.e., in the physiological (shikimate pathway) direction: NADPH + DHS → SA + NADP, and in the reverse direction: SA + NADP → NADPH + DHS (Fig. 3). The Michaelis constants and maximal velocities are summarized in Table 1. The maximal reaction rate for the reverse reaction from SA to DHS was 4.6-fold higher than in the shikimate pathway direction (DHS reduction). Because the saturating concentrations of NADP and SA were high, we also determined the apparent Michaelis constant at approximate conditions (Table

1). Furthermore, excess substrate DHS inhibited the reaction (Fig. A.1) with a substrate inhibition constant of K_{SS} = 0.12 ± 0.07 mM (Table 1).

2.3. Product inhibition analysis confirmed the ordered mechanism of the SDH-catalyzed reaction in both directions

The kinetic mechanism of the bisubstrate SDH reaction was analyzed in both directions. To identify the type of mechanism, we constructed Lineweaver-Burk diagnostical plots (Fig. 3), a Hanes plot and an Eadie-Hofstee plot (data not shown) and performed product inhibition assays (Fig. 4, Table 2). All kinetic parameters including V_{max}, K_m, K_A, K_{ic}, K_{iu}, K_i, V^*_{max}, K_{SS}, $S_{0.5}$ were calculated from non-linear regression using Eqs. 1-7.

The initial rate of the reaction in the physiological direction was measured using several concentrations of DHS and NADPH, showing the typical Lineweaver-Burk plot of a sequential mechanism: straight lines with an intercept left to the ordinate (Fig. 3) and K_A 0.25 ± 0.13 mM. In this direction, the free enzyme binds to NADPH, which allows DHS, but not SA, binding in an ordered mechanism, thus partly explaining the mutual competition between NADPH and SA. NADPH binding apparently prevents NADP binding, and *vice versa*, leading to bilateral mutual competitive inhibition (Fig. 5, Table 2).

The direction of SA oxidation confirmed the strong affinity between the free enzyme and NADP. The mechanism was sequential but with a very low, almost immeasurable, dissociation constant for the complex enzyme – substrate (K_A), thus it seems to look like a ping-pong. Obviously, the complex enzyme-NADP is very thermodynamically stable (Fig. 3).

NADP binding enables both DHS and SA binding. The latter follows a classical ordered mechanism in the direction of SA + NADP → NADPH + DHS; in contrast, the former results in the formation of a dead-end complex. Its origin explains the competitive inhibition of DHS against the substrate SA. Thus, these findings further confirm the competition between NADP and NADPH (Fig. 5, Table 2).

DHS binding to the free enzyme prevents NADPH binding by forming a dead-end complex (enzyme-DHS) that precludes a disordered mechanism in the direction of NADPH + DHS → SA + NADP. In addition, another dead-end complex (enzyme-DHS-NADP) is also formed when NADP binds to the enzyme-DHS (Fig. 5).

SA binding to the free enzyme prevents both NADP and NADPH binding also by forming a dead-end complex, which, in the case of NADP, prevents a disordered mechanism in the direction of SA + NADP → NADPH + DHS. In the case of NADPH, the formation of the dead-end complex completes the explanation for the competitive inhibition by the SA inhibitor against the NADPH substrate. Thus, SA competes with NADPH to bind to free enzyme, but not the other way around, that is, NADPH does not compete with SA since SA binding to the enzyme leads to a dead-end complex. Therefore, we proposed an ordered mechanism of the bi-substrate reaction catalyzed by SDH in both directions with three dead-end complexes (enzyme-DHS, enzyme-SA, and enzyme-NADP-DHS) (Fig. 5).

2.4. Identification of all SDH products and cofactor specificity

The activity of SDH was monitored by LC-MS (Table 3), focusing on side reactions. GA was formed non-enzymatically since it was also detected without SDH in the mixtures. PCA was produced from SA and DHS in the parsley shikimate pathway. No products were detected for DHQ with NADH and for QA with NAD as substrates. The parsley SDH active routes are shown in Fig. 6.

2.5. Tannic acid and some phenylpropanoids, as well as Zn^{2+} and Cu^{2+} ions, inhibit SDH activity

Various compounds that participate in phenylpropanoid metabolism and/or are related to SDH were studied as potential modulators of its activity in a screening performed at inhibitor concentrations ranging from 0.006 to 3.5 mM. Aromatic amino acids (Phe, Tyr, Trp), which are synthesized in the shikimate pathway, had no effect on SDH activity.

Concurrently, the first product of the phenylpropanoid pathway (*t*-cinnamic acid) and the potential SDH product (quinic acid) did not affect SDH activity, similarly to umbelliferone (7-hydroxycoumarine) and resveratrol (trans–3,4',5–trihydroxystilbene) (Fig. 7). One-way ANOVA confirmed that the effect of these compounds was non-significant (data not shown). In turn, salicylic, *p*-coumaric, *t*-ferulic, sinapic, syringic, caffeic, chlorogenic (caffeic acid and quinic acid ester) acids and the polyphenolic compound tannic acid had an inhibitory effect on parsley SDH activity, with tannic acid showing the lowest IC_{50} (Fig. 7). Caffeic acid and chlorogenic acid were also effective inhibitors. Hydroxycinnamic acids, such as *p*-coumaric, *t*-ferulic, sinapic, syringic and salicylic acids, showed much higher IC_{50} values (Fig. 7). In the irreversible inhibition test, the activity of the enzyme incubated with individual inhibitors did not decrease over time (data not shown). Therefore, all inhibitors mentioned above are reversible.

Although gallic acid was also tested, it strongly interfered with the formation of color complexes, making it impossible to determine its effect. Furthermore, the color of flavanone or any representative of the flavonoids interfered with the colorimetric method, also precluding the analysis of their inhibitory activity.

Table 4 summarizes the effects on SDH activity when adding different ions to the reaction mixture. Generally, among the ions tested in this study (Ca^{2+}, Na^{+}, K^{+}, Mg^{2+}, Mn^{2+}, Zn^{2+}, and Cu^{2+}), only Zn^{2+} and Cu^{2+} had a significant effect on SDH activity. At 0.1 mM and 0.01 mM, $Zn^{2+}$and Cu^{2+} decreased SDH activity to 10 and 21 %, respectively.

3. Discussion

The kinetic study of SDH purified from non-photosynthetic tissue parsley root containing evaluation of product inhibitors, Michaelis constants and pH optima of both reversible reactions resulted in establishing an ordered mechanism and shift of the equilibrium

in favor of physiological shikimate pathway direction in the cell. Furthermore, parsley SDH exclusively used NADP(H) and SA (DHS) as a coenzyme and a substrate, respectively, while forming PCA as a by-product but not being involved in GA production. Furthermore, phenylpropanoids of one branch were found responsible for feedback regulation of parsley SDH.

3.1. Parsley root extracts show high SDH activity

One of the reasons why SDH activity is low in plant crude extracts is the presence of phenolics. In general, when exposed to air, plant phenolics are readily oxidized, generating products that form complexes with proteins and inhibit enzyme activity (Buchanan et al., 2000), as shown in Fig. 1. Since the total phenolic content is very high in plants, especially in medicinal herbs (Tupec et al., 2017), a group of vegetables was chosen to identify a source of high SDH activity from non-photosynthetic tissue. From the group of 8 vegetable sources, the parsley root (*Petroselinum crispum*) exhibited the highest SDH activity.

3.2. The directions of SDH-catalyzed SA oxidation and DHS reduction is controlled by the pH optimum and differ in maximal reaction rate

SDHs catalyze a reversible reaction, both DHS reduction and SA oxidation. For parsley SDH, the optimal pH was 9.5-10 for SA oxidation and 7-8.5 for DHS reduction (i.e., shikimate pathway direction) (Table 1). Accordingly, pH likely participates in the regulation of SDH activity *in vivo*. In photosynthetic tissues, the optimal pH 8 of the SDH reaction in the shikimate pathway direction matches the pH of the illuminated chloroplast, which ensures that the reactions of the shikimate pathway coincide with photosynthesis, and thus NADPH and ATP are readily available. Although SDH purified from parsley root is not a chloroplastic enzyme, SDH regulation by pH in non-photosynthesizing plastids is likely similar. NADPH is provided by the oxidative pentose phosphate pathway, and the optimal pH of glucose-6-phosphate dehydrogenase from barley root plastids is also approximately pH 8 (Esposito et

al., 2001). Conversely, SDHs have a non-physiologically high optimal pH in the SA oxidation direction (Avitia-Dominguez et al., 2014; Diaz and Merino, 1997; Guo et al., 2014; Lourenco and Neves, 1984; Lourenco et al., 1991). The unusually high optimal pH of the reverse reaction may be a mechanism of physiological protection against metabolite flowback through the shikimate pathway (Table 1). The pH profiles of SDH suggest that catalysis and substrate binding involve acid/base chemistry (Fonseca et al., 2007). The amino acids residues Lys385 and Asp423 (numbered with respect to the *Arabidopsis* protein), located in the SDH active site, which are conserved in DHD/SHD enzymes and which have been proposed to be involved in proton transfer during catalysis, are most likely responsible for such a high optimal pH (Singh and Christendat, 2006).

Furthermore, other factors favor the direction of shikimate pathway: metabolite channeling, which prevents the accumulation of substrates or products (Singh and Christendat, 2006), high Michaelis constants in the direction of SA oxidation (Table 1), product competitive inhibition against NADP and SA (Fig. 4, 5) and the formation of dead-end complexes (Fig. 5). The comparison of the maximal reaction rate in both directions shows that the reaction is 4.6 times higher in the non-physiological direction. These data were obtained at the pH optimum of the respective reactions, so they are not likely relevant to cellular context. However, this reaction is often used to study the properties of SDH from various sources.

For many SDHs, the bisubstrate reaction follows a typical sequential mechanism, as found for SDH from other sources, e. g., *Pisum sativum* (Balinsky et al., 1971; Dowsett et al., 1972) or *Capsicum annuum* (Diaz and Merino, 1997) or from *Mycobacterium tuberculosis* (Fonseca et al., 2007). In pea epicotyls, the sequential mechanism of the bisubstrate reaction was further specified to be ordered, with NADPH binding followed by DHS (Balinsky et al., 1971; Dowsett et al., 1972). The mechanism of mycobacterial SDH was also classified as steady-state ordered, albeit with DHS binding first, followed by NADPH (Fonseca et al., 2007).

Bacterial and plant SDHs also differ in their genetic framework in that each enzyme of the shikimate pathway is encoded by monofunctional genes in bacteria. In turn, DHD and SDH are fused to a bifunctional enzyme complex in plants, and even 5 enzymes of the shikimate pathway are fused to a penta-functional complex in fungi (Derrer et al., 2013). Parsley SDH has the typical molecular weight of plant SDHs (Fig. 2) (Bontpart et al., 2016; Diaz and Merino, 1997; Fiedler and Schultz, 1985; Koshiba, 1978; Lourenco and Neves, 1984; Lourenco et al., 1991; Muir et al., 2011) and is likely a monomer with both domains, DHD and SDH. The initial reaction rate (Fig. 3) and product inhibition pattern (Fig. 4) are in line with an ordered bi-bi mechanism with NADPH or NADP binding to the enzyme first except that SA is a competitive inhibitor with respect to NADPH and DHS is a competitive product inhibitor with respect to SA (Fig. 5). These findings indicate that not only NADPH and NADP but also SA may interact with the free enzyme, most likely in the form of a dead-end complex (enzyme-SA). Both NADP and SA prevent the first substrate, NADPH, from binding to SDH, but DHS has no competitive inhibitor. Therefore, in accordance with an ordered mechanism, DHS is the second substrate. Nevertheless, the enzyme-DHS complex acts as a dead-end complex, similarly to enzyme-NADP-DHS (Fig. 5). Hence, the formation of dead-end complexes with SA and DHS explains the key role that the NADP/NADPH ratio plays in establishing an equilibrium between the two directions. In parsley, the shikimate pathway *via* NADPH continues with the phenylpropanoid pathway, specifically with the synthesis of coumarins, where psoralen, bergapten, isoimperatorin, oxypeucedanin, xanthoxin, trioxalen, and angelicin are the most important coumarins in parsley, or with the synthesis of flavonoids (apiin and luteolin) (Kolarovic et al., 2010). In addition to the shikimate pathway, NADPH is also needed for the antioxidant system and for nitrate assimilation.

3.3. SDH also catalyzes the formation of PCA but not GA and QA

Other SDH-catalyzed reactions that may provide phenolic compounds or intermediates have been reported. Muir et al. (2011) demonstrated that SDH from walnut (*Juglans regia*) catalyzed not only the NADP-dependent dehydrogenation of SA to DHS but also the dehydrogenation of DHS to 3,5-diDHS, which provides GA after enolization. Recombinant EcDQD/SDH2 and 3 enzymes also catalyze NADP-dependent oxidation of 3-DHS to produce gallate, which is in some Eucalyptus species essential for the biosynthesis of the aluminum-detoxifying metabolite (Tahara et al., 2021). Two SDH isoforms showed a similar activity in grape wine berries (Bontpart et al., 2016). However, when analyzing parsley SDH, we also detected GA in the mixtures without the enzyme (Table 3). Therefore, we confirmed that GA could form non-enzymatically, as found in an *in vitro* study of recombinant isoforms of *Camellia sinensis* SDHs of grape wine berries (Huang et al., 2019) and also non-enzymatic formation of gallic acid was previously described (Kambourakis and Frost, 2000). Moreover, the reaction mechanism of parsley SDH showed that the binding of NADP and DHS to the SDH leads to the dead-end complex (Fig. 5). Consequently, enzymatic GA formation is not possible.

We also studied the pathway from DHQ to QA and back, but no products were detected in both directions. Thus, parsley SDH also belongs to the *bona fide* SDH group, using exclusively NADP as a coenzyme and SA as a substrate (Garcia-Guevara et al., 2017), whereas, e.g., some poplar and *Eucalyptus camaldulensis* SDH isoforms prefer NAD and also use QA as a substrate (Guo et al., 2014; Tahara et al., 2021). In-depth sequencing and *in vitro* biochemical assays showed that 3 poplar enzymes from 5 originally annotated as DHD/SDHs should be rather classified as QA dehydrogenases (Guo et al., 2014). In turn, we found that PCA is a byproduct in the parsley SDH pathway (Table 3, Fig. 6). As previously hypothesized (Guo et al., 2014), this reaction is ensured by SDH in parsley.

3.4. Parsley SDH is regulated by metabolites of the phenylpropanoid pathway

Because the shikimate pathway is absent in mammals, searching and designing inhibitors against enzymes of this pathway may lead to the development of antimicrobials (such as the bacterial *Mycobacterium tuberculosis* and *Helicobacter pylori* SDH) and antiparasitic (malaria parasite SDH) and herbicidal (plant SDH) agents, which are harmless to humans (Diaz-Quiroz et al., 2018). There are 3 strategies for identifying compounds with an inhibitory effect on a particular enzyme: i) analyzing substrate structural analogs (Baillie et al., 1972; Diaz and Merino, 1997; Fiedler and Schultz, 1985; Koshiba, 1978; Lemos Silva et al., 1985; Lourenco and Neves, 1984; Lourenco et al., 1991; Rothe, 1974), ii) screening thousands of compounds (Avitia-Dominguez et al., 2014; Han et al., 2006; Peek et al., 2014), and iii) searching for feedback inhibitors among products of the whole pathway. The first strategy has led to the discovery of the herbicide 2,4-dichlorphenoxy acetic acid (2,4-D) (Diaz and Merino, 1997). Concurrently, several studies have demonstrated that PCA (possible byproduct of SDH) inhibits plant SDH (Diaz and Merino, 1997; Koshiba, 1978; Lemos Silva et al., 1985; Lourenco and Neves, 1984; Lourenco et al., 1991). In this study, we have shown that parsley SDH forms PCA in the irreversible reaction (Fig. 6). Using a screening strategy, different research groups have identified SDH inhibitors, for example, 5 novel *Helicobacter pylori* SDH inhibitors, including the natural product curcumin (Han et al., 2006), and polyphenolic inhibitors (epigallocatechin gallate and epicatechin gallate) of *Pseudomonas putida* and *Arabidopsis thaliana* SDH (Peek et al., 2014). A limited number of inhibition/activation studies have identified dihydroxybenzoic acid and its derivatives as SDH inhibitors (Fiedler and Schultz, 1985; Koshiba, 1978; Nandy and Ganguli, 1961), thus showing that SDH inhibitors are not limited to herbicides and organic reagents.

In this study, we chose the third strategy to identify plant SDH inhibitors among the products of the phenylpropanoid pathway (representative compounds of simple phenols, flavonoid, stilbene, and polyphenols). The strongest parsley SDH inhibitor was tannic acid (Fig. 7).

Tannins have strong astringent properties, which may induce complexation with enzymes and substrates (Tintino et al., 2016). They bind to proteins (by hydrophobic, hydrophilic, non-specific, and specific interactions), pigments, low-molecular-weight compounds, and metallic ions (Kato et al., 2017). In microorganisms, interactions between tannic acid and the cell membrane can affect its permeability through the inhibition of the efflux pump, which may be associated with an antimicrobial effect (Tintino et al., 2016). Furthermore, the potentially extracellular localization of tannic acid may contribute to this effect because leaf mesophyll cell walls are the typical site of origin and deposition of hydrolysable tannins in oak leaves (Grundhofer et al., 2001). Furthermore, in the outer peels of pomegranate (*Punica granatum* L.), SDHs play a role in controlling the biosynthesis of hydrolysable tannins (Habashi et al., 2019).

Our results also showed that parsley SDH is inhibited at 0.15 and 0.19 mM IC_{50} by caffeic acid and chlorogenic acid (with 2 and 5 hydroxyl groups in the structure), respectively (Fig. 7). Chlorogenic acids are esters formed between caffeic acid and quinic acid, which are strong antioxidants found in many vegetable species and coffee beans (Colon and Nerin, 2016; Guo et al., 2014; Liang and Kitts, 2015; Niggeweg et al., 2004). In plants, chlorogenic acids serve as protecting compounds against stress, e.g., viral infection (Spoustova et al., 2015), or as feeding deterrents (Ikonen et al., 2001). The *p*-coumaric, *t*-ferulic, sinapic, syringic, and salicylic acids, all with only one hydroxyl group, were milder SDH inhibitors, with IC_{50} above 5 mM, and they are not involved in regulation under physiological conditions. Salicylic acid is an important signal molecule; however, its concentration does not reach the value of the experimentally determined IC_{50}, even during stress (Belonoznikova et al., 2020). In their study, Belinsky and Davies concluded that the both carbonyl group at the C1 position and a hydroxyl group at the 4-OH position are significant determinants of ligand binding. This is true for syringic acid with IC_{50} 5.1 ± 1.0 mM. Tannic acid contains several hydroxyl groups

on phenyl rings; thus, their hydroxyl groups may interact with the amino acid residue in the enzyme active center.

Under non-stress conditions, plant SDH may be inhibited by some phenylpropanoid compounds. In our previous study, we found significant chlorogenic and quinic acid depletion in tobacco plants exposed to potyviral stress and heat shock (Hyskova et al., 2021). Such a depletion could in turn favor the shikimate pathway, producing precursors of defense compounds by enhancing SDH activity.

Plant SDH inhibition by divalent metal ions, particularly Zn^{2+} and Cu^{2+}, is known and correlated with the inactivation of functional sulfhydryl groups of SDH and also confirmed with the inhibition of plant SDH by *p*-chloromercuribenzoate which could be reversed by cysteine (Balinsky and Davies, 1961; Koshiba, 1978; Lourenco and Neves, 1984). SDH from parsley root was also inhibited by Zn^{2+} and Cu^{2+}, particularly by Cu^{2+} ions (Table 4).

4. Conclusions

Parsley root SDH follows an ordered reaction mechanism with three dead-end complexes in both directions. PCA was identified as a side product of SDH, whereas GA was formed non-enzymatically and quinate was not detected. As such, the phenylpropanoid pathway leading to the synthesis of precursors of monolignols (initiating with cinnamic acid and continuing with *p*-coumaric acid, caffeic acid, ferulic acid, 5-hydroxyferulic and sinapic acid) affects SDH activity through feedback regulation. Moreover, their number of hydroxyl groups increases their inhibition effect on SDH. Accordingly, tannic acid, chlorogenic acid, and caffeic acid are the most effective inhibitors of parsley root SDH, which may be feedback-regulated by phenylpropanoids under stress conditions.

5. Material and methods

5.1. Extraction and Purification of SDH

The amount of 1 g of each vegetable (parsley root, zucchini and pumpkin fruit, celery, ginger, carrot, broccoli, or onion) was homogenized in 3 ml of 100 mM Tris-HCl, pH 7.8 buffer containing 1 mM dithiothreitol, 1 mM EDTA, 5 mM $MgCl_2$, and 5 % (v/v) glycerol) with 0.02 g/ml of poly(vinylpyrrolidone) and centrifuged at 16600*g* for 15 min. The supernatant was used to measure SDH activity. SDH was purified from 100 g of parsley root by ammonium sulfate precipitation, ion exchange chromatography on DEAE-cellulose, and gel filtration on Sephacryl S-300, as described previously (Ryšlavá et al., 2007).

5.2. SDH activity assay

SDH activity was monitored spectrophotometrically at 20 °C, following the formation of NADPH during the oxidation of SA into DHS by the increase of absorbance at 340 nm. The SDH assay mixture (total volume of 1 ml) contained 100 mM AMP-NaOH buffer (pH 9.0), 0.2 mM NADP and 3 mM SA. The reaction was initiated by adding the enzyme (50 µl).

Potential regulatory effects of Zn^{2+} (0.1 mM), Cu^{2+} (0.01 mM); Na^+, K^+, Mg^{2+}, Ca^{2+}, Mn^{2+} and NH_4^+ (5 mM) ions on SDH activity were tested.

5.3. Determination of pI, pH optimum, and relative molecular weight of SDH

Isoelectric focusing was performed using the Pharmacia system FBE-3000 and 125 x 125 mm gels Servalyt, Precotes 3-10, according to the Pharmacia manual, as published previously (Ryšlavá et al., 2007). A standard protein mixture (IEF Markers from Serva with pI 3.5-10.65) was used for calibration. SDH activity was detected by incubating 0.2 mM NADP, 3 mM SA and 10 mg/ml of iodonitroterazolium chloride with 5 µg/ml phenazine methosulfate in 100 mM AMP-NaOH buffer (pH 9.0).

The optimum pH of the enzyme was determined over the following pH ranges: 80 mM MES-NaOH buffer (pH 5.2 – 7.2), 80 mM Tris-HCl buffer (pH 6.8 – 8.6), 80 mM glycine-NaOH buffer (pH 8.6 – 10.6), 80 mM AMP buffer (pH 9.0 – 10.5), 80 mM Na_2CO_3-$NaHCO_3$ buffer (pH 9.5 – 11.0) and 80 mM Na_2HPO_4-NaOH buffer (pH 11.0 – 12.0). SDH activity was measured as described in 2.2.

The relative molecular weight of SDH was determined by gel chromatography on a Sephacryl S-300 column (1.2 x 57 cm). Red native electrophoresis was also used for molecular weight determination (Drab et al., 2011). SDH activity was assessed as described above after isoelectric focusing.

5.4. Determination of kinetic parameters and mechanism of the bisubstrate reaction catalyzed by SDH

The reaction rate was measured by the change of absorbance at 340 nm. In 500 mM Tris-HCl buffer (pH 8), the concentration of one of the substrates ranged from 0.005 to 0.7 mM NADPH and from 0.05 to 2 mM DHS, whereas the saturating concentration of the second substrate DHS and NADPH were 2 mM and 0.7 mM, respectively. The reverse reaction was determined similarly but in 500 mM AMP-NaOH buffer (pH 9.0) with 0.05 – 10 mM NADP and 0.2 – 10 mM SA, whereas the concentration of the second substrate was at saturation, i.e., 10 mM SA and 3 mM NADP, respectively. Kinetic parameters were determined by fitting the data to the Michaelis-Menten Eq. (1) or to an equation characterizing substrate inhibition Eq. (2) and the Michaelis constant (K_m), the maximum reaction rate (V_{max}), the hypothetical maximal reaction rate corresponding to the rate that the enzyme reached in the absence of inhibition by an excess of substrate (V^*_{max}) and the substrate inhibition constant (K_{ss}) were calculated by non-linear regression. All measurements were performed at 20 °C.

$$v = \frac{V_{max}[S]}{K_m + [S]}$$

$$v = \frac{V^*_{max}[S]}{K_m + [S] + \frac{[S]^2}{K_{ss}}} \quad \text{Eq. (1)}$$

Eq. (2)

The kinetic mechanism of SDH was studied in both directions by varying the concentration of NADP (0.05-0.5 mM) or NADPH (0.05-0.4 mM) and the concentration of SA (0.2-3 mM) or DHS (0.05-2 mM).

The experimental data of the reaction rate as a function of the substrate (SA, NADP) concentration were fit into general reaction rate equations for the bisubstrate reactions, classified as ping – pong: Eq. (3) and sequential: Eq. (4), and linearization methods, as the double reciprocal plot, Hanes plot or Eadie-Hofstee plot.

$$v = \frac{V_{max}[A][B]}{[B]K_{mA} + [A]K_{mB} + [A][B]} \quad \text{Eq. (3)}$$

$$v = \frac{V_{max}[A][B]}{[B]K_{mA} + [A]K_{mB} + [A][B] + K_A K_{mB}} \quad \text{Eq. (4)}$$

V_{max} is the maximal reaction rate of the enzyme reaction, K_{mA} and K_{mB} are the Michaelis constants for the substrate A and B, respectively, and K_A is the dissociation constant for the complex enzyme-substrate. Equations derived for the determination of dead-end complexes are summarized in supplementary material Eq. A.1- A.32.

5.5. Product inhibition study

In the direction from DHS to SA, the reaction mixture contained: 500 mM Tris-HCl buffer (pH 8) and a variable concentration of DHS (0.2; 0.3, 0.5, and 1 mM) or NADPH (0.05; 0.1, 0.2, and 0.3 mM) with a subsaturating concentration of the second substrate, i.e.,

0.2 mM NADPH or 0.75 mM DHS. The concentrations of the inhibitors, NADP and SA, were in the 0.1-0.3 mM and 0.5-2 mM ranges, respectively. In this direction, saturating product concentrations could not be measured for technical reasons (NADPH absorbance above 3).

In the direction from SA to DHS, the reaction mixture contained: 375 mM AMP-NaOH buffer (pH 9.0) and a variable concentration of SA and NADP. The final variable concentrations of SA (2; 0.5; 0.3; and 0.15 mM) and NADP (0.5; 0.2; 0.1; and 0.05 mM) were tested at saturating and subsaturating concentrations of the second substrate. The saturating concentrations were 20 mM and 2 mM, and the subsaturating concentrations were 0.3 mM and 0.1 mM for SA and NADP, respectively. The concentrations of the inhibitors, NADPH and DHS, were in the 0.05-0.1 and 0.5-1 mM ranges, respectively.

The data derived from the product inhibition studies were fitted to the equation describing the relevant type of inhibition: competitive Eq. (5) and non-competitive Eq. (6), where [S] is the substrate concentration, [I] is the inhibitor concentration, and K_{ic} and K_{iu} are the inhibition constants for the inhibitor derived by slope and intercept, respectively, in the Lineweaver-Burk plot.

$$v = \frac{V_{max}[S]}{K_m\left(1+\frac{[I]}{K_{ic}}\right)+[S]} \qquad \text{Eq. (5)}$$

$$v = \frac{V_{max}[S]}{K_m\left(1+\frac{[I]}{K_{ic}}\right)+\left(1+\frac{[I]}{K_{iu}}\right)[S]} \qquad \text{Eq. (6)}$$

5.6. Identification of all SDH products

SDH isolated from parsley root (10 µl with specific activity 470 $nmol.min^{-1}.mg^{-1}$) was incubated in the 280 µL reaction mixture containing either 100 mM Tris-HCl pH 8 (in the

physiological direction, see Fig. 6) or 100 mM AMP-NaOH pH 9 buffers, 0.14 mM NADP(H)/NAD(H) and 2 mM SA/DHS/DHQ/QA/GA/PCA for 30 min at 20 °C. The reaction was initiated by adding the enzyme and stopped by adding 10 µl of 99 % (v/v) formic acid. Blank experiments were prepared similarly, albeit adding formic acid before the enzyme. The calibration standards were purchased from Sigma-Aldrich (USA) and Carl Roth (Germany).

The reaction mixtures were assayed by reversed-phase liquid chromatography coupled to electrospray mass spectrometry (LC-MS). The injection volume was 5 µL (Dionex UltiMate 3000, Thermo Fisher Scientific, USA). A Zorbax C18 reversed-phase silica-based column was used for all separations (150 × 2.1 mm, 3.5 µm, Agilent, USA). The mobile phase consisted of 0.5 % (v/v) formic acid in 10 % (v/v) acetonitrile in water (eluent A); and 0.3 % (v/v) formic acid in 100 % (v/v) acetonitrile (eluent B). The flow rate was set to 0.250 ml/min at 37 °C. The following elution program was used: isocratic A for 7 min, 0-100 % B for 1 min, isocratic B for 2 min, isocratic A for 3 min. MS analysis was performed on a ESI-Q-TOF maXis II (Bruker, USA). All mass spectrometric data were acquired in negative ionization mode.

5.7. Effect of secondary metabolites on the SDH

Selected secondary metabolites were tested for their potential regulatory effect on SDH activity. The reversibility of inhibition by these compounds was tested simultaneously (Appendix A Supplementary material). Tannic acid was dissolved in distilled water, caffeic acid, chlorogenic acid, *t*-ferulic acid, *p*-coumaric acid, and salicylic acid were dissolved in 96 % ethanol, and sinapic and syringic acids were dissolved in 50 % ethanol. The final concentration of ethanol did not affect SDH activity. Since phenylpropanoids interfered with the spectrophotometric assay (increasing absorbance at 340 nm), this assay was replaced with the colorimetric microplate method. A reaction mixture (280 ul) consisting of 180 mM AMP-NaOH buffer (pH 9.0), 0.14 mM NADP, 2.1 mM SA, 5 mg/ml iodonitrotetrazolium with 5

µg/ml phenazine methosulfate, and 20 µl of potential inhibitor compound was incubated with 10 µl of enzyme for 15 minutes. The reaction was terminated with 10 µl of 99 % formic acid, measuring the absorbance at 500 nm.

Simultaneously, blank reactions were prepared in which 10 µl of enzyme was first treated with 10 µl of 99 % (v/v) formic acid and then with the reaction mixture. Another blank was prepared as the individual reaction (including incubation time), albeit replacing the enzyme with distilled water.

The half maximal inhibitory concentration IC_{50} was calculated from Eq. (7). [I] is the inhibitor concentration, a and b are the maximal and minimal values of reaction rate, respectively, and c corresponds to the slope of the sigmoid function.

$$v = b + \frac{a - b}{1 + \left(\frac{[I]}{IC_{50}}\right)^{c}} \qquad \text{Eq. (7)}$$

5.8. Determination of protein and total phenolic content

Soluble proteins were determined according to Bradford (Bradford, 1976), and total phenolics compounds were quantified according to Tupec et al. (Tupec et al., 2017).

5.9. Statistics

SDH isolation was performed in 20 independent biological replicates, repeating each measurement at least three times. Data were analyzed and processed in SigmaPlot v. 12 (Systat Software, Inc.) and Microsoft Excel 2019 (Microsoft Corp.).

Table 1 Kinetic parameters of parsley SDH

V_{max} - maximal reaction rate of enzyme reaction, K_m- Michaelis constant of the specific substrate, $K´_m$ -apparent Michaelis constant at a given concentration of the second substrate), K_{SS} - inhibition constant at an excess substrate concentration, K_A - dissociation constant of the enzyme – substrate complex, ♣for technical reasons (absorbance above 3 or excess substrate inhibition), this parameter could not be determined. Kinetic constants were calculated as an average of values from at least 3 experiments performed in doublets, S. D. are shown.

	Direction of the reaction catalyzed by SDH	
	SA → DHS	**DHS → SA**
pH optimum	9.5-10	7-8.5
V_{max} [µmol.min^{-1}.mg^{-1}] for SA (DHS)	1.34	0.29
V_{max} [µmol.min^{-1}.mg^{-1}] for NADP(H)	1.32	0.28
K_m for SA (DHS) [mM]	0.71 ± 0.13	♣
K_m for NADP(H) [mM]	0.47 ± 0.16	♣
$K´_m$ for SA (with 0.2 mM NADP)	0.16 ± 0.01	-
$K´_m$ for DHS (with 0.4 mM NADPH)	-	0.23 ± 0.03
$K´_m$ for NADP (with 3 mM SA)	0.054 ± 0.011	-
$K´_m$ for NADPH (with 2 mM DHS)	-	0.016 ± 0.03
K_{SS} for SA (DHS) [mM]	-	0.12 ± 0.07
K_A	0.030 ± 0.008	0.25 ± 0.13

Table 2 Results of the product inhibition study for the determination of the bisubstrate reaction mechanism of parsley SDH. Inhibition constants were calculated as an average of values from 2-4 experiments carried out in doublets, S.D. are shown.

Patterns and values in brackets mean that the reaction is saturated with the 2nd substrate.

	Product inhibitor				Product inhibitor			
	Q (NADP)		P (SA)		A (NADPH)		B (DHS)	
	Varied substrate				Varied substrate			
i.e.	1/NADPH	1/DHS	1/NADPH	1/DHS	1/NADP	1/SA	1/NADP	1/SA
2nd substrate	subsaturated				subsaturated (saturated)			
Pattern	C	NC	C	NC	C (C)	NC (N.I.)	NC (N.I.)	C (C)
Ki [mM]	0.22±0.02	0.4±0.1	0.7±0.1	0.7±0.3	0.12±0.07 (0.49±0.03)	0.36± 0.08	1.4±0.2	0.13±0.03 (0.33±0.03)
Mechanism	steady state sequential order				steady state sequential order			

Table 3 Identification of SDH products by LC-MS analysis. List of products detected after 30 min incubation with (and without) SDH enzyme at 20 °C. DHS, 3-dehydroshikimate; DHQ, 3-dehydroquinate; PCA, protocatechuic acid; SA, shikimic acid; QA, quinate. *the incubation time was 60 min at 20 °C. Each determination was done at least 3-times, the average values and S.D. are shown.

reaction	products [nmol]
SA+NADP	DHS: 5.7 ± 0.7
	PCA: 0.1 ± 0.0
*DHS+NADPH	SA: 4.9 ± 0.2
	GA: 0.5 ± 0.0
	PCA: 0.7 ± 0.1
	DHQ: 1.1 ± 0.0
DHS+NADP	GA: 0.1 ± 0.0
	PCA: 0.3 ± 0.2
DHS+NADP	GA: 2.1 ± 0.4
– without SDH	PCA: 2.7 ± 0.6
DHQ+ NADP	DHS: 17.4 ± 1.4
	PCA: 4.9 ± 0.4
*DHQ+ NADPH	DHS: 3.4 ± 0.8
	SA: 1.4 ± 0.2
	GA: 1.1 ± 0.5
	PCA: 1.3 ± 0.2
DHQ+NADH	No products detected.
QA+NAD	No products detected.
PCA+NADPH	No products detected.

Table 4 The effect of various ions on parsley SDH activity. Screening was performed spectrophotometrically at 340 nm in the presence of 3 mM SA, 0.2 mM NADP and 5 mM*, 0.1 mM**, or 0.01 mM*** concentration of potential modulator. Each determination was done at least 3-times, the average values and S.D. are shown.

Compound	**% of activity**
$(NH_4)_2SO_4$	115.6±9.8 *
$CaCl_2$	113.2±8.2 *
NaCl	105.2±3.7 *
KCl	107.0±7.3 *
$MgCl_2$	99.3±15.0 *
$MnCl_2$	77.6±23.1 *
$ZnSO_4$	10.1±4.8 **
$CuSO_4$	21.2±8.3 ***

Figures

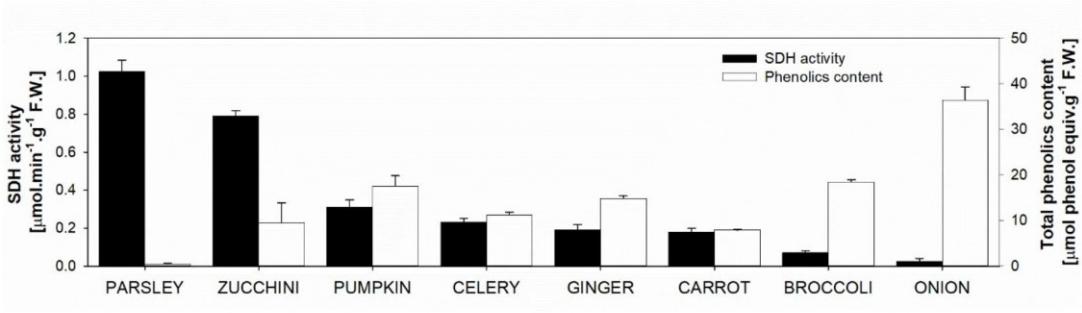


Fig. 1 Searching for plant sources of SDH activity. High SDH activity (black columns) correlates with low total phenolics content (white columns) and *vice versa*. Each determination was done at least 3-times, the average values and S.D. are shown.

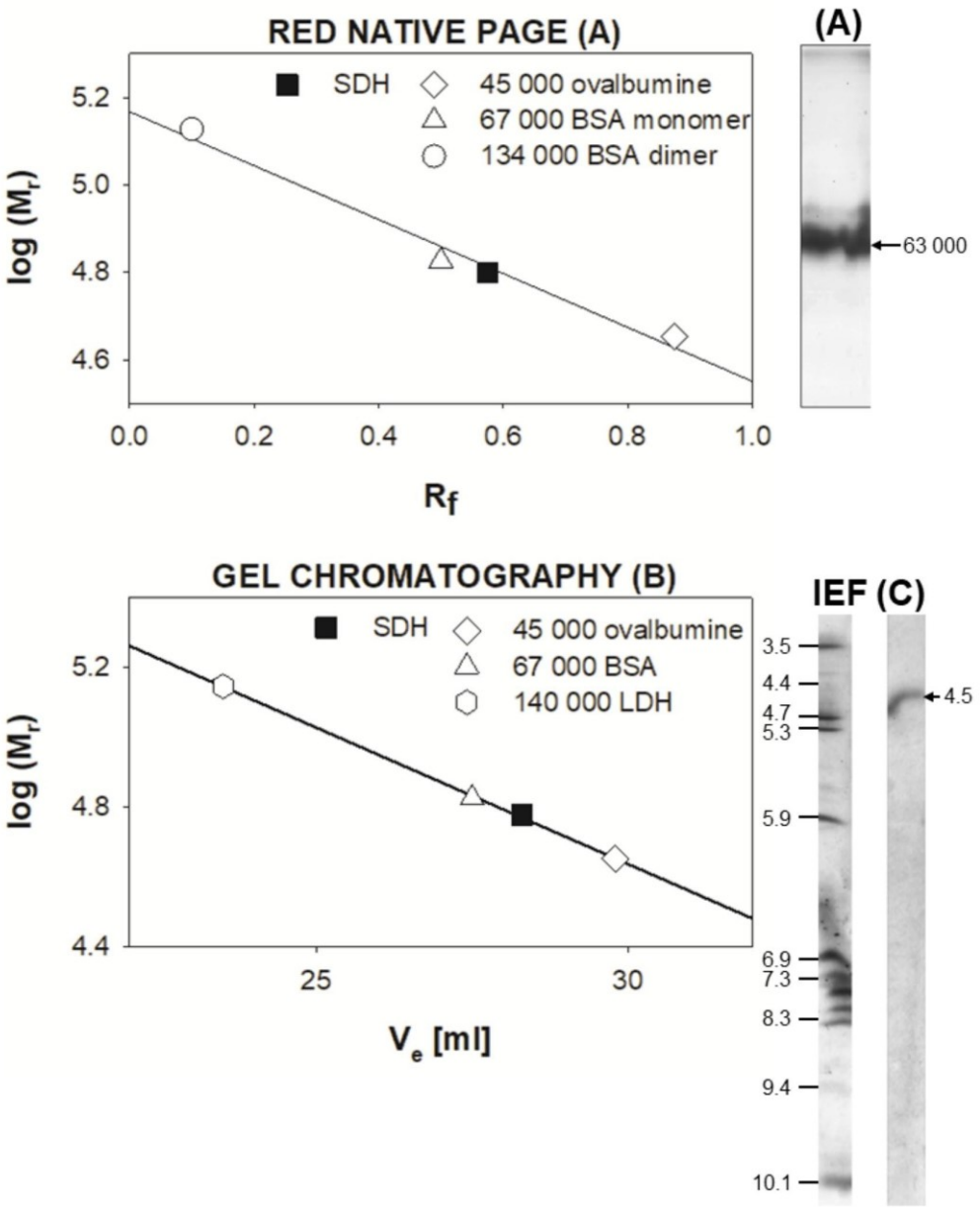


Fig. 2 Estimation of the relative molecular mass of SDH using red native PAGE (A) and gel chromatography on a Sephacryl-S300 column (B) and determination of pI using isoelectric focusing (C). The arrows indicate the position of SDH. R_f corresponds to the retention factor.

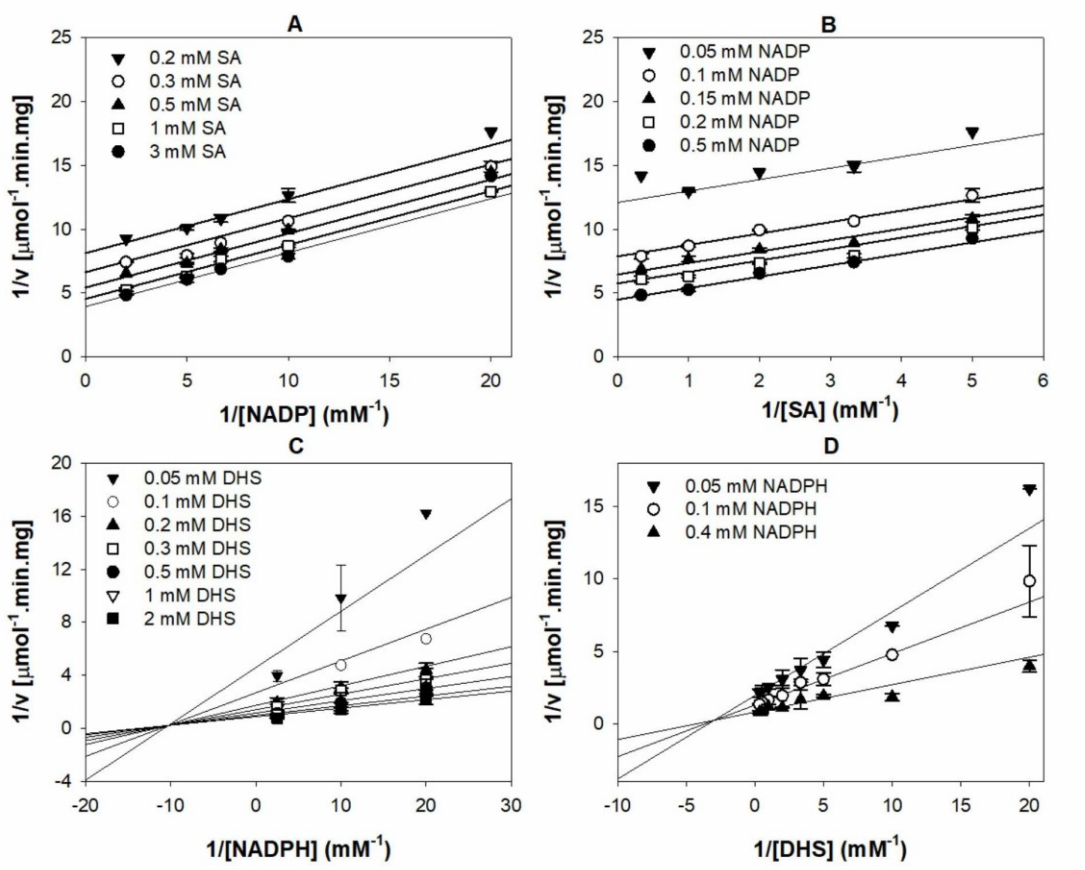


Fig. 3 Determination of the type of SDH reaction mechanism based on Lineweaver-Burk diagnostical plots for the direction from SA to DHS (A,B) and from DHS to SA (C,D)

Double reciprocal plots are fitted to an equation corresponding to a sequential mechanism.

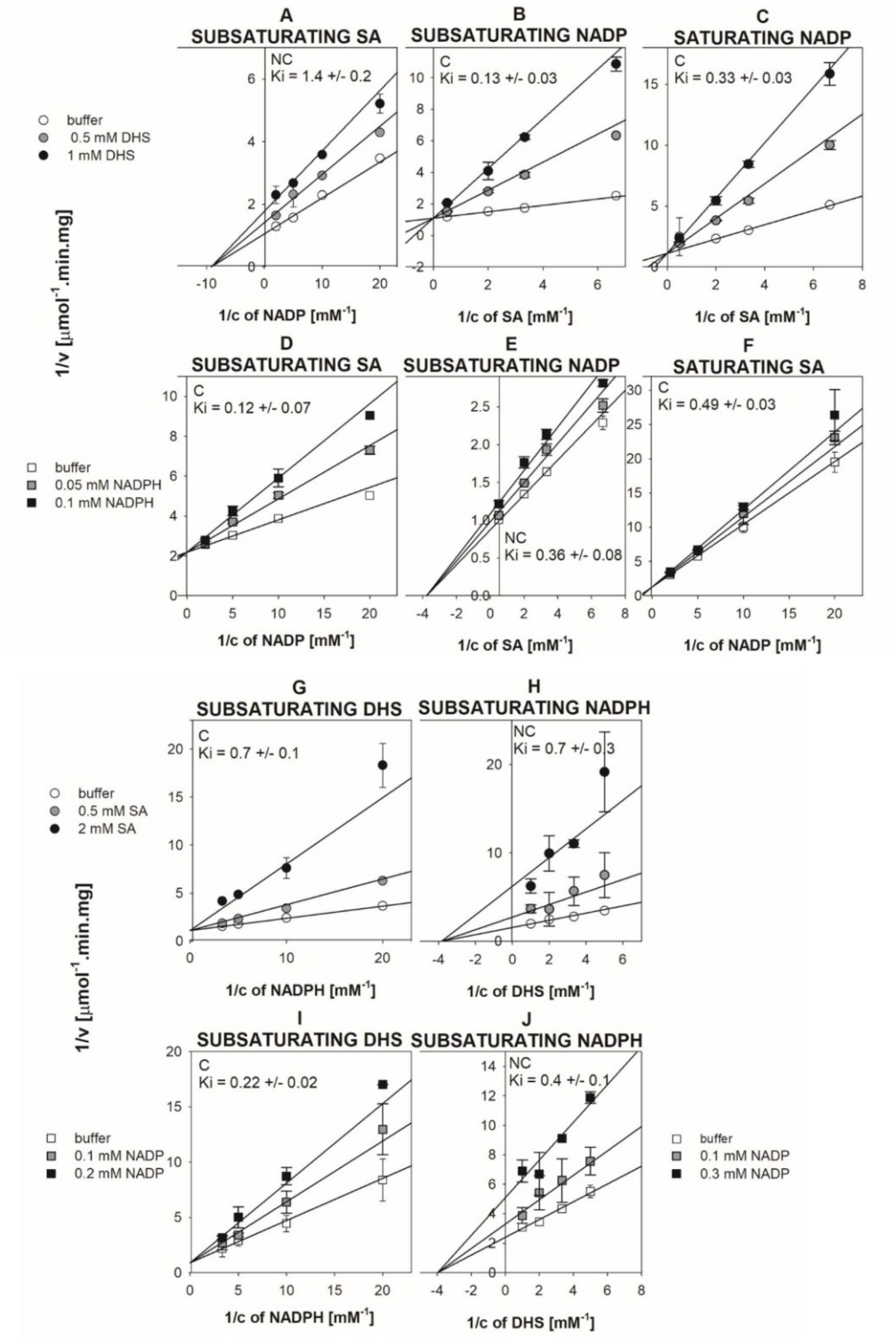


Fig. 4 Product inhibition analysis for the determination of the mechanism of bisubstrate reaction in the direction from SA to DHS (A-F) and in the direction from DHS to SA (G-

J). Experimental data are fitted with calculated values determined by non-linear regression using equations charactering competitive and non-competitive inhibition, respectively. SDH products DHS (A,B,C) and NADPH (D,E,F) served as competitive (B,C,D,F) and non-competitive (A,E) inhibitors. The saturating (C,F) and subsaturating (A,B,D,E) concentrations of SA and NADP were 20 mM and 2 mM, and 0.3 (2) mM and 0.5 mM, respectively. Saturating concentrations of NADP and variable concentrations of SA caused no inhibition (N.I.) of NADPH and saturating concentrations of SA and variable concentrations of NADP caused N.I. of DHS (data not shown). SDH products SA (G,H) and NADP (I,J) served as competitive (G,I) and non-competitive (H,J) inhibitors at 0.75 mM (subsaturating concentration) DHS (G,I) and 0.2 mM (subsaturating concentration) NADPH (H,J) as a second substrate. K_i indicates inhibition constants in mM. Measurements were performed in doublets (S.D. are shown) and at least 2-4 times (enzyme preparations from different isolations).

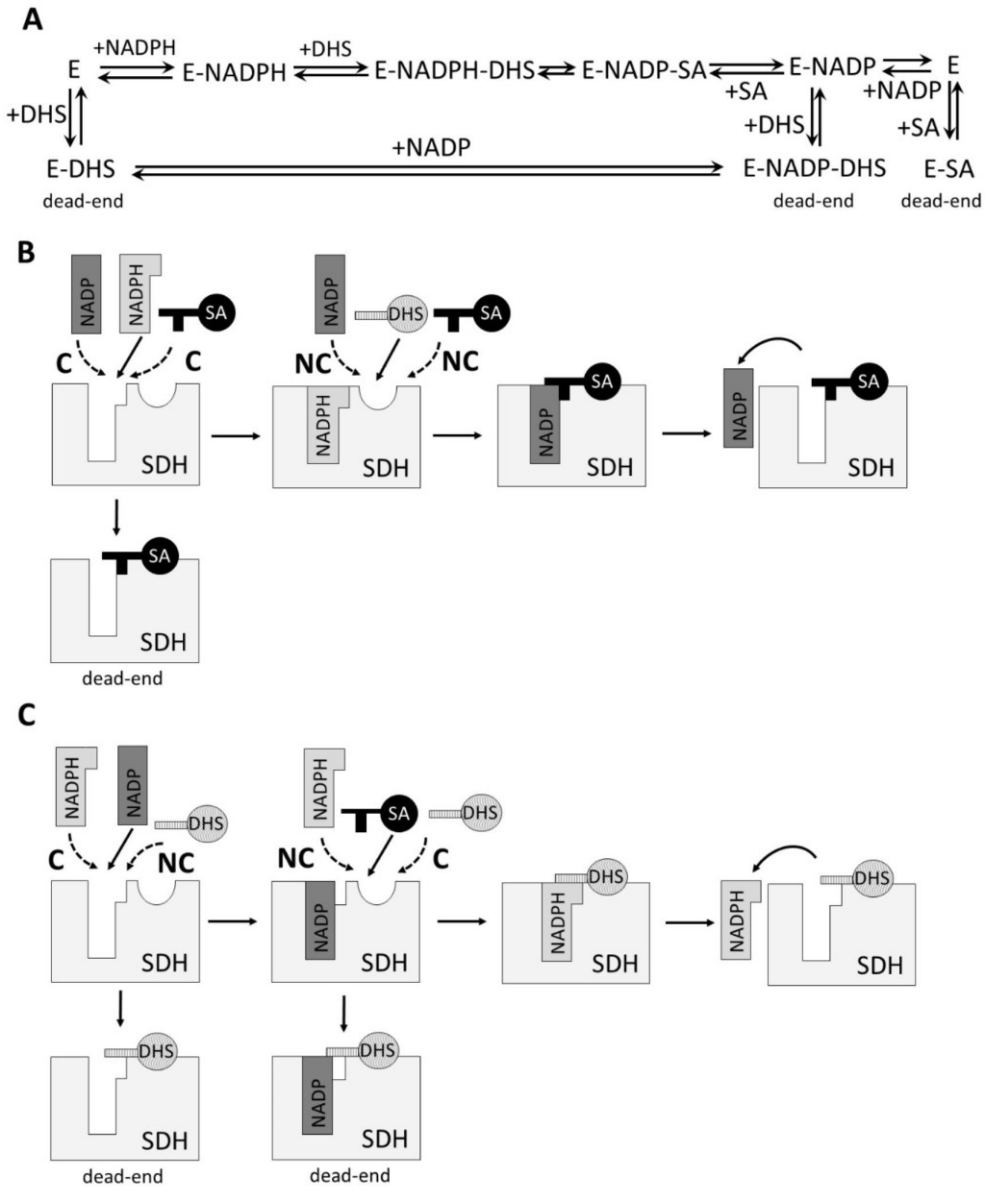
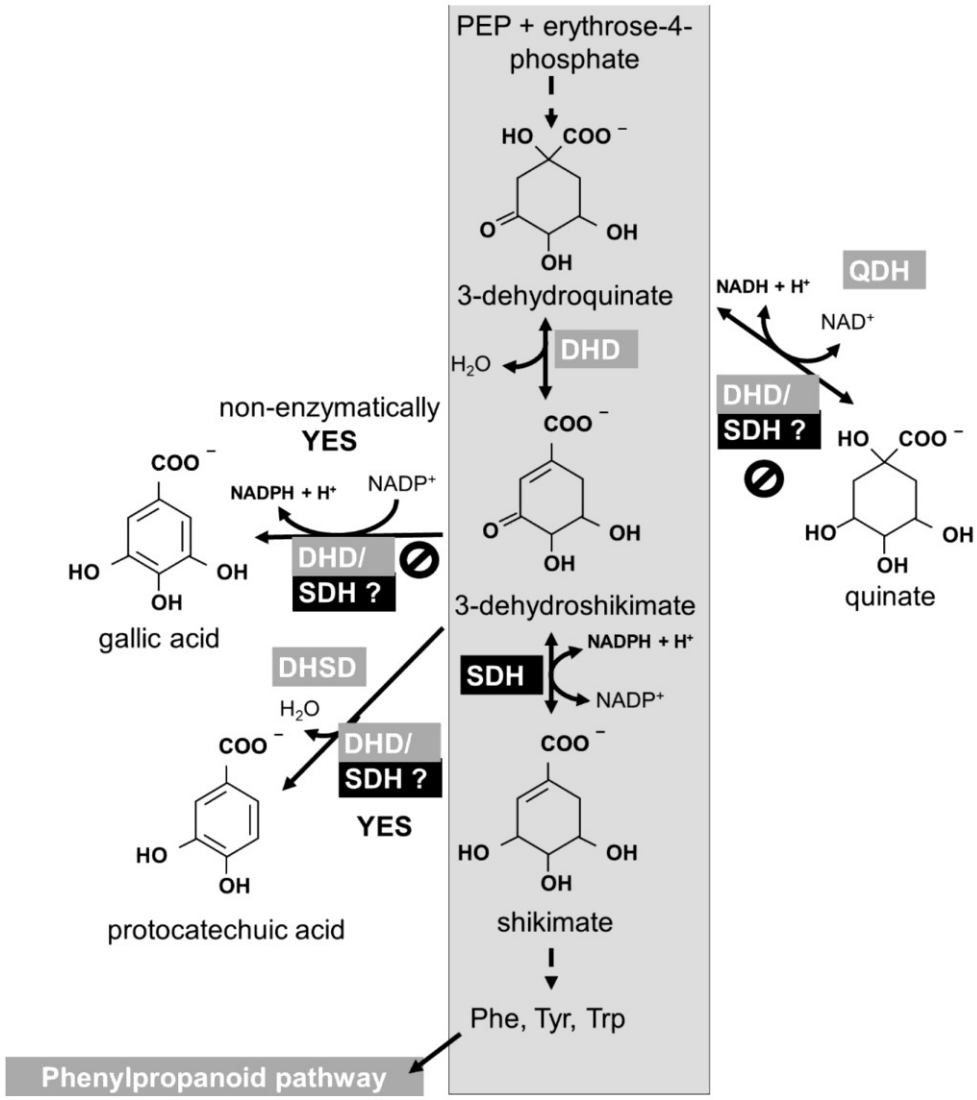


Fig. 5 Proposed kinetic mechanism of the bisubstrate reaction catalyzed by parsley SDH from non-photosynthetic tissue. SDH reaction scheme (A), graphical representation of the product inhibition study in DHS reduction direction (B) and in SA oxidation direction (C) with a formation of dead-end complexes. Non-Competitive (NC) and competitive (C) product inhibitors are indicated.



584

585 **Fig. 6 Identification of parsley SDH products by reversed-phase liquid chromatography**

586 **coupled to electrospray mass spectrometry**. The symbol ∅ indicates that no potential

587 parsley SDH byproduct was identified in the reaction mixtures by mass spectrometry. QDH,

588 quinate dehydrogenase; QD, quinate dehydratase; DHSD, dehydroshikimate dehydratase.

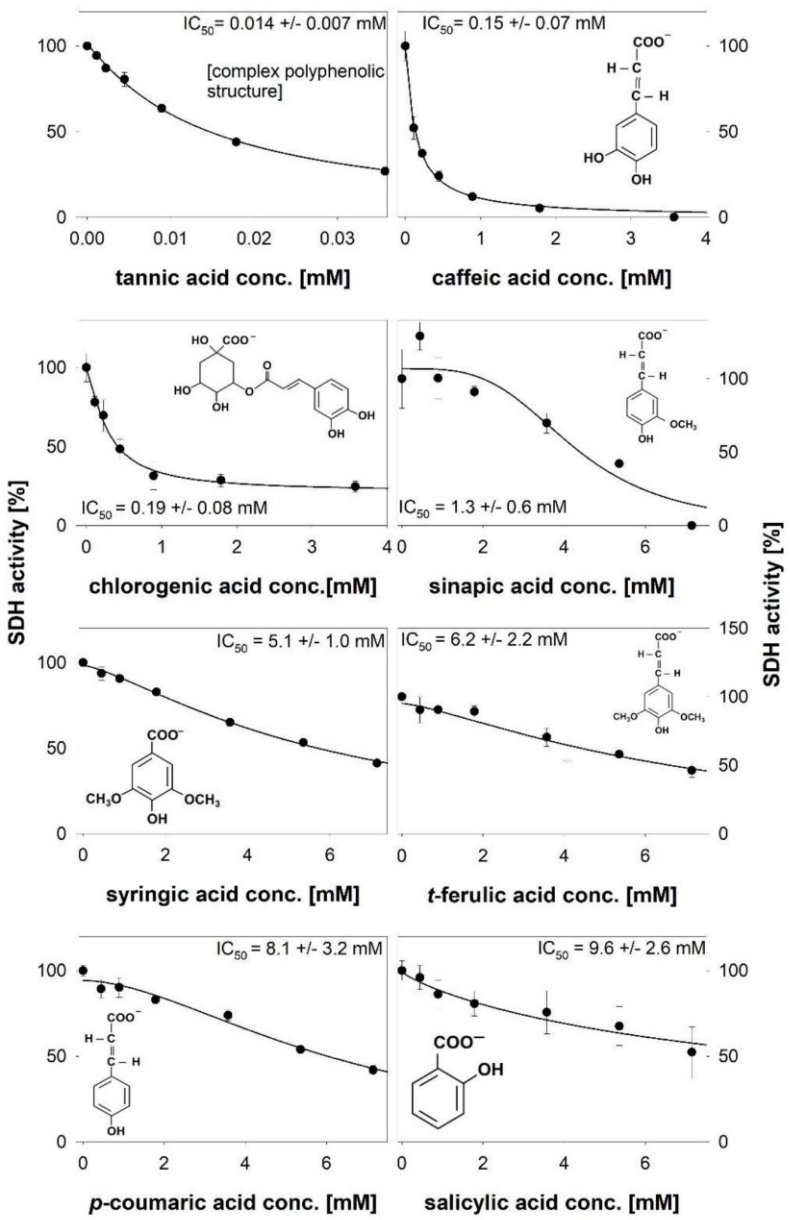


Fig. 7 Inhibition effect of various phenylpropanoids on the activity of parsley SDH.

The specific activity of the enzyme preparations was 0.17 ± 0.07 μmol.min^{-1}mg^{-1}. Controls in 96 and 50 % ethanol were only slightly different from the distilled water control, with specific activities of 0.18 ± 0.06 and 0.19 ± 0.11 μmol.min^{-1}mg^{-1}, respectively. IC_{50} was calculated from

nonlinear regression with Eq. (7). Each determination was done at least 3-times, the average values and standard deviations are shown.

Declaration of competing interest

The authors declare that they have no known competing financial interests or personal relationships that could have appeared to influence the work reported in this table.

Author Contributions: V.H. conceptualization, data curation, formal analysis, investigation, resources, writing-original draft, K.B. investigation, data curation, methodology, validation, formal analysis, funding acquisition, writing-original draft, I.S. investigation, D.K. investigation, data curation, and methodology, M.I. software, validation, writing-review and editing, H.R. supervision, project administration, funding acquisition, resources, writing-review and editing.

Acknowledgement: This work was supported (in part) by Charles University (SVV260572/2020). The authors thank Dr. Carlos V. Melo for English editing the manuscript.

Reference

Avitia-Dominguez, C., Sierra-Campos, E., Salas-Pacheco, J. M., Najera, H., Rojo-Dominguez, A., Cisneros-Martinez, J., Tellez-Valencia, A., 2014. Inhibition and biochemical characterization of methicillin-resistant *Staphylococcus aureus* shikimate dehydrogenase: an in silico and kinetic study. Molecules 19, 4491-4509. https://doi.org/10.3390/molecules19044491.

Baillie, A. C., Corbett, J. R., Dowsett, J. R., McCloskey, P., 1972. Inhibitors of shikimate dehydrogenase as potential herbicides. Pestid. Sci. 3, 113-120. https://doi.org/10.1002/ps.2780030202.

Balinsky, D., Davies, D. D., 1961. Aromatic biosynthesis in higher plants. 1. Preparation and properties of dehydroshikimic reductase. Biochem. J. 80, 292-296. https://doi.org/10.1042/bj0800292.

Balinsky, D., Dennis, A. W., Cleland, W. W., 1971. Kinetic and isotope-exchange studies on shikimate dehydrogenase from *Pisum sativum*. Biochemistry 10, 1947-1952. https://doi.org/10.1021/bi00786a032.

Belonoznikova, K., Vaverova, K., Vanek, T., Kolarik, M., Hyskova, V., Vankova, R., Dobrev, P., Krizek, T., Hodek, O., Cokrtova, K., Stipek, A., Ryslava, H., 2020. Novel insights into the effect of Pythium strains on rapeseed metabolism. Microorganisms 8, doi: 10.3390/microorganisms8101472. https://doi.org/10.3390/microorganisms8101472.

Bontpart, T., Marlin, T., Vialet, S., Guiraud, J. L., Pinasseau, L., Meudec, E., Sommerer, N., Cheynier, V., Terrier, N., 2016. Two shikimate dehydrogenases, VvSDH3 and VvSDH4, are involved in gallic acid biosynthesis in grapevine. J. Exp. Bot. 67, 3537-3550. https://doi.org/ 10.1093/jxb/erw184.

Bradford, M. M., 1976. A rapid and sensitive method for the quantitation of microgram quantities of protein utilizing the principle of protein-dye binding. Anal. Biochem. 72, 248-254. https://doi.org/210.1006/abio.1976.9999.

Buchanan, B. B., Gruissem, W., L.Jones, R., 2000. Biochemistry & Molecular Biology of Plants. American Society of Plant Physiologists, Rockville, Maryland.

Cabane, M., Pireaux, J. C., Leger, E., Weber, E., Dizengremel, P., Pollet, B., Lapierre, C., 2004. Condensed lignins are synthesized in poplar leaves exposed to ozone. Plant Physiol. 134, 586-594. https://doi.org/ 10.1104/pp.103.031765.

Carrington, Y., Guo, J., Le, C. H., Fillo, A., Kwon, J., Tran, L. T., Ehlting, J., 2018. Evolution of a secondary metabolic pathway from primary metabolism: shikimate and quinate biosynthesis in plants. Plant J. 95, 823-833. https://doi.org/ 10.1111/tpj.13990.

Colon, M., Nerin, C., 2016. Synergistic, antagonistic and additive interactions of green tea polyphenols. Eur. Food Res. Technol. 242, 211–220. https://doi.org/ 10.1007/s00217-015-2532-9.

Deng, Y., Lu, S., 2017. Biosynthesis and regulation of phenylpropanoids in plants. Crit. Rev. Plant Sci. 36, 257-290. https://doi.org/10.1080/07352689.2017.1402852.

Derrer, B., Macheroux, P., Kappes, B., 2013. The shikimate pathway in apicomplexan parasites: implications for drug development. Front. Biosci. 18, 944-969. https://doi.org/ 10.2741/4155

Diaz-Quiroz, D. C., Cardona-Felix, C. S., Viveros-Ceballos, J. L., Reyes-Gonzalez, M. A., Bolivar, F., Ordonez, M., Escalante, A., 2018. Synthesis, biological activity and molecular modelling studies of shikimic acid derivatives as inhibitors of the shikimate dehydrogenase enzyme of *Escherichia coli.* J. Enzyme Inhib. Med. Chem. 33, 397-404.

https://doi.org/ 10.1080/14756366.2017.1422125.
Diaz, J., Merino, F., 1997. Shikimate dehydrogenase from pepper (*Capsicum annuum*) seedlings. Purification and properties. Physiol. Plantarum 100, 147-152. https://doi.org/10.1111/j.1399-3054.1997.tb03465.x.
Dowsett, J. R., Middleton, B., Corbett, J. R., Tubbs, P. K., 1972. The anomalous inhibition of shikimate dehydrogenase by analogues of dehydroshikimate. Biochim. Biophys. Acta 276, 344-349. https://doi.org/ 10.1016/0005-2744(72)90994-1.
Drab, T., Kracmerova, J., Ticha, I., Hanzlikova, E., Ticha, M., Ryslava, H., Doubnerova, V., Manaskova-Postlerova, P., Liberda, J., 2011. Native red electrophoresis--a new method suitable for separation of native proteins. Electrophoresis 32, 3597-3599. https://doi.org/ 10.1002/elps.201100310.
Esposito, S., Carfagna, S., Massaro, G., Vona, V., Di Martino Rigano, V., 2001. Glucose-6-phosphate dehydrogenase in barley roots: kinetic properties and localisation of the isoforms. Planta 212, 627-634. https://doi.org/ doi: 10.1007/s004250000443.
Esposito, S., Massaro, G., Vona, V., Di Martino Rigano, V., Carfagna, S., 2003. Glutamate synthesis in barley roots: the role of the plastidic glucose-6-phosphate dehydrogenase. Planta 216, 639-647. https://doi.org/ 10.1007/s00425-002-0892-4.
Fiedler, E., Schultz, G., 1985. Localization, purification, and characterization of shikimate oxidoreductase-dehydroquinate hydrolyase from stroma of spinach chloroplasts. Plant Physiol. 79, 212-218. https://doi.org/ 10.1104/pp.79.1.212.
Fonseca, I. O., Silva, R. G., Fernandes, C. L., de Souza, O. N., Basso, L. A., Santos, D. S., 2007. Kinetic and chemical mechanisms of shikimate dehydrogenase from *Mycobacterium tuberculosis.* Arch. Biochem. Biophys. 457, 123-133. https://doi.org/ 10.1016/j.abb.2006.11.015.
Garcia-Guevara, F., Bravo, I., Martinez-Anaya, C., Segovia, L., 2017. Cofactor specificity switch in shikimate dehydrogenase by rational design and consensus engineering. Protein Eng. Des. Sel. 30, 533-541. https://doi.org/ 10.1093/protein/gzx031.
Grundhofer, P., Niemetz, R., Schilling, G., Gross, G. G., 2001. Biosynthesis and subcellular distribution of hydrolyzable tannins. Phytochemistry 57, 915-927. https://doi.org/ 10.1016/s0031-9422(01)00099-1.
Guo, J., Carrington, Y., Alber, A., Ehlting, J., 2014. Molecular characterization of quinate and shikimate metabolism in *Populus trichocarpa*. J. Biol. Chem. 289, 23846-23858. https://doi.org/ 10.1074/jbc.M114.558536.
Habashi, R., Hacham, Y., Dhakarey, R., Matityahu, I., Holland, D., Tian, L., Amir, R., 2019. Elucidating the role of shikimate dehydrogenase in controlling the production of anthocyanins and hydrolysable tannins in the outer peels of pomegranate. BMC Plant Biol. 19, 476-491. https://doi.org/410.1186/s12870-12019-12042-12871.
Han, C., Wang, L., Yu, K., Chen, L., Hu, L., Chen, K., Jiang, H., Shen, X., 2006. Biochemical characterization and inhibitor discovery of shikimate dehydrogenase from *Helicobacter pylori.* FEBS J. 273, 4682-4692. https://doi.org/ 10.1111/j.1742-4658.2006.05469.x.
Heldt, H.-W., Piechulla, B., Heldt, F., 2011. Plant Biochemistry-Translation of the 4th German edition. Elsevier Academic Press, Amsterdam, Boston, Heildelberg, London, New York, Oxford, Paris, San Diego, San Francisco, Singapore, Sydney, Tokyo.

Huang, K., Li, M., Liu, Y., Zhu, M., Zhao, G., Zhou, Y., Zhang, L., Wu, Y., Dai, X., Xia, T., Gao, L., 2019. Functional analysis of 3-dehydroquinate dehydratase/shikimate dehydrogenases involved in shikimate pathway in Camellia sinensis. Front. Plant Sci. 10, doi: 10.3389/fpls.2019.01268. https://doi.org/10.3389/fpls.2019.01268

Hyskova, V., Belonoznikova, K., Doricova, V., Kavan, D., Gillarova, S., Henke, S., Synkova, H., Ryslava, H., Cerovska, N., 2021. Effects of heat treatment on metabolism of tobacco plants infected with *Potato virus Y*. Plant Biol. doi: 10.1111/plb.13234. https://doi.org/10.1111/plb.13234

Hyskova, V., Pliskova, V., Cerveny, V., Ryslava, H., 2017. NADP-dependent enzymes are involved in response to salt and hypoosmotic stress in cucumber plants. Gen. Physiol. Biophys. 36, 247-258. https://doi.org/ 10.4149/gpb_2016053.

Ikonen, A., Tahvanainen, J., Roininen, H., 2001. Chlorogenic acid as an antiherbivore defence of willows against leaf beetles. Entomol. Exp. Appl. 99, 47–54. https://doi.org/10.1046/j.1570-7458.2001.00800.x.

Kambourakis, S., Frost, J. W., 2000. Synthesis of gallic acid: Cu(2+)-mediated oxidation of 3-dehydroshikimic acid. J. Org. Chem. 65, 6904-6909. https://doi.org/ 10.1021/jo000335z.

Kato, C. G., Goncalves, G. A., Peralta, R. A., Seixas, F. A. V., de Sa-Nakanishi, A. B., Bracht, L., Comar, J. F., Bracht, A., Peralta, R. M., 2017. Inhibition of alpha-amylases by condensed and hydrolysable tannins: focus on kinetics and hypoglycemic actions. Enzyme Res. 2017, doi: 10.1155/2017/5724902. https://doi.org/ 10.1155/2017/5724902.

Kolarovic, J., Popovic, M., Zlinska, J., Trivic, S., Vojnovic, M., 2010. Antioxidant activities of celery and parsley juices in rats treated with doxorubicin. Molecules 15, 6193-6204. https://doi.org/ 10.3390/molecules15096193.

Koshiba, T., 1978. Purification of two forms of the associated 3-dehydroquinate hydro-lyase and shikimate:NADP+ oxidoreductase in *Phaseolus mungo* seedlings. Biochim. Biophys. Acta 522, 10-18. https://doi.org/ 10.1016/0005-2744(78)90317-0.

Kovacik, J., Klejdus, B., Backor, M., 2009. Phenolic metabolism of *Matricaria chamomilla* plants exposed to nickel. J. Plant Physiol. 166, 1460-1464. https://doi.org/ 10.1016/j.jplph.2009.03.002.

Lemos Silva, G. M., Lourenco, E. J., Neves, V. A., 1985. Inhibition of shikimate dehydrogenase from heart-of-palm (*Euterpe oleracea* Mart.). J. Food Biochem. 9, 105-116. https://doi.org/10.1111/j.1745-4514.1985.tb00342.x.

Liang, N., Kitts, D. D., 2015. Role of chlorogenic acids in controlling oxidative and inflammatory stress conditions. Nutrients 8, doi:10.3390/nu8010016. https://doi.org/ 10.3390/nu8010016.

Lourenco, E. J., Neves, V. A., 1984. Partial purification and some properties of shikimate dehydrogenase from tomatoes. Phytochemistry 23, 497-499. https://doi.org/10.1016/S0031-9422(00)80366-0.

Lourenco, E. J., Silva, G. M., Neves, V. A., 1991. Purification and properties of shikimate dehydrogenase from cucumber (*Cucumis sativus* L.). J. Agric. Food Chem. 39, 458-462. https://doi.org/ https://doi.org/10.1021/jf00003a006.

Moura, J. C., Bonine, C. A., de Oliveira Fernandes Viana, J., Dornelas, M. C., Mazzafera, P., 2010. Abiotic and biotic stresses and changes in the lignin content and composition in plants. J. Integr. Plant Biol. 52, 360-376. https://doi.org/ 10.1111/j.1744-7909.2010.00892.x

Muir, R. M., Ibanez, A. M., Uratsu, S. L., Ingham, E. S., Leslie, C. A., McGranahan, G. H., Batra, N., Goyal, S., Joseph, J., Jemmis, E. D., Dandekar, A. M., 2011. Mechanism of gallic acid biosynthesis in bacteria (*Escherichia coli*) and walnut (*Juglans regia*). Plant Mol. Biol. 75, 555-565. https://doi.org/ 10.1007/s11103-011-9739-3.

Nandy, M., Ganguli, N. C., 1961. Studies on 5-dehydroshikimic reductase from mung bean seedlings (*Phaseolus aureus*). Arch. Biochem. Biophys. 92, 399-408. https://doi.org/ 10.1016/0003-9861(61)90378-2.

Niggeweg, R., Michael, A. J., Martin, C., 2004. Engineering plants with increased levels of the antioxidant chlorogenic acid. Nat. Biotechnol. 22, 746-754. https://doi.org/ 10.1038/nbt966.

Peek, J., Shi, T., Christendat, D., 2014. Identification of novel polyphenolic inhibitors of shikimate dehydrogenase (AroE). J. Biomol. Screen 19, 1090-1098. https://doi.org/10.1177/1087057114527127.

Rothe, G. M., 1974. Intracellular compartmentation and regulation of two shikimate dehydrogenase isoenzymes in *Pisum sativum*. Z. Pflanzenphysiol. Bd. 74, 152-159. https://doi.org/10.1016/S0044-328X(74)80168-6.

Ryšlavá, H., Doubnerová, V., Müller, K., Baťková, P., Schnablová, R., Liberda, J., Synková, H., Čeřovská, N., 2007. The enzyme kinetics of the NADP-malic enzyme from tobacco leaves. Czech. Chem. Commun. 72, 1420-1434. https://doi.org/1410.1135/cccc20071420.

Singh, S. A., Christendat, D., 2006. Structure of Arabidopsis dehydroquinate dehydratase-shikimate dehydrogenase and implications for metabolic channeling in the shikimate pathway. Biochemistry 45, 7787-7796. https://doi.org/10.1016/S0044-328X(74)80168-6.

Spoustova, P., Hyskova, V., Muller, K., Schnablova, R., Ryslava, H., Cerovska, N., Malbeck, J., Cvikrova, M., Synkova, H., 2015. Tobacco susceptibility to *Potato virus Y*-NTN infection is affected by grafting and endogenous cytokinin content. Plant Sci. 235, 25-36. https://doi.org/ 10.1016/j.plantsci.2015.02.017.

Tahara, K., Nishiguchi, M., Funke, E., Miyazawa, S.-I., Miyama, T., Milkowski, C., 2021. Dehydroquinate dehydratase/shikimate dehydrogenases involved in gallate biosynthesis of the aluminum‐tolerant tree species *Eucalyptus camaldulensis*. Planta 253, doi: 10.1007/s00425-020-03516-w. https://doi.org/10.1007/s00425-00020-03516-w.

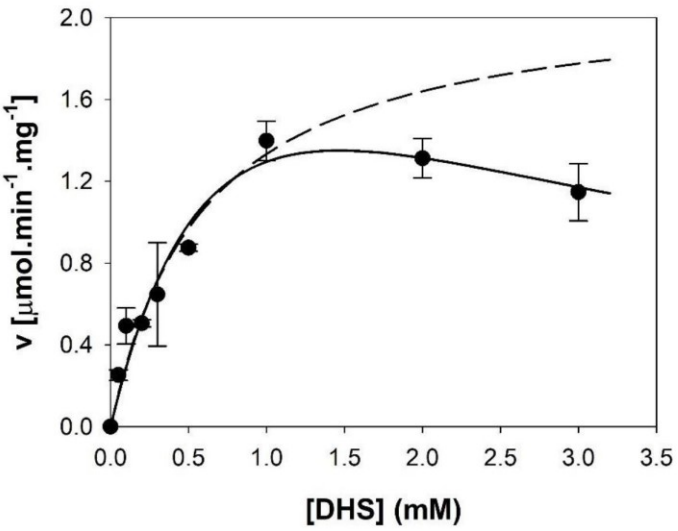
Tintino, S. R., Oliveira-Tintino, C. D., Campina, F. F., Silva, R. L., Costa Mdo, S., Menezes, I. R., Calixto-Junior, J. T., Siqueira-Junior, J. P., Coutinho, H. D., Leal-Balbino, T. C., Balbino, V. Q., 2016. Evaluation of the tannic acid inhibitory effect against the NorA efflux pump of *Staphylococcus aureus*. Microb. Pathog. 97, 9-13. https://doi.org/ 10.1016/j.micpath.2016.04.003.

Tupec, M., Hyskova, V., Belonoznikova, K., Hranicek, J., Cerveny, V., Ryslava, H., 2017. Characterization of some potential medicinal plants from Central Europe by their antioxidant capacity and the presence of metal elements. Food Biosci. 20, 43-50. https://doi.org/10.1016/j.fbio.2017.08.001.

Tzin, V., Galili, G., 2010. New insights into the shikimate and aromatic amino acids biosynthesis pathways in plants. Mol. Plant 3, 956-972. https://doi.org/ 10.1093/mp/ssq048.

Appendix A. Supplementary Data

Supplementary figure



Suppl. Fig. A.1 Inhibition of parsley SDH by excess of substrate DHS. Dashed line: fit with Michaelis-Menten equation, solid line: fit with Eq. (2) for the inhibition by excess of the substrate.

Supplementary methods

Effect of secondary metabolites on SDH –determination of the reversibility of inhibition
The reversibility of inhibition was tested as follows 30-µl aliquots from the incubation mixture consisting of 200 µl of SDH and 400 µl of 5 mM compound were collected at 0, 1, 5, 10, 15, 20, 30, and 60 mins and assayed, as described above. The blank incubation mixture consisted of 200 µl of SDH, 200 µl of 99 % (v/v) formic acid, and 400 µl of 5 mM inhibitor. The inhibitors primarily dissolved in 96 % ethanol and were diluted to a final 30 % concentration in the reaction mixtures. This percentage of ethanol had no effect on activity in the reference samples.

Derived equations used for the determination of the kinetic mechanism
In order to determine the kinetic parameters of the reaction mechanism, the initial reaction rates were measured for different combinations of the reactants in one or another direction. Under such conditions the reaction-products concentration can be considered as zero and thus the reactions in which they appear as reactants can be dismissed from the mechanism. The reaction scheme of the reaction

$P + Q \rightarrow A + B,$

will therefore adopt the following shape:

$$E + Q \underset{k_{-Q}}{\overset{k_Q}{\rightleftarrows}} EQ \qquad \text{Eq.}(A.1)$$

$$E + P \underset{k_{-P}}{\overset{k_P}{\rightleftarrows}} EP \qquad \text{Eq.}(A.2)$$

$$EQ + P \underset{k_{-1}}{\overset{k_1}{\rightleftarrows}} EPQ \qquad \text{Eq.}(A.3)$$

$$EPQ \xrightarrow{k_B} EA + B \qquad Eq.(A.4)$$

$$EA \xrightarrow{k_A} E + A \qquad Eq.(A.5)$$

In accord with the steady-state approximation we assume the steady state of all the enzyme forms taking place in the mechanism which leads to the following equations:

$$\frac{d[EQ]}{dt} = k_Q[E][Q] - k_{-Q}[EQ] - k_1[EQ][P] + k_{-1}[EPQ] = 0 \qquad Eq.(A.6)$$

$$\frac{d[EP]}{dt} = k_P[E][P] - k_{-P}[EP] = 0 \qquad Eq.(A.7)$$

$$\frac{d[EPQ]}{dt} = k_1[EQ][P] - k_{-1}[EPQ] - k_B[EPQ] = 0 \qquad Eq.(A.8)$$

$$\frac{d[EA]}{dt} = k_B[EPQ] - k_A[EA] = 0 \qquad Eq.(A.9)$$

A similar equation for the last enzyme form, i.e. free enzyme E, is linearly dependent on the previous equation and therefore not used here. In addition, the mass-balance equation

$$[E]_0 = [E] + [EQ] + [EP] + [EPQ] + [EA] \qquad Eq.(A.10)$$

is taken into account – it expresses the fact that all the concentrations of the enzyme forms sum up to the total enzyme concentration present in the reaction mixture.

The reaction rate can be defined as the rate of the conversion of the EPQ complex to a complex EA and the product B (eq. A.4):

$$v = k_B[EPQ]. \qquad Eq.(A.11)$$

(Considering only the initial rates, there are no reverse reaction steps behind the EPQ complex. Therefore, we can equally define the overall reaction rate as a rate of eq. A.5, i.e. $v = k_A[EA]$, obviously obtaining the same result. From the same reason it is not necessary to consider more detailed mechanism of converting the EPQ complex to the final products, e.g. including its transformation to an EAB complex.)

Hence, we express all the concentrations of the enzyme forms as functions of $[EPQ]$. Eq. (A.9) and A.8 give the following relations:

$$[EA] = \frac{k_B}{k_A}[EPQ] \qquad Eq.(A.12)$$

$$[EQ] = \frac{k_{-1} + k_B}{k_1[P]}[EPQ] \qquad Eq.(A.13)$$

Eq. A.7 gives

$$[EP] = \frac{k_P}{k_{-P}}[E][P] \qquad Eq.\ (A.14)$$

and from eq. A.6 we obtain

$$k_Q[E][Q] = \big(k_{-Q} + k_1[P]\big)[EQ] - k_{-1}[EPQ]$$

$$= \big(k_{-Q} + k_1[P]\big)\frac{k_{-1} + k_B}{k_1[P]}[EPQ] - k_{-1}[EPQ] \qquad Eq.(A.15)$$

and thus

$$k_Q k_1[P][Q][E] = \big(k_{-Q} + k_1[P]\big)(k_{-1} + k_B)[EPQ] - k_{-1}k_1[P][EPQ] \qquad Eq.(A.16)$$

$$k_Q k_1[P][Q][E] = \left(k_{-Q}k_{-1} + k_{-Q}k_B + k_B k_1[P]\right)[EPQ] \qquad Eq.(A.17)$$

$$[E] = \frac{\left(k_{-Q}k_{-1} + k_{-Q}k_B + k_B k_1[P]\right)}{k_Q k_1[P][Q]}[EPQ]. \qquad Eq.(A.18)$$

Substituting this expression into eq. A.14 gives

$$[EP] = \frac{k_P}{k_{-P}}\frac{\left(k_{-Q}k_{-1} + k_{-Q}k_B + k_B k_1[P]\right)}{k_Q k_1[Q]}[EPQ]. \qquad Eq.(A.19)$$

Expressions given by eqs. A.12, A.13, A.18, A.19 can be substituted to eq. A.10 which leads to

$$[E]_0 = \left(\frac{k_{-Q}k_{-1} + k_{-Q}k_B + k_B k_1[P]}{k_Q k_1[P][Q]} + \frac{k_{-1} + k_B}{k_1[P]} + \frac{k_P}{k_{-P}}\frac{k_{-Q}k_{-1} + k_{-Q}k_B + k_B k_1[P]}{k_Q k_1[Q]} + 1 + \frac{k_B}{k_A}\right)[EPQ]$$

$$= \frac{1}{[P]}\frac{1}{[Q]}\left(\frac{k_{-Q}}{k_Q}\frac{k_{-1} + k_B}{k_1} + \frac{k_B k_1}{k_Q k_1}[P] + \frac{k_{-1} + k_B}{k_1}[Q] + \frac{k_P}{k_{-P}}\frac{k_{-Q}}{k_Q}\frac{k_{-1} + k_B}{k_1}[P] + \frac{k_P}{k_{-P}}\frac{k_B k_1}{k_Q k_1}[P]^2 + \frac{k_A + k_B}{k_A}[P][Q]\right)[EPQ]$$

$$= \frac{1}{[P]}\frac{1}{[Q]}\left[\frac{k_{-Q}}{k_Q}\frac{k_{-1} + k_B}{k_1} + \frac{k_{-1} + k_B}{k_1}[Q] + \left(\frac{k_P}{k_{-P}}\frac{k_{-Q}}{k_Q}\frac{k_{-1} + k_B}{k_1} + \frac{k_B k_1}{k_Q k_1}\right)[P] + \frac{k_P}{k_{-P}}\frac{k_B k_1}{k_Q k_1}[P]^2 + \frac{k_A + k_B}{k_A}[P][Q]\right][EPQ] \qquad Eq.(A.20)$$

From this equation we obtain

$$[EPQ] = \frac{[E]_0[P][Q]}{\frac{k_{-Q}}{k_Q}\frac{k_{-1} + k_B}{k_1} + \frac{k_{-1} + k_B}{k_1}[Q] + \left(\frac{k_P}{k_{-P}}\frac{k_{-Q}}{k_Q}\frac{k_{-1} + k_B}{k_1} + \frac{k_B k_1}{k_Q k_1}\right)[P] + \frac{k_P}{k_{-P}}\frac{k_B k_1}{k_Q k_1}[P]^2 + \frac{k_A + k_B}{k_A}[P][Q]} \qquad Eq.(A.21)$$

and, considering eq. A.11,

$$v = k_B[EPQ] = \frac{k_A k_B}{k_A + k_B}[E]_0[P][Q]\left[\frac{k_A}{k_A + k_B}\frac{k_{-Q}}{k_Q}\frac{k_{-1} + k_B}{k_1} + \frac{k_A}{k_A + k_B}\frac{k_{-1} + k_B}{k_1}[Q] + \frac{k_A}{k_A + k_B}\left(\frac{k_P}{k_{-P}}\frac{k_{-Q}}{k_Q}\frac{k_{-1} + k_B}{k_1} + \frac{k_B}{k_Q}\right)[P] + \frac{k_A}{k_A + k_B}\frac{k_P}{k_{-P}}\frac{k_B}{k_Q}[P]^2 + [P][Q]\right]^{-1}$$

$$= \frac{v_{max}[P][Q]}{K_A + K_{mP}[Q] + K_{mQ}[P] + K_x[P]^2 + [P][Q]} \qquad Eq.(A.22)$$

The constants in eq. A.22 are defined as follows:

$$v_{max} = \frac{k_A k_B}{k_A + k_B}[E]_0 \qquad Eq.(A.23)$$

$$K_A = \frac{k_A}{k_A + k_B}\frac{k_{-Q}}{k_Q}\frac{k_{-1} + k_B}{k_1} \qquad Eq.(A.24)$$

$$K_{mP} = \frac{k_A}{k_A + k_B}\frac{k_{-1} + k_B}{k_1} \qquad Eq.(A.25)$$

$$K_{mQ} = \frac{k_A}{k_A + k_B}\left(\frac{k_P}{k_{-P}}\frac{k_{-Q}}{k_Q}\frac{k_{-1} + k_B}{k_1} + \frac{k_B}{k_Q}\right) \qquad Eq.(A.26)$$

$$K_x = \frac{k_A}{k_A + k_B}\frac{k_P}{k_{-P}}\frac{k_B}{k_Q} \qquad Eq.(A.27)$$

All the symbols, except for K_x, were chosen in analogy with the conventions used at the ordered two-substrate mechanism. The symbol v_{max}, in the current mechanism, does not have the meaning of the limit maximum reaction rate, since at high concentrations of P inhibition by substrate takes place inevitably. Therefore, it is only a formal symbol resembling the ordered mechanism that adopts the original meaning in case that $K_x \to 0$.

The reciprocal dependence of $\frac{1}{v}$ on $\frac{1}{[P]}$ and $\frac{1}{[Q]}$ then reads

$$\frac{1}{v} = \frac{1}{v_{max}}\left(K_A\frac{1}{[P]}\frac{1}{[Q]} + K_{mP}\frac{1}{[P]} + K_{mQ}\frac{1}{[Q]} + K_x\frac{[P]}{[Q]} + 1\right) \qquad Eq.(A.28)$$

The following relations can be found among the constants in eq. A.28:

$$K_A = \frac{k_{-Q}}{k_Q}K_{mP} \qquad Eq.(A.29)$$

$$K_{mQ} = \frac{k_P}{k_{-P}}K_A + \frac{k_{-P}}{k_P}K_x \qquad Eq.(A.30)$$

As K_{mP} is independent of k_Q and k_{-Q} and K_A is independent of k_P and k_{-P}, the constants K_A, K_{mP}, K_{mQ}, K_x are independent in the sense that they may adopt any combination of values without being determined by one another. Thus, when determining them from the experimental data we need not work with the individual rate constants but we can only take these cumulative constants into account.

Eqs. A.22 and A.28 can be analogously applied at the initial-velocity experiments with the reverse reaction, i.e.

$A + B \to P + Q$.

In this case we substitute $Q \to A$ and $P \to B$ and obtain

$$v = \frac{v_{max}[B][A]}{K'_A + K_{mB}[A] + K_{mA}[B] + K'_x[B]^2 + [B][A]} \qquad Eq.(A.31)$$

and

$$\frac{1}{v} = \frac{1}{v_{max}}\left(K'_A\frac{1}{[B]}\frac{1}{[A]} + K_{mP}\frac{1}{[B]} + K_{mQ}\frac{1}{[A]} + K'_x\frac{[B]}{[A]} + 1\right). \qquad Eq.(A.32)$$

3.2.5 Side effects of triazoles on treated crops

In 2021, we published our first results from the pot experiments with *Solanum lycopersicum* L. plants that were treated with triazole fungicides cyproconazole, penconazole, tebuconazole and all their combinations (Jakl et al 2021a, Jakl et al 2021b). We already showed that triazole interactions lead to more distinct "cocktail" effects (Jaklová Dytrtová et al 2020, Jaklová Dytrtová et al 2021, Jaklová Dytrtová et al 2018). The plants were treated weekly with triazole foliar application as performed in the agriculture practice for 53 days. Samples of leaves and tomatoes were harvested twice during the experiment (Fig. 16).

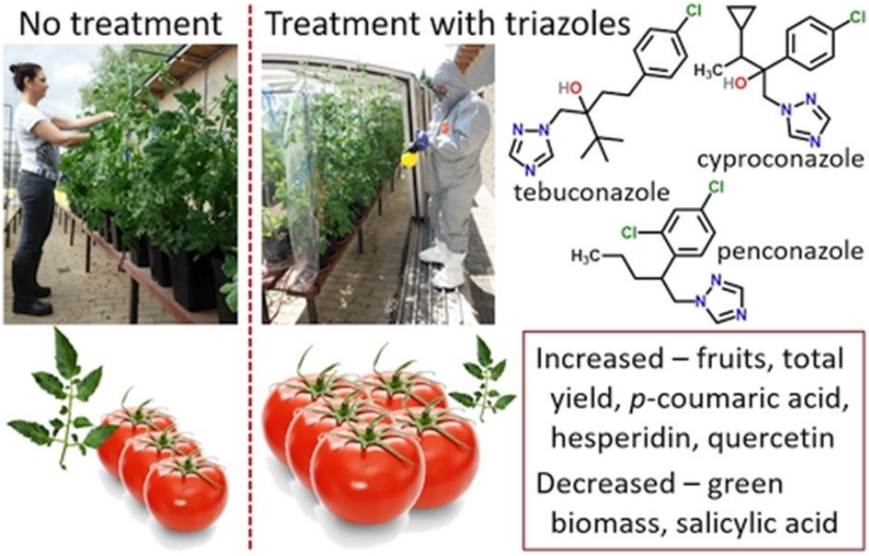


Fig. 16: Graphical abstract (Jakl et al 2021a).

In the 1st harvest, we observed a significant increase in the tomato yield and size but a decreased concentration of chlorophyll *a* and *b* in the comparison with the control (untreated) plants (Fig. 2, 4 in Jakl et al 2021a). We supposed that triazoles could interfere with enzymes involved in the chlorophyll biosynthesis. Also, triazoles could have fallen from the leaves (or by inaccurate spraying) and got into the soil where they can create complexes with cations and influence the plant uptake of some essential minerals (Jakl et al 2021a, Jakl et al 2017).

The main goal was to follow the content of phenolic acids as potential antioxidants in the peel of tomato fruit because we supposed that triazoles may represent a significant stress factor. Also, higher activities of antioxidant enzymes such as superoxide dismutase and peroxidase were reported after triazole application (Tuna 2014). In all treated variants (except for tebuconazole mixtures)

the content of chlorogenic acid (CGA, Fig. 5 in Jakl et al 2021a) was significantly increased in the 1st tomato harvest. The elevated CGA concentration compared to the control in the single-azole variants during the first ripening could be related to the protection mechanisms against triazoles-induced oxidation. In the 2nd tomato harvest the CGA content decreased approx. to 40% after penconazole and cyproconazole treatments in comparison with the 1st harvest. It may indicate a response to oxidation stress however, this adaptation was not observed for single tebuconazole treatment. Another detected phenolic acid was *p*-coumaric acid and its content in the 1st tomato harvest was higher than in the 2nd one (Fig.5 in Jakl et al 2021a). It was slightly higher in the treated groups, except for cyproconazole-treated (significantly higher) and tebuconazole-treated (significantly lower), also suggesting its role in triazole treatment response. We also tried to analyze the trends of the detected phenolic compounds between the 1st and 2nd harvests. We observed negative correlations – a decrease of quercetin and *p*-coumaric acid which serve as the respective precursors for quercitrin and CGA which increased. Then mild positive correlations were calculated for CGA and hesperidin, and CGA and quercitrin (Table SI5, Fig. 5 in Jakl et al 2021a).

The information of triazole impact on the plant metabolism are still rather scarce, especially for the effect of cocktails of triazoles. In our future research, we would like to focus on various plant metabolic enzymes to determine which pathway (e.g., antioxidant, biotransformation systems) might be affected the most.

My contribution:

I was kindly invited to analyze the data statistically. I prepared the resulting tables and helped in editing the manuscript as well as in critical reading.

Chemosphere 277 (2021) 130242

Contents lists available at ScienceDirect

Chemosphere

journal homepage: www.elsevier.com/locate/chemosphere

Side effects of triazoles on treated crops

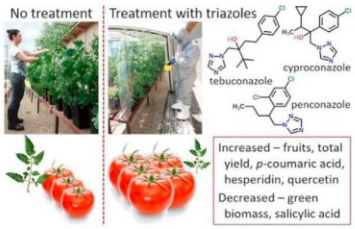
Michal Jakl [a], Sanja Ćavar Zeljković [b, c], Ishak Kovač [d, e], Kateřina Bělonožníková [f], Jana Jaklová Dytrtová [d, g, *]

[a] Czech University of Life Sciences Prague, Faculty of Agrobiology, Food and Natural Resources, Department of Agro-Environmental Chemistry and Plant Nutrition, Prague – Suchdol, Czech Republic
[b] Centre of the Region Haná for Biotechnological and Agricultural Research, Department of Genetic Resources for Vegetables, Medicinal and Special Plants, Crop Research Institute, Olomouc, Czech Republic
[c] Centre of Region Haná for Biotechnological and Agricultural Research, Palacký University, Department of Phytochemistry, Olomouc, Czech Republic
[d] Czech Academy of Sciences, Institute of Organic Chemistry and Biochemistry, Prague 6, Czech Republic
[e] Charles University, Faculty of Science, Department of Analytical Chemistry, Prague 2, Czech Republic
[f] Charles University, Faculty of Science, Department of Biochemistry, Prague 2, Czech Republic
[g] Charles University, Faculty of Physical Education and Sport, Department of Physiology and Biochemistry, Prague 6, Czech Republic

HIGHLIGHTS

- Triazoles foliar treatment induces significant stress for tomato plants.
- The stress is manifested by the green biomass decrease and fructification increase.
- Content of the majority of determining phenolic compounds increased.
- Content of chlorophylls in leaves decreased.

GRAPHICAL ABSTRACT



ARTICLE INFO

Article history:
Received 19 January 2021
Received in revised form
8 March 2021
Accepted 9 March 2021
Available online 15 March 2021

Handling Editor: Willie Peijnenburg

Keywords:
Chlorophylls
Foliar treatment
Phenolic compounds
Redox conditions

ABSTRACT

Triazolic fungicides are widely applied in crop production to protect plants against fungal pathogens. However, they may influence the biochemical processes in plants and other non-target species. This paper is aimed at the effect of triazoles (namely tebuconazole, cyproconazole, and penconazole) single/mixed applications on the phenolics production in tomato (*Solanum lycopersicum* L.) fruit peel, amount of chlorophyll *a and b* in tomato leaves as well as on basic plant growth parameters. For this purpose, cherry tomatoes were planted in the pot experiment and foliarly-treated weekly, with the same total triazoles dose of 3.52 μmol per plant (in mixtures of 1.71 or 1.17 μmol of each in two or three components, respectively). The treatments increased the weight of fruits in the 1st harvest about 43%, however, this effect was not observed in the next harvest. Increased oxidative stress in the triazoles presence was observed, based on the elevated production of antioxidant phenolics in the 1st harvest. Most alarming is the decrease of the weight of thin stems and foliage and the concentration of chlorophyll *a* (*b*) in leaves in

Abbreviations: Cyp, cyproconazole; Pen, penconazole; Teb, tebuconazole; CGA, chlorogenic acid; PCA, *p*-coumaric acid.

* Corresponding author. Czech Academy of Sciences, Institute of Organic Chemistry and Biochemistry, Flemingovo nám. 542/2, 166 10 Prague 6, Czech Republic; Charles University, Faculty of Physical Education and Sport, Department of Physiology and Biochemistry, José Martího 269/31, 162 52, Prague 6, Czech Republic.
E-mail addresses: dytrtova@uochb.cas.cz, dytrtova@ftvs.cuni.cz (J. Jaklová Dytrtová).

https://doi.org/10.1016/j.chemosphere.2021.130242
0045-6535/© 2021 Elsevier Ltd. All rights reserved.

Tomato
Triazolic mixtures

all triazoles-treated variants. The non-target impacts on plant biochemical processes (related to the phenolics or chlorophylls production and functionality) were confirmed.

© 2021 Elsevier Ltd. All rights reserved.

1. Introduction

The group of **triazolic fungicides** (tebuconazole, penconazole, cyproconazole, and others) is being widely used in the protection of vegetables, fruits, etc. in crop production. The presence of azoles in the environment influences not only the target enzymes (14α-demethylase) and the target species (fungi), but also other enzymes like aromatase (Conner et al., 2012; Jaklová Dytrtová et al., 2020), superoxide dismutase and peroxidase (Tuna, 2014), α-amylase and β-amylase (Gopi et al., 2007), and probably other enzymes from the large cytochrome P450 family, which are widely present in the plant, animal as well as fungi kingdoms (Chen and Ying, 2015; Beijer et al., 2018). It means that the presence of triazoles might also influence directly the enzymes or mechanisms in the protected plants responsible for plant growth, fructification, oxidation, chlorophylls synthesis, production of phenolic compounds etc. (Gopi et al., 2007; Tuna, 2014; Jakl et al., 2021). Besides, it is important to know how the antifungal plant protection with triazoles influences the quality of fruits and also the physiological functions and fitness of the plant. This information is still not well discovered.

In the research, we have focused on the description of basic plant growing parameters (amount of green biomass, size of fruits, the total yield of fruits), chlorophyll *a and b* contents, and the content of selected flavonoids (quercetin, quercitrin), flavanones (hesperidin) (Rice-Evans et al., 1996), chlorogenic acid, salicylic acid, and *p*-coumaric acid being among the most abundant polyphenolic compounds in tomato (García-Valverde et al., 2013; Martí et al., 2016). In general, the synthesis of phenolics in plants can be affected by the application of various pesticides (mostly herbicides, insecticides, and fungicides) (Daniel et al., 1999). However, this finding is too general. Even between fungicides based on the triazole ring, there are huge differences in the attached chains, and thus in their effect. They affect several P450 enzymes, and thus also the synthesis of biologically active substances, not excluding phenolic ones (Tietjen, 2017). The situation complicates when the triazoles are applied in a mixture. For this pilot study, 3 similar, often agriculturally applied triazoles with a relatively "uncomplicated" structure were selected. It is expected that the effect of triazoles on the system is not one-level and the cocktail interactions have to be further included and intensively studied.

Among phenolics, especially **flavonoids** are considered as important biologically active compounds produced in several plants. Their activities (Heim et al., 2002; Khoddami et al., 2013; Kumar and Pandey, 2013; Karak, 2019) are dependent on their structure, mainly on their structural class, degree of hydroxylation, other substitutions and conjugations, and degree of polymerization. Within plants, mostly they have a function as signal molecules, allopathic compounds, phytoalexins, detoxifying agents, and antimicrobial defensive compounds (Panche et al., 2016; Mathesius, 2018). Among others, the presence of phenolic antioxidants protecting against pathogens attack may be beneficial also for consumers (Jaklová Dytrtová et al., 2018). **Chlorogenic acid** (CGA) is implicated in biotic and abiotic stress responses (Lallemand et al., 2012). ***p*-Coumaric acid** (4-hydroxycinnamic acid) belongs among natural esters of hydroxycinnamic acid compounds modulating plant growth and metabolism. **Salicylic acid** is a plant hormone participating in many processes such as growth, development, photosynthesis, transpiration, ion uptake, and transport (Vlot et al., 2009). It is involved in endogenous signaling, mediating, and plant defense against pathogens (Hayat and Ahmad, 2007), in the pathogen attack signaling system its methyl salicylate serves as a volatile agent (ester) enable to transfer the signal into other parts of the plant.

As the information about the effect of triazoles on the whole system is incomplete, this paper aims to characterize the effect of selected triazole fungicides on the production of phenolic compounds and chlorophylls in tomato (*Solanum lycopersicum* L.) as a model plant, as well as production of the fruits.

2. Materials and methods

2.1. Pot experiment and treatments

The pot experiment was performed with five-week-old tomato (*Solanum lycopersicum* L. var. 'Sweet Cherry') seedlings from their first filial generation from one parent tomato plant. Each 4L pot contained 500 g dwt of ready-mix "Horticultural Substrate with Active Humus" and added mineral nutrients (AGRO CS a.s., Czech Republic) and one randomly-selected tomato seedling. They were grown for 53 days in a vegetation hall with natural temperature and light (Fig. SI1) and root irrigation with demineralised water. After four and seven weeks the plants were planted, a mixture of mineral macronutrients in liquid form (Lovoflor NPK 4—2.5-3, Lovochemie a.s., Czech Republic) in an optional fertiliser dose (0.75 mL/kg) was added to the soil of each plant to provide for its basic needs.

To determine the effect of the individual fungicidal substances directly in the form in which they are applied (including additives), commercial products containing given active substances were used. For application, the dose was always based on the ranges in application sheets given by the manufacturer for spraying tomatoes to meet the total triazoles amount of $3.52 \cdot 10^{-6}$ mol per plant (calculated from their declared content).

The experiment was set up in seven different triazole treatments and control (**Table 1**), in five replicates each, i.e. in five pots, with one plant each. Treatments were carried out *via* foliar application, i.e. by precise gentle spraying (preventing losses) of the above-ground biomass with a suspension of a given triazole or a given mixture of triazoles, every week during the tomato plantation, in the same dose as the initial. The control variant sprayed with demineralised water served as a comparison.

For the determination of phenolic compounds, the ripened tomato fruits of all plants were harvested twice, after four weeks from the first treatment and after six weeks, within the termination. For chlorophylls determination, the green biomass was sampled at the same time as the fruits. The pictures from the pot experiment are comprised in Fig. 1.

2.2. Chlorophylls determination

An aliquot (1 g) of fresh leaves samples was weighed into a ceramic mortar and quartz sand was added. To neutralize the organic acids released from the tissues a teaspoon of $MgCO_3$ (p.a., Sigma-Aldrich) was added. The leaves were then ground using a pestle. After complete comminution, the sample was quantitatively

Table 1
Setup of triazoles equimolar treatment in the pot experiment.

No.	Abbreviation	Triazole(s) applied in a mixture	Amount[a] of each triazole (μmol/plant)
1	Con	control	0
2	Cyp	cyproconazole	3.52
3	Pen	penconazole	3.52
4	Teb	tebuconazole	3.52
5	Cyp-Pen	cyproconazole + penconazole	1.76
6	Cyp-Teb	cyproconazole + tebuconazole	1.76
7	Pen-Teb	penconazole + tebuconazole	1.76
8	Cyp-Pen-Teb	cyproconazole + penconazole + tebuconazole	1.17

[a] In all treatments, the sum of the triazoles was the same - 3.52 μmol per plant.

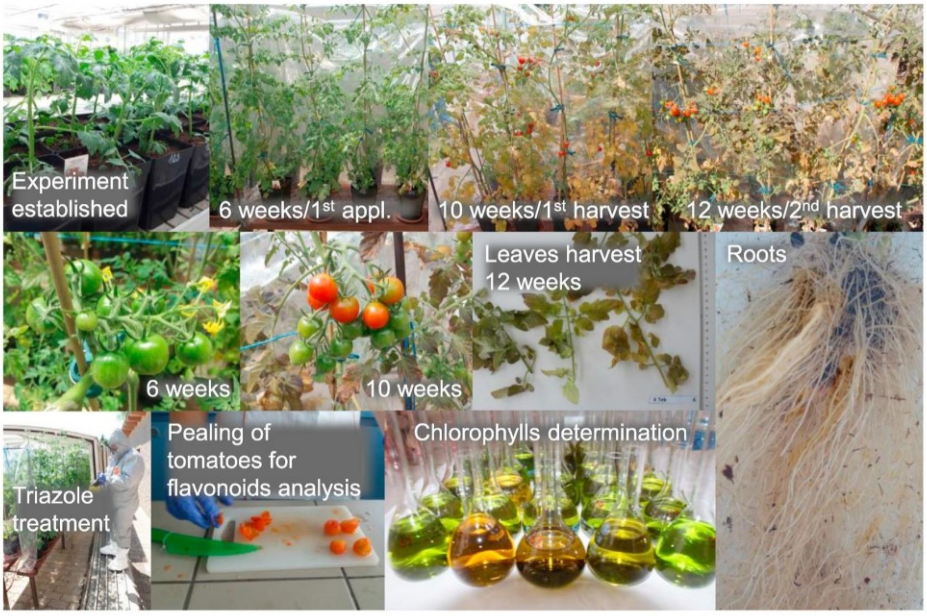


Fig. 1. Selection of pictures comprising the most important milestones of the pot experiment.

transferred with 80% acetone (ACS, Sigma-Aldrich) onto a paper filter, filtered directly into a 50 mL volumetric flask, rinsed thoroughly, and filled up to the mark with 80% acetone. The samples were analyzed using a spectrophotometer (LAMBDA 25, PerkinElmer, USA) at 663 and 647 nm wavelengths and empirical formulas (Wellburn, 1994):

$$\text{chlorophyll } a \text{ (CHL}a\text{)} = 12.25A_{663} - 2.79\ A_{647}\ \text{(mg/L)}$$

$$\text{chlorophyll } b \text{ (CHL}b\text{)} = -5.1A_{663} + 20.5\ A_{647}\ \text{(mg/L)}$$

Results were expressed in milligrams of chlorophylls per kilogram of dry biomass (105 °C).

2.3. Determination of phenolic compounds

A sample extract was prepared from freshly harvested tomatoes. Before the extraction, tomato samples were peeled and gained peel was used for phenolic determination. For extraction of the phenolic compounds, a mixture of acetone and water (7:3) was used. All samples were weighted to the approximate value of 2 g. Appropriate volume of the solvent for the weighted sample is calculated from the ratio that 5 mL of extraction mixture is needed for 1 g of sample.

The extraction of the phenolic compounds was performed in a sonication bath for 10 min. After sonication, all samples were centrifuged for 10 min at 5G. Subsequently, 1.5 mL of supernatant were transferred into Eppendorf vials and stored at −80 °C until they were analyzed.

A 50 μL of sample extract was evaporated under vacuum and then reconstituted in the mobile phase. UHPLC-MS/MS analysis of the extracts was performed on Nexera X2 UHPLC (Shimadzu Handels GmbH) coupled with a MS-8050 (Shimadzu Handels GmbH). Chromatographic separation was performed on an UHPLC Acquity BEH C18 (150 × 3.0 mm; 1.7 μm particle size) column (Waters Corp., Milford, MA, USA) that was kept at 40 °C. The mobile phase consisted of 10 mmol/L formic acid in water (component A) and acetonitrile (component B). Totally 32 analytes were separated using a binary gradient starting at 5% B for 3 min, 5–25% B for next 4 min, 25–30% B for 6 min, 30–35% B for next 4 min, 35–60% B for 6 min, 60–100% for next 4 min, then isocratic for 1.5 min, back to 5% B within 0.1 min, and equilibration for 3.4 min. The flow rate was 0.4 mL/min and the injection volume 10 μL.

All analytes were analyzed in negative ionization mode ESI-, using multiple reaction monitoring (MRM) mode for their identification and quantification (Supplementary **Table SI1**). The spray

voltage was 3 kV, and the vaporizer and the ion transfer tube temperatures were 320 °C. Standard solutions of 32 target compounds (Supplementary **Table SI1**), purchased from Sigma-Aldrich (Czech Republic), were firstly prepared in methanol at 1 mmol/L concentration. All solutions were gradually diluted in the mobile phase to the working concentrations ranged from 0.01 to 50 μmol/L. Quantification was performed by isotope diluting method with *p*-coumaric acid-d_6 and salicylic acid-d_4 (Toronto Research Chemicals, Canada) as internal standards.

2.4. Statistical analysis

The results of the analyses performed in Five replicates and two technical repeats were statistically processed by One Way ANOVA (Tukey method), and *t*-test, using the statistical software TIBCO Statistica (v. 13.5.0.17; TIBCO Software Inc.) and by Pearson Product Moment Correlation using SigmaPlot (v.12.5; Systat Software Inc.). The differences were considered statistically significant at $P \leq 0.05$.

3. Results and discussion

3.1. Fructification

The weight of tomato fruits, as well as the weight of whole plants, are some of the basic parameters of the triazoles treatment impact (Fig. 2, **Table 2**, **Table SI2**). In the 1st harvest, the average weight of tomato fruits from the control was significantly the smallest in contrast to all treated variants. In the 2nd harvest, there were no significant differences in fruit weight among variants. The tomato fruits of the 2nd harvest were significantly smaller (42% on average) than the tomato fruits in the 1st harvest. This difference can be explained by the depletion of nutrients in the soil medium during the plants growth (Jakl et al., 2021), by colder weather or by visibly worse plant fitness during the last two weeks of the experiment. Nitrogen and potassium uptake is slow at the beginning of the plant growth, and then it rapidly increases during the flowering stages. Potassium is highly required during fruit development, and nitrogen uptake is increased mainly after the formation of the first fruits, other nutrients (P, Ca, and Mg) are required constantly (Ozores-Hampton et al., 2015). We have compensated the nutrition demands *via* regular fertilization with N, P, and K. Nevertheless, probably this compensation was not absolute and the tomatoes in the 1st harvest (Fig. 2a) were above 43% bigger (9.0 g/tomato on average including the control) than the tomatoes in the 2nd harvest (Fig. 2b) (5.2 g/tomato on average including the control). The average atmospheric temperature during the last 2 weeks before the 1st harvest was 28 °C and during the last 2 weeks before the 2nd it was 23 °C. Also the number of sunny days decreased, the full sunlight decreased from 11.5 h to 6 h a day (Fig. SI1). In the 1st harvest the weight of tomato fruits of the control was the smallest (6.7 g/tomato) comparing to the treated variants (9.4 g/tomato on the average), which is 40.3% more (Fig. 2a). Whereas in the 2nd harvest the weight of tomato fruits of the control was 4.6 g/tomato and 5.3 g/tomato on the average of the treated variants, which is 15.2% more (Fig. 2b). In the 2nd harvest all the weights were more unified. As a result, the weight decrease of the non-treated tomatoes (control) was 31% and the treated tomatoes it was 44%. Therefore, the higher weight decay (above 13%) in the treated tomatoes can be ascribed to the triazoles application. However it is relative; it seems that at the beginning the treated tomato plants were protected against pathogens by the triazole application, therefore tomato plants had invested the energy sources into the fruit growth instead of the protection against pathogens. Whereas the level of protection was different among the treated variants. It seems that the highest protection against pathogens was for the treatment with Teb (because the weight of tomato fruits was 10.8 g/tomato), the smallest one (among the treated variants) was for the Teb*Pen treatment (8.1 g/tomato). From this viewpoint, it seems that the foliar application of triazoles induces a bigger size of tomato fruits; however, this benefit was almost lost at the end of the experiment because the plants visibly suffered from fungal infection as well as by cloudy weather. This benefit loss can be also caused by the created resistance of fungal pathogens at the end of the experiment (Vanden Bossche et al., 1998). Additionally, the total weight of the plants (1st and 2nd harvest together) shows a similar trend as the size of the tomatoes. The smallest weight of the total tomatoes yield was for the control (55.81 g), while the average weight of the treated plants was 92.93 g (**Table SI2**). It is visible that

Table 2
Decrease of the average fruit weight (percentage) from the 1st to the 2nd harvest.

treatment	weight decrease (%)
Teb	48.2
Pen	50.6
Cyp	38.0
Teb*Pen	40.5
Teb*Cyp	37.7
Pen*Cyp	43.2
Teb*Pen*Cyp	47.8
control	30.8
average of all variants	43.7

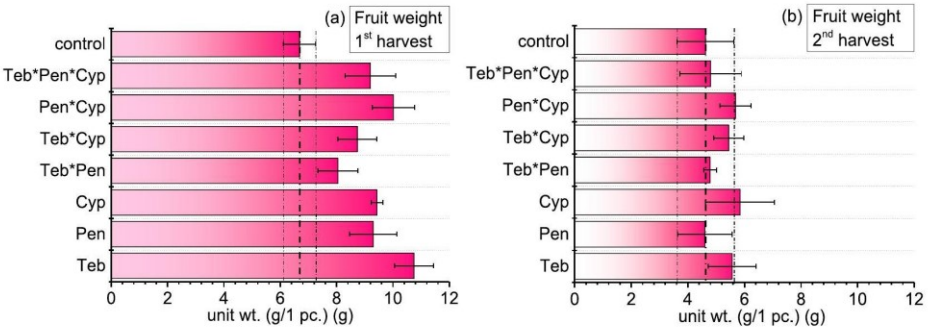


Fig. 2. Average fruit weight (g) within the variants for (a) the first and (b) the second harvest. Intervals represent confidence intervals ($n = 10$, $P < 0.05$).

the triazole treatment significantly increase the yield, as well as the size of the fruit.

3.2. Green biomass and chlorophyll

The green biomass was harvested at the end of the experiment (Fig. SI2) at the same time as the 2nd fruits harvest and divided into stems (Fig. 3a,b,c) and leaves (Fig. 3d). In the weight of the thick stems (Fig. 3a), there are no significant differences among variants. The differences were seen in thin stem weight (Fig. 3b), where the number of thin stems was slightly lower for the majority of treated variants (significant for Teb*Pen*Cyp, Teb*Cyp, and Teb treatment). Only the Cyp variant had a higher amount of thin stems than the control. There is also a significant difference in the weight of leaves between the treated variants and the control (Fig. 3d). The leaves weight is higher in the control, the treated variants have a lower weight of leaves (significantly for Teb*Pen*Cyp, Teb*Cyp, Teb*Pen, and Teb). The green leaves are the most responsible tissue for photosynthesis (Sarlikioti et al., 2011), therefore the decrease of the leaves weight caused by the treatment can be considered alarming from the photosynthetic point of view. On the other hand, the whole view has to be completed with the information on the content of chlorophylls (Fig. 4).

The content of chlorophylls *a and b* was measured in two harvests (1st harvest at the same time as the first harvest of ripe tomato fruits and the 2nd at the end of the experiment) (Fig. 4, Table SI3). In the 1st harvest, the content of chlorophyll *a* is significantly higher in the control in contrast to all treated variants (Fig. 4a, Table SI4). The content of chlorophyll *b* in the 1st harvest is also higher in the control than in treated variants, but mostly not significantly (Fig. 4b, Table SI4). These differences might be caused by the changed uptake of some essential minerals from the soil (because the part of foliar-applied triazoles can get into the soil (Takala et al., 2019). It is known, that triazoles can create complexes with dications, with unexpected changes in the chemistry of the triazoles (Jaklová Dytrtová et al., 2014; Jakl et al., 2017; Kovač et al., 2020). On the other hand, the presence of triazoles might influence directly the enzymes or mechanisms responsible for chlorophylls synthesis. The possible impact of triazoles can be on the level of enzymes or even gene expression (transcription as well as translation). For example, it is known that the overexpression of H3K27me3 demethylase REF 6 accelerates the degradation of chlorophylls (Wang et al., 2019). On the other hand, it is also well known that triazoles inhibit the activity of demethylases. Nevertheless, we have not at disposal yet any relevant data that triazoles directly or indirectly influence the biosynthesis of chlorophylls. Therefore, the discussion of the chlorophylls content in tomato leaves after different triazoles cocktail applications occurs on a theoretical level. Further research is essential.

The data about the chlorophylls *a and b* content in the 2nd harvest (Fig. 4c and d, Table SI4) indicate that the lower content of chlorophyll *a and b* were equalized at the end of the vegetation period. This indicates that plants can compensate for the negative impact of triazoles treatment within the time, which is a positive finding.

From the comparison between the 1st and the 2nd harvests, it can be seen that the content of chlorophyll *a* (Fig. 4a,c) in the control is relatively stable or slightly decreased (378 mg/kg and

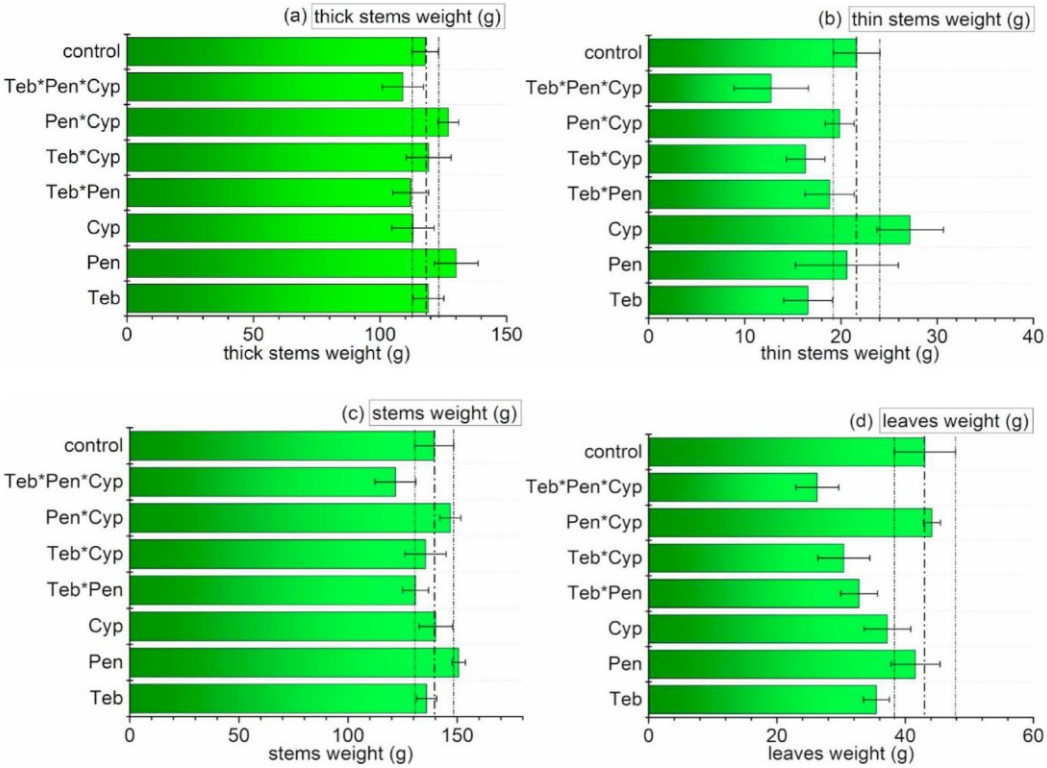


Fig. 3. Average weight (g) of tomato (a) thick stems, (b) thin stems, (c) whole stems, (d) leaves. Intervals represent confidence intervals (n = 5, P < 0.05).

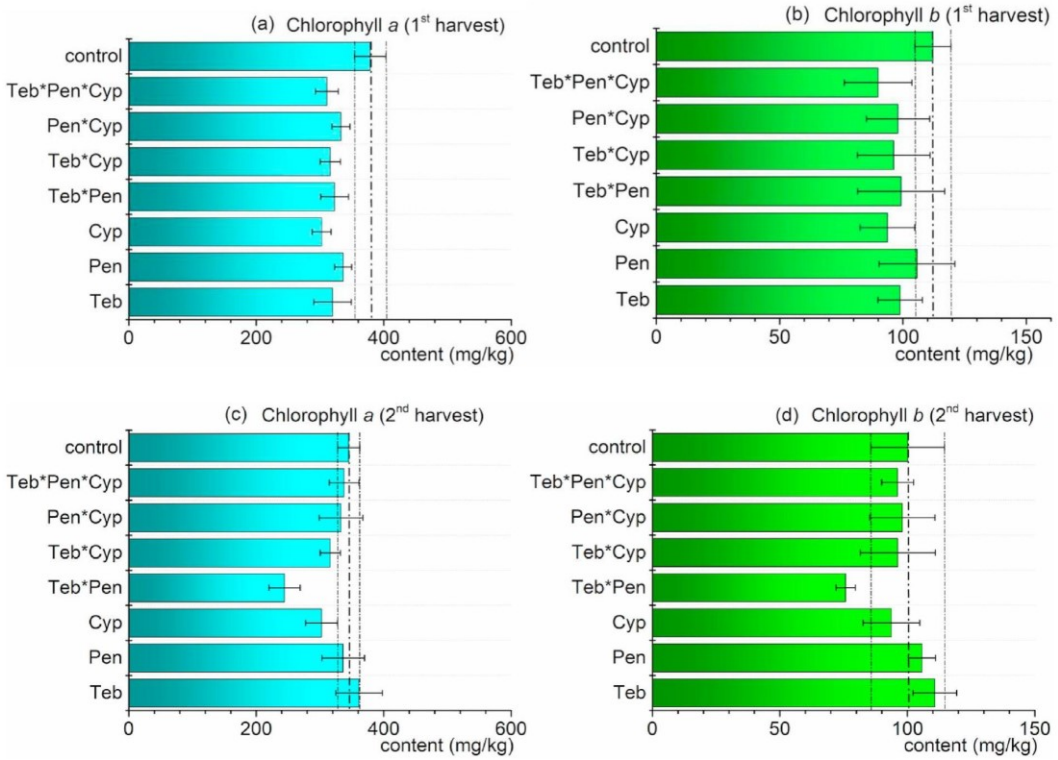


Fig. 4. Average concentrations of chlorophylls *a and b* in two harvests. Intervals represent confidence intervals (n = 10, P < 0.05).

346 mg/kg, respectively). The amount of chlorophyll *a* from the 1st to the 2nd harvest remained approximately the same (average for all treated variant in the 1st harvest is 320 mg/kg and in the 2nd is 319 mg/kg). The amount of chlorophyll *b* in the control remained similar (112 and 100 mg/kg in the 1st and 2nd harvests) as well as in the treated variants (97 mg/kg, as an average for all treated variants, remained the same in both harvests). It also means that the content of chlorophylls in the control variant decreased from the 1st to the 2nd harvest while its content in the treated variants remained mostly unchanged (**Table SI3**). However, in the 2nd harvest in the Teb*Pen treatment the content of both chlorophylls significantly decreased among all treated variants (**Table SI4**). The content of chlorophyll *a* was 244 mg/kg in Teb*Pen treatment and 331 mg/kg as the average for other treated variants. A similar trend can be seen also for the content of chlorophyll *b*, where its content in the Teb*Pen treated variant was 76 mg/kg and for average for the rest of the treated variants 100 mg/kg. From this point of view, it seems that especially the combination of Teb*Pen treatment has a highly negative effect on chlorophyll production. The information about this cocktail effect on the enzymes is limited; there is only some particular information about the impact on the aimed enzymes such as aromatase (Jaklová Dytrtová et al., 2020). It opens another possible direction for the research – to study how different combinations influence the activity of specific enzymes, which are not primarily considered as target enzymes.

3.3. Phenolic compounds

For the determination of phenolic compounds (Fig. 5), the tomato fruits were harvested twice. The 1st harvest was provided during the vegetation (week 10); once all plants had at least some tomato fruits ripened. The 2nd harvest was provided at the end of the period (harvested when the pot experiment was terminated). Between the 1st and 2nd harvest, there were found significant differences even in the same variant (**Table SI3**). The difference between the 1st and the 2nd harvest is 14 days only, however, the plants had slightly different conditions during the ripening. Two weeks before the 1st harvest, the average maximum temperature was 28.5 °C, the day sunlight was for 11.45 h on the average, without any precipitation. In 2 weeks before the 2nd harvest, the average temperature was 23.7 °C only, the day sunlight was 6.05 h/day on the average, with high precipitation (Fig. SI1). Under these natural conditions, there is an increased tendency for fungal pathogens incidence related to a higher risk of the plant infection and changes of its behavior before the 2nd harvest.

In the further text, the significant (on the statistical level of 95%) differences are discussed only; the statistical comparison according to One Way ANOVA between all experimental groups can be found in Supplemetary **Table SI4**. Phenolic profiles of the tomato peel samples are summarised in Supplementary Fig. SI3.

The content of **chlorogenic acid** (CGA) (Fig. 5a, **Table SI3**) in the control of the 1st harvest is significantly lower than of the 2nd harvest. This natural trend is in relation to the increased incidence of fungal pathogens in the time before the 2nd harvest and with the natural strategy of plant protection against them (Ruelas et al., 2006). Because of the fungal pathogens during the second ripening, the CGA content in the control increased approx. 4times compare to the 1st harvest. The trend of CGA increase from the 1st

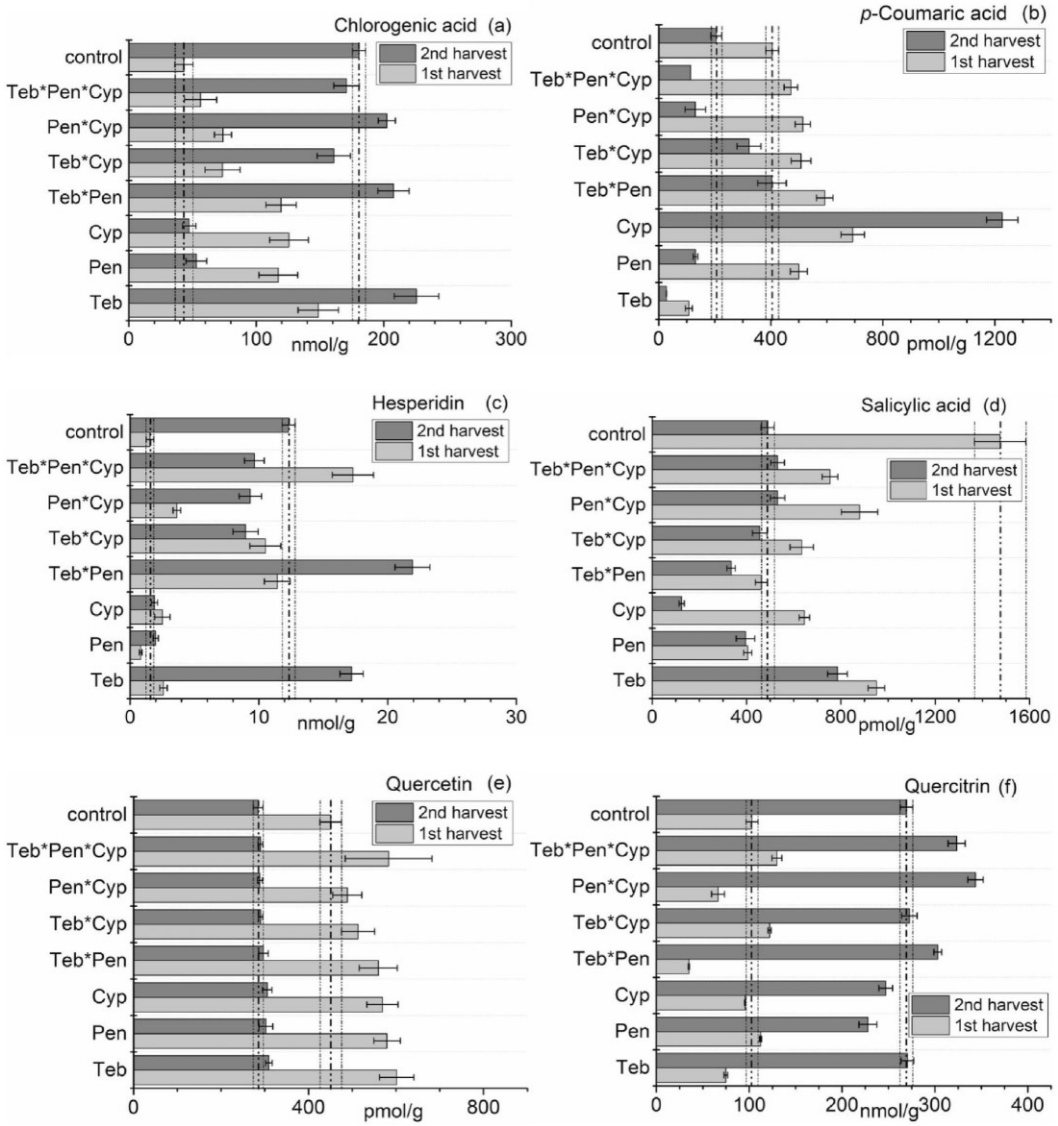


Fig. 5. Concentrations (nmol/g or in pmol/g) of phenolic compounds: (a) chlorogenic acid, *p*-coumaric acid, (c) hesperidin, (d) salicylic acid, (e) quercetin and (f) quercitrin in fruits. Intervals represent confidence intervals ($n = 10$, $P < 0.05$).

to the 2nd harvest is also visible for all triazole-mixed variants and slightly for the tebuconazole treated variant. For the single triazole-treated variants with cyproconazole and penconazole the trend is opposite.

Let's look at this problem in more detail. Before the 1st harvest, the self-protection against fungal pathogens was not necessary; therefore the CGA was not naturally produced (in the control). At that time the triazolic treatment was redundant. However, when the treatments were provided as prevention, the reaction of plants on the triazoles presence was also observed on the elevated CGA production as the anti-stress strategy (Mahesh et al., 2007) against triazoles-induced oxidation. This elevation of CGA in the 1st harvest was observed for all triazole-treated variants. The smallest elevation of CGA was observed in the mixed treatments (least in the Teb*Pen*Cyp mixture) and highest in the single-treated variants (the highest for Teb). It seems that in the case of CGA production the smallest disrupting effect (in the weather with a low incidence of fungal pathogens) have the mixtures. The explanation might be seen in the dissipation of the impact or in some side reactions among the triazoles leading to less reactive products (Jaklová Dytrtová et al., 2020). In the 2nd harvest it is visible, that the triazolic mixtures and single tebuconazole treatments were not sufficient in the protection against fungal pathogens and CGA production had to be increased similarly (or even more – Pen*Cyp, Teb*Pen and Teb) to the control. Only the single treatment with cyproconazole and penconazole has not elevated the CGA content

in the 2nd harvest in contrast to the 1st harvest. If we consider the elevated CGA level with elevated plant stress, the problem is the single tebuconazole treatment, which elevated the level of CGA in the 1st as well as in the 2nd harvest. The explanation may lie in the possible redox behavior of tebuconazole (Jaklová Dytrtová et al., 2011).

***p*-Coumaric acid** (PCA) is considered to create hydrogen bonds with receptors of the photoactive yellow protein, responsible for the absorption of the blue light (Kort et al., 1996). It is known that the content of the blue light is higher at the beginning of the vegetation period (Thomas and Vince-Prue, 1997). Also, the light duration and intensity were higher before the 1st harvest. There is a significant difference in the intensity and the spectrum of light during the sunny (before 1st harvest) and cloudy (before the 2nd harvest) days. During cloudy weather, the diffuse light spectrum is mostly decreased in higher wavelengths (from yellow to infrared), whereas the intensity of the light (from UV to visible) is more or less on 50% of the sunny weather (Andrews and Pearce, 2013). The filtration of the low wavelength (mostly infrared) is also related to the lower temperature, typical for cloudy weather. Therefore, it is not surprising that the PCA content in the 1st harvest was higher than in the 2nd (Fig. 5b) in the majority of treated variants (except the variant treated with Cyp) including the control. Moreover, the content of PCA in the majority (excepting Teb variant) of treated variants was higher than in the control. PCA is also considered as a plant antioxidant (Castelluccio et al., 1995), therefore it is expected the higher oxidation stress caused by triazoles presence can be reflected in an elevated level of PCA. This effect was not observed in the single tebuconazole treatment only, which can be explained by the lower stability of tebuconazole on the plant body under higher light intensity (Matadha et al., 2020) leading to its degradation. In the 2nd harvest, the PCA content in the majority of treated variants and control decreased. The PCA content in the majority of treated variants in the 2nd harvest was lower than in the control. Only in the treatment with Teb*Cyp, Teb*Pen and Cyp the PCA content was elevated in the 2nd harvest compared to the control.

Hesperidin (Fig. 5c) is well-known for its benefits for human health (Man et al., 2019), it is expected to have not only antioxidant properties but also protective against UV-radiation. The UV-radiation is the light with short wavelengths, therefore its amount was not decreased so much during the cloudy weather contrary to the visible or infrared light. The trend of hesperidin content from the 1st to the 2nd harvest (6times increased) indicates that before the 2nd harvest the oxidative conditions were increased (Fig. 5c). Plants produced more hesperidin to compensate for the higher oxidative conditions. In the 1st harvest the amount of hesperidin was extremely high in all treated variants with triazole mixtures and slightly higher for the cyproconazole or tebuconazole single treatments comparing to the control. Therefore, it seems that the mixtures increase the oxidative conditions more than the single triazole treatments. The redox properties of triazoles depend on the conditions, it is found to be similar to strong natural antioxidant resveratrol (Jaklová Dytrtová et al., 2018). From this point of view, the reactivity of triazole mixtures is more variable than the single triazole-containing environments. The elevation of hesperidin by single tebuconazole and cyproconazole can be explained by the presence of two enantiomers of these triazoles. For example, cyproconazole is a racemic mixture of two enantiomers, which theoretically (under model conditions) have different behaviour and allow reactions between them (Jakl et al., 2017). Therefore it can be expected that these two enantiomers will react differently also in the environment. In the 2nd harvest the significantly higher content of hesperidin than in the control was found in the Teb*Pen and Teb variant (**Table SI4**).

Salicylic acid (Fig. 5d) is considered as an important plant hormone participating in many processes such as growth, development, photosynthesis, transpiration, ion uptake, and transport (Vlot et al., 2009) as well as in the protection against pathogens (Hayat and Ahmad, 2007). The concentration of salicylic acid in the 1st harvest is enormous in the control contrary to the treated plants. The lower content of salicylic acid in the treated variant correlates with lower growth of green biomass as well as lower content of chlorophyll *a* (**Table SI5**). The trend is decreasing (from the 1st to the 2nd harvest) in the majority of the variants including the control (except the single treatment with penconazole, where the concentrations are similar in both harvests). In the 2nd harvest, the contents of salicylic acid in plants treated with triazoles mixtures were similar to the control. It seems here that the impact of triazoles was dissipated if the mixtures were used instead of the single triazole treatments.

Quercetin (3,5,7,3′,4′-pentahydroxyflavone) is considered a strong antioxidant (Mendoza and Burd, 2011). Its concentration in the 1st harvest was significantly higher than in the 2nd harvest (Fig. 5e, Table SI3) for all treated variants including the control. It indicates that the demands of oxidants quenching decreased in cloudy weather with higher humidity. Whereas in the 1st harvest, the quercetin concentration in the control was the smallest among variants. The highest contents were found in single treatments and Teb*Pen*Cyp.

Quercitrin is the glycosylated form of quercetin and rhamnose (quercetin-3-rhamnoside). Its concentration in tomato fruits is almost 3-orders higher than the concentration of quercetin. Because of the glycosylation, its antioxidant activity might be lower; it might be a more stable compound than quercetin. From this point of view, the concentration of quercitrin in the 1st harvest is significantly lower than in the 2nd harvest (Fig. 5f, Table SI3) for all variants including the control. It can signify that during the vegetation period plants are creating some pool of antioxidants, which can be potentially used. This effort is significantly higher for variants treated with the cocktails of triazoles (Teb*Pen*Cyp, Pen*Cyp, and Teb*Pen) than for control or plants treated with single triazole (Cyp and Pen, **Table SI4**).

The trends of phenolic compounds of the 1st and 2nd harvest were analyzed according to the Pearson's correlation coefficient (**Table SI5**). A strong negative correlation was observed for the content of quercitrin and quercetin and a negative mild correlation was shown for CGA and PCA. Both, quercetin and PCA serve as the respective precursors for quercitrin and CGA. Therefore, the stress conditions between the harvests likely led to both CGA and quercitrin accumulation. Also, mild positive correlations were determined for CGA and hesperidin, and CGA and quercitrin. CGA represents a powerful antioxidant but is also related to the biosynthesis of lignin, and thus the plant cell wall fortification against biotic stressors (Hýsková et al., 2021). Hesperidin, as well as quercitrin, were shown as effective inhibitors of various fungal pathogens (Salas et al., 2011; Jin, 2019). Therefore, the increased and conjoint accumulation of these phenolic compounds could be related to antifungal defense. The complex interactions between triazoles and phenolics should be evaluated independently to understand the mechanism of the impact. It rdepends on the type of given phenolic compound and triazole and also on other chemicals present.

4. Conclusions

It is clearly visible that the presence of triazoles influences also plant behaviour significantly. The stress might be visible on the increased weight of fruits as well as on the increased total weight of

tomato yield. This tendency can be explained by the investment of remaining energy into the filial generation (seeds production). What is alarming is a consequence of triazole treatment with the decrease in thin stems and leaves weight – the parts responsible for the photosynthesis. Moreover, the effect on photosynthesis by triazole treatment can be seen in the decreased concentration of chlorophyll *a and b* in the 1st harvest. This may cause a decrease in the photosynthesis yield and consequently the decrease of plant growth. This finding corresponds with the decreased weight of tomato fruits in the 2nd harvest in contrast to the 1st harvest.

The two harvests bring also situations with different conditions during the ripening. Before the 1st harvest, the conditions were ideal (low humidity, high temperature, high sunlight), therefore the fungi development was low and the self-protection of plants was sufficient. Before the 2nd harvest, the weather conditions were ideal for the fungi development (high humidity, lower temperature, and low sunlight), therefore the triazole treatment might be useful. However, despite the triazole treatment the plants were not in good conditions in the end of the experiment.

The classification of different phenolics content brings interesting conclusions. Mostly it seems that the triazoles foliar treatment (especially with triazole mixtures) induces higher oxidation conditions in plants. The production of some phenolics was higher in triazole-treated plants (quercetin, *p*-coumaric acid, and hesperidin). On the other hand, salicylic acid content in the triazoles-treated plants was much lower than in the control (especially in the 1st harvest). Chlorogenic acid is probably a very powerful tool for plant protection against fungal pathogens (seen from the control) because its content was 4times lower in the 1st harvest (before which the high plant protection was not naturally necessary) than in the 2nd harvest (where the fungi infection was visibly present). On the other hand, chlorogenic acid also protects plants against higher oxidative conditions, which were caused by the high amount of (unutilised) triazoles (from single treatments).

There were seen also some contrasts between the single-triazole treatment and the mixed-triazole treatment. However, it cannot be said which is less harmful to the plant. It depends on the weather conditions as well as on the type of the process. Generally, the triazolic mixture application brings additional variability in the interactivity among the triazoles to the system. The result of this interactivity always depends on the current conditions; therefore it cannot be decided now if the final effect on the system will be positive or negative.

Author statement

Michal Jakl: Investigation, Formal analysis, Visualization, Supervision, Validation; Sanja Ćavar Zeljković: Investigation, Methodology, writing; Ishak Kovač: Investigation, Formal analysis, Validation; Kateřina Bělonožníková: Formal analysis; Jana Jaklová Dytrtová: Conceptualization, Methodology, Investigation, Formal analysis, Writing, Funding acquisition, Visualization, Supervision, Project administration.

Funding

J.J.D. thanks to the Czech Science Foundation (project no. 18-01710S) for the financial support.

Declaration of competing interest

The authors declare that they have no known competing financial interests or personal relationships that could have appeared to influence the work reported in this paper.

Appendix A. Supplementary data

Supplementary data to this article can be found online at https://doi.org/10.1016/j.chemosphere.2021.130242.

References

Andrews, R.W., Pearce, J.M., 2013. The effect of spectral albedo on amorphous silicon and crystalline silicon solar photovoltaic device performance. Sol. Energy 91, 233–241.
Beijer, K., Jonsson, M., Shaik, S., Behrens, D., Brunström, B., Brandt, I., 2018. Azoles additively inhibit cytochrome P450 1 (EROD) and 19 (aromatase) in rainbow trout (*Oncorhynchus mykiss*). Aquat. Toxicol. 198, 73–81.
Castelluccio, C., Paganga, G., Melikian, N., Bolwell, G.P., Pridham, J., Sampson, J., Rice-Evans, C., 1995. Antioxidant potential of intermediates in phenylpropanoid metabolism in higher plants. FEBS Lett. 368, 188–192.
Chen, Z.F., Ying, G.G., 2015. Occurrence, fate and ecological risk of five typical azole fungicides as therapeutic and personal care products in the environment: a review. Environ. Int. 84, 142–153.
Conner, K.P., Vennam, P., Woods, C.M., Krzyaniak, M.D., Bowman, M.K., Atkins, W.M., 2012. 1,2,3-triazole-heme interactions in cytochrome P450: functionally competent triazole-water-heme complexes. Biochemistry 51, 6441–6457.
Daniel, O., Meier, M.S., Schlatter, J., Frischknecht, P., 1999. Selected phenolic compounds in cultivated plants: ecologic functions, health implications, and modulation by pesticides. Environ. Health Perspect. 107, 109–114.
García-Valverde, V., Navarro-González, I., García-Alonso, J., Periago, M.J., 2013. Antioxidant bioactive compounds in selected industrial processing and fresh consumption tomato cultivars. Food Bioprocess Technol. 6, 391–402.
Gopi, R., Jaleel, C.A., Sairam, R., Lakshmanan, G.M.A., Gomathinayagam, M., Panneerselvam, R., 2007. Differential effects of hexaconazole and paclobutrazol on biomass, electrolyte leakage, lipid peroxidation and antioxidant potential of *Daucus carota* L. Colloids Surf. B Biointerfaces 60, 180–186.
Hayat, S., Ahmad, A. (Eds.), 2007. Salicylic Acid: A Plant Hormone. Springer, Dordrecht.
Heim, K.E., Tagliaferro, A.R., Bobilya, D.J., 2002. Flavonoid antioxidants: chemistry, metabolism and structure-activity relationships. J. Nutr. Biochem. 13, 572–584.
Hýsková, V., Bělonožníková, K., Doričová, V., Kavan, D., Gillarová, S., Henke, S., Synková, H., Ryšlavá, H., Čeřovská, N., 2021. Effects of heat treatment on metabolism of tobacco plants infected with Potato virus Y. Plant Biol. https://doi.org/10.1111/plb.13234. In press.
Jakl, M., Fanfrlík, J., Jaklová Dytrtová, J., 2017. Mimicking of cyproconazole behavior in the presence of Cu and Zn Rapid Commun. Mass Spectrom. 31, 2043–2050.
Jakl, M., Kovač, I., Ćavar Zeljković, S., Jaklová Dytrtová, J., 2021. Triazole fungicides in soil affect the yield of fruit, green biomass, and phenolics production of *Solanum lycopersicum* L. Food Chem. 351, 129328.
Jaklová Dytrtová, J., Jakl, M., Schröder, D., Čadková, E., Komárek, M., 2011. Complexation between the fungicide tebuconazole and copper(II) probed by electrospray ionization mass spectrometry. Rapid Commun. Mass Spectrom. 25, 1037–1042.
Jaklová Dytrtová, J., Fanfrlík, J., Norková, R., Jakl, M., Hobza, P., 2014. Theoretical insight into the stabilization of triazole fungicides via their interactions with dications. Int. J. Mass Spectrom. 359, 38–43.
Jaklová Dytrtová, J., Straka, M., Bělonožníková, K., Jakl, M., Ryšlavá, H., 2018. Does resveratrol retain its antioxidative properties in wine? Redox behaviour of resveratrol in the presence of Cu(II) and tebuconazole. Food Chem. 262, 221–225.
Jaklová Dytrtová, J., Bělonožníková, K., Jakl, M., Ryšlavá, H., 2020. Triazoles and aromatase: the impact of copper cocktails. Environ. Pollut. 266 (1), 115201.
Jin, Y.S., 2019. Recent advances in natural antifungal flavonoids and their derivatives. Bioorg. Med. Chem. Lett 29, 126589.
Karak, P., 2019. Biological activities of flavonoids: an overview. Int. J. Pharmaceut. Sci. Rev. Res. 10, 1567–1574.
Khoddami, A., Wilkes, M.A., Roberts, T.H., 2013. Techniques for analysis of plant phenolic compounds. Molecules 18, 2328–2375.
Kort, R., Vonk, H., Xu, X., Hoff, W.D., Crielaard, W., Hellingwerf, K.J., 1996. Evidence for trans-cis isomerization of the p-coumaric acid chromophore as the photochemical basis of the photocycle of photoactive yellow protein. FEBS Lett. 382, 73–78.
Kovač, I., Jakl, M., Fanfrlík, J., Andrushchenko, V., Jaklová Dytrtová, J., 2020. Complexation and stability of the fungicide penconazole in the presence of zinc and copper ions. Rapid Commun. Mass Spectrom. 34, e8714.
Kumar, S., Pandey, A.K., 2013. Chemistry and biological activities of flavonoids: an overview. Sci. World J. 2013, 162750.
Lallemand, L.A., Zubieta, C., Lee, S.G., Wang, Y.C., Acajjaoui, S., Timmins, J., McSweeney, S., Jez, J.M., McCarthy, J.G., McCarthy, A.A., 2012. A structural basis for the biosynthesis of the major chlorogenic acids found in coffee. Plant Physiol. 160, 249–260.
Mahesh, V., Million-Rousseau, R., Ullmann, P., Chabrillange, N., Bustamante, J., Mondolot, L., Morant, M., Noirot, M., Hamon, S., de Kochko, A., Werck-Reichhart, D., Campa, C., 2007. Functional characterization of two *p*-coumaroyl ester 3'-hydroxylase genes from coffee tree: evidence of a candidate for chlorogenic acid biosynthesis. Plant Mol. Biol. 64, 145–159.
Man, M.Q., Yang, B., Elias, P.M., 2019. Benefits of hesperidin for cutaneous functions.

Evid. Based Complement. Altern. Med. 2019, 2676307.
Martí, R., Rosello, S., Cebolla-Cornejo, J., 2016. Tomato as a source of carotenoids and polyphenols targeted to cancer prevention. Cancers 8 (6), 58.
Matadha, N.Y., Mohapatra, S., Siddamallaiah, L., Udupi, V.R., Gadigeppa, S., Raja, D.P., Donagar, S.P., Hebbar, S.S., 2020. Persistence and dissipation of fluopyram and tebuconazole on bell pepper and soil under different environmental conditions. Int. J. Environ. Anal. Chem. https://doi.org/10.1080/03067319.2019.1704745. In press.
Mathesius, U., 2018. Flavonoid functions in plants and their interactions with other organisms. Plants-Basel 7, 30.
Mendoza, E.E., Burd, R., 2011. Quercetin as a systemic chemopreventative agent: structural and functional mechanisms. Mini Rev. Med. Chem. 11, 1216–1221.
Ozores-Hampton, M., Di Gioia, F., Sato, S., Simonne, E., Morgan, K., 2015. Effects of nitrogen rates on nitrogen, phosphorous, and potassium partitioning, accumulation, and use efficiency in seepage-irrigated fresh market tomatoes. Hortscience 50, 1636–1643.
Panche, A.N., Diwan, A.D., Chandra, S.R., 2016. Flavonoids: an overview. J. Nutr. Sci. 5, 1–15.
Rice-Evans, C.A., Miller, N.J., Paganga, G., 1996. Structure-antioxidant activity relationships of flavonoids and phenolic acids. Free Radic. Biol. Med. 20, 933–956.
Ruelas, C., Tiznado-Hernandez, M.E., Sanchez-Estrada, A., Robles-Burgueno, M.R., Troncoso-Rojas, R., 2006. Changes in phenolic acid content during *Alternaria alternata* infection in tomato fruit. J. Phytopathol. 154, 236–244.
Salas, M.P., Céliz, G., Geronazzo, H., Daz, M., Resnik, S.L., 2011. Antifungal activity of natural and enzymatically-modified flavonoids isolated from citrus species. Food Chem. 124, 1411–1415.
Sarlikioti, V., de Visser, P.H.B., Buck-Sorlin, G.H., Marcelis, L.F.M., 2011. How plant architecture affects light absorption and photosynthesis in tomato: towards an ideotype for plant architecture using a functional-structural plant model. Ann. Bot. 108, 1065–1073.
Takala, N., Sirén, H., Jakl, M., Jaklová Dytrtová, J., 2019. Determination of important azoles in soil solution using CE. Monatsh. Chem. 150, 1625–1631.
Thomas, B., Vince-Prue, D., 1997. Photoperiodism in Plants, 2 ed. Academic Press, London.
Tietjen, K., 2017. Contribution of plant responses to efficacy of fungicides – a perspective. In: Deising, H.B., Fraaije, B., Mehl, A., Oerke, E.C., Sierotzki, H., Stammler, G. (Eds.), Modern Fungicides and Antifungal Compounds. Phytomedizinische Gesellschaft, Braunschweig, pp. 33–50.
Tuna, A.L., 2014. Influence of foliarly applied different triazole compounds on growth, nutrition, and antioxidant enzyme activities in tomato ('*Solanum lycopersicum*' L.) under salt stress. Aust. J. Crop. Sci. 8, 71–79.
Vanden Bossche, H., Dromer, F., Improvisi, I., Lozano-Chiu, M., Rex, J.H., Sanglard, D., 1998. Antifungal drug resistance in pathogenic fungi. Med. Mycol. 36, 119–128.
Vlot, A.C., Dempsey, D.A., Klessig, D.F., 2009. Salicylic acid, a multifaceted hormone to combat disease. Annu. Rev. Phytopathol. 47, 177–206.
Wang, X.L., Gao, J., Gao, S., Song, Y., Yang, Z., Kuai, B.K., 2019. The H3K27me3 demethylase REF6 promotes leaf senescence through directly activating major senescence regulatory and functional genes in *Arabidopsis*. PLoS Genet. 15, e1008068.
Wellburn, A.R., 1994. The spectral determination of chlorophylls *a* and *b*, as well as total carotenoids, using various solvents with spectrophotometers of different resolution. J. Plant Physiol. 144, 307–313.

3.3 Antioxidants and their impact on humans and the environment

3.3.1 Characterization of some potential medicinal plants from Central Europe by their antioxidant capacity and the presence of metal elements

Medicinal plants have been used for thousands of years to treat various health issues. They are commonly rich in terpenes (carvacrol, citral, linalool, and geraniol) and phenolics (flavonoids and phenolic acids) (Ortega-Ramirez et al 2014). We analyzed 15 medicinal plants, commonly available in Central Europe, by the total phenolics and flavonoids, three different antioxidant capacity assays and the content of some essential minerals (Na, K, Mg, Ca, Zn and Se) (Fig. 17). We prepared the plant extracts in the form of hot water extracts, simulating herbal teas, and methanolic extracts as tinctures. The main aim of this study was to correlate the total phenolic content with antioxidant capacity and with the nutritionally key metal elements.

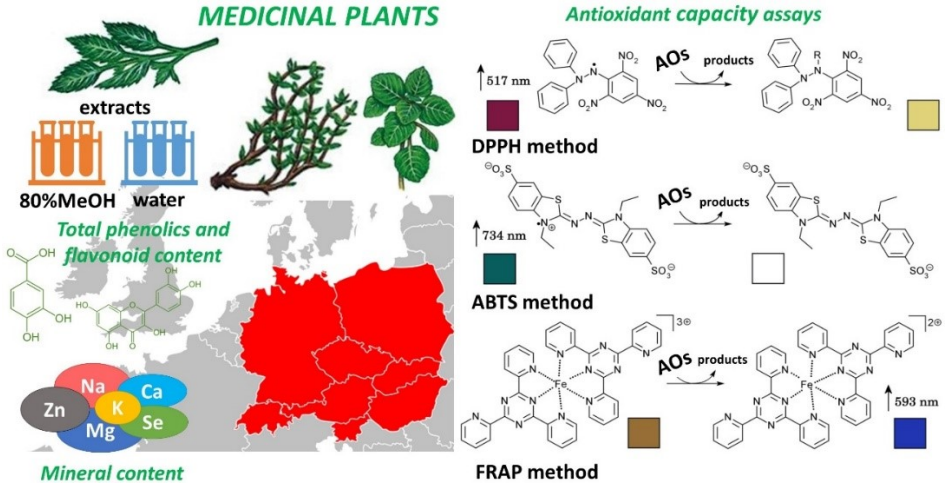


Fig. 17: A summary of the publication (Tupec et al 2017). *Abbreviations: ABTS - 2,2'-azino-bis(3-ethylbenzothiazoline-6-sulfonate), AOs - antioxidants, DPPH - N,N-di(phenyl)picryl hydrazyl, FRAP - ferric ion reducing antioxidant power.*

The most promising plants that showed high phenolics content and high antioxidant capacity were *Agrimonia eupatoria*, *Origanum vulgare* and *Mentha × piperita.* For most medicinal plants, the antioxidant capacities were comparable in the aqueous and methanolic extracts with exceptions of *Origanum vulgare, Marrubium vulgare* and *Camellia sinensis* (Fig. 1, 2 in Tupec et al 2017).

The results of the correlation analysis confirmed the assumption that, in principle, antioxidant capacities determined by methods using a similar mechanism (here mainly single electron transfer versus hydrogen atom transfer) show a very good linear correlation. In the case of total phenolics content and antioxidant capacity, a good correlation was also found. The content of flavonoid in relation to antioxidant capacity showed only a weak correlation (Fig. 3 in Tupec et al 2017). Flavonoids are one of the subgroups of phenolic compounds; thus, they do not have strongly correlate. The flavonoids bound in the form of glycosides are also not detectable by the used method based on Al^{3+} chelation (complex flavonoid-Al^{3+} increases absorbance at 400-450 nm) because carbohydrate substituents may be directly attached to one of the complexing oxygen atoms or sterically inhibit the aluminum ion coordination. The primary hydrolysis of all glycosides in the sample could have led to a more accurate determination of the total flavonoids.

Nowadays, the human diet is full of more NaCl than necessary. Except for, methanolic extracts *Agrimonia eupatoria, Plantago lanceolata, Thymus vulgaris*, all the tested medicinal plants contained more K^+ than Na^+ thus these extracts could support balanced Na/K ratio (Fig. 4 in Tupec et al 2017). Also, high amounts of Zn that were found in *Stevia rebaudiana, Thymus vulgaris,* and *Salvia officinalis* could supply this element significantly (Table 1, 2 in Tupec et al 2017). Selen is an essential element, found in organisms mainly in selenoproteins, e.g., thioredoxin reductase (Allmang et al 2009), however, in the plant extracts the Se content was below the detection limit. However, it was found by a more sensitive method in the analysis of the plant ash (Table 2 in Tupec et al 2017), supporting the use of *Achillea millefolium* and *Salvia officinalis* as spice.

My contribution:

I participated in the antioxidant capacity determination and helped to edit the manuscript.

Food Bioscience 20 (2017) 43–50

Contents lists available at ScienceDirect

Food Bioscience

journal homepage: www.elsevier.com/locate/fbio

Characterization of some potential medicinal plants from Central Europe by their antioxidant capacity and the presence of metal elements

Michal Tupec[a], Veronika Hýsková[a], Kateřina Bělonožníková[a], Jakub Hraníček[b], Václav Červený[b], Helena Ryšlavá[a,*]

[a] Department of Biochemistry, Faculty of Science, Charles University, Czech Republic
[b] Department of Analytical Chemistry, Faculty of Science, Charles University, Czech Republic

ARTICLE INFO

Keywords:
Antioxidant capacity
Medicinal plant
Metal element
Total flavonoids
Total phenolic compounds

ABSTRACT

Plants contain polyphenolic compounds such as phenolic acids, flavonoids, stilbenes, lignans, etc., which are endowed with antioxidant properties. The aim of this study was to correlate the total phenolic compound and flavonoid content of 15 medicinal plants with their antioxidant properties and to determine some important essential elements (Na, K, Ca, Mg, Zn, Se). The antioxidant capacity was tested by three methods (ABTS, DPPH, and FRAP) for the ability to provide electrons or hydrogen to various compounds, or to scavenge free radicals. The highest content of total phenolic compounds in aqueous extracts was found in *Agrimonia eupatoria*. In addition to this plant, high antioxidant capacities were also present in *Origanum vulgare* and *Mentha* × *piperita*. The positive correlation between the total phenolic compound content and the antioxidant capacity was strong, whereas flavonoids were correlated to antioxidant properties to a lesser extent. All the aqueous plant extracts contain larger amounts of potassium than sodium, which could be beneficial for humans with low NaCl diets. The significance of replenishing of calcium, magnesium, zinc, and selenium by drinking herbal teas is discussed.

1. Introduction

Natural products from plants have been used for health maintenance, treatment of various diseases and for lifespan extension since ancient times. The contents of secondary metabolites (above all phenylpropanoids including flavonoids, isoflavonoids, stilbenes, lignans and tannins) in medicinal plants, fruits, and vegetables are related to their antioxidant properties and in some cases to antimicrobial, anti-inflammatory, and hypolipidic effects or even to their anti-carcinogenic potential in biological systems (Marti, Rosello, & Cebolla-Cornejo, 2016; Martins, Petropoulos, & Ferreira, 2016; Szajdek & Borowska, 2008; Wojdylo, Oszmianski, & Czemerys, 2007). Polyphenolic compounds usually have high redox potentials, which allow them to act as reducing agents, hydrogen donors, radical scavengers, and singlet oxygen quenchers. In addition, they have a metal-chelating ability. Therefore these compounds play an important role in bodily defence systems against the harmful by-products (reactive oxygen species ROS) formed during normal aerobic cell respiration and especially in oxidative stress under pathological conditions (Ou, Huang, Hampsch-Woodill, Flanagan, & Deemer, 2002; Song et al., 2016; Tramutola, Lanzillotta, Perluigi, & Butterfield, 2016).

Polyphenols together with antioxidant enzymes and low-molecular-weight antioxidant compounds, such as ascorbate, vitamin E or glutathione, control not only oxidative stress but also stabilize lipids against peroxidation and inhibit various types of oxidizing enzymes (Yao, Sang, Zhou, & Ren, 2010). A consensus is emerging that polyphenols, rather than antioxidant vitamins alone, are responsible for the anti-aging benefits of the Mediterranean diet (Baxter, 2008).

The maintenance of ion homeostasis in the whole organism, tissues, extracellular medium, and inside the cell is quite important. Ions are stored, excreted and taken up from food or beverages or added as mineral supplements. Some ions are present in organisms in relatively high concentrations, such as Na^+, K^+. Although Na^+ ions are prevalent in extracellular fluids and K^+ can be found in the cell, both are involved in water balance and osmotic pressure regulation, and in transport processes across the plasma membrane. The localization of both ions and thus the membrane potential is maintained by Na^+-K^+ ATPase (Penton, Czogalla, & Loffing, 2015; Terker et al., 2015). Further ions important for human metabolism are bivalent Ca^{2+} and Mg^{2+}, which specifically act in metabolic and physiological processes (Blaine,

Abbreviations: ABTS, 2,2'-azino-bis(3-ethylbenzothiazoline-6-sulfonate); a. s. l., above sea level; DPPH, *N,N* di(phenyl)picryl hydrazyl; dw, dry weight; FRAP, ferric ion reducing antioxidant power; ROS, reactive oxygen species; TPTZ, 2,4,6-tris(2-pyridyl)-*s*-triazine

* Correspondence to: Department of Biochemistry, Faculty of Science, Charles University, Hlavova 2030, Prague 2 128 40, Czech Republic.
E-mail address: helena.ryslava@natur.cuni.cz (H. Ryšlavá).

http://dx.doi.org/10.1016/j.fbio.2017.08.001
Received 3 March 2017; Received in revised form 10 July 2017; Accepted 1 August 2017
Available online 02 August 2017
2212-4292/ © 2017 Elsevier Ltd. All rights reserved.

Chonchol, & Levi, 2015; Tai, Leung, Grey, Reid, & Bolland, 2015). While Na^+ ions are supplied in large amounts in the human diet, other ions are obviously not available in sufficient amounts. Some elements are also essential for metabolism, but they are required in small quantities, because higher concentrations are toxic for the organism. Selenium is a component of proteins containing selenocysteine e.g. glutathione peroxidases, thioredoxin reductases, and methionine sulfoxide (Kurokawa & Berry, 2013). Zinc is not stored in organisms and a continuous external supply for metabolic requirements is necessary; this is correlated with the function of the phagocytosis of macrophages and natural killer cells and the reduction of inflammatory mediators; it possesses antioxidant properties and has been found to be useful in preventing damage by UV light. Zinc could induce the synthesis of metallothioneins, the low molecular weight proteins involved in detoxification and scavenging of free radicals (Cruz, de Oliveira, & Marreiro Ddo, 2015; Gupta, Mahajan, Mehta, & Chauhan, 2014; Zastrow & Pecoraro, 2014).

The aim of this study was to correlate the total phenolic compound content with the antioxidant properties (tested by three various methods) and with the important metal elements in some potential medicinal plants. In addition to the typical medicinal plants used in Central Europe, other interesting plants such as *Camellia sinensis* L., known as a rich source of phenolic compounds, or *Stevia rebaudiana Bert.* were also chosen. In addition to plants traditionally used as herbal teas, also potentially toxic plants, recommended only for external use, were tested. Moreover, the content of essential micronutrients for humans, Zn and Se, which are important for antioxidant and immunity systems, were determined in extracts of the tested plants. In addition, the ratio of the elements Ca and Mg, Na and K, which are present in larger amounts, was determined. The studied plants were tested in the form of hot water extracts (herbal tea) and methanolic extracts (tincture).

2. Materials and methods

2.1. Plant material

All the medicinal plants were grown at the same place in the country near Prague GPS N 49°52.24997', E 14°24.61278' (altitude 321 m a. s. l., average annual temperature 7–8 °C, average growing season temperature 13–14 °C, average annual precipitation 600 mm of water column). Thus, the content of nutrients in the soil, the actual precipitations, irradiation, etc. were identical for all the species during cultivation. Only *Camellia sinensis* L. was bought from the local market; this plant material is rich in phenolic compounds and therefore suitable for comparison with other medicinal herbs. The plants were collected in August, the shoots of plant species were dried and then the shoots were homogenized and stored as mixed samples for the subsequent analyses. Flowers were also present in the samples of *Lamium album* L, *Levandula angustifolia Mill.,* and *Achillea millefolium* L.

2.2. Sample preparation

2.5 g of the ground air-dried plant material was submerged in 50 ml of extracting solvent, which was an 80% (w/w) methanol/water mixture or deionized water. The mixture was heated under reflux for 30 min at 70 °C for the methanol/water mixture or at 80 °C for the deionized water. The resulting crude extract was first filtered through four layers of gauze and then centrifuged at 9, 400 × g (Hettich Universal 32 R, Tuttlingen, Germany) for 10 min (4 °C). The supernatant was subsequently filtered through a syringe filter with a pore diameter of 0.2 μm (Schleicher-Schuell, Dassel, Germany) and the obtained extract was stored below − 20 °C until further use. The dry weight for unification of the results was obtained by heating about 0.5 g of the corresponding plant material to dryness at 100 °C for at least an hour.

2.3. Determination of the total phenolic compounds content

The total phenolic compound content was determined by the standard Folin-Ciocâlteu colorimetric method with slight modifications (Cai, Luo, Sun, & Corke, 2004; Dudonne, Vitrac, Coutiere, Woillez, & Merillon, 2009). First, 1.0 ml of 10% (v/v) Folin-Ciocâlteu reagent (Dr. Kulich Pharma, Hradec Králové, Czech Republic) was added to the extract, which was previously diluted to the appropriate concentration with water and neutralized after two minutes by addition of 800 μl of 75 g/l sodium carbonate solution (Lach-Ner, Neratovice, Czech Republic). After incubation (28 min) at ambient temperature, the absorbance of the solution was measured against a blank solution at 760 nm using an Ultrospec 1000 UV–VIS spectrophotometer (Pharmacia Biotech, Uppsala, Sweden). A phenol solution (Sigma-Aldrich, St. Louis, MO, USA) was used as a standard for the calibration. The results are expressed as mmol of phenol equivalents per kg of dry weight.

2.4. Determination of total flavonoids

The flavonoids were determined by a modified Dowd method according to Liu et al. (2002). 1.50 ml of deionized water and 70 μl of 50 g/l potassium nitrite solution (Sigma-Aldrich, St. Louis, MO, USA), were added to 200 μl of the appropriately diluted extract. After 5 min, 150 μl of 100 g/l aluminium chloride solution (Sigma-Aldrich, St. Louis, MO, USA) was added, followed by another 5 min incubation period and a final addition of 500 μl of 1 mol/l sodium hydroxide solution. After 2 min, the absorbance of the solution was measured against a blank solution (without $AlCl_3$) at 510 nm using an Ultrospec 1000 UV–VIS spectrophotometer (Pharmacia Biotech, Uppsala, Sweden). A solution of quercetin (Sigma-Aldrich, St. Louis, MO, USA) was used as a standard in calibration. The results are expressed as mmol of quercetin equivalents per kg of dry weight.

2.5. Trolox Equivalent Antioxidant Capacity assay (TEAC) with $ABTS^{\cdot+}$

The Trolox Equivalent Antioxidant Capacity assay with ABTS radical cation was performed according to Wojdylo et al. (2007) and according to Yao, Sang, Zhou, and Ren, Yao et al. (2010). The ABTS radical cation was generated a day before the measurement by dissolving 10 mg of ABTS diammonium salt (Sigma-Aldrich, St. Louis, MO, USA) in 3.0 ml of 82 μg/ml potassium persulphate solution (Sigma-Aldrich, St. Louis, MO, USA); the resulting solution was incubated in the dark at ambient temperature for at least 16 h. The stock solution of ABTS radical cation was then made by dilution with deionized water to an absorbance of about 1.3 at 734 nm (1 cm optical path) using an Ultrospec 1000 UV–VIS spectrophotometer (Pharmacia Biotech, Uppsala, Sweden). 1.0 ml of the previously prepared solution of ABTS radical cation (~ 0.1 mmol/l) was added to 200 μl of the appropriately diluted extract, followed by incubation at ambient temperature for 10 min. Finally, the absorbance was measured at 734 nm against a reference solution without the extract. The calibration curve was performed using a trolox (Sigma-Aldrich, St. Louis, MO, USA) solution in 50% ethanol as a standard. The results are expressed as mmol of trolox equivalents per kg of dry weight.

2.6. Trolox Equivalent Antioxidant Capacity assay with DPPH

The TEAC assay with the DPPH radical was carried out as previously described by Brand-Williams, Cuvelier, and Berset (1995) and by Re et al. (1999)., 1.0 ml of 96% ethanol was mixed with 500 μl of the extract diluted with water. 500 μl of 400 μmol/l DPPH (Sigma-Aldrich, St. Louis, MO, USA) solution in ethanol were added to this mixture. After 10 min incubation at ambient temperature, the absorbance was measured at 517 nm against a blank solution without the extract using an Ultrospec 1000 UV–VIS spectrophotometer (Pharmacia Biotech, Uppsala, Sweden). Trolox (Sigma-Aldrich, St. Louis, MO, USA) was used

for the calibration. The results are expressed as mmol of trolox equivalents per kg of dry weight.

2.7. Ferric Ion Reduction Antioxidant Power assay

The Ferric Ion Reduction Antioxidant Power assay (FRAP) was performed accordingly to Dudonne et al. (2009) and accordingly to Tsao, Yang, Xie, Sockovie and Khanizadeh (2005). The FRAP reagent consisted of (1) 700 µmol/l TPTZ (Sigma-Aldrich, St. Louis, MO, USA) solution in 40 mmol/l HCl, (2) 20 mmol/l ferric chloride solution (Sigma-Aldrich, St. Louis, MO, USA) and (3) 300 mmol/l acetate buffer (pH 3.6). The volume ratio of components (1), (2) and (3) was 25:10:65. 1.0 ml of the FRAP reagent was added to 200 µl of the extract previously diluted with water. After incubation for 10 min at ambient temperature, the absorbance was read at 593 nm against a reference solution without the extract using an Ultrospec 1000 UV–VIS spectrophotometer (Pharmacia Biotech, Uppsala, Sweden). The calibration curve was obtained using an ascorbic acid (Sigma-Aldrich, St. Louis, MO, USA) solution as a standard. The results are expressed as mmol of ascorbic acid equivalents per kg of dry weight.

2.8. Determination of metal elements

Measurements of the sodium, potassium, magnesium, calcium, manganese, zinc, and selenium concentrations in water and methanolic extracts were acquired using a GBC 933 AA (GBC Scientific Equipment, Melbourne, Australia) atomic absorption spectrometer with a flame atomization unit (Na, K, Mg, Ca and Zn) or hydride generation unit (Se). The spectrometer was operated using predefined optimal settings. Variant Na, K, Mg, Ca, Zn and Se hollow cathode lamps were operated at 589.0, 766.5, 285.2, 422.7, 213.9 and 196.0 nm, respectively, with 0.5 nm spectral band passes. A lamp current of 10 mA was used in all cases. Atomization was performed with an air-acetylene flame for Na, K, Zn and Mg or a nitrous oxide-acetylene flame for Ca. An optimized laboratory-made hydride generation unit based on the BH_4^-/acid reaction was used for selenium determination. The concentration of zinc was determined without adding any chemical agents. To suppress partial ionization during sodium, potassium and magnesium determination, cesium nitrate was added to all the samples at a final concentration of 2000 µg/ml. To overcome the most common interferences in an air-acetylene flame, a known excess of a releasing agent (lanthanum, 10 mg/ml) was added. To avoid calcium ionization during its measurement, a small amount of potassium chloride was added to all the samples at a final concentration of 3000 mg/l. All the reagents used were of analytical reagent grade or higher purity. Deionized water (< 0.1 mS cm^{-1}, Milli-QPLUS, EMD Millipore, Billerica, MA, USA) was used to prepare all solutions. Working standards were prepared by diluting standard 1.000 g/l stock solutions of Na^+, K^+, Mg^{2+}, Ca^{2+}, Zn^{2+} and Se^{4+} (Merck, Darmstadt, Germany). The same methods were used for solid samples of plants (dried ashes). These samples were weighed without previous rinsing and were digested in 5 ml of 65% nitric acid (Analpure®, Analytika, Prague, Czech Republic) using a Digestion MDS-2000 microwave system with Lined Digestion Vessels. The original solutions were transferred to 10 ml volumetric flasks and filled to the mark with deionized water.

2.9. Statistical analysis

All the measurements were carried out in triplicate/quadruplicate and standard deviations or variations were calculated. The data were analyzed by analysis of variance ANOVA (all the pairwise multiple comparison procedures by the Holm-Sidak method) and the differences were considered statistically significant at $P \leq 0.05$.

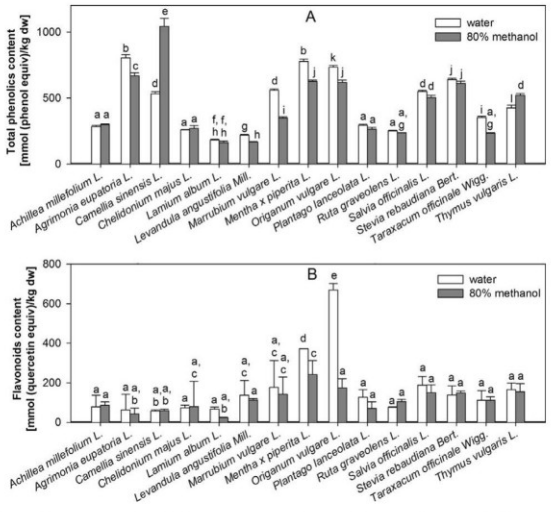


Fig. 1. The contents of total phenolic compounds (A) and flavonoids (B) in the hot water (white columns) and 80% methanolic (grey columns) extracts of 15 herbal plants. The contents of total phenolic compounds and flavonoids are expressed as mmol of phenol equivalents per kg of dry weight (dw) and mmol of quercetin equivalents per kg of dw, respectively. The determination was repeated 4-times and the variation is shown. Different letters next to each bar denote significant differences ($P \leq 0.05$) among the plant groups according to ANOVA. The same letters next to a bar which corresponds to a particular plant indicate no statistically significant differences between the extraction procedures.

3. Results

3.1. The phenolic compounds are correlated to antioxidant properties

The aqueous and methanolic extracts of the experimental plants were tested for the contents of phenolic compounds using the Folin-Ciocâlteu method and the results are given as molar phenol equivalents in the dry material. The aqueous extracts contained 180–800 mmol of phenol equivalent per kg, corresponding to 17–76 g of phenol per kg. For the methanolic extracts, the values were 160–1040 mmol of phenol equivalent per kg, or 15–98 g of phenol per kg (Fig. 1A). In many plants, such as *Origanum vulgare* L., *Agrimonia eupatoria* L., *Mentha* × *piperita* L., the contents of the phenolic compounds were slightly higher in the hot water extracts than in the methanolic ones, but significantly more total phenolic compound contents were present in the methanolic extract of *Camellia sinensis* L. plant. Both the aqueous and methanolic extracts of *Lamium album* L. exhibited the lowest phenolic contents.

The next tested parameter was the content of flavonoids determined using the aluminium complex-based method. The contents of flavonoids in the aqueous and methanolic extracts were similar in most plant species. The methanolic extracts contained 25–240 mmol of quercetin equivalents per kg, which corresponds to 7–73 g of quercetin per kg. The largest amount was present in *Mentha* × *piperita* L., the lowest amount was found in *Lamium album* L. Hot water extracts yielded 57–670 mmol of quercetin equivalents per kg, corresponding to 17–200 g of quercetin per kg. The highest concentration of flavonoids was found in the aqueous extracts of *Origanum vulgare* L. and in *Mentha* × *piperita* L. (Fig. 1B).

The antioxidant properties were tested by three methods: ABTS/DPPH, and FRAP (Fig. 2). The methods are based on different principles, so the results could be expected to be diverse. The ABTS compound treated with $K_2S_2O_8$ forms a cation radical, which can be reduced by an antioxidant compound and monitored by a decrease in the absorbance. Among the tested aqueous extracts, the highest capacity was determined in *Agrimonia eupatoria* L., *Origanum vulgare* L., and

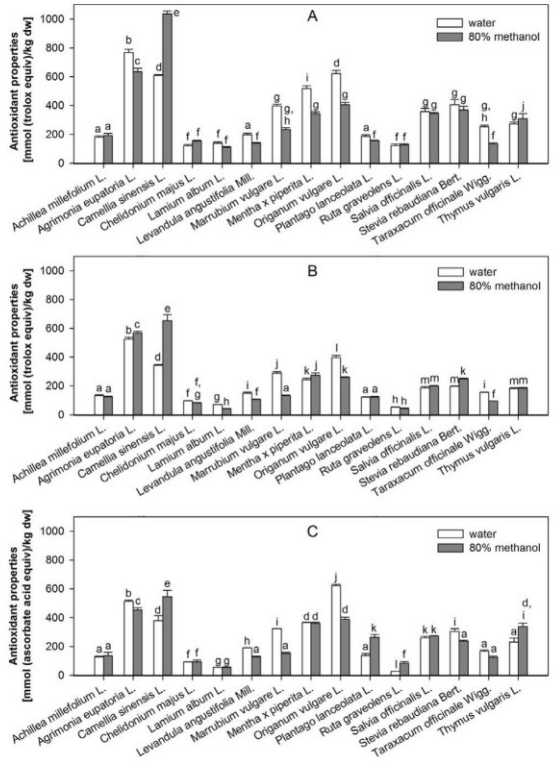


Fig. 2. The antioxidant properties of the hot water (white columns) and 80% methanolic (grey columns) extracts of 15 herbal plants determined by ABTS (A), DPPH (B), and FRAP (C) method. The antioxidant properties are expressed as mmol of trolox equivalents per kg of dry weight for ABTS and DPPH method and as mmol of ascorbate acid equivalents per kg of dry weight for FRAP assay. The determination was repeated 4-times, and the variation is shown. The different letters next to each bar denote significant differences ($P \leq 0.05$) among the plant groups according to ANOVA. The same letters next to a bar which corresponds to a particular plant indicate no statistically significant differences between the extraction procedures.

Camellia sinensis L. (Fig. 2A). In contrast, *Thymus vulgaris* L. and *Taraxacum officinale* Wigg. aqueous and methanolic extracts had the lowest antioxidant capacities determined by the ABTS method. DPPH forms a stable radical, which can bind a hydrogen atom or a radical. This process can be monitored as a decrease in absorbance. The highest values using this technique were obtained for *Agrimonia eupatoria* L. and *Origanum vulgare* L., the lowest ones were for *Ruta graveolens* L. and *Lamium album* L. (Fig. 2B). The FRAP method functions as one electron transfer; 2,4,6-tris(2-pyridyl)-*s*-triazine forms a complex with Fe^{3+} and this ion is reduced by an antioxidant compound to Fe^{2+}, which can be monitored as an increase in the absorbance. High antioxidant capacity values measured by FRAP were obtained for *Origanum vulgare* L. and *Agrimonia eupatoria* L., *Camellia sinensis* L., *Mentha* × *piperita* L., and *Stevia rebaudiana* Bert. (Fig. 2C). The lowest antioxidant capacity determined by FRAP was again found in *Ruta graveolens* L. and *Lamium album* L. aqueous and methanolic extracts, similar to the values determined by the DPPH method. In most plant species, the antioxidant capacity was comparable in the aqueous and methanolic extracts. The aqueous extracts of some plant species, such as *Origanum vulgare* L. and *Marrubium vulgare* L., had higher antioxidant capacities than the methanolic extracts. In some cases, the results were the opposite: the most significant plant with high antioxidant capacity in the methanolic extract was *Camellia sinensis* L.; this was consistent for all the tested methods (Fig. 2).

Correlation of the values obtained by the individual methods for the plant species was followed (Fig. 3). All three datasets were characterized by Pearson correlation coefficients, which were greater than 0.9 (Fig. 3). The correlations between the antioxidant capacities and the contents of phenolic compounds were strong; however, when the antioxidant capacity was compared for only flavonoids, the correlation was weaker (Fig. 3). We can conclude that the high content of total phenolic compounds measured by the Folin-Ciocâteu method corresponded to the high antioxidant capacity measured by all the three tested methods.

3.2. Metal elements are present in herbal extracts

The presence of some metal elements was also evaluated in the plant extracts. Monovalent Na^+ and K^+ and divalent Ca^{2+} and Mg^{2+} ions are among the plentifully represented metal ions in living cells. The content of Na^+ was relatively low in all the plants (0.06–1.4 g per kg of dw and 0.014–2 g per kg of dw in the aqueous and methanolic extracts, respectively), higher values were found in *Plantago lanceolata* L. and *Taraxacum officinale* Wigg. aqueous extracts. On the other hand, K^+ was present in herbal extracts in higher concentrations; high contents of this cation were found in *Chelidonium majus* L., *Lamium album* L. and *Taraxacum officinale* Wigg. The content of K^+ was significantly higher than that of Na^+ in the aqueous extracts of all the plant species, so that their ratio could be propitious for human metabolism when consumed as tea (Fig. 4). A high content of Ca^{2+} ions was found in almost all the plant extracts, the only exception being *Lamium album* L. with a low concentration of Ca^{2+} ions. The highest Ca^{2+} contents were detected in *Chelidonium majus* L., *Plantago lanceolata* L. and *Ruta graveolens* L. The Mg^{2+} content was also relatively high, especially in *Marrubium vulgare* L., *Agrimonia eupatoria* L., *Lamium album* L., *Salvia officinalis* L., and *Mentha* × *piperita* L. The ratio of the two divalent ions in the herbal extracts varied; in *Agrimonia eupatoria* L., *Mentha* × *piperita* L., *Salvia officinalis* L., and *Stevia rebaudiana* Bert., the ratio was nearly 1, in many plants more Ca^{2+} than Mg^{2+} was determined but the ratios were the opposite in *Marrubium vulgare* L., *Achillea millefolium* L., and *Lamium album* L. Notably, the corresponding ratio was 0.01 in *Camellia sinensis* L. with a low Ca^{2+} concentration in the aqueous extract.

In addition to these more available elements, the amounts of Zn and Se were also measured, because they participate in important pathways and are not always present in sufficient amounts in the human diet. Zn was detected in plant aqueous extracts in amounts of 0.06–0.25 g per kg of dw and in methanolic extracts in amounts of 0.002–0.17 g per kg of dw, while the highest contents were found in *Chelidonium majus* L., *Stevia rebaudiana* Bert., and *Thymus vulgaris* L. (Fig. 4). The selenium content was under the detection limit in the herbal extracts, i.e. less than 0.34 μg/l, corresponding to 14.2 μg/kg. However, when the plant samples were analyzed in the form of dried ashes, higher concentrations were found. *Achillea millefolium* L., *Agrimonia eupatoria* L., *Camellia sinensis* L., *Chelidonium majus* L., and *Salvia officinalis* L. contained hundreds μg of Se per kg (Table 2). The content of other tested elements Zn, Ca, and Mg were also significantly greater in the ashes than in aqueous or methanolic extracts (Fig. 5, Table 1, 2).

4. Discussion

The harmful effects of the free radicals and ROS on the cell components and their relationship to many serious diseases are well known. The human diet contains vitamins, i.e. ascorbic acid, carotenoids, and vitamin E, while fruits and vegetables are rich in phenolic compounds with antioxidant capacity, but their intake in the human diet is not always adequate. Medicinal plants used in natural healing from everlasting plants also contain various phenolic compounds in their tissues, which could be effective in prevention and/or healing. The simplest application is in the form of a hot water extract, i.e. herbal tea. All the plants tested in this study had relatively high contents of phenolic compounds and the content of total phenolic compounds was correlated

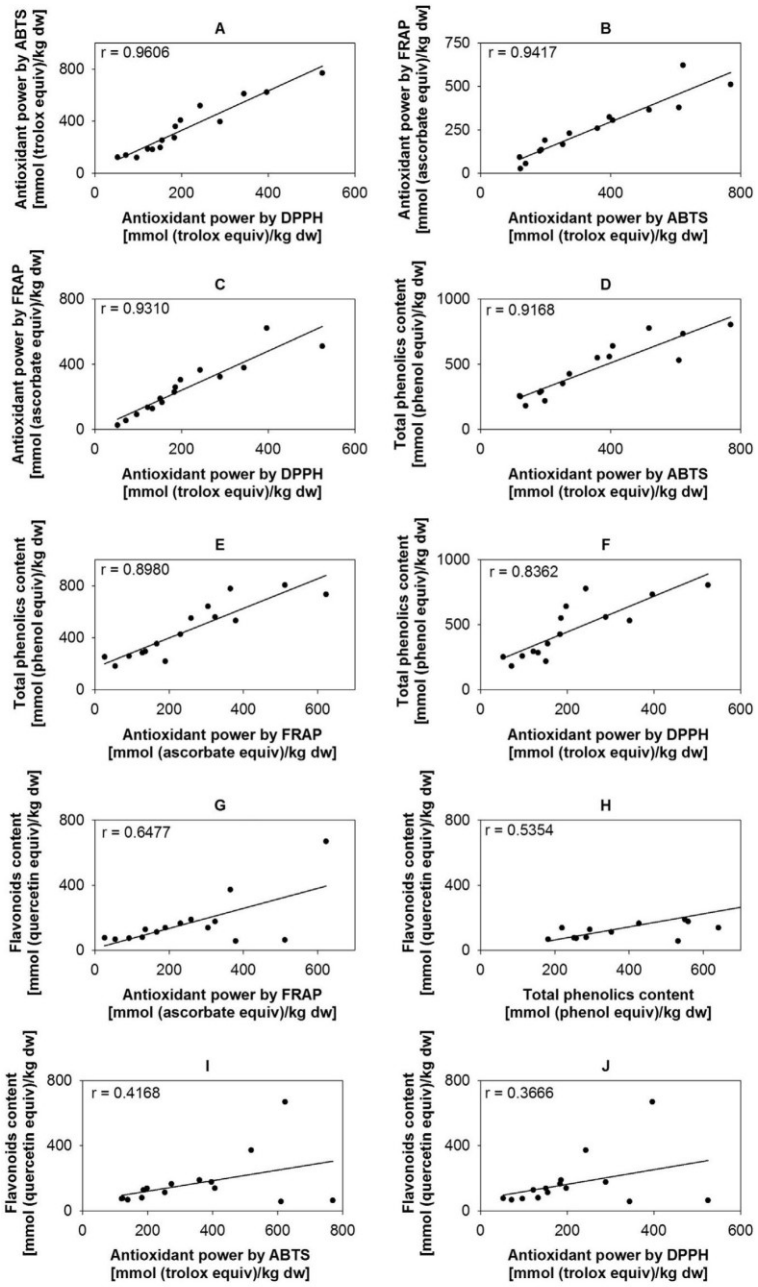


Fig. 3. Correlation analysis of the results of 5 different methods (determination of total phenolic compounds and flavonoid content and determination of the antioxidant capacity by ABTS, DPPH, and FRAP) for 15 herbal plants. The graphs are ordered according to Pearson's correlation coefficients (r), which are indicated in the plots.

well with the antioxidant properties (Figs. 1–3). The ratio of antioxidant capacity and total phenolic compounds indicates specific antioxidant capacity. The comparison of specific antioxidant capacity determined by ABTS, DPPH and FRAP in both water and methanolic extracts showed the most potent extracts to be those of: *Levandula angustifolia* Mill, *Agrimonia eupatoria* L., and *Origanum vulgare* L. *Camellia sinensis* L. also belongs among plants with high specific antioxidant capacity. In contrast, aqueous and methanolic extracts of *Ruta graveolens* L. and *Chelidonium majus* L. have low specific antioxidant capacity.

Comparison of our results with the literature is complicated, because various extraction methods (solvents, time of extraction, temperature) were used and determinations of the antioxidant capacity were not identical (Molnar et al., 2017). Nevertheless, high contents of phenolic compounds and high antioxidant capacity were reported for *Agrimonia eupatoria* L.(Kuczmannova et al., 2015; Santos et al., 2017) and for *Origanum vulgare* L. (Goncalves et al., 2017; Nile, Nile, & Keum, 2017). Many compounds with antioxidant properties could act synergistically. No compound is present in a large excess in the mixtures and there is not any great danger from the pro-oxidative properties of these compounds.

Recently, the analysis of trace elements in human tissues has shown that they can be important markers for biochemical and physiological

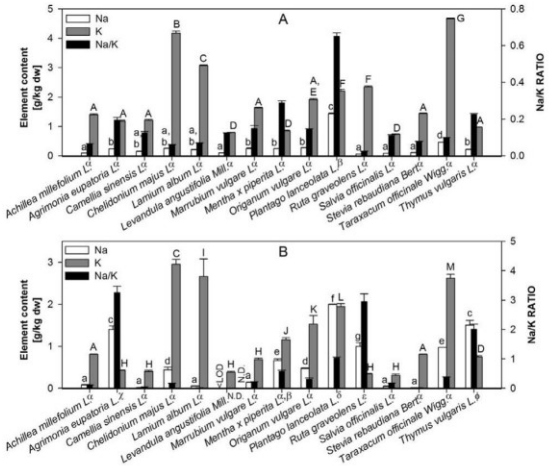


Fig. 4. The contents of Na and K in the aqueous (A) and methanolic (B) extracts of 15 herbal plants. The z axis presents Na/K ratio. The determination was repeated 3-times and the uncertainty in the measurement is expressed as the standard deviations. The different letters next to each bar denote significant differences ($P \leq 0.05$) among the plant groups according to ANOVA. The small letters correspond to Na, the capitals to K and the Greek letters to the Na/K ratio. The same letters next to a bar which corresponds to a particular plant indicate no statistically significant differences between the extraction procedures.

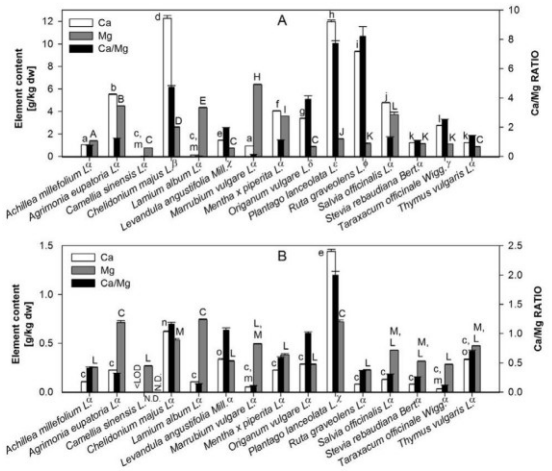


Fig. 5. The contents of Ca and Mg in the aqueous (A) and methanolic (B) extracts of 15 herbal plants. The z axis represents the Ca/Mg ratio. The different letters next to each bar denote significant differences ($P \leq 0.05$) among the plant groups according to ANOVA. The small letters correspond to Ca, the capitals to Mg and Greek letters to the Ca/Mg ratio. The same letters next to a bar which corresponds to a particular plant indicate no statistically significant differences between the extraction procedures.

processes, where some elements show high correlation with pathological disorders (Czerny, Krupka, Ozarowski, & Seremak-Mrozikiewicz, 2014).

Metal elements are required in different amounts and they play different roles in the metabolism. In this work we studied the concentrations of Zn and Se, which could contribute to ROS scavenging, and Na, K, Ca and Mg, whose metal ions are present in larger amounts in organisms. Enhanced demands on Zn are associated with oxidative stress, such as hyperglycaemia, infection or UV radiation (Cruz et al., 2015; Gupta et al., 2014). The herbal extracts tested in this study also contained Zn; thus drinking herbal tea made from *Stevia rebaudiana* Bert., *Thymus vulgaris* L., or *Salvia officinalis* L. could supply Zn to the human organism and improve defense mechanisms against ROS. The content of Zn in an aqueous extract from *Chelidonium majus* L. was even greater; however, considering the relative toxicity of the plant, it cannot be used as an herbal tea. However, the presence of Zn could participate in the effect when used in dermal application. Depending on the herbal species, a differences was found between aqueous and methanolic extracts; zinc is probably bound in various types of compounds (Table 1). It can be seen from comparison of Tables 1, 2 that the ash contains more Zn than the extracts, which is probably due to the fact that Zn interacts with compounds that are not extracted into water or methanol. Using the whole herbs as spices, and thus addition of *Thymus vulgaris* L. or *Salvia officinalis* L. to foods, could possibly enhance the intake of Zn.

Se is an essential semimetal microelement, both abnormally low and high intakes are a health risk (Kurokawa & Berry, 2013; Vinceti et al., 2017). Se is present in organisms primarily in selenoproteins, which function as enzymes in redox reactions, e. g. thioredoxin reductases, glutathione peroxidases or methionine sulfoxide reductase (Allmang, Wurth, & Krol, 2009). Dietary deficiencies of Se have been reported in some countries (Panchal, Wanyonyi, & Brown, 2017). The Se content in the herbal extracts studied in this work was very low and below the detection limit. However, the content of Se in ash could be measured using a more sensitive method (Table 2) and significant differences were apparent among the plant species. Higher concentrations were found in *Achillea millefolium* L., *Agrimonia eupatoria* L., *Camellia sinensis* L., *Chelidonium majus* L., *Salvia officinalis* L., and *Stevia rebaudiana* Bert., compared to the other tested plant species. We could suppose that *Salvia officinalis* L. as a spice and *Camellia sinensis* L. or *Achillea millefolium* L. and *Agrimonia eupatoria* L. in a herbal mixture could improve Se intake in human metabolism. Similar to Se, Zn, Ca and Mg were also present in higher concentrations in the dried solid samples than in the solvent extracts. It seems that using whole dried medicinal plants (or fresh) for food preparation as spices or additives could be more beneficial than consuming infusions in relation to element intake (Table 1, 2).

The human diet in modern society contains much more NaCl than the organism requires; on the other hand, the consumption of K^+ is relatively low. A high Na^+/K^+ ratio is associated with hypertension and cardiovascular diseases (He et al., 2015; Penton et al., 2015; Terker et al., 2015). From this point of view, an increased content of K^+ in the diet and drinking herbal teas could contribute to the balance of both ions because all the tested herbs contained more K than Na, where the ratio Na/K varied from 0.02 to 0.22. The only exception of a higher ratio (0.65) was the aqueous extract of *Plantago lanceolata* L. (Fig. 4).

The intake of Ca in the diet is not always sufficient, especially among seniors. The supplementation of Ca recommended for osteoporosis prevention had only a minor effect on bone mineral density but many negative effects (Bolland et al., 2015; Tai et al., 2015). Some diseases are associated with low levels of Mg in the serum; people with metabolic and diabetic syndromes need a greater supply of Mg (Mooren, 2015). Hyperglycaemia and the resulting osmotic diuresis lead to Mg excretion. Low levels of magnesium have been found after treatment with some drugs (Blaine et al., 2015). Increased Ca and Mg intake in foods seems to be better compared to inorganic supplements. In the presented study, all the herbal extracts contained Ca and Mg, so that drinking herbal tea could make a beneficial contribution to replenishing insufficient amounts of calcium and magnesium (Fig. 5).

5. Conclusion

Our results clearly demonstrated that the extracts of all the tested potential medicinal plants possessed antioxidant capacity, which was correlated with the content of total phenolic compounds. Thus using these plant species, especially *Agrimonia eupatoria* L., *Origanum vulgare* L., and *Mentha* × *piperita* L. in the form of herbal tea or spices could protect the organism from ROS that has arisen in the metabolism or during pathological events. The plant tissues and extracts also

Table 1
The contents of Zn and Se in the aqueous and methanolic extracts of 15 herbal plants. The different letters next to each value denote significant differences ($P \leq 0.05$) among the plant groups according to ANOVA. The same letters next to a value which corresponds to a particular plant indicate no statistically significant differences between the extraction procedures.

Extract	Aqueous Zinc		Methanolic		Aqueous Selenium	Methanolic
	[g/kg dw]	±	[g/kg dw]	±	[g/kg dw]	[g/kg dw]
Achillea millefolium L.	0.086^{a}	0.003	0.028^{b}	0.0013	< LOD	< LOD
Agrimonia eupatoria L.	0.066^{b}	0.009	0.018^{b}	0.0013	< LOD	< LOD
Camellia sinensis L.	0.089^{a}	0.004	0.024^{b}	0.0022	< LOD	< LOD
Chelidonium majus L.	0.259^{c}	0.007	0.017^{b}	0.0067	< LOD	< LOD
Lamium album L.	0.112^{d}	0.011	0.112^{d}	0.0067	< LOD	< LOD
Levandula angustifolia Mill.	0.060^{b}	0.004	0.008^{b}	0.007	< LOD	< LOD
Marrubium vulgare L.	0.083^{a}	0.004	0.029^{b}	0.013	< LOD	< LOD
Mentha × piperita L.	$0.082^{a,b}$	0.006	0.040^{b}	0.006	< LOD	< LOD
Origanum vulgare L.	0.066^{b}	0.003	0.002^{b}	0.001	< LOD	< LOD
Plantago lanceolata L.	0.111^{d}	0.003	0.002^{b}	0.001	< LOD	< LOD
Ruta graveolens L.	0.092^{a}	0.005	0.014^{b}	0.002	< LOD	< LOD
Salvia officinalis L.	0.130^{e}	0.006	0.014^{b}	0.001	< LOD	< LOD
Stevia rebaudiana Bert.	0.189^{f}	0.008	0.018^{b}	0.005	< LOD	< LOD
Taraxacum officinale Wigg.	$0.076^{a,b}$	0.003	0.034^{b}	0.005	< LOD	< LOD
Thymus vulgaris L.	0.153^{g}	0.008	0.050^{b}	0.003	< LOD	< LOD

Table 2
The contents of Ca, Mg, Zn, and Se in ash dried at 525 °C. The different letters next to each value denote significant differences ($P \leq 0.05$) among the plant groups according to ANOVA.

	Calcium		Magnesium		Zinc		Selenium	
	[g/kg dw]	±	[g/kg dw]	±	[g/kg dw]	±	[µg/kg dw]	±
Achillea millefolium L.	20.45^{a}	0.44	4.01^{a}	0.09	0.22^{a}	0.02	477.9^{a}	13.9
Agrimonia eupatoria L.	15.66^{b}	1.31	4.15^{a}	0.35	0.31^{b}	0.01	468.7^{a}	5.62
Camellia sinensis L.	32.52^{c}	0.32	7.45^{b}	0.12	0.08^{c}	0.00	395.3^{b}	11.1
Chelidonium majus L.	10.97^{d}	0.12	2.95^{c}	0.03	0.31^{b}	0.00	352.2^{c}	7.40
Lamium album L.	16.98^{e}	0.50	9.23^{d}	0.27	$0.33^{b,d}$	0.00	52.39^{d}	5.13
Levandula angustifolia Mill.	25.65^{f}	0.40	5.05^{e}	0.08	0.55^{e}	0.00	58.19^{d}	0.87
Marrubium vulgare L.	27.51^{g}	0.57	7.62^{b}	0.04	0.11^{f}	0.00	67.57^{d}	2.09
Mentha × piperita L.	49.40^{h}	0.59	5.35^{e}	0.06	0.39^{g}	0.01	18.73^{e}	0.49
Origanum vulgare L.	$26.48^{f,g}$	0.24	$4.49^{a,f}$	0.04	0.41^{h}	0.00	35.59^{f}	1.60
Plantago lanceolata L.	34.35^{i}	0.58	4.34^{a}	0.07	0.44^{i}	0.00	$43.24^{d,f}$	3.98
Ruta graveolens L.	53.44^{j}	0.49	$5.43^{e,g}$	0.05	0.48^{j}	0.00	$53.42^{d,g}$	5.29
Salvia officinalis L.	48.97^{h}	0.41	7.12^{b}	0.06	0.76^{k}	0.00	339.2^{c}	6.78
Stevia rebaudiana Bert.	17.75^{e}	0.49	6.34^{h}	0.17	0.76^{k}	0.01	$326.5^{c,h}$	8.16
Taraxacum officinale Wigg.	11.04^{d}	0.17	3.55^{i}	0.05	0.55^{e}	0.00	$27.41^{f,e}$	0.58
Thymus vulgaris L.	29.96^{k}	0.64	5.37^{e}	0.11	0.71^{l}	0.00	16.97^{e}	0.32

contained some tested essential microelements required for human metabolism (Mg, Ca, K, Zn, Se). These facts showed that medicinal plants could provide many benefits for human nutrition and in the prevention of chronic diseases.

Conflict of interest

The authors declare no conflict of interest.

Acknowledgement

This work was supported by Charles University (project UNCE 204025/2012).

References

Allmang, C., Wurth, L., & Krol, A. (2009). The selenium to selenoprotein pathway in eukaryotes: More molecular partners than anticipated. *Biochimica et Biophysica Acta, 1790*(11), 1415–1423.

Baxter, R. A. (2008). Anti-aging properties of resveratrol: Review and report of a potent new antioxidant skin care formulation. *Journal of Cosmetic Dermatology, 7*(1), 2–7.

Blaine, J., Chonchol, M., & Levi, M. (2015). Renal control of calcium, phosphate, and magnesium homeostasis. *Clinical Journal of the American Society of Nephrology, 10*(7), 1257–1272.

Bolland, M. J., Leung, W., Tai, V., Bastin, S., Gamble, G. D., Grey, A., & Reid, I. R. (2015). Calcium intake and risk of fracture: systematic review. *British Medical Journal (Clinical Research ed), 351*, h4580. http://dx.doi.org/10.1136/bmj.h4580:1-14.

Brand-Williams, W., Cuvelier, M. E., & Berset, C. (1995). Use of a free-radical method to evaluate antioxidant activity. *Food Science and Technology, 28*(1), 25–30.

Cai, Y. Z., Luo, Q., Sun, M., & Corke, H. (2004). Antioxidant activity and phenolic compounds of 112 traditional Chinese medicinal plants associated with anticancer. *Life Sciences, 74*(17), 2157–2184.

Cruz, K. J., de Oliveira, A. R., & Marreiro Ddo, N. (2015). Antioxidant role of zinc in diabetes mellitus. *World Journal of Diabetes, 6*(2), 333–337.

Czerny, B., Krupka, K., Ozarowski, M., & Seremak-Mrozikiewicz, A. (2014). Screening of trace elements in hair of the female population with different types of cancers in Wielkopolska region of Poland. *The Scientific World Journal, 2014*, 1–15.

Dudonne, S., Vitrac, X., Coutiere, P., Woillez, M., & Merillon, J. M. (2009). Comparative study of antioxidant properties and total phenolic content of 30 plant extracts of industrial interest using DPPH, ABTS, FRAP, SOD, and ORAC assays. *Journal of Agricultural and Food Chemistry, 57*(5), 1768–1774.

Goncalves, S., Moreira, E., Grosso, C., Andrade, P. B., Valentao, P., & Romano, A. (2017). Phenolic profile, antioxidant activity and enzyme inhibitory activities of extracts from aromatic plants used in Mediterranean diet. *Journal of Food Science Technology, 54*(1), 219–227.

Gupta, M., Mahajan, V. K., Mehta, K. S., & Chauhan, P. S. (2014). Zinc therapy in dermatology: A review. *Dermatology Research and Practice, 2014*, 709152. http://dx.doi.org/10.1155/2014/709152:1-11.

He, M., Mu, J., Liu, F., Ren, K., Wang, Y., Guo, T., & Wang, D. (2015). Effects of a high salt intake and potassium supplementation on QT interval dispersion in normotensive healthy subjects. *Internal Medicine (Tokyo, Japan), 54*(3), 295–301.

Kuczmannova, A., Gal, P., Varinska, L., Treml, J., Kovac, I., Novotny, M., ... Mucaji, P. (2015). *Agrimonia eupatoria* L. and *Cynara cardunculus* L. water infusions: Phenolic profile and comparison of antioxidant activities. *Molecules, 20*(11), 20538–20550.

Kurokawa, S., & Berry, M. J. (2013). Selenium. Role of the essential metalloid in health. *Metal Ions in Life Sciences, 13*, 499–534.

Liu, M., Li, X. Q., Weber, C., Lee, C. Y., Brown, J., & Liu, R. H. (2002). Antioxidant and anti proliferative activities of raspberries. *Journal of Agricultural and Food Chemistry, 50*(10), 2926–2930.

Marti, R., Rosello, S., & Cebolla-Cornejo, J. (2016). Tomato as a source of carotenoids and polyphenols targeted to cancer prevention. *Cancers*, *8*(6), 58.

Martins, N., Petropoulos, S., & Ferreira, I. C. (2016). Chemical composition and bioactive compounds of garlic (*Allium sativum* L.) as affected by pre- and post-harvest conditions: A review. *Food Chemistry*, *211*, 41–50.

Molnar, M., Jerkovic, I., Suknovic, D., Bilic Rajs, B., Aladic, K., Subaric, D., & Jokic, S. (2017). Screening of six medicinal plant extracts obtained by two conventional methods and supercritical CO_2 extraction targeted on coumarin content, 2,2-diphenyl-1-picrylhydrazyl radical scavenging capacity and total phenols content. *Molecules*, *22*(3), 1–10.

Mooren, F. C. (2015). Magnesium and disturbances in carbohydrate metabolism. *Diabetes, Obesity and Metabolism*, *17*(9), 813–823.

Nile, S. H., Nile, A. S., & Keum, Y. S. (2017). Total phenolics, antioxidant, antitumor, and enzyme inhibitory activity of Indian medicinal and aromatic plants extracted with different extraction methods. *3 Biotech*, *7*(76), http://dx.doi.org/10.1007/s13205-017-0706-9.

Ou, B. X., Huang, D. J., Hampsch-Woodill, M., Flanagan, J. A., & Deemer, E. K. (2002). Analysis of antioxidant activities of common vegetables employing oxygen radical absorbance capacity (ORAC) and ferric reducing antioxidant power (FRAP) assays: A comparative study. *Journal of Agricultural and Food Chemistry*, *50*(11), 3122–3128.

Panchal, S. K., Wanyonyi, S., & Brown, L. (2017). Selenium, vanadium, and chromium as micronutrients to improve metabolic syndrome. *Current Hypertension Reports*, *19*(10), http://dx.doi.org/10.1007/s11906-11017-10701-x.

Penton, D., Czogalla, J., & Loffing, J. (2015). Dietary potassium and the renal control of salt balance and blood pressure. *Pflugers Archiv-European Journal of Physiology*, *467*(3), 513–530.

Re, R., Pellegrini, N., Proteggente, A., Pannala, A., Yang, M., & Rice-Evans, C. (1999). Antioxidant activity applying an improved ABTS radical cation decolorization assay. *Free Radical Biology & Medicine*, *26*(9–10), 1231–1237.

Santos, T. N., Costa, G., Ferreira, J. P., Liberal, J., Francisco, V., Paranhos, A., ... Batista, M. T. (2017). Antioxidant, anti-Inflammatory, and analgesic activities of *Agrimonia eupatoria* L. infusion. *Evidence-Based Complementary and Alternative Medicine*, 1–13. http://dx.doi.org/10.1155/2017/8309894.

Song, J. H., Han, Y. M., Kim, W. H., Park, J. M., Jeong, M., Go, E. J., ... Hahm, K. B. (2016). Oxidative stress from reflux esophagitis to esophageal cancer: The alleviation with antioxidants. *Free Radical Research*, *50*(10), 1071–1079.

Szajdek, A., & Borowska, E. J. (2008). Bioactive compounds and health-promoting properties of berry fruits: A review. *Plant Foods for Human Nutrition*, *63*(4), 147–156.

Tai, V., Leung, W., Grey, A., Reid, I. R., & Bolland, M. J. (2015). *Calcium intake and bone mineral density: Systematic review and meta-analysis. British Medical Journal (Clinical Research ed)*, *351*, h4183. http://dx.doi.org/10.1136/bmj.h4183:1-14.

Terker, A. S., Zhang, C., McCormick, J. A., Lazelle, R. A., Zhang, C., Meermeier, N. P., ... Ellison, D. H. (2015). Potassium modulates electrolyte balance and blood pressure through effects on distal cell voltage and chloride. *Cell Metabolism*, *21*(1), 39–50.

Tramutola, A., Lanzillotta, C., Perluigi, M., & Butterfield, D. A. (2016). Oxidative stress, protein modification and Alzheimer disease. *Brain Research Bulletin*. http://dx.doi.org/10.1016/j.brainresbull.2016.06.005.

Tsao, R., Yang, R., Xie, S., Sockovie, E., & Khanizadeh, S. (2005). Which polyphenolic compounds contribute to the total antioxidant activities of apple? *Journal of Agricultural and Food Chemistry*, *53*(12), 4989–4995.

Vinceti, M., Filippini, T., Cilloni, S., Bargellini, A., Vergoni, A. V., Tsatsakis, A., & Ferrante, M. (2017). Health risk assessment of environmental selenium: Emerging evidence and challenges (Review). *Molecular Medicine Reports*, *15*(5), 3323–3335.

Wojdylo, A., Oszmianski, J., & Czemerys, R. (2007). Antioxidant activity and phenolic compounds in 32 selected herbs. *Food Chemistry*, *105*(3), 940–949.

Yao, Y., Sang, W., Zhou, M. J., & Ren, G. X. (2010). Phenolic composition and antioxidant activities of 11 celery cultivars. *Journal of Food Science*, *75*(1), C9–C13.

Zastrow, M. L., & Pecoraro, V. L. (2014). Designing hydrolytic zinc metalloenzymes. *Biochemistry*, *53*(6), 957–978.

3.3.2 Does resveratrol retain its antioxidative properties in wine? Redox behaviour of resveratrol in the presence of Cu(II) and tebuconazole

In 2018, we established a fruitful cooperation and friendship with Jana Jaklová Dytrtová and her group. During the preparation of this manuscript, we relied on our knowledge on antioxidant capacity methods (Tupec et al 2017).

Red wine is the most important source of resveratrol for humans. This molecule is probably the most important factor in the so-called French paradox. It describes an epidemiological finding of a low incidence of cardiovascular disease in the French population, even though their diet is rich in saturated fats, but also includes a daily intake of an adequate amount of red wine. Resveratrol is biosynthesized by vines (and other plants) especially in response to the pathogen *Botrytis cinerea* (Kasiotis et al 2013, Šmidrkal et al 2001). Also, wine usually contains high amounts of Cu^{2+} because vineyard soils used to be sprayed by bluestone (copper sulphate) as an antifungal agent (contact fungicide). Nowadays, systemic fungicides such as tebuconazole are used and may linger in wine. Tebuconazole is a reactive triazole, eager to create complexes with metal cations (Jaklová Dytrtová et al 2011). The main aim of this project was to analyze the interactions between resveratrol, Cu^{+}/Cu^{2+} and tebuconazole by mass spectrometry, antioxidant capacity assay and quantum-chemical calculations (Fig. 18).

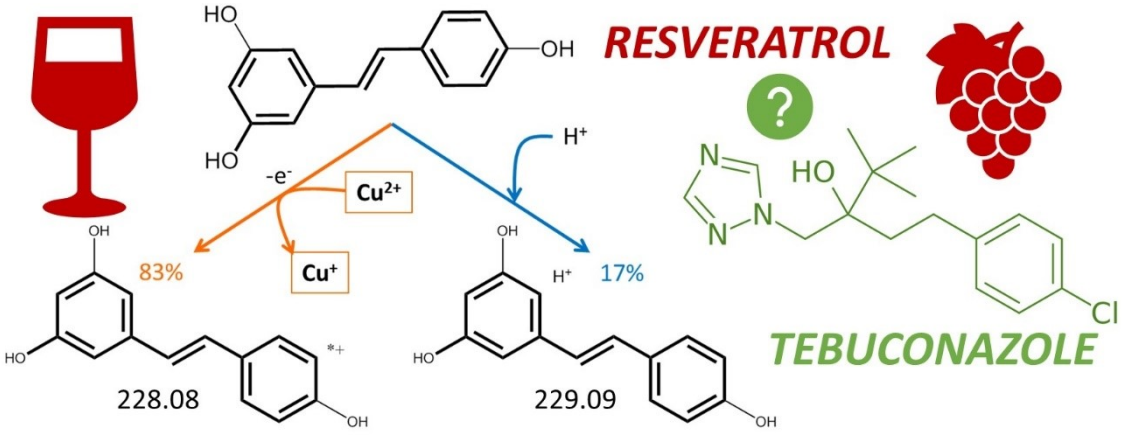


Fig. 18: Scheme of suggested formation of Res*+ (228.08) and (HRes)+ (229.09) in the presence of Cu^{2+}. The role of tebuconazole in the (anti)oxidant interactions was analyzed in this project.

We found that resveratrol turns oxidative in the presence of Cu^{2+} (Fig. 1, SI3 in Jaklová Dytrtová et al 2018). The mixture of resveratrol and tebuconazole was

measured in both positive and negative modes of ESI-MS (Fig. 2, Fig. SI8 in Jaklová Dytrtová et al 2018). In the negative mode, we detected compounds with antioxidant capacity $(Resveratrol\text{-}H)^-$, $[Resveratrol(Resveratrol\text{-}H)]^-$ and expected antioxidant capacity $[Tebuconazole(Resveratrol\text{-}H)]^-$. No resveratrol radicals or cations were observed in the positive mode. After the addition of Cu^{2+}, we focused mainly on the $[Cu(Resveratrol\text{-}H)(Tebuconazole)]^+$ and its daughter ion $[CuTebuconazole]^+$ found in the positive mode (Fig. 3, 4 in Jaklová Dytrtová et al 2018). The interaction between Cu^+ and tebuconazole can be *via* the electron lone pair of the hydroxyl group, N2 of the triazole ring and the phenol ring. In the experiment, performed on the electrochemical device coupled online with ESI-MS, we found that resveratrol first interacts with tebuconazole and subsequently with Cu^{2+}. No products of Cu-resveratrol were detected as resveratrol is bound in $[Tebuconazole(Resveratrol\text{-}H)]^-$. In the antioxidant capacity assays, we found that Resveratrol-Cu^{2+} showed significant decrease while Resveratrol-Tebuconazole-Cu^{2+} demonstrated slightly higher capacity (or equal) to single resveratrol. The results were significantly time dependent in the antioxidant assay (liquid phase), distinct differences between various mixtures showed after 7 days of incubation at 4°C (Fig. 6, SI12 in Jaklová Dytrtová et al 2018).

In conclusion, tebuconazole's high affinity for Cu^{2+} can protect resveratrol. Also, tebuconazole strongly binds to resveratrol and blocks the positions attacked by Cu^{2+}.

My contribution:

I measured the antioxidant capacity of resveratrol with or without the presence of triazoles and Cu^{2+}. I prepared the resulting figures.

Food Chemistry 262 (2018) 221–225

Contents lists available at ScienceDirect

Food Chemistry

journal homepage: www.elsevier.com/locate/foodchem

Does resveratrol retain its antioxidative properties in wine? Redox behaviour of resveratrol in the presence of Cu(II) and tebuconazole

Jana Jaklová Dytrtová[a,b,*], Michal Straka[a], Kateřina Bělonožníková[c], Michal Jakl[d], Helena Ryšlavá[c]

[a] Institute of Organic Chemistry and Biochemistry, The Czech Academy of Sciences, Flemingovo náměstí 2, 166 10 Prague 6, Czech Republic
[b] Department of Physiology and Biochemistry, Faculty of Physical Education and Sport, Charles University, Jose Martího 31, 162 52 Prague 6, Czech Republic
[c] Department of Biochemistry, Faculty of Science, Charles University, Hlavova 2030, 128 43 Praha 2, Czech Republic
[d] Department of Agro-Environmental Chemistry and Plant Nutrition, Faculty of Agrobiology, Food and Natural Resources, Czech University of Life Sciences Prague, Kamýcká 129, 165 00 Prague – Suchdol, Czech Republic

ARTICLE INFO

Keywords:
Polyphenols
Triazoles
Copper
Antioxidant capacity
ESI-MS
DFT
FRAP

ABSTRACT

Resveratrol is antioxidant naturally occurring in wine grapes. It is thought to have a preventive biological activity against number of diseases. However, it has been recently shown that in the presence of metal ions, such as Cu^{2+}, resveratrol forms oxidative radicals. Cu^{2+} is usually present in wine due to former usage of bluestone in vineyards. Fungicide tebuconazole has substituted bluestone and is presently one of the most widely used agrochemicals in wine industry; wine thus may contain traces of tebuconazole. Here, we study the ternary system of resveratrol, Cu^{2+}, and tebuconazole experimentally and theoretically (using mass spectrometry, antioxidant capacity assay and quantum-chemical calculations) to model the redox behaviour of resveratrol in wine. We show that tebuconazole prevents formation of oxidative resveratrol radicals (induced by Cu^{2+} reaction with resveratrol) via preferential Cu^{2+} capture and protection of the binding sites of resveratrol. This positive effect of tebuconazole has not been observed before.

1. Introduction

Resveratrol (Res) belongs to the family of polyphenol (polyhydroxide) compounds. It is thought to have a strong biological activity against a number of diseases, such as cancer or cardiovascular diseases (Baur et al., 2006; Bradamante, Barenghi, & Villa, 2004; Jang et al., 1997; Quideau, Deffieux, & Pouysegu, 2012; Smoliga, Baur, & Hausenblas, 2011). The positive healing effect of Res is based on its antioxidant properties, i.e., ability to quench free radicals. Its most common natural resource are wine grapes; esp. red wine contains up to 14 mg L^{-1} of Res (Stervbo, Vang, & Bonnesen, 2007). Wine is also rich in copper cations (milligrams per litter, depending on the variety of the grape) (Clark, Wilkes, & Scollary, 2015) because of contamination of vineyard soils by copper cations due to historical antifungal spraying of vineyards with bluestone (copper sulphate).

It has been shown recently that in the presence of Cu^{2+} ions Res forms radicals with strong oxidative activity and a Cu^{2+}-Res complex (Fig. 1; see below), which can intercalate DNA (Hadi et al., 2010; Tamboli, Defant, Mancini, & Tosi, 2011; Tamboli et al., 2012). Wine is a complex mixture containing many natural and artificial chemicals. One of them, tebuconazole (Teb) is heavily used for protection of grapes against fungal diseases and can be present also in the final wine products (Alister et al., 2014). It is a reactive agrochemical with high affinity to metal cations (Jaklová Dytrtová, Jakl, Schröder, Čadková, & Komárek, 2011), and can thus be expected to strongly interact with Cu^{2+} and even with resveratrol. The purpose of this study was to investigate the ternary system of resveratrol, tebuconazole, and Cu^{2+} to mimic the redox behaviour of resveratrol in wine. Mixtures of resveratrol with Cu^{2+}, resveratrol with tebuconazole, and resveratrol with Cu^{2+} and tebuconazole were studied by means of electrospray ionization mass spectrometry to understand basic reactivity of these systems and structures of created products. Density functional calculations were used to quantify the interactions among studied molecules. The change in the antioxidant capacity of Res in solution was measured in relation to the individual interactions and time.

* Corresponding author at: Institute of Organic Chemistry and Biochemistry, The Czech Academy of Sciences, Flemingovo náměstí 2, 166 10 Prague 6, Czech Republic.
E-mail addresses: dytrtova@ftvs.cuni.cz, dytrtova@uochb.cas.cz (J. Jaklová Dytrtová).

https://doi.org/10.1016/j.foodchem.2018.04.096
Received 11 September 2017; Received in revised form 23 February 2018; Accepted 21 April 2018
Available online 25 April 2018
0308-8146/ © 2018 Elsevier Ltd. All rights reserved.

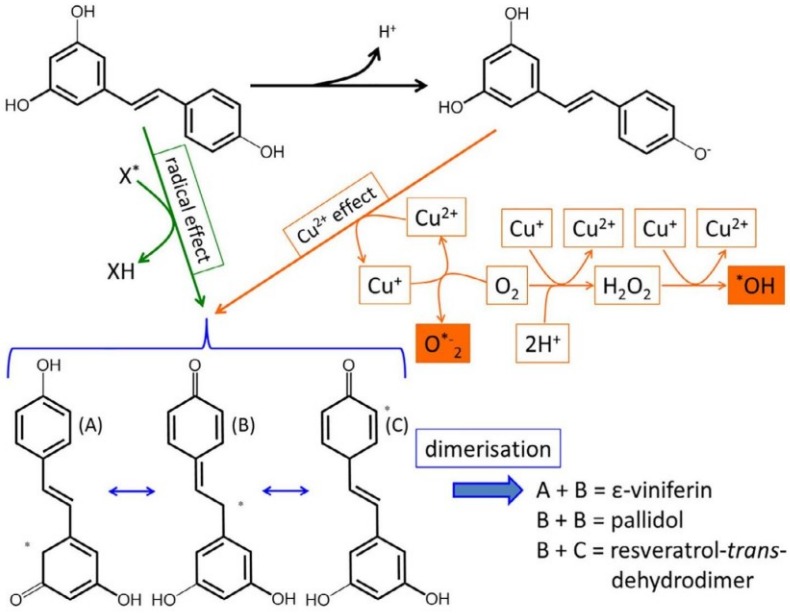


Fig. 1. Summary of the known actions of resveratrol (Res) alone (black arrows) and resveratrol in the presence of Cu^{2+} (orange arrows). The blue arrow indicates dimerization of deprotonated resveratrol radicals on the left. Based on general knowledge of Fenton reaction (Takaya et al., 2005; Tamboli et al., 2012). (For interpretation of the references to colour in this figure legend, the reader is referred to the web version of this article.)

2. Experimental

2.1. Mass spectrometry studies

The mass-spectrometry studies were performed using ion-trap mass spectrometer (ESI-MS; Finnigan LCQ Advantage, ThermoFinnigan, USA) fitted with an electrospray ion source operated in the positive-ion and negative-ion modes. The exact masses were measured using a QToF mass spectrometer (SYNAPT G2, Waters, UK). The sample solutions were continuously fed (0.6 mL h^{-1}) into the ion source through a silica capillary. Nitrogen was used as the nebulizer gas. Operating conditions of the ion trap were set as follows: spray voltage of 4.0 kV, capillary voltage of 0–10 V, tube lens offset of −5 to 10 V, heated capillary temperature of 200 °C, and sheath-gas flow rate as well as auxiliary-gas flow rate of 10–50 arbitrary units. For the QToF the conditions were set as follows: capillary voltage of 3.0 kV, sampling and extraction cones of 28 V and 2 V, source and desolvation temperatures of 100 and 350 °C, cone and desolvation gas of 50 and 450 L h^{-1}. Stability of the complexes was experimentally determined in an ion trap using collision-induced dissociation (CID) experiments of mass selected ions by comparing appearance energies (*AE*, kJ mol^{-1}) of daughter ions for fragmentation of Res, Res/Cu, Teb/Res/Cu parent ions (Zins, Pepe, & Schröder, 2010).

The sample solutions were prepared at desired concentrations using resveratrol and tebuconazole (Sigma-Aldrich, Czech Republic) stock solution (10^{-2} mol L^{-1}) in ethanol (Maneko, Czech Republic) and $CuCl_2$ (Sigma-Aldrich, Czech Republic) stock solution (10^{-2} mol L^{-1}) in pure water (> 18 MΩ). The experiments were mostly realized for an equimolar mixture of Res, Teb, and $CuCl_2$ ($5 \cdot 10^{-5}$ mol L^{-1}) in methanol/water (1:1).

2.2. EC/ESI-MS

For mimicking of Res and Teb interactions with copper an electrochemical device (EC) coupled online with ESI-MS (EC/ESI-MS) depicted in Reference Jaklová Dytrtová, Jakl, Navrátil, Cvačka, and Pačes (2016) was used. The sample solutions were continuously (0.45 mL h^{-1}) fed into the EC through a silica capillary. The operating potential inserted to the copper working electrode was +700 mV, the operating time was 120 s. During this time the mass spectra detecting the reaction products were online recorded. Parameters of ESI-MS were the same as above. The sample solution consisted of equimolar mixtures (both $5 \cdot 10^{-5}$ mol L^{-1}) of Res and Teb in methanol/electrolyte (25 mmol L^{-1} ammonium acetate) mixture (1:1).

2.3. Theoretical calculations

Molecular structures were optimized with Gaussian 09 code (Frisch et al., 2009) using the B3LYP density functional (Becke, 1988) and the 6-311G* basis set (Jakl, Straka, Jaklová Dytrtová, & Roithová, 2014).

Different mutual orientations of molecules in complexes were calculated to assure the global minima. Only the lowest energy isomers found are discussed. Frequency analysis was performed for each structure to assure the minimum and to determine the zero-point energy correction. The theoretical bonding energies (BDE) refer to the energies at 0 K, i.e., the sum of electronic energy and zero-point energy.

2.4. Antioxidant capacity assay

The Free Radical Scavenging by the use of the DPPH radical (2,2-diphenyl-1-picrylhydrazyl), and the Ferric Reducing Antioxidant Potential assays (FRAP) were used for the antioxidant capacity determination, both accordingly to Tupec et al. (Tupec et al., 2017), and Dudonne et al. (Dudonné, Vitrac, Coutière, Woillez, & Mérillon, 2009). The detailed procedures are described in SI. The experiments were realized for an equimolar mixture of Res, Teb, and $CuCl_2$ (100 μmol L^{-1} for FRAP, 800 μmol L^{-1} for DPPH), or Res, Teb, $[(CH_3CN)_4Cu]PF_6$ (2.5 mmol L^{-1} for DPPH). For FRAP, Teb and Cu^{2+} solutions were also tested in 1–10 mmol L^{-1} concentrations but they did not cause any changes in absorbance, thus they were considered of no antioxidant capacity. All the samples were measured at least 4-times. The data were analysed by One Way ANOVA (Bonferroni method); the differences were considered statistically significant at $P \leq 0.05$.

3. Results and discussion

The behaviour of Res in the presence of Cu^{2+} was studied previously by Tamboli *et al.* (Tamboli et al., 2012). We were able to

reproduce their experiments in most part; the details are given in SI. We shortly summarize in Fig. 1 the recent knowledge about Res interactions in the presence of Cu^{2+}. Res itself forms a preferentially deprotonated anion $(Res\text{-}H)^-$ and its adduct with neutral Res, $[Res(Res\text{-}H)]^-$ in the negative mode (Fig. SI1). The addition of $CuCl_2$ to the system (Fig. SI2) initiates a plethora of Res transformations, particularly creation of phenoxyl radical $Res^{\bullet+}$ (m/z 228.08). Its recombination with Res yields several dehydrodimers, particularly the resveratrol-*trans*-dehydrodimer and ε-viniferin. The details are shown in Fig. 1.

The system with Cu^{2+} yields phenoxyl radical $Res^{\bullet+}$ (m/z = 228.08), which has pro-oxidative properties, and $(HRes)^+$ product (m/z = 229.09) (Fig. SI3) (Tamboli et al., 2012). The $Res^{\bullet+}$ was also found by Tamboli *et al.* (Tamboli et al., 2012) after treatment of Res with Fe^{3+}. We note that due to the delocalization of the unpaired electron, the $(Res\text{-}H)^{\bullet}$ is a weaker oxidant than, e.g., oxygen or hydroxyl radicals. Phenoxyradicals $(Res\text{-}H)^{\bullet}$ in Fig. 1 are sufficiently reactive to combine into dimers (Fig. SI4). Two of the three previously proposed dimers (Takaya et al., 2005) we confirmed in the mixture. Fragmentation of 455^+ – the Res dimer (Fig. SI5) – revealed that the signal belongs to a mixture of resveratrol-*trans*-dehydrodimer (Tamboli et al., 2012) and ε-viniferin.

Let us now to discuss the mixture of Res and Teb (Fig. 2). Res itself gives raise to two compounds with an anti-oxidant activity in the negative mode: the deprotonated $(Res\text{-}H)^-$ and its complex with neutral Res, $[Res(Res\text{-}H)]^-$. Additionally, the $[Teb(Res\text{-}H)]^-$ complex with expected antioxidant activity is formed. Teb is also present in the deprotonated form, $(Teb\text{-}H)^-$, Fig. 2.

The positive mode spectrum of Teb + Res mixture (Fig. SI8) shows various Teb adducts typical for Cu^{2+}-Teb systems (Jaklová Dytrtová et al., 2011; Jaklová Dytrtová, Jakl, Schröder, & Norková, 2013). Neither the Res cations, nor the Res radicals are observed in the positive mode spectrum. Fragmentation spectrum of $[Teb(Res\text{-}H)]^-$ (Fig. SI9) shows that the preferred degradation pathway goes via loss of the neutral Teb, with an appearance energy (*AE*) (Zins et al., 2010) of 121 kJ mol^{-1}. The calculated energy for $[Teb(Res\text{-}H)]^- \rightarrow Teb + (Res\text{-}H)^-$ fragmentation of 110 kJ mol^{-1} is in a nice agreement with the experiment. No changes of Res antioxidant properties promoted by Teb presence were observed under electrospray conditions in the gas phase; this is supported also by the antioxidant capacity determination in solution (see further).

To study the impact of Cu^{2+} on the Res-Teb system, the mixture of Res, Teb, and $CuCl_2$ was introduced into ESI-MS and measured in both the positive (Fig. 3) and the negative modes (Fig. SI10). The following species are present in the positive mode spectrum: the H^+ adducts of Res and Teb ($(HRes)^+$ and $(HTeb)^+$), Teb complexes of Cu^+, $[Cu(Teb)_{1,2}]^+$, described previously (Jaklová Dytrtová et al., 2011, 2013), and a ternary complex $[Cu(Res\text{-}H)(Teb)]^+$, which we studied in detail.

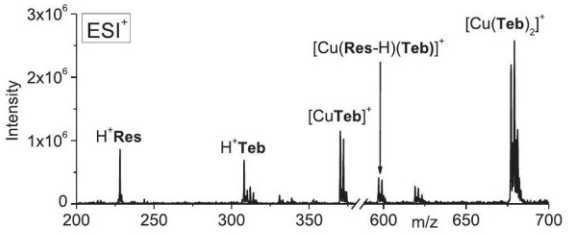


Fig. 3. Positive mode spectrum of equimolar mixture ($2.5 \cdot 10^{-5}$ mol L^{-1}) of resveratrol (Res), tebuconazole (Teb), and $CuCl_2$ in ethanol/methanol/water (1:1:2).

The $[Cu(Res\text{-}H)(Teb)]^+$ complex has an exact m/z = 597.15 and its favoured daughter ion is $[CuTeb]^+$ with the AE = 154 kJ mol^{-1} (Fig. SI11). The copper is present as Cu^{2+} in $[Cu(Res\text{-}H)(Teb)]^+$ and is stabilized by the negative charge (Jakl, Fanfrlík, & Jaklová Dytrtová, 2017) carried by $(Res\text{-}H)^-$. We assume that the electron from $(Res\text{-}H)^-$ "ligand" is transferred to Cu^{2+} during the fragmentation, leading to generation of $(Res\text{-}H)^{\bullet}$ via a Fenton-like reaction. The calculated energy for $[Cu(Res\text{-}H)(Teb)]^+ \rightarrow [Cu(Teb)]^+ + (Res\text{-}H)^{\bullet}$ fragmentation of 208 kJ mol^{-1} exceeds the experimental AE of 154 kJ mol^{-1} by about 30% (Jakl et al., 2014).

The calculated structures of $[Cu(Res\text{-}H)(Teb)]^+$ and $[Cu(Teb)]^+$ are compared in Fig. 4. In $[Cu(Teb)]^+$ the Cu^+ binds to Teb via: (i) the electron lone-pair of the OH group, $r_{Cu\text{-}O}$ = 2.162 Å, (ii) N2 of the triazole ring, $r_{Cu\text{-}N2}$ = 1.949 Å, and (iii) via the phenol ring in a cation-π interaction, the shortest $r_{Cu\text{-}C}$ = 2.023–2.193 Å.

In $[Cu(Res\text{-}H)(Teb)]^+$ the Res further binds to Cu^{2+} with $r_{Cu\text{-}O4'}$ = 1.864 Å. The bond to the Teb hydroxyl elongates from 2.162 Å in $[Cu(Teb)]^+$ to 2.237 Å in $[Cu(Res\text{-}H)(Teb)]^+$ due to the *trans* effect, while the Cu-N2 bond shortens from 1.949 to 1.885 Å. The interaction with the phenolic ring is lost in $[Cu(Res\text{-}H)(Teb)]^+$, the closest Cu-C contacts are 2.804 and 2.884 Å.

In the negative mode spectrum (Fig. SI11), no copper complex is observed. The spectrum shows deprotonated $(Res\text{-}H)^-$ and $(Teb\text{-}H)^-$, dimer $[Res(Res\text{-}H)]^-$, Teb, and Res adducts with Cl^-, such as $ResCl^-$ and $TebCl^-$, mixed $[Teb(Res\text{-}H)]^-$ dimer and its adduct with water $[Teb(Res\text{-}H)(H_2O)_2]^-$.

The electrochemical device coupled *online* with ESI-MS (EC/ESI-MS) (Jaklová Dytrtová et al., 2016) enables electrochemical activation (marking) of various substances via their reactions with metallic ions *in statu nascendi*, produced from the working electrode, therefore it is a welcome tool for *in situ* study of redox reactions. Its utilization allows to study subsequent reactions of Res/Teb adducts with oxidizing of the copper working electrode ($Cu^0 \rightarrow Cu^{1+} \rightarrow Cu^{2+}$). The sample was

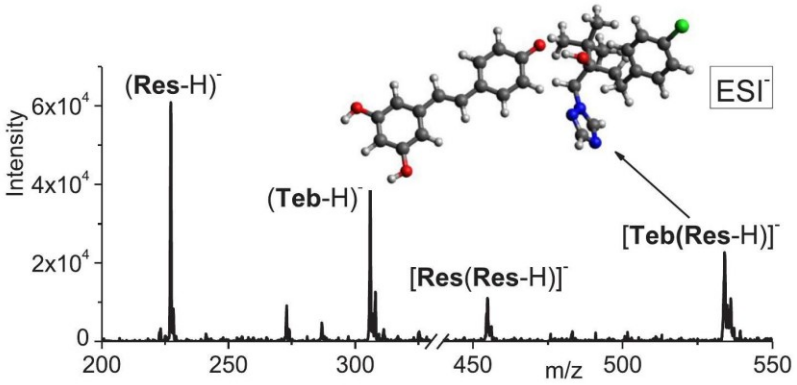


Fig. 2. Negative mode spectrum of equimolar ($5 \cdot 10^{-5}$ mol L^{-1}) mixture of resveratrol (Res) and tebuconazole (Teb) in ethanol/water (1:1).

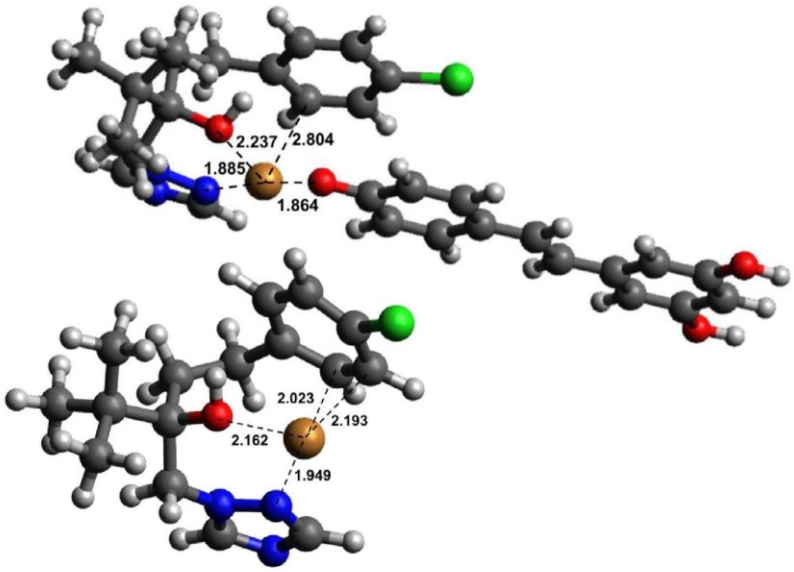


Fig. 4. B3LYP/6-311G* calculated structures of $[Cu(Res\text{-}H)(Teb)]^+$ (top) and $[Cu(Teb)]^+$ (bottom).

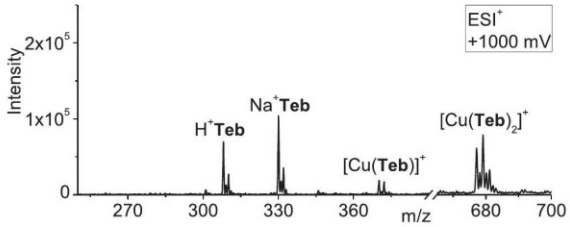


Fig. 5. Positive mode spectrum obtained by the EC-ESI-MS when inserting 1000 mV potential to the copper working electrode. The sample is an equimolar ($2.5 \cdot 10^{-5}$ mol L^{-1}) mixture of resveratrol (Res) and tebuconazole (Teb) in ethanol/methanol/25 mM NH_4Ac in H_2O (1:1:2).

created by mixing the equimolar amount of Teb and Res and subsequently introduced into EC (*online* coupled with ESI-MS). In this setup, Res interacts first with Teb and subsequently with Cu^{2+}. The reaction scheme is: Res + Teb → Res-Teb products → interaction with copper working electrode → Cu^q/Res/Teb (q = 1,2) products. The reaction products are shown in Fig. 5. In contrast to spectrum in Fig. 3 describing the products of reaction scheme Cu^{2+} + Res + Teb → $[CuTeb(Res\text{-}H)]^+$, no Cu/Res products are present here. The reactions of Res with Cu^{2+} are not allowed, as it is now bounded in $[Teb(Res\text{-}H)]^-$ complex, hence the Res binding sites for Cu^{2+} are largely blocked by Teb. Apparently, the $[CuTeb(Res\text{-}H)]^+$ complex forms only under conditions where Res, Teb, and Cu^{2+} are present simultaneously in the reaction mixture, see examples above.

The influence of Teb and Cu^{2+}/Cu^+ on Res was also characterized by the antioxidant capacity. FRAP method detects an antioxidant as an electron donor. The 7 days incubation of Res:Teb did not change the Res

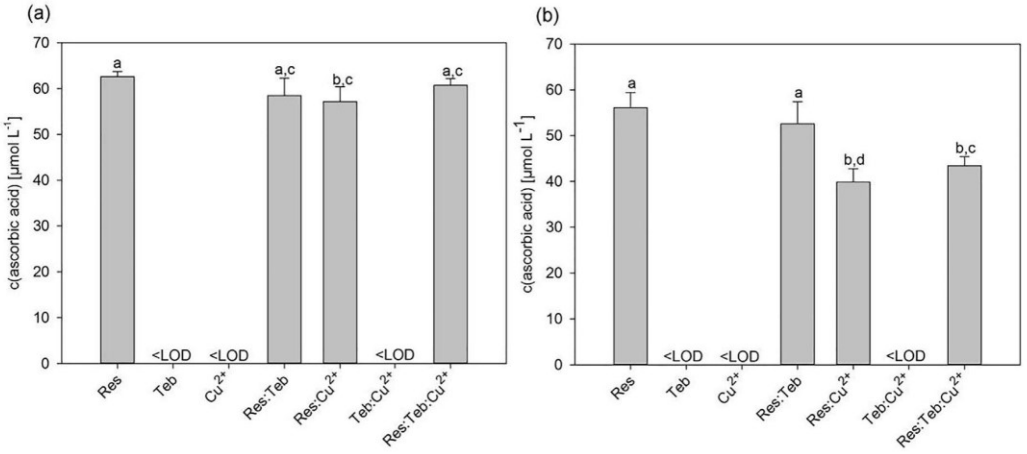


Fig. 6. Antioxidant capacity measured by FRAP method (a) immediately and (b) after 7 days incubation in the dark at 4 °C. The samples were prepared as equimolar mixtures of Res, Teb, and $CuCl_2$ (100 µmol L^{-1}). Values shown represent the mean ± SD (n = 4 replicates). Different letters next to each bar denote significant differences ($P \leq 0.05$) among the groups according to ANOVA. The same letters next to a bar indicate no statistically significant differences between the groups.

antioxidant capacity, while Res:Cu^{2+} significantly decreased its antioxidant capacity. Res:Teb:Cu^{2+} showed slightly higher antioxidant capacity than Res:Cu^{2+} (Fig. 6). The antioxidant capacity clearly depends on time. The protection of Res by Teb against Cu^{2+} was visible after longer incubation period. In FRAP method we worked in aqueous solution with Cu^{2+}, which probably described authentically the real situation in wine.

We also tested both Cu^{2+} and Cu^{+} by DPPH method, which recognizes an antioxidant as an H^{+} donor. Cu^{+} significantly decreased Res antioxidant capacity immediately after mixing. In acetonitrile Res:Teb showed significantly higher antioxidant capacity in comparison with Res. Res:Teb:Cu^{+} antioxidant capacity was slightly higher than Res:Cu^{+} after 7 days incubation. On the other hand, Cu^{2+} slightly increased Res antioxidant capacity (Fig. SI12). The H^{+} mechanism of DPPH method could be related to the different behaviour of Res in the presence of Cu^{2+}.

4. Conclusions

The simulated behaviour of antioxidant resveratrol in the presence of Cu^{2+} and fungicide tebuconazole as an example of simplified ternary system in wine was studied by electrospray ionization mass spectrometry. It was confirmed that resveratrol turns oxidative in the presence of Cu^{2+}. However, in the presence of tebuconazole, the Cu^{2+} cations preferentially bind to tebuconazole due to its high affinity for copper. Moreover, tebuconazole strongly binds to resveratrol, and thus effectively blocks the Cu-binding positions of resveratrol. Therefore, the presence of fungicide tebuconazole in wine has an unexpected two-fold protective effect for resveratrol antioxidant properties. The experimental data were supported by results of DFT calculations as well as by experimental results of determination of antioxidant capacity. The process is fast in the gas phase whereas it requires longer times in the liquid phase. The observed behaviour of the resveratrol should be taken into account with respect to the broader discussion of the effects of resveratrol in wine on our health.

Acknowledgements

This work was supported by the Czech Science Foundation, Czech Republic (18-01710S).

Appendix A. Supplementary data

Supplementary data associated with this article can be found, in the online version, at https://doi.org/10.1016/j.foodchem.2018.04.096.

References

Alister, C., Araya, M., Morande, J. E., Volosky, C., Saavedra, J., Cordova, A., & Kogan, M. (2014). Effects of wine grape cultivar, application conditions and the winemaking process on the dissipation of six pesticides. *Ciencia E Investigacion Agraria, 41*(3), 375–386.

Baur, J. A., Pearson, K. J., Price, N. L., Jamieson, H. A., Lerin, C., Kalra, A., ... Sinclair, D. A. (2006). Resveratrol improves health and survival of mice on a high-calorie diet. *Nature, 444*(7117), 337–342.

Becke, A. D. (1988). Density-functional exchange-energy approximation with correct asymptotic behavior. *Physical Review A, 38*(6), 3098–3100.

Bradamante, S., Barenghi, L., & Villa, A. (2004). Cardiovascular protective effects of resveratrol. *Cardiovascular Drug Reviews, 22*(3), 169–188.

Clark, A. C., Wilkes, E. N., & Scollary, G. R. (2015). Chemistry of copper in white wine: A review. *Australian Journal of Grape and Wine Research, 21*(3), 339–350.

Dudonné, S., Vitrac, X., Coutière, P., Woillez, M., & Mérillon, J. M. (2009). Comparative study of antioxidant properties and total phenolic content of 30 plant extracts of industrial interest using DPPH, ABTS, FRAP, SOD, and ORAC assays. *Journal of Agricultural and Food Chemistry, 57*(5), 1768–1774.

Frisch, M. J., Trucks, G. W., Schlegel, H. B., Scuseria, G. E., Robb, M. A., Cheeseman, J. R., ... Fox, D. J. (2009). *Gaussian 09, Revision A.1*. Wallingford CT: Gaussian, Inc.

Hadi, S. M., Ullah, M. F., Azmi, A. S., Ahmad, A., Shamim, U., Zubair, H., & Khan, H. Y. (2010). Resveratrol mobilizes endogenous copper in human peripheral lymphocytes leading to oxidative DNA breakage: A putative mechanism for chemoprevention of cancer. *Pharmaceutical Research, 27*(6), 979–988.

Jakl, M., Fanfrlík, J., & Jaklová Dytrtová, J. (2017). Mimicking of cyproconazole behavior in the Cu and Zn presence. *Rapid Communications in Mass Spectrometry, 31*(23), 2043–2050.

Jakl, M., Straka, M., Jaklová Dytrtová, J., & Roithová, J. (2014). Formation and stability of calcium complexes of dimethyl sulfoxide in water. *International Journal of Mass Spectrometry, 360*, 8–14.

Jaklová Dytrtová, J., Jakl, M., Navrátil, T., Cvačka, J., & Pačes, O. (2016). An electrochemical device generating metal ion adducts of organic compounds for electrospray mass spectrometry. *Electrochimica Acta, 211*, 787–793.

Jaklová Dytrtová, J., Jakl, M., Schröder, D., Čadková, E., & Komárek, M. (2011). Complexation between the fungicide tebuconazole and copper(II) probed by electrospray ionization mass spectrometry. *Rapid Communications in Mass Spectrometry, 25*, 1037–1042.

Jaklová Dytrtová, J., Jakl, M., Schröder, D., & Norková, R. (2013). In situ generation of copper cations and complexation with tebuconazole in a hyphenation of electrochemistry with mass spectrometry. *International Journal of Mass Spectrometry, 338*, 45–49.

Jang, M. S., Cai, E. N., Udeani, G. O., Slowing, K. V., Thomas, C. F., Beecher, C. W. W., ... Pezzuto, J. M. (1997). Cancer chemopreventive activity of resveratrol, a natural product derived from grapes. *Science, 275*(5297), 218–220.

Quideau, S., Deffieux, D., & Pouysegu, L. (2012). Resveratrol still has something to say about aging!. *Angewandte Chemie-International Edition, 51*(28), 6824–6826.

Smoliga, J. M., Baur, J. A., & Hausenblas, H. A. (2011). Resveratrol and health – A comprehensive review of human clinical trials. *Molecular Nutrition & Food Research, 55*(8), 1129–1141.

Stervbo, U., Vang, O., & Bonnesen, C. (2007). A review of the content of the putative chemopreventive phytoalexin resveratrol in red wine. *Food Chemistry, 101*(2), 449–457.

Takaya, Y., Terashima, K., Ito, J., He, Y. H., Tateoka, M., Yamaguchi, N., & Niwa, M. (2005). Biomimic transformation of resveratrol. *Tetrahedron, 61*(43), 10285–10290.

Tamboli, V., Defant, A., Mancini, I., & Tosi, P. (2011). A study of resveratrol-copper complexes by electrospray ionization mass spectrometry and density functional theory calculations. *Rapid Communications in Mass Spectrometry, 25*(4), 526–532.

Tamboli, V. F., Re, N., Coletti, C., Defant, A., Mancini, I., & Tosi, P. (2012). A joint experimental and theoretical investigation on the oxidative coupling of resveratrol induced by copper and iron ions. *International Journal of Mass Spectrometry, 319–320*, 55–63.

Tupec, M., Hýsková, V., Bělonožníková, K., Hraníček, J., Červený, V., & Ryšlavá, H. (2017). Characterization of some potential medicinal plants from Central Europe by their antioxidant capacity and the presence of metal elements. *Food Bioscience, 20*, 43–50.

Zins, E.-L., Pepe, C., & Schröder, D. (2010). Energy-dependent dissociation of benzylpyridinium ions in an ion-trap mass spectrometer. *Journal of Mass Spectrometry, 45*(11), 1253–1260.

3.3.3 Triazoles and aromatase: The impact of copper cocktails

The main use of triazoles lies in their antifungal properties (systemic fungicides) as they inhibit 14-α-demethylase (CYP51A - EC 1.14.14.154) responsible for ergosterol biosynthesis, subsequently resulting in destabilization of fungal plasma membrane. However, triazoles also inhibit aromatase (CYP19A1 - EC 1.14.14.14), a crucial enzyme for aromatization of androgens into estrogens. Although the depletion of estrogens is the principle of the use of azoles in the estrogen-dependent adenocarcinoma and breast cancer therapy; for healthy organisms triazoles represent potential endocrine disruptors (Egbuta et al 2014, Taxvig et al 2008).

In this project, we focused on three triazoles tebuconazole, penconazole, cyproconazole, their mutual interactions with or without the presence of copper ions and the impact on aromatase activity (Fig. 19).

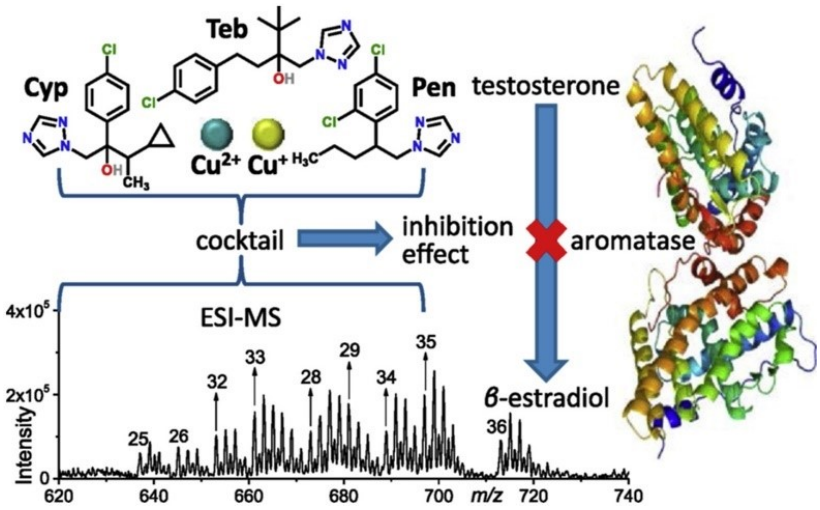


Fig. 19: Graphical abstract (Jaklová Dytrtová et al 2020).

It is generally assumed, that the effect of all triazoles is more or less similar. However, it is visible from our results (Table 1 in Jaklová Dytrtová et al 2020) that this statement is rather wrong. Penconazole showed the highest inhibition effect on aromatase activity (decrease to 41±5%) in comparison with the other two tested compounds (average to 75±3%). To understand possible group effects, e.g., inter-reaction among the triazoles, we prepared their mixtures. We calculated the hypothetical activity as a simple addition (i.e., average of experimental activities). For the triazoles mixtures, we detected no statistically significant differences between the hypothetical and experimental effects, i.e., no significant

(group) interactions. In accordance, we observed no adequate products in the mass spectra.

On the other hand, the addition of copper significantly shuffled the score. Suddenly, we could have estimated statistically significant cocktail effects of the triazole/copper mixtures from the hypothetical activity and the experimental activity. Additionally, the cocktail impact resulted in a greater decrease of the aromatase activity in contrast to the hypothetical expectation. Therefore, we assumed that the copper cations had caused some reactions yielding more effective triazole metabolites/products/adducts/complexes. The biggest cocktail effect decreasing the aromatase activity more than 40% (compared to hypothetical activity) was observed for the mixture of penconazole and Cu^{2+}. Also, other mixtures with penconazole showed significant cocktail effects (Table 1, Fig. 2 in Jaklová Dytrtová et al 2020). We also described previously that penconazole in the presence of Cu^{2+} is transformed to several metabolites (Kovač et al 2020). Potentially, these adducts are more effective in aromatase inhibition than single penconazole.

The most complex system tebuconazole-penconazole-cyproconazole-Cu^{2+} was carefully followed in the mass spectrometry analysis (Fig. 1, 2, 4, Table 2 in Jaklová Dytrtová et al 2020). The analysis of other mixtures can be found in the Supplement. We observed that the presence of copper ions is crucial for the formation of triazole metabolites. Namely, tebuconazole loses the *tert*-butyl group, cyproconazole loses the cyclopropyl group, and penconazole loses one chloride anion (Fig. 3 in Jaklová Dytrtová et al 2020). Additionally, in the presence of copper ions, triazoles deprotonated although being considered weak bases.

My contribution:

I measured the impact of triazoles and their various mixtures on the aromatase activity. I analyzed the data statistically and prepared the resulting tables. I helped to edit the manuscript.

Environmental Pollution 266 (2020) 115201

Contents lists available at ScienceDirect

Environmental Pollution

journal homepage: www.elsevier.com/locate/envpol

Triazoles and aromatase: The impact of copper cocktails☆

Jana Jaklová Dytrtová [a, b, *], Kateřina Bělonožníková [c], Michal Jakl [d], Helena Ryšlavá [c]

[a] Institute of Organic Chemistry and Biochemistry of the Czech Academy of Sciences, Flemingovo nám. 542/2, 166 10, Prague 6, Czech Republic
[b] Charles University, Faculty of Physical Education and Sport, Department of Physiology and Biochemistry, José Martího 269/31, 162 52, Prague 6, Czech Republic
[c] Charles University, Faculty of Science, Department of Biochemistry, Hlavova 2030, 128 43, Prague 2, Czech Republic
[d] Czech University of Life Sciences Prague, Faculty of Agrobiology, Food and Natural Resources, Department of Agro-Environmental Chemistry and Plant Nutrition, Kamýcká 129, 165 00, Prague – Suchdol, Czech Republic

ARTICLE INFO

Article history:
Received 3 March 2020
Received in revised form
30 June 2020
Accepted 5 July 2020
Available online 9 July 2020

Keywords:
Cocktail effect
Azoles
Cytochrome P450 monooxygenases
Fenton reaction

ABSTRACT

Triazoles are used as antifungal agents, they mostly inhibit two enzymes: 14α-demethylase and aromatase. These enzymes are utilised also in other species and therefore the affection in non-target species in the environment is expected as well. Besides, triazoles are often being applied in a mixture and they can also interact with other substances present. This study clarifies how three selected representative triazoles (tebuconazole, penconazole and cyproconazole) interact with each other (group effect) and in mixtures (cocktail effect) with copper, essential/toxic for all organisms. Within the experiments on electrospray and collision-induced dissociations (both ESI-MS), it has been found that the fragments correspond to typical triazole metabolites. For their formation, the presence of copper ions is crucial. The inhibitory effect of Cu cocktails on aromatase enzymatic activity has been studied. The presence of Cu ions together with triazole(s) significantly increases the inhibitory effect on aromatase activity. The highest inhibitory effect (more than 60%) on aromatase activity is produced by cocktails containing penconazole and Cu ions, namely by penconazole/Cu and penconazole/tebuconazole/Cu. The reactivity of triazoles in groups is not significantly affected by the interactions among them. Additionally, the role of triazoles in copper Fenton reaction regulation has been observed and described. These changes may be attributed to the formation and stabilization of the complexes with the central Cu ion, with usually one, two or three triazolic ligands, depending on the mixture. The study demonstrates that the interaction of triazoles and Cu ions is a complex process; their impact on metabolism seems to be rather extensive and must be evaluated in the context of biochemical reactions.

© 2020 Elsevier Ltd. All rights reserved.

1. Introduction

Triazoles (belonging to the group of azoles) are systemic fungicides frequently used to crop protection against yeast and mildew. In these target species, azoles inhibit the biosynthesis of steroids (Egbuta et al., 2014; Zarn et al., 2003) mainly by blocking fungal cytochrome P450 monooxygenase sterol 14α-demethylase (CYP51A1, EC 1.14.14.154). The inhibition of fungal CYP51 leads to the depletion of ergosterol, essential in fungal plasma membranes and thus the destabilization of the membrane (Alcazar-Fuoli et al., 2008). For humans, inhibition of CYP51 is not crucial because diet supplies cholesterol (an intermediate).

Many azoles also inhibit aromatase (CYP19A1, EC 1.14.14.14) (Conner et al., 2012). Cyp19 catalyses the conversion of androstenedione, testosterone or 16α-hydroxytestosterone to estrone, 17β-estradiol or 17β,16α-estriol, respectively (Conley et al., 2001; Trösken et al., 2004). The depletion of estrogens is the principle of the use of azoles in the antiestrogen therapy against estrogen-dependent adenocarcinoma and breast cancer cells (Egbuta et al., 2014; Lang et al., 1993).

Since most azoles are not completely specific, they are able to inhibit additional key cytochrome P450 enzymes, e.g. lanosterol-14-demethylase (CYP1) (Beijer et al., 2018), cholesterol side-chain

Abbreviations: Cyp, cyproconazole; Pen, penconazole; RFU, relative fluorescence units; Teb, tebuconazole; AE, appearance energy.

☆ This paper has been recommended for acceptance by Klaus Kümmerer.

* Corresponding author. Institute of Organic Chemistry and Biochemistry of the Czech Academy of Sciences, Flemingovo nám. 542/2, 166 10, Prague 6, Czech Republic.
E-mail addresses: dytrtova@uochb.cas.cz, dytrtova@ftvs.cuni.cz (J. Jaklová Dytrtová).

https://doi.org/10.1016/j.envpol.2020.115201
0269-7491/© 2020 Elsevier Ltd. All rights reserved.

cleavage (CYP11A) steroid 11β-hydroxylase (CYP11B and CYP11C1) and steroid 17α-hydroxylase/17,20 lyase (CYP17) responsible for transformation of steroid hormone (Chen and Ying, 2015).

These effects on highly conserved cytochrome P450 monooxygenases such as CYP51, are similar to those observed in mammals including human (Chen and Ying, 2015; Lepesheva et al., 2003). In healthy non-target organisms, azoles are consequently considered to be potential endocrine disruptors (Taxvig et al., 2008; Trösken et al., 2004; Zarn et al., 2003).

The individual influence of various azoles on the target enzymes has been well described. Because of the treatment strategies, the issue of the possible effect of (tri)azoles in a mixture (cocktail effect) on given enzymes is of great interest (Kjaerstad et al., 2010; Rieke et al., 2014; Seeger et al., 2019; Schmidt et al., 2016).

Triazoles as fungicides are widely used in agriculture, in the field from which they easily spread through the soil; and contaminate groundwater and even reach urban centres. Moreover, these compounds are also used in therapeutic and personal care products (shampoos, dermal creams, and soaps etc.) (Assress et al., 2020). Their removal rate in wastewater treatment plant is rather low. Azole fungicides are generally detected in surface water and sediment of the aquatic environment (Chen and Ying, 2015). In our previous studies it was found that the behaviour of the triazoles and their degradation pathways are also strongly influenced by their reactions with the ions of various elements present (Jaklová Dytrtová et al., 2014; Kovač et al., 2020).

Besides triazoles, especially copper compounds are also widely applied as fungicides for crops (Komárek et al., 2010; Vazquez-Blanco et al., 2020). There has been evidence that triazole fungicides can create complexes with copper ions and change their behaviour in the environment, i.e., their accumulation in soils, degradation, mobility, and stability (Arias et al., 2006; Jakl et al., 2017; Jakl and Jaklová Dytrtová, 2018; Jaklová Dytrtová et al., 2011). Copper as an ion coordinated in many enzymes plays an essential role in the biochemistry of all living organisms. On the other hand, its free ions in cells may be toxic *via* the catalysis of Fenton (Haber-Weiss) reactions forming reactive oxygen species and hydroxyl radicals. In addition to the oxidative damages, the presence of free Cu ions may lead to the direct impairment of redox-sensitive signalling and to functional changes of activator protein 1 (AP-1), a transcription factor regulating gene expression (Letelier et al., 2009). In the presence of copper ions, the activity of cytochrome P450 monooxygenases could be passivated by their oxidation, by copper ions binding to their amino acids and by other structural changes (Letelier et al., 2009).

This research has focused on three triazolic compounds: tebuconazole, penconazole and cyproconazole, which are often used in crop protection. Tebuconazole is even the world's most widely used triazolic fungicide (as a seed dressing and foliar spray against rusts, smuts, bunt, powdery mildew, leaf spots, and blights) with the potentially most harming impact on the environment (Li et al., 2019; Sharma et al., 2019). Only a few studies have been focused on penconazole, however its toxic effects were reported on various organisms, including mice and fish (Aksakal and Ciltas, 2018; Meng et al., 2020). Cyproconazole has been widely used in restraining and curing plant diseases and deeply studied since it was shown to have stereoselective toxicity against *Chlorella pyrenoidosa* and *Pelophylax nigromaculatus* (black-spotted frog) (He et al., 2019).

All of these compounds have a relatively similar structure (see the Graphical Abstract), which concerns not only the nitrogen heterocycle but also the chlorinated benzene ring on their aliphatic chains. On the contrary, they do not contain other halogens or epoxy chains, which could fundamentally change their reactivity. The main aim here is to bring the information on how the cocktails of these similar triazoles in their different (typically racemic) mixtures and with copper ions influence the activity of aromatase and thus to predict their environmental behaviour and impact.

2. Material and methods

2.1. Chemicals

Tebuconazole (**Teb**; 1-(4-chlorophenyl)-4,4-dimethyl-3-(1H-1,2,4-triazol-1-ylmethyl)pentan-3-ol), penconazole (**Pen**; 1-[2-(2,4-dichlorophenyl)pentyl]-1,2,4-triazole) and cyproconazole (**Cyp**; 2-(4-chlorophenyl)-3-cyclopropyl-1-(1H-1,2,4-triazol-1-yl) butan-2-ol) were of analytical grade purity (Pestanal®), and $CuCl_2$ of 99.999% (trace metal basis) purity. All of these chemicals were purchased from Sigma-Aldrich (Czech Republic). The solid standards were used for the preparation of stock solutions. The stock solutions of triazoles (10^{-2} mol/L) were prepared in acetonitrile (Sigma-Aldrich) for biochemical experiments or in ethanol (99.9%; VWR s.r.o.) and the stock solutions of metal salt ($CuCl_2$) were prepared in deionised water (18.2 MΩ purity, Milli-Q®, Millipore). All the stock solutions were stored in a freezer (−25 °C). A rigid number of heterocyclic rings in the mixtures was required. The overall problem was focused on equimolar mixtures of triazoles with unchanged total heterocycles concentration. This approximation allows to use average to estimate hypothetical values, which may serve as comparison for the experimental values.

2.2. Effect on human recombinant aromatase (CYP19A) studied in vitro

The effect of the test triazoles and Cu ions on aromatase activity was evaluated in the samples prepared with the equimolar concentration of triazoles (10^{-6} mol/L) with/without the presence of $CuCl_2$ equimolar to their sum (Table 1). The activity of aromatase was experimentally determined using a NADPH-generating system (based on glucose-6-phosphate dehydrogenase) and a fluorogenic substrate of two-fold K_m concentration, which after reduction turns into a highly fluorescent metabolite. For this purpose, the Aromatase (CYP19A) Inhibitor Screening Kit (Fluorometric) (BioVision, Milpitas, USA) was used. The stock solutions of triazoles were prepared in acetonitrile (Sigma-Aldrich) because it was shown to have the least impact on aromatase activity at the final concentration $\leq$ 1% according to the manufacturer. The aromatase substrate was also dissolved in acetonitrile according to the manual (0.12% in reaction). The presence of 10^{-6} mol/L triazole solution meant an only 0.01% increase in the total acetonitrile concentration in the reaction mixture. The increase of acetonitrile had no effect on aromatase activity (data not shown). The fluorescent metabolite was measured using a multi-well fluorescence microplate reader (Infinite M200 PRO, Tecan, Switzerland) in the kinetic mode at 488/527 nm (Ex/Em) according to the manufacturer's instructions (60 min, 37 °C) with the use of white 96-well plates with a flat bottom (Costar, Corning, USA).

The activity of aromatase was expressed in percentage, whereas the activity of 100% was related to the reference control sample containing no triazoles. The activities measured in single-component samples (consisting of 10^{-6} mol/L **Teb** or **Pen** or **Cyp** or $CuCl_2$) served for the estimation of the hypothetical activity (A_{hypot}) of aromatase in multicomponent samples. For instance, in the sample that consisted of an equimolar mixture of **Teb**/**Pen**/**Cyp** ($3.33 \cdot 10^{-7}$ mol/L each, triazoles together 10^{-6} mol/L), the hypothetical activity was calculated as the average of the experimental activities (A_{exp}) determine in the single-compound samples:

$$\mathbf{A}_{hypot} = \frac{A_{exp}(\mathbf{Teb}) + A_{exp}(\mathbf{Pen}) + A_{exp}(\mathbf{Cyp})}{3}$$

Table 1
Activity of aromatase in different reaction mixtures. The activity of the control sample was 1.3 ± 0.1 RFU/min/μg. The different letters above each reaction mixture denote significant differences ($P \leq 0.05$) between the groups according to one-way ANOVA. The same minuscule letters indicate no statistically significant differences. A_{exp} … experimental activity, A_{hypot} … hypothetical (calculated) activity, D … hypothetical decrease of aromatase activity. The significant difference between A_{exp} and A_{hypot} indicated by * was analysed by *t*-test ($P \leq 0.05$).

Reaction mixture	A_{exp} (%)	error	A_{hypot} (%)	error	A_{exp}-A_{hypot}	aromatase activity
Control (buffer)[a,f]	100.00	2.60				
Teb[b,g]	**77.30**	**10.10**				
Pen[c]	**41.00**	**5.30**				
Cyp[b,d]	**72.30**	**8.00**				
Teb-Pen-Cyp[b,d,e]	69.20	8.40	63.53	6.00	5.67	
Teb-Pen[c,d]	55.30	9.80	59.15	7.70	−3.85	
Teb-Cyp[a,b]	81.20	5.00	74.80	9.05	6.40	
Pen-Cyp[c,e]	50.10	8.00	56.65	6.65	−6.55	
Cu^{2+}, [f]	118.50	2.90				
Teb-Cu^{2+}, [b,d]	72.10	3.20	97.90*	10.10	−25.80	D
Pen-Cu^{2+},[c]	**39.10**	**2.60**	**79.75***	**5.30**	**−40.65**	**D**
Cyp-Cu^{2+},[b,d,e]	70.10	3.90	95.40*	8.00	−25.30	D
Teb-Pen-Cyp-Cu^{2+},[c,d,g]	**58.80**	**9.50**	**93.85***	**6.00**	**−35.05**	**D**
Teb-Pen-Cu^{2+},[c]	**48.20**	**1.50**	**88.83***	**7.70**	**−40.63**	**D**
Teb-Cyp-Cu^{2+},[a,b]	79.80	5.50	96.65	9.05	−16.85	
Pen-Cyp-Cu^{2+},[c]	**47.80**	**6.40**	**87.58***	**6.65**	**−39.78**	**D**

The A_{hypot} for the mixture containing an equimolar mixture of **Teb**/**Pen**/**Cyp** ($3.33 \cdot 10^{-7}$ mol/L each, triazoles together 10^{-6} mol/L) and 10^{-6} mol/L of $CuCl_2$ is expressed as:

$$\mathbf{A}_{hypot} = \left(\frac{A_{exp}(\mathbf{Teb}) + A_{exp}(\mathbf{Pen}) + A_{exp}\mathbf{Cyp}}{3} + \mathbf{A}_{exp}(Cu) \right) \Big/ 2$$

The determinations were performed in three replicates, each together with a reference control sample (without azoles and metals). The data were analysed by One Way ANOVA (Tukey method, Sigmaplot 12.5, Systat Software, Inc.); the differences were considered statistically significant at $P \leq 0.05$.

2.3. Creation of metal/triazole adducts studied using ESI-MS

The experiments were performed using a quadrupole ion-trap mass spectrometer (Finnigan LCQ Advantage, ThermoFinnigan, USA) in the positive mode. The samples were prepared from the stock solutions of triazoles and metals (10^{-2} mol/L) in a manner similar to that used in the preparation of the samples from biochemical experiments (to keep the same proportion of mixing – see Table 1). In contrast, the total concentration of azoles (as well as metals) in the samples was 50 times higher because of the sensitivity of the instrument. For example, the sample **Teb**-**Pen**-**Cyp**-Cu^{2+} (in Table 1) contained $5 \cdot 10^{-5}$ mol/L of $CuCl_2$ and $1.67 \cdot 10^{-5}$ mol/L of each triazole (**Teb**, **Pen** and **Cyp**). The sample solutions were continuously fed into the ion source at 0.5 mL/h through a silica capillary. Nitrogen was used as the nebuliser gas and sweep/auxiliary gas (8–15 arbit. units) and helium as the collision gas. The other conditions of the ion source were set as follows: spray voltage: 4.50 kV, capillary temperature: 200 °C, capillary voltage 20 V, tube lens offset 15 V.

Collision-induced dissociation (CID) experiments were used for the study of the dissociation of metal-triazole complexes. The methodology was based on the dissociation of benzylpyridinium ions (Zins et al., 2010). The mass spectra of mass-selected ions were measured as fragmentation thresholds in percentages of normalised collision energy (%NCE), optimised by the manufacturer in the range of 0–100%, and corresponded to a resonance-excitation alternating-current signal of 0–2.5 V (zero-to-peak) (Zins et al., 2010). Normalised collision energies were converted into kilojoules per mole *via* phenomenological conversion; phenomenological appearance energies (*AEs*) are in correlation with the NCE framework (Révész et al., 2010). The phenomenological conversion factor (which is an individual parameter depending on the instrument) was experimentally determined as follows: E_{coll} (kJ/mol) = (7.3 ± 0.3) · E_{coll} (%).

3. Results and discussion

Each individually assessed triazole significantly reduced the aromatase activity (Table 1), in the case of penconazole even to 41%. Their combinations had a similar effect as was expected from hypothetical calculations. On the other hand, the addition of Cu^{2+} to the triazole mixtures decreased the aromatase activity in contrast to the hypothetical expectations. It is generally assumed that the effect of all triazoles is more or less similar. However, it is visible from our results (Table 1) that this assumption is completely wrong.

In the first three lines of Table 1, showing the activities of aromatase in the presence of **Teb**, **Pen** and **Cyp** (as singles), it is visible that the biggest inhibitory effect on aromatase is produced by **Pen**, followed by **Cyp** and **Teb**.

To understand the possible **group effect** (which can be attributed e.g. to some inter-reactions) of these three triazoles, we prepared their mixtures. The hypothetical activity of aromatase is estimated as a simple addition. The difference from this hypothetical (additive) activity can be ascribed to the group effect. It arises from the lines 4–7 of Table 1, that this group effect is small (on the level of error) and not statistically significant. This result means that there are no significant reactions or interactions among these three triazoles. This fact can also be supported by the absence of those products in the mass spectra (Fig. SI1-3).

If we switch to a potentially more reactive system – triazoles with copper cations, we can estimate the **cocktail effect** of those triazole/copper mixtures from the hypothetical activity (assumed as a simple addition) and the experimental activity. From the last part of Table 1, it is visible that the difference between the experimental and hypothetical activity is bigger than the error and therefore statistically significant ($P \leq 0.05$). Additionally, the cocktail effect of copper/triazole mixtures reduces the aromatase activity in contrast to hypothetical expectation.

The biggest cocktail effect, decreasing the aromatase activity by more than 40% (in comparison with hypothetical expectations), has been observed for the mixtures of **Pen** and Cu^{2+}, **Teb**/**Pen** and Cu^{2+}, and **Cyp**/**Pen** and Cu^{2+}. All of these mixtures contain **Pen**. **Pen** in the presence of Cu^{2+} is transformed into several metabolites (Kovač

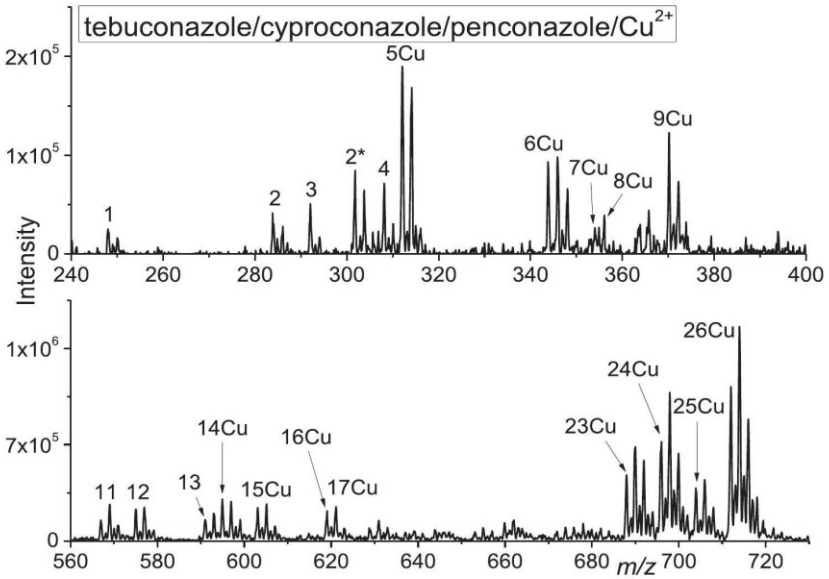


Fig. 1. Full MS spectrum of the mixture of $CuCl_2$ ($5 \cdot 10^{-5}$ mol/L), tebuconazole ($1.67 \cdot 10^{-5}$ mol/L), cyproconazole ($1.67 \cdot 10^{-5}$ mol/L) and penconazole ($1.67 \cdot 10^{-5}$ mol/L) in the ESI positive mode. The cations are listed in Table 2.

et al., 2020). These adducts are potentially more effective in aromatase inhibition than single penconazole.

It is evident that the interactions of triazoles with copper ions influence their effect on aromatase. It is essential to know which reaction products are formed. For this purpose, it is useful to use the gas phase approach to study the variety of possible reactions or complexes using ESI-MS. The data obtained must, of course, be thoroughly evaluated, because the experiments in the gas phase do not always give the same picture that is provided in the liquid phase (Agrawal and Schröder, 2011; Schröder, 2004).

According to our previous results (Jakl et al., 2017; Jaklová Dytrtová et al., 2014), the reactivity of triazoles in the presence of some metals might be modified *via* the creation of complexes or at least of metabolites. Our previous studies (Jakl et al., 2017; Jaklová Dytrtová et al., 2014; Jaklová Dytrtová et al., 2018; Norková et al., 2012) have also shown that triazoles (**Cyp** and **Teb**) bind to

Table 2
List of all the cations present in the full spectra (Fig. 1) of $CuCl_2$ ($5 \cdot 10^{-5}$ mol/L), tebuconazole (**Teb**, $1.67 \cdot 10^{-5}$ mol/L), cyproconazole (**Cyp**, $1.67 \cdot 10^{-5}$ mol/L) and penconazole (**Pen**, $1.67 \cdot 10^{-5}$ mol/L).

no.	m/z	formula	absolute intensity	relative intensity (%)	*AE* (kJ/mol)
1	248.10	$(Pen\text{-}Cl)^+$	3.64E+04	0.74	216
2	284.07	$(HPen)^+$	3.21E+04	0.66	190
3	292.12	$(HCyp)^+$	8.20E+04	1.68	189
2*	302.08	$(HPen)^+(H_2O)$	8.40E+04	1.72	156
4	308.15	$(HTeb)^+$	7.09E+04	1.45	174
5Cu	**312.00**	**$[Cu(Teb^*)]^+$/$[Cu(Cyp^*)]^+$/$[Cu(HPen\text{-}Cl)]^+$**	**2.11E+05**	4.31	219
6Cu	345.99	$[Cu(Pen)]^+$	8.83E+04	1.80	164
7Cu	353.04	$[Cu(Cyp\text{-}H)]^+$	1.86E+04	0.38	12
8Cu	354.04	$[Cu(Cyp)]^+$	2.86E+04	0.58	168
9Cu	370.08	$[Cu(Teb)]^+$	8.52E+04	1.74	224
10Cu	405.04	$[Cu(Teb)Cl]^+$	2.81E+04	0.57	138
11	**567.14**	**$[H(Pen)_2]^+$**	**1.65E+05**	3.37	208
12	**575.19**	**$[H(Pen)(Cyp)]^+$**	**2.23E+05**	4.56	183
13	**591.22**	**$[H(Teb)(Pen)]^+$**	**1.71E+05**	3.49	157
14Cu	595.10	$[Cu(HPen\text{-}Cl)(Pen\text{-}H)]^+$	2.07E+05	4.23	188
15Cu	603.15	$[Cu(HPen\text{-}Cl)(Cyp\text{-}H)]^+$	2.47E+05	5.05	175
16Cu	**629.06**	**$[Cu(Pen)_2]^+$**	**1.07E+05**	2.19	197
17Cu	637.11	$[Cu(Pen)(Cyp)]^+$	6.84E+04	1.40	178
18Cu	644.16	$[Cu(Cyp)(Cyp\text{-}H)]^+$	8.40E+04	1.72	12
19Cu	645.16	$[Cu(Cyp)_2]^+$	8.40E+04	1.72	188
20Cu	653.16	$[Cu(Teb)(Pen)]^+$	4.87E+04	1.00	165
21Cu	**660.19**	**$[Cu(Teb)(Cyp\text{-}H)]^+$**	**1.35E+05**	2.76	201
22Cu	661.19	$[Cu(Teb)(Cyp)]^+$	8.65E+04	1.77	158
23Cu	**688.11**	**$[Cu(Teb)(Pen)Cl]^+$**	**4.16E+05**	8.50	187
24Cu	**696.16**	**$[Cu(Teb)(Cyp)Cl]^+$**	**7.27E+05**	14.86	195
25Cu	704.00	$[Cu(Pen)_2(C_3H_5)]^+$	3.84E+05	7.85	203
26Cu	**712.19**	**$[Cu(Teb)_2Cl]^+$**	**9.74E+05**	19.91	137

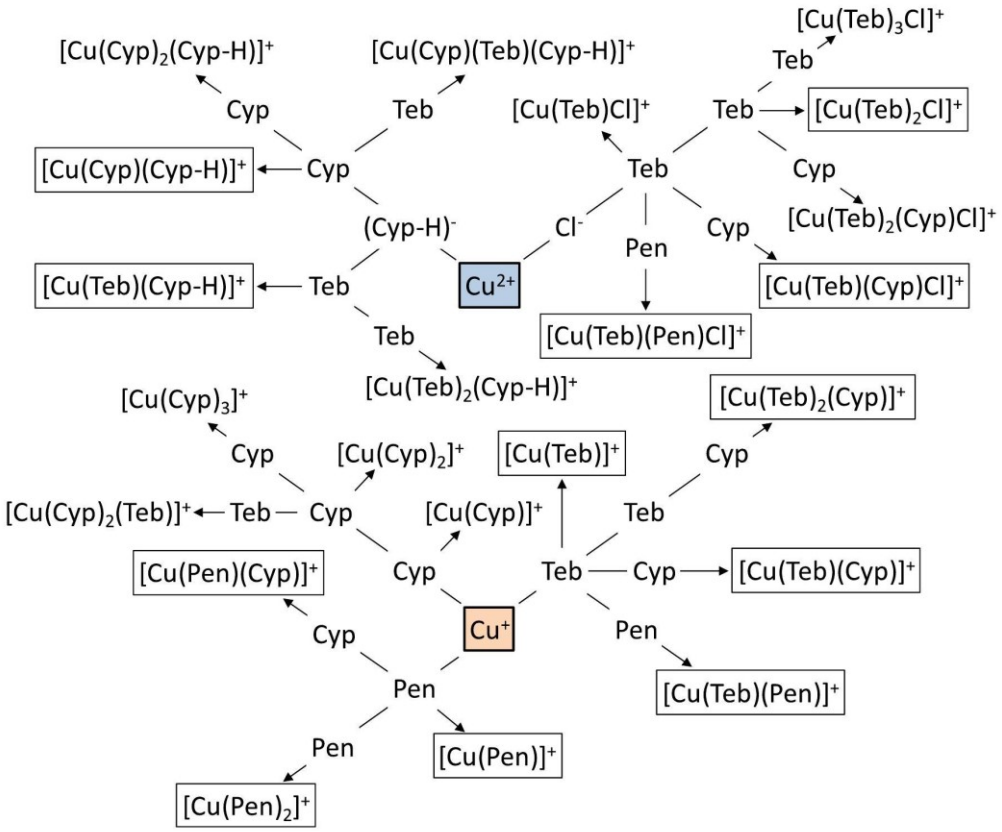


Fig. 2. Generative system of Cu^{2+} and Cu^{+} complexes with penconazole (**Pen**), cyproconazole (**Cyp**), tebuconazole (**Teb**).

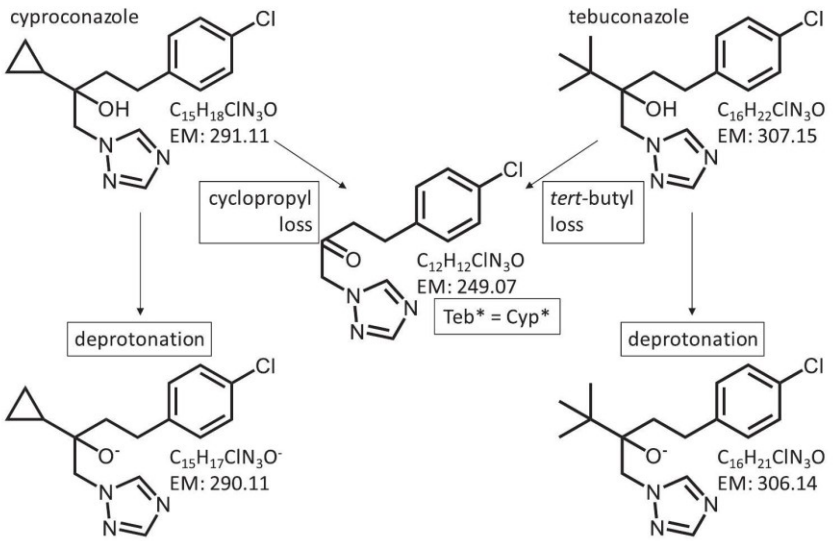


Fig. 3. Metabolites/degradation products in the presence of Cu coming from cyproconazole (**Cyp**) and tebuconazole (**Teb**) through deprotonation or the loss of *tert*-butyl or cyclopropyl moiety (**Cyp***, **Teb***).

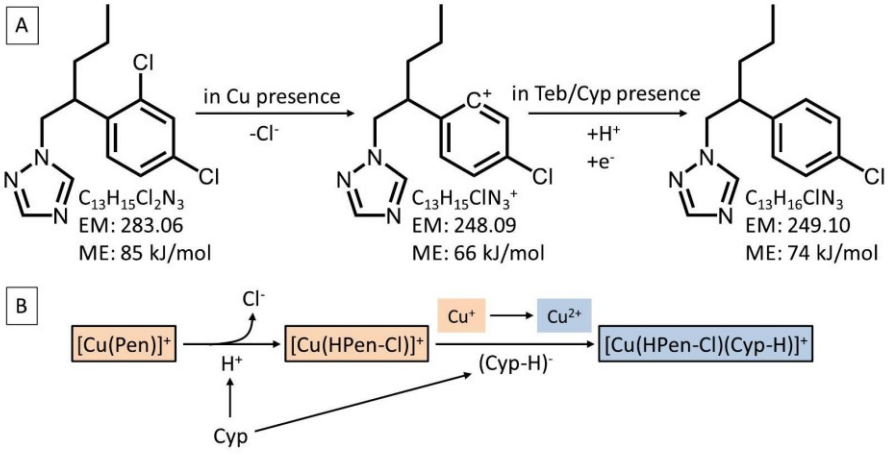


Fig. 4. A. Transformation of penconazole in the presence of Cu^{2+} and tebuconazole (**Teb**) or cyproconazole (**Cyp**). *EM* is exact mass and *ME* is the minimum energy calculated using molecular dynamics (Chem3D Pro 19.0, PerkinElmer Informatics). B. Transformation of the penconazole (**Pen**) complex with copper in the presence of **Cyp**.

dications *via* the 4N of the triazole ring, *via* the π-electrons of the chlorophenyl ring and *via* the oxygen atom of the OH group. The creation of this type of bonds also explains the deprotonation of **Cyp** (Jakl et al., 2017) and **Pen** (Kovač et al., 2020).

The strong tendency to create stable complexes with dications can be taken to advantage in triazoles analysis in environmental matrixes (Jaklová Dytrtová et al., 2016; Jaklová Dytrtová et al., 2013). On the other hand, we have taken into account that this tendency significantly influences the reactivity of triazoles (Jaklová Dytrtová et al., 2018).

The experimental aromatase activity in cocktails (copper ions and triazoles together) was at least 16% lower than hypothetically expected. The highest aromatase decrease effect occurred in the cocktails containing **Pen** (more than 35%). The system consisting of Cu^{2+} and **Pen** was described in detail in Kovač et al. (2020). The most important information on this system here is the creation of **Pen** metabolites. The presence of copper ions induces the loss of one chlorine from **Pen** to create (**Pen**-Cl)$^+$ with *m/z* 248$^+$, and the loss of two hydrogens, which could be explained by the creation of a double bond or an additional ring (Kovač et al., 2020; Schwack and Hartmann, 1994).

The most complex system is **Teb**/**Pen**/**Cyp**/Cu^{2+}, which contains all the possible adducts, complexes as well as degradation products (Fig. 1). Other spectra of each particular systems are shown in the supplementary material.

The spectrum received from the **Teb**/**Pen**/**Cyp**/Cu^{2+} system (Fig. 1) mostly contains Cu^+ complexes. The most abundant as well as the most stable (based on *AE*s values) are [Cu(**Teb**)$_2$Cl]$^+$, [Cu(**Teb**)(**Pen**)(H_2O)Cl]$^+$, [Cu(**Teb**)(**Pen**)Cl]$^+$, [Cu(**Pen**)(**Pen**-Cl)]$^+$, [Cu(**Teb***)]$^+$ and [Cu(**Teb**)(**Teb***)]$^+$. Selected CID spectra of these mass-selected ions together with their *AE*s are shown in the supplementary material (Fig. SI5). The complete image of the Cu^{2+}/Cu^+, **Teb**, **Pen** and **Cyp** complexes/adducts listed in Table 2 is depicted in Fig. 2.

The most important complexes created from copper cations with **Teb**, **Cyp** and **Pen** are summarised in Fig. 2. Copper is present in the complexes as Cu^{2+}, where the negative charge coming from Cl^- or deprotonated **Cyp** or **Teb** (Fig. 3) has a stabilizing effect on the higher oxidation state of copper. Some part of the Cu^{2+} state has also been reduced in the electrospray to Cu^+. The preservation of the Cu^{2+} requires the stabilizing impact of a negatively-charged counter-ion or at least four neutral ligands (Jaklová Dytrtová et al., 2011; Tintaru et al., 2009).

Fig. 2 shows the genealogy of the generation of complexes. It is not a reaction scheme, only an explanation of which $Cu^{2+/+}$ complexes are created. Theoretically, all the statistical combinations are possible, but some of the complexes are preferred more than others. These preferences might be explained by high *AE*s of those complexes as well as by their abundance in the spectra (Table 2).

In the presence of Cu^{2+} several types of **Cyp**, **Teb** (Fig. 3) and **Pen** degradation products are created. Namely: (i) **Pen** loses its chlorine atom (details in (Kovač et al., 2020)), (ii) **Teb** loses its *tert*-butyl group (also observed in (Jakl et al., 2017; Jaklová Dytrtová et al., 2013)) (Fig. 3), and **Cyp** loses its isopropyl group (Jakl et al., 2017) (Fig. 3) to receive the same metabolite as from **Teb**.

For the **Teb**/**Pen**/Cu^{2+} cocktail the experimental aromatase activity was almost about 41% lower than expected. The mass spectrum in the positive-ion mode is depicted in Fig. SI1. It shows the same complexes, as those that can be seen in the spectrum received from the system consisting of **Teb**/**Pen**/**Cyp**/Cu^{2+} (Fig. 1). Of course, the complexes/adducts containing **Cyp** are not present. However, the spectrum of **Teb**/**Pen**/Cu^{2+} (Fig. SI1) contains three complexes [Cu(**Teb**)(**Teb***)]$^+$, [Cu(**Teb**)(**Teb**-H)]$^+$, and [Cu(**Teb**)$_2$]$^+$ that are not present in the **Teb**/**Pen**/**Cyp**/Cu^{2+} mixture (Fig. 1). These complexes contain $Cu^{2+/+}$ and **Teb** only and their abundance in the spectrum (Fig. SI1) is not high. Only [Cu(**Teb**)(**Teb***)]$^+$ appears in a relatively high amount (4.04% of the total signal of all the complexes). These complexes are not abundant in the **Teb**/**Pen**/**Cyp**/Cu^{2+} mixture (Fig. 1) probably because of their thermodynamic competition with more stable complexes.

The spectrum of the **Pen**/**Cyp**/Cu^{2+} system (Fig. SI2) contains the expected complexes/adducts, which are present also in **Teb**/**Pen**/**Cyp**/Cu^{2+} (Fig. 1). The system of **Teb**/**Cyp**/Cu^{2+} is shown in Fig. SI4.

A detailed comparison of the spectra of different cocktails with Cu has revealed interesting facts. First of all, the signal with *m/z* 312.00 is attributable to two cations, [Cu(**Teb***)]$^+$ and [Cu(**Cyp***)]$^+$, because **Cyp*** and **Teb*** are the same fragments ($C_{12}H_{12}ClN_3O$, Fig. 3). Additionally, there is [Cu(H**Pen**-Cl)]$^+$, where H**Pen**-Cl is a neutral fragment transformed from the (**Pen**-Cl)$^+$ ion created in Cu ions presence (Kovač et al., 2020) by **Teb** or **Cyp** (Fig. 4). It means the catalysis of Cl^- cleavage by Cu^{2+} leads to $C_{13}H_{15}ClN_3^+$ formation, which is relatively unstable, and in the presence of H^+, it is

transformed into neutral $C_{13}H_{16}ClN_3$. The 3D structures of Pen metabolites are depicted in Fig. SI6. In this case, the source of H^+ is **Teb** or **Cyp**; in liquids, however, it can be something more willing to release a proton (e.g. H_2O). Triazoles are considered to be weak bases with pK_a around 1.5 (Konášová et al., 2015).

The completion of this redox reaction requires an electron. There is only one candidate to give electrons (be oxidised) – it is Cu^+. Cu^+ is easily created from Cu^{2+} in electrospray in the presence of **Teb** (Jaklová Dytrtová et al., 2011) as well as **Cyp** (Jakl et al., 2017). This one-electron reduction of copper ion under electrospray conditions is explained in detail in (Agrawal and Schröder, 2011; Schröder, 2004). The first step of the **Pen**/Cu reaction is just a simple decay (the loss of Cl^-). In the second step, $(Pen\text{-}Cl)^+$ gains one H^+, after which it gains an e^- from Cu^+. This redox reaction is also confirmed in the spectra (Figs. 1 and 4A), where all the participants of the redox reaction are present. The $Cu^{2+/+}$ system is considered to be a radical induction system (Jaklová Dytrtová et al., 2018), known as a Fenton reaction. In real environmental systems, where the cocktail of the present chemicals is richer and more complicated than our triazolic cocktails, the risk of the generation of free radicals is more reasonable. Additionally, the presence of triazoles in the system has the quenching effect on the $Cu^{2+/+}$ system (Jaklová Dytrtová et al., 2018).

We have demonstrated that the interaction of triazoles and metals is a complex process and its impact on metabolism seems to be rather extensive and must be evaluated in the context of biochemical reactions *in vivo*.

4. Conclusion

The group effects did not differ significantly from the calculated average of the effects of every particular triazoles in a mixture. This means that the reactivity of triazoles in groups is not significantly affected by interactions among them. On the other hand, the presence of copper together with triazole(s) (cocktail effect) considerably increases the inhibitory effect to aromatase activity. The highest inhibitory effect (greater than 60%) has been observed in the mixtures containing penconazole with Cu. The presence of copper in ionic forms is crucial for the formation of triazole metabolites. Namely, tebuconazole loses the *tert*-butyl group, cyproconazole loses the cyclopropyl group, and penconazole loses one chloride anion. Additionally, although the triazoles are considered to be weak bases, in the presence of Cu ions they deprotonate.

Under electrospray conditions in the presence of triazoles, Cu^{2+} is reduced to Cu^+. Cu^+ is known to initiate the Fenton reaction, which leads to radical production. However, in the presence of triazoles (mostly penconazole) Cu^+ is oxidised back to Cu^{2+}. Therefore, triazoles can be considered as possible quenchers of this copper Fenton reaction.

Evidently, the situation is really complicated even in the case of several possibly reactive members (e.g. Cu^{2+}, penconazole and cyproconazole). Further, it is essential to predict the real impact of an applied treatment and to include all possibly important parts of the system.

Funding

J.J.D. thanks to the Grantová agentura České republiky (project no. 18-01710S) for the financial support.

CRediT authorship contribution statement

Jana Jaklová Dytrtová: Conceptualization, Methodology, Investigation, Formal analysis, Writing - original draft, Funding acquisition. **Kateřina Bělonožníková:** Investigation, Formal analysis, Writing - original draft. **Michal Jakl:** Investigation, Formal analysis, Writing - original draft. **Helena Ryšlavá:** Conceptualization, Methodology, Writing - original draft.

Declaration of competing interest

The authors declare that there are no competing interests associated with the manuscript.

Appendix A. Supplementary data

Supplementary data to this article can be found online at https://doi.org/10.1016/j.envpol.2020.115201.

References

Agrawal, D., Schröder, D., 2011. Insight into solution chemistry from gas-phase experiments. Organometallics 30, 32–35.
Aksakal, F.I., Ciltas, A., 2018. Developmental toxicity of penconazole in Zebrfish (*Danio rerio*) embryos. Chemosphere 200, 8–15.
Alcazar-Fuoli, L., Mellado, E., Garcia-Effron, G., Lopez, J.R., Grimalt, J.O., Cuenca-Estrella, J.M., Rodriguez-Tudela, J.L., 2008. Ergosterol biosynthesis pathway in *Aspergillus fumigatus*. Steroids 73, 339–347.
Arias, M., Paradelo, M., López, E., Simal-Gándara, J., 2006. Influence of pH and soil copper on adsorption of metalaxyl and penconazole by the surface layer of vineyard soils. J. Agric. Food Chem. 54, 8155–8162.
Assress, H.A., Nyoni, H., Mamba, B.B., Msagati, T.A.M., 2020. Occurrence and risk assessment of azole antifungal drugs in water and wastewater. Ecotoxicol. Environ. Saf. 187. Unsp. 109868.
Beijer, K., Jonsson, M., Shaik, S., Behrens, D., Brunström, B., Brandt, I., 2018. Azoles additively inhibit cytochrome P450 1 (EROD) and 19 (aromatase) in rainbow trout (*Oncorhynchus mykiss*). Aquat. Toxicol. 198, 73–81.
Chen, Z.F., Ying, G.G., 2015. Occurrence, fate and ecological risk of five typical azole fungicides as therapeutic and personal care products in the environment: a review. Environ. Int. 84, 142–153.
Conley, A., Mapes, S., Corbin, C.J., Greger, D., Walters, K., Trant, J., Graham, S., 2001. A comparative approach to structure-function studies of mammalian aromatases. J. Steroid Biochem. Mol. Biol. 79, 289–297.
Conner, K.P., Vennam, P., Woods, C.M., Krzyaniak, M.D., Bowman, M.K., Atkins, W.M., 2012. 1,2,3-triazole-heme interactions in cytochrome P450: functionally competent triazole-water-heme complexes. Biochemistry 51, 6441–6457.
Egbuta, C., Lo, J., Ghosh, D., 2014. Mechanism of inhibition of estrogen biosynthesis by azole fungicides. Endocrinology 155, 4622–4628.
He, R.J., Mai, B.L., Fan, J., Jiang, Y., Chen, G., Guo, D., Chen, G.D., Yao, X.S., Gao, H., Zhang, W.G., 2019. Identification, quantification, and stereoselective degradation of triazole fungicide cyproconazole in two matrixes through chiral liquid chromatography-tandem mass spectrometry. J. Agric. Food Chem. 67, 10782–10790.
Jakl, M., Jaklová Dytrtová, J., 2018. Penconazole and its behavior in the presence of copper. In: Navrátil, T., Fojta, M., Schwarzová, K. (Eds.), Modern Electrochemical Methods XXXVIII. Lenka Srsenova-Best Servis, Ústí nad Labem, pp. 105–108.
Jakl, M., Fanfrlík, J., Jaklová Dytrtová, J., 2017. Mimicking of cyproconazole behavior in the presence of Cu and Zn. Rapid Commun. Mass Spectrom. 31, 2043–2050.
Jaklová Dytrtová, J., Jakl, M., Schröder, D., Čadková, E., Komárek, M., 2011. Complexation between the fungicide tebuconazole and copper(II) probed by electrospray ionization mass spectrometry. Rapid Commun. Mass Spectrom. 25, 1037–1042.
Jaklová Dytrtová, J., Jakl, M., Schröder, D., Norková, R., 2013. *In situ* generation of copper cations and complexation with tebuconazole in a hyphenation of electrochemistry with mass spectrometry. Int. J. Mass Spectrom. 338, 45–49.
Jaklová Dytrtová, J., Fanfrlík, J., Norková, R., Jakl, M., Hobza, P., 2014. Theoretical insight into the stabilization of triazole fungicides via their interactions with dications. Int. J. Mass Spectrom. 359, 38–43.
Jaklová Dytrtová, J., Jakl, M., Navrátil, T., Cvačka, J., Pačes, O., 2016. An electrochemical device generating metal ion adducts of organic compounds for electrospray mass spectrometry. Electrochim. Acta 211, 787–793.
Jaklová Dytrtová, J., Straka, M., Bělonožníková, K., Jakl, M., Ryšlavá, H., 2018. Does resveratrol retain its antioxidative properties in wine? Redox behaviour of resveratrol in the presence of Cu(II) and tebuconazole. Food Chem. 262, 221–225.
Kjaerstad, M.B., Taxvig, C., Andersen, H.R., Nellemann, C., 2010. Mixture effects of endocrine disrupting compounds *in vitro*. Int. J. Androl. 33, 425–433.
Komárek, M., Čadková, E., Chrastný, V., Bordas, F., Bollinger, J.-C., 2010. Contamination of vineyard soils with fungicides: a review of environmental and toxicological aspects. Environ. Int. 36, 138–151.
Konášová, R., Jaklová Dytrtová, J., Kašička, V., 2015. Determination of acid dissociation constants of triazole fungicides by pressure assisted capillary electrophoresis. J. Chromatogr. A 1408, 243–249.
Kovač, I., Jakl, M., Fanfrlík, J., Andrushchenko, V., Jaklová Dytrtová, J., 2020. Complexation and stability of the fungicide penconazole in the presence of zinc

and copper ions. Rapid Commun. Mass Spectrom. 34, e8714.
Lang, M., Batzl, C., Furet, P., Bowman, R., Hausler, A., Bhatnagar, A.S., 1993. Structure-activity relationships and binding model of novel aromatase inhibitors. J. Steroid Biochem. Mol. Biol. 44, 421–428.
Lepesheva, G.I., Virus, C., Waterman, M.R., 2003. Conservation in the CYP51 family. Role of the B' helix/BC loop and helices F and G in enzymatic function. Biochemistry 42, 9091–9101.
Letelier, M.E., Faundez, M., Jara-Sandoval, J., Molina-Berrios, A., Cortes-Troncoso, J., Aracena-Parks, R., Marin-Catalan, R., 2009. Mechanisms underlying the inhibition of the cytochrome P450 system by copper ions. J. Appl. Toxicol. 29, 695–702.
Li, S.Y., Sun, Q.Q., Wu, Q., Gui, W.J., Zhu, G.N., Schlenk, D., 2019. Endocrine disrupting effects of tebuconazole on different life stages of zebrafish (*Danio rerio*). Environ. Pollut. 249, 1049–1059.
Meng, Z.Y., Liu, L., Xi, Y.X., Jia, M., Yan, S., Tian, S.N., Sun, W., Zhu, W.T., Li, X.F., Zhou, Z.Q., 2020. Different effects of exposure to penconazole and its enantiomers on hepatic glycolipid metabolism of male mice. Environ. Pollut. 257, 113555.
Norková, R., Jaklová Dytrtová, J., Jakl, M., Schröder, D., 2012. Formation of tebuconazole complexes with cadmium(II) investigated by electrospray ionization mass spectrometry. Water Air Soil Pollut. 223, 2633–2640.
Révész, Á., Milko, P., Žabka, J., Schröder, D., Roithová, J., 2010. Reduction from copper(II) to copper(I) upon collisional activation of $(pyridine)_2CuCl^+$. J. Mass Spectrom. 45, 1246–1252.
Rieke, S., Koehn, S., Hirsch-Ernst, K., Pfeil, R., Kneuer, C., Marx-Stoelting, P., 2014. Combination effects of (tri)azole fungicides on hormone production and xenobiotic metabolism in a human placental cell line. Int. J. Environ. Res. Publ. Health 11, 9661–9680.
Schmidt, F., Marx-Stoelting, P., Haider, W., Heise, T., Kneuer, C., Ladwig, M., Banneke, S., Rieke, S., Niemann, L., 2016. Combination effects of azole fungicides in male rats in a broad dose range. Toxicology 355, 54–63.
Schröder, D., 2004. Coulomb explosions and stability of multiply charged ions in the gas phase. Angew. Chem. Int. Ed. 43, 1329–1331.
Schwack, W., Hartmann, M., 1994. Fungicides and photochemistry: photodegradation of the azole fungicide penconazole. Zeitschrift Fur Lebensmittel-Untersuchung Und-Forschung 198, 11–14.
Seeger, B., Mentz, A., Knebel, C., Schmidt, F., Bednarz, H., Niehaus, K., Albaum, S., Kalinowski, J., Noll, T., Steinberg, P., Marx-Stoelting, P., Heise, T., 2019. Assessment of mixture toxicity of (tri)azoles and their hepatotoxic effects in vitro by means of omics technologies. Arch. Toxicol. 93, 2321–2333.
Sharma, K.K., Tripathy, V., Rao, C.S., Bhushan, V.S., Reddy, K.N., Jyot, G., Sahoo, S.K., Singh, B., Mandal, K., Banerjee, H., Banerjee, T., Bhattacharya, S., George, T., Beevi, N., Sharma, K., Tayade, A., Gopal, M., Walia, S., 2019. Persistence, dissipation, and risk assessment of a combination formulation of trifloxystrobin and tebuconazole fungicides in/on tomato. Regul. Toxicol. Pharmacol. 108. Unsp. 104471.
Taxvig, C., Vinggaard, A.M., Hass, U., Axelstad, M., Metzdorff, S., Nellemann, C., 2008. Endocrine-disrupting properties *in vivo* of widely used azole fungicides. Int. J. Androl. 31, 170–176.
Tintaru, A., Charles, L., Milko, P., Roithová, J., Schröder, D., 2009. Redox reactions of copper(II) upon electrospray ionization in the presence of acridine ligands with an amide side chain. J. Phys. Org. Chem. 22, 229–233.
Trösken, E.R., Scholz, K., Lutz, R.W., Völkel, W., Zarn, J.A., Lutz, W.K., 2004. Comparative assessment of the inhibition of recombinant human CYP19 (aromatase) by azoles used in agriculture and as drugs for humans. Endocr. Res. 30, 387–394.
Vazquez-Blanco, R., Arias-Estevez, M., Baath, E., Fernandez-Calvino, D., 2020. Comparison of Cu salts and commercial Cu based fungicides on toxicity towards microorganisms in soil. Environ. Pollut. 257, 113585.
Zarn, J.A., Bruschweiler, B.J., Schlatter, J.R., 2003. Azole fungicides affect mammalian steroidogenesis by inhibiting sterol 14a-demethylase and aromatase. Environ. Health Perspect. 111, 255–261.
Zins, E.-L., Pepe, C., Schröder, D., 2010. Energy-dependent dissociation of benzylpyridinium ions in an ion-trap mass spectrometer. J. Mass Spectrom. 45, 1253–1260.

3.3.4 Cocktail effects of triazoles and zinc on cytochrome 3A4 and 19A1

Generally, azoles belong to the most efficient fungicides for the treatment of human, animal, and plant fungal pathogens (Bhagat et al 2021). They serve as the primary therapy of fungal infections, but also as prophylactic or supporting cure for immune suppressed patients (anticancer chemotherapy, HIV, organ transplants etc.) (Dvořák 2011). Their mechanism of action lies in the interaction with CYP450 which are involved in the metabolism of hydrophobic compounds. The lone pair of nitrogen in azoles can directly coordinate the heme iron in CYP450 and cause activity inhibition (Godamudunage et al 2018, Yamazoe et al 2020). Nowadays, azoles can be also found in daily used products such as washing powder, personal care products like shampoo, foam, toothpaste, hair products or so-called anti-aging creams. This excessive use of azoles has led to their accumulation in water, soil, and aquatic organisms, influencing a wide range of non-target species (Bhagat et al 2021).

After the analysis of interactions among copper ions and triazoles on the aromatase (CYP19A1) activity (Jaklová Dytrtová et al 2020), we decided to explore the effect of exchanging copper for zinc and to also assess the impact on a major biotransformation enzyme CYP3A4 (Fig. 20).

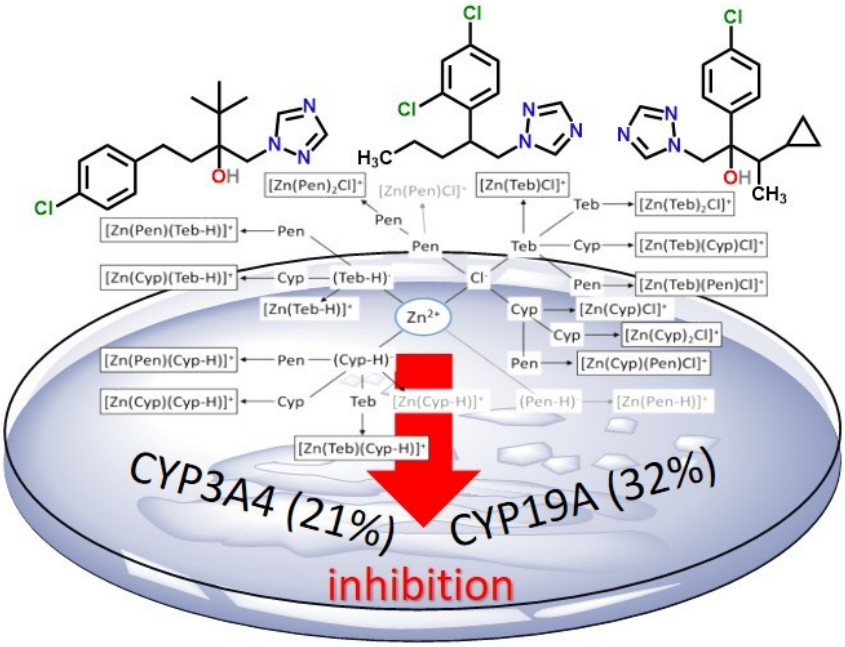


Fig. 20: Graphical abstract (Jaklová Dytrtová et al 2021).

As shown previously, single penconazole showed highest inhibition effect on CYP19A1 (Jaklová Dytrtová et al 2020) while tebuconazole most decreased

CYP3A4 activity to 57±7% (Table 1 in Jaklová Dytrtová et al 2021). The calculated cocktail effect (additional decrease of activity) in the presence of Zn^{2+} in the triazole mixtures was 20% in average for CYP3A4 and 32% in average for CYP19A1. For copper ions, we explained the cocktail effect by the creation of various complexes or adducts (Jaklová Dytrtová et al 2020). However, in the presence of Zn^{2+} we did not detect any triazole metabolites. Therefore, we supposed that the increase of inhibitory effect could be provided by the deprotonated triazoles [$(Tebuconazole\text{-}H)^-$ and $(Cyproconazole\text{-}H)^-$ mostly], which are present as ligands in the complexes with Zn^{2+}, or *via* creation of Zn^{2+} complexes with triazoles with Cl^- as a counter ion ($[Zn(TPC)_{1,2,3}Cl]^+$) or double charged complexes ($[Zn(TPC)_{3,4,5}]^{2+}$), where tebuconazole and cyproconazole are preferred as ligands (Fig. 5, Fig. 6 in Jaklová Dytrtová et al 2021). TPC means that all variants (tebuconazole, penconazole and cyproconazole) as ligands in the complex are possible.

My contribution:

I measured the impact of triazoles on the cytochrome 3A4 and 19A activities. I analyzed the data statistically and prepared the resulting tables. I helped to edit the manuscript.

Cocktail effects of triazoles and zinc on cytochrome 3A4 and 19A

Jana Jaklová Dytrtová [a, b, *], Kateřina Bělonožníková [c], Michal Jakl [d], Helena Ryšlavá [c]

[a] *Czech Academy of Sciences, Institute of Organic Chemistry and Biochemistry, Flemingovo nám. 542/2, 166 10 Prague 6, Czech Republic; dytrtova@uochb.cas.cz*

[b] *Charles University, Faculty of Physical Education and Sport, Department of Physiology and Biochemistry, José Martího 269/31, 162 52 Prague 6, Czech Republic; dytrtova@ftvs.cuni.cz*

[c] *Charles University, Faculty of Science, Department of Biochemistry, Hlavova 2030, 128 43 Prague 2, Czech Republic; k.belonoznikova@gmail.com, helena.ryslava@natur.cuni.cz*

[d] *Czech University of Life Sciences Prague, Faculty of Agrobiology, Food and Natural Resources, Department of Agro-Environmental Chemistry and Plant Nutrition, Kamýcká 129, 165 00 Prague – Suchdol, Czech Republic; jakl@af.czu.cz*

Highlights

- Additive effect of reaction mixtures of triazoles – cocktails cannot be neglected.
- Description of the creation of triazoles complexes in the presence of zinc cations.
- Aromatase activity is inhibited by triazolic cocktails with zinc by approx. 30%.
- CYP3A4 activity is inhibited by triazolic cocktails with zinc by approx. 20%.

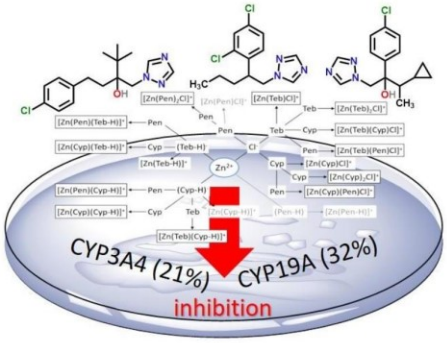
* Corresponding author. Czech Academy of Sciences, Institute of Organic Chemistry and Biochemistry, Flemingovo nám. 542/2, 166 10 Prague 6, Czech Republic; Charles University, Faculty of Physical Education and Sport, Department of Physiology and Biochemistry, José Martího 269/31, 162 52 Prague 6, Czech Republic

E-mail addresses: dytrtova@uochb.cas.cz; dytrtova@ftvs.cuni.cz (J. Jaklová Dytrtová)

Abstract

Triazoles as antifungal agents inhibit 14α-demethylase to block the biosynthesis of ergosterol. However, they also interact with other cytochrome P450 enzymes (CYP) and the resulting effects can be either advantageous or adverse. Practically, triazoles are often being applied in their mixtures, whereas possible interactions among each other (the group effect) are not considered. Moreover, their interactions with other substances naturally present in the environment (the cocktail effect) are not assessed as well. In this study, the inhibitory effect of the triazoles as singles, groups as well as cocktails on aromatase (CYP19A1) and CYP3A4 activities was investigated. The highest inhibitory effect on aromatase activity was observed for penconazole (59%) and on CYP3A4 activity was observed for tebuconazole (33%). Moreover, additional inhibitory effect on the enzyme activities, which can be attributed to the cocktail effect, was found. The most effective on aromatase inhibition are the mixtures containing penconazole and Zn, namely penconazole/cyproconazole/Zn and penconazole/cyproconazole/tebuconazole/Zn. The additional inhibitory effect on CYP3A4, attributed to the cocktail effect (of triazoles with Zn), is usually around 21% on average. The exact knowledge of triazoles behaviour in the Zn(II) presence may clarify the reasons for some macroscopic changes of plants/animal behaviour, fitness or healthiness.

Graphical abstract



Abstract

Triazoles as antifungal agents inhibit 14α-demethylase to block the biosynthesis of ergosterol. However, they also interact with other cytochrome P450 enzymes (CYP) and the resulting effects can be either advantageous or adverse. Practically, triazoles are often being applied in their mixtures, whereas possible interactions among each other (the group effect) are not considered. Moreover, their interactions with other substances naturally present in the environment (the cocktail effect) are not assessed as well. In this study, the inhibitory effect of the triazoles as singles, groups as well as cocktails on aromatase (CYP19A1) and CYP3A4 activities was investigated. The highest inhibitory effect on aromatase activity was observed for penconazole (59%) and on CYP3A4 activity was observed for tebuconazole (33%). Moreover, additional inhibitory effect on the enzyme activities, which can be attributed to the cocktail effect, was found. The most effective on aromatase inhibition are the mixtures containing penconazole and Zn, namely penconazole/cyproconazole/Zn and penconazole/cyproconazole/tebuconazole/Zn. The additional inhibitory effect on CYP3A4, attributed to the cocktail effect (of triazoles with Zn), is usually around 21% on average. The exact knowledge of triazoles behaviour in the Zn(II) presence may clarify the reasons for some macroscopic changes of plants/animal behaviour, fitness or healthiness.

Key words: CYP19A1; CYP3A4; antifungals; enzyme activity; inhibitory effect

1. Introduction

Azoles represent a large group of drugs used to treat yeast and fungal infections, but also work as prophylactic or supporting treatment of immune suppressed patients (Balding et al., 2008; Dvořák, 2011). They are a substrate for and inhibitors of cytochrome P450 enzymes (CYP450), as well as inhibitors of membrane transporters such as P-glycoprotein (Brüggemann et al., 2009). Azoles inhibit the biosynthesis of steroids (Egbuta et al., 2014; Zarn et al., 2003), namely they block sterol 14α-demethylase (CYP51, EC 1.14.14.154) which yields to the depletion of ergosterol leading to destabilization of fungal plasma membranes (Dvořák, 2011; Lepesheva et al., 2003). For example, triazoles appear as an important class of drugs to treat and prevent invasive aspergillosis by inhibiting fungal CYP3A4 enzyme (Groll et al., 2017).

However, as a side effect of the antifungal treatment azoles also inhibit the activity of aromatase (CYP19A1, EC 1.14.14.14) which catalyses the conversion of androstenedione or testosterone to oestrone or beta-oestradiol (Conley et al., 2001). In a healthy organism, this inhibition leads to the harmful depletion of oestrogens and therefore, azoles are considered as potential endocrine disruptors (Trösken et al., 2006). On the other hand, the aromatase inhibitors (e.g., letrozole, anastrozole) are being applied in postmenopausal breast cancer therapy because high amounts of oestrogen would promote cancer cells growth and spread (Egbuta et al., 2014).

In general, CYP450 is involved in the metabolism of various hydrophobic chemicals. The nitrogen lone pair in azoles can directly coordinate the heme iron in CYP450 to elicit inhibition (Godamudunage et al., 2018; Yamazoe et al., 2020). CYP3A4 (EC 1.14.14.1), a major CYP form, expressed in human liver and small intestine, serves for degradation of most of xenobiotics,

being responsible for metabolism of more than 50% of medicines (Lynch and Price, 2007; Yamazoe et al., 2020). Therefore, binding of azoles to CYP3A4 – resulting in its inhibition or induction – often also leads to adverse drug-drug interactions and has been in the centre of scientific interest (Balding et al., 2008; Godamudunage et al., 2018; Groll et al., 2017; Yamazoe et al., 2020). It may be well described how (tri)azoles influence the target enzymes individually (Lang et al., 1993; Trösken et al., 2006). However, the cocktail effect of triazoles on the metabolic enzymes has not been sufficiently clarified yet.

Triazoles (**Cyp** and **Teb**) bind to dications (e.g., Zn^{2+}) *via* the 4N of the triazole ring, *via* the π-electrons of the chlorophenyl ring and *via* the oxygen atom of the OH group (Jakl et al., 2017; Jaklová Dytrtová et al., 2014; Jaklová Dytrtová et al., 2011; Jaklová Dytrtová et al., 2013; Jaklová Dytrtová et al., 2018). The creation of this type of bonds also explains the deprotonation of **Cyp** (Jakl et al., 2017) and **Pen** (Kovač et al., 2020) in the presence of Zn^{2+}; the deprotonation yields to more stable bond to Zn^{2+}. In general, triazoles have strong tendency to create stable complexes with dications (Jaklová Dytrtová et al., 2014; Jaklová Dytrtová et al., 2011). This tendency can be taken to advantage for triazoles analysis in environmental matrixes (Jaklová Dytrtová et al., 2013). On the other hand, we have considered that this tendency significantly influences the reactivity of triazoles (Jaklová Dytrtová et al., 2018).

The rather excessive use of azoles in agriculture, pharmaceuticals, and personal care products has led to their accumulation in water, soil, and aquatic organisms (Bhagat et al., 2021). Triazoles are commonly used as systemic fungicides to crop protection against yeast and mildew (Ribas e Ribas et al., 2016). As the number of various mixtures and newly developed azoles increases in the environment, the more frequent and larger the exposure to non-target organisms is (Bhagat et al., 2021; Casida, 2009; Schmidt et al., 2016). This research study aims

to bring information on how different cocktails of triazoles, namely tebuconazole, penconazole and cyproconazole, and Zn(II) influence the activity of aromatase and CYP3A4 and which triazoles and Zn complexes predominantly form.

2. Material and methods

2.1. Chemicals

Tebuconazole (1-(4-chlorophenyl)-4,4-dimethyl-3-(1H-1,2,4-triazol-1-ylmethyl)pentan-3-ol; **Teb**), penconazole (1-[2-(2,4-dichlorophenyl)pentyl]1,2,4-triazole; **Pen**) and cyproconazole (2-(4-chlorophenyl)-3-cyclopropyl-1-(1H-1,2,4-triazol-1-yl)butan-2-ol; **Cyp**) were of the analytical grade purity (Pestanal®), and anhydrous $ZnCl_2$ of 99.99% (trace metal basis) purity, all purchased from Sigma-Aldrich (Czech Republic). The solid standards served for preparation of the stock solutions. Stock solutions of triazoles (10^{-2} mol/L) were prepared in ethanol (99.9%; VWR s.r.o.) or in acetonitrile (Sigma-Aldrich) for biochemical experiments and the stock solution of $ZnCl_2$ was prepared in deionised water (18.2 MΩ purity, Milli-Q®, Millipore). All the stock solutions were stored in a freezer (-25°C).

2.2. Effect on human recombinant aromatase (CYP19A1) and CYP3A4 in vitro

The effect of the test triazoles and Zn^{2+} on the aromatase or CYP3A4 activity was evaluated in the samples prepared with the equimolar concentration of triazole (10^{-6} mol/L) with/without the presence of $ZnCl_2$ equimolar to triazoles (**Table 1**). The activity of CYP19A and CYP3A4 (*RFU*/min/μg) was experimentally determined using a NADPH-generating system (based on glucose-6-phosphate dehydrogenase) and a fluorogenic substrate, which after reduction turns into a highly fluorescent metabolite. For this purpose, the Aromatase and Cytochrome P450 3A4 Inhibitor Screening Kits (Fluorometric) (BioVision, Milpitas, USA) were used. The stock

solutions of triazoles were prepared in acetonitrile (Sigma-Aldrich) because it was shown to have the least impact on cytochrome activities at the final concentration <1% according to the manufacturer. The substrate was also dissolved in acetonitrile according to the manual (0.1% in reaction). The presence of 10^{-6} mol/L triazole solution meant an only 0.01% increase in the total acetonitrile concentration in the reaction mixture. The increase of acetonitrile had no effect on aromatase activity (data not shown). The fluorescent metabolite was measured using a multi-well fluorescence microplate reader (Infinite M200 PRO, Tecan, Switzerland) in the kinetic mode at 488/527 nm for CYP19A1 and 535/587 nm for CYP3A4 according to the manufacturer's instructions (60 min, 37°C) with the use of black 96-well plates with a flat bottom (Costar, Corning, USA). The activity was expressed in percentage, whereas the activity of 100% was related to the reference control sample containing no triazoles. The activities measured in single component samples (consisting of 10^{-6} mol/L **Teb** or **Pen** or **Cyp** or $ZnCl_2$) served for the estimation of the hypothetical activity (A_{hypoth}) of CYP19A1 and CYP3A4 in multicomponent samples.

E.g., in the sample that consisted of equimolar mixture of triazoles **Teb**/**Pen**/**Cyp** ($3.33 \cdot 10^{-7}$ mol/L each, 10^{-6} mol/L in sum) the A_{hypoth} was estimated as the weighted average of the experimental activities (A_{exp}) determined in the single-compound samples:

$$\mathrm{A_{hypoth}} = \frac{\mathrm{A_{exp}(Teb)} + \mathrm{A_{exp}(Pen)} + \mathrm{A_{exp}(Cyp)}}{3}$$

or the A_{hypoth} for the mixture containing equimolar mixture of **Teb**/**Pen**/**Cyp** ($3.33 \cdot 10^{-7}$ mol/L each, 10^{-6} mol/L in sum) and 10^{-6} mol/L of $ZnCl_2$ is expressed (with the respect of concentrations of individual components):

$$\mathrm{A_{hypoth}} = \left(\frac{\mathrm{A_{exp}(Teb)} + \mathrm{A_{exp}(Pen)} + \mathrm{A_{exp}(Cyp)}}{3} + \mathrm{A_{exp}(Zn)}\right)/2$$

The determinations were performed in three replicates, each together with a reference control sample (without triazoles and Zn). The data were analysed by One Way ANOVA (Tukey method) and t-test (Sigmaplot 12.5, Systat Software, Inc.); the differences were considered statistically significant at $P \leq 0.05$.

2.3. Creation of Zn/triazoles adducts studied using ESI-MS

The experiments were performed using a quadrupole ion-trap mass spectrometer (Finnigan LCQ Advantage, ThermoFinnigan, USA) in the positive mode. The samples were prepared from the stock solutions of triazoles and $ZnCl_2$ (10^{-2} mol/L) with the similar manner (to keep the same proportion of mixing) as the samples from biochemical experiments (**Table 1**). In contrast the total concentration of triazoles (as well as Zn^{2+}) in the samples was 50 times higher, because of the sensitivity of the instrument. For example, the sample **Teb**/**Pen**/**Cyp**/Zn^{2+} (in **Table 1**) contained $5 \cdot 10^{-5}$ mol/L of $ZnCl_2$ and $1.67 \cdot 10^{-5}$ mol/L of each triazole (**Teb**, **Pen** and **Cyp**). The sample solutions were continuously fed into ion source at 0.5 mL/h through silica capillary. Nitrogen was used as a nebulizer gas and sweep/auxiliary-gas (8 to 15 arb units) and helium as the collision gas. Other conditions of ion source were set as follows: spray voltage: 4.50 kV, capillary temperature: 200°C, capillary voltage 20 V, tube lens offset 15 V.

Collision-induced dissociation (CID) experiments were used for the study of the dissociation of complexes metal/azole complexes. The methodology was based on the dissociation of benzylpyridinium ions (Zins et al., 2010). Mass spectra of mass-selected ions were measured as fragmentation thresholds in percentages of normalised collision energy (%NCE), optimised by the manufacturer in the range from 0 to 100% and corresponded to a resonance excitation alternating current signal from 0-2.5 V (zero-to-peak) (Jaklová Dytrtová et al., 2011; Zins et al.,

2010). *NCE*s were converted into kilojoules per mole via phenomenological conversion (Jaklová Dytrtová et al., 2011; Norková et al., 2012), phenomenological appearance energies (*AE*s) are in correlation with *NCE* framework (Révész et al., 2010). The phenomenological conversion factor (which is an individual parameter depending on the instrument) was experimentally determined as follows: E_{coll} (kJ/mol) = (7.3 ± 0.3) · E_{coll} (%).

3. Results and discussion

The influence of triazoles and zinc ions on the activity of human recombinant aromatase and CYP3A4 was followed in liquid solution using a fluorogenic substrate of 2-fold Michaelis-Menten constant concentration and measured continuously in kinetic mode. The activity of aromatase or CYP3A4 was expressed in percentage, whereas the activity of 100 % was related to the reference control sample containing no triazoles (**Table 1**). The activities measured in the single component samples (consisted of 10^{-6} mol/L **Teb** or **Pen** or **Cyp** or $ZnCl_2$) served for estimation of the hypothetical activity (A_{hypoth}) of aromatase or CYP3A4 in multicomponent samples (Jaklová Dytrtová et al., 2020).

Table 1 The impact of triazoles on CYP19A1 (aromatase) and CYP3A4 activity in the liquid phase. The activity of control samples was 1.3±0.1 *RFU*/min/µg for CYP19A1 and 161±7 *RFU*/min/µg for CYP3A4. The different letters above each reaction mixture denote significant differences ($P \leq 0.05$) among the groups according to one-way ANOVA. The same minuscule letters indicate no statistically significant differences. A_{exp} … experimental activity, A_{hypoth} … estimated activity, *AIE* … additional inhibitory effect (calculated as a difference between A_{exp} and A_{hypoth}; established in [20]). The significant difference between A_{exp} and A_{hypoth} indicated by * was analysed by t-test ($P \leq 0.05$).

reaction mixture	Cytochrome 19A (aromatase)					Cytochrome 3A4				
	A_{exp} (%)	error	A_{hypoth} (%)	error	*AIE*	A_{exp} (%)	error	A_{hypoth} (%)	error	*AIE*
Control (buffer)	100.00[a]	2.60				100.00[h,j]	3.30			
Teb	**77.30[b]**	**10.10**				**57.00[i,l]**	**7.00**			
Pen	**41.00[c]**	**5.30**				**64.50[i,k,l]**	**12.40**			
Cyp	**72.30[b,d]**	**8.00**				**77.10[i,k]**	**7.50**			
Teb/Pen/Cyp	69.20[b,d,e]	8.40	63.53	6.00	5.67	61.60[i,l]	6.30	66.20	7.57	-4.60
Teb/Pen	55.30[c,d]	9.80	59.15	7.70	-3.85	57.20[i,l]	8.40	60.75	9.70	-3.55
Teb/Cyp	81.20[a,b]	5.00	74.80	9.05	6.40	64.10[i,k,l]	8.80	67.05	7.25	-2.95
Pen/Cyp	50.10[c,e,g]	8.00	56.65	6.65	-6.55	66.50[i,k,l]	12.10	70.80	9.95	-4.30
Zn^{2+}	**123.90[f]**	**6.00**				**104.80[h]**	**5.70**			
Teb/Zn^{2+}	76.50[b,d]	0.90	100.60*	8.05	**-24.10**	57.90[i,l]	8.60	80.90*	6.35	**-23.00**
Pen/Zn^{2+}	48.70[c,e,g]	2.30	82.45*	5.65	**-33.75**	64.40[i,k,l]	12.00	84.65*	9.05	**-20.25**
Cyp/Zn^{2+}	88.30[a,b]	3.80	98.10	7.00	-9.80	83.40[j,k]	7.90	90.95	6.60	-7.55
Teb/Pen/Cyp/Zn^{2+}	47.60[c,e]	13.20	93.72*	6.90	**-46.12**	62.90[i,l]	8.90	85.50*	7.33	**-22.60**
Teb/Pen/Zn^{2+}	55.10[c,d]	8.10	91.53*	6.85	**-36.43**	56.30[l]	9.40	82.78*	7.70	**-26.48**
Teb/Cyp/Zn^{2+}	69.80[b,d,g]	5.30	99.35*	7.53	**-29.55**	61.00[i,l]	7.10	85.93*	6.48	**-24.93**
Pen/Cyp/Zn^{2+}	44.20[c]	7.90	90.28*	6.33	**-46.08**	68.40[i,k,l]	12.30	87.80*	7.83	**-19.40**

3.1. Inhibition of aromatase (CYP19A1)

The direct inhibitory effect of single triazoles on aromatase increases: **Teb** (23%) < **Cyp** (28%) << **Pen** (59%). It means penconazole is the most effective inhibitor of aromatase in pure model samples from the three selected triazoles. Following to that, the mixtures of triazoles containing penconazole are the most effective in aromatase inhibition: **Teb**/**Cyp** (19%) < **Teb**/**Pen**/**Cyp** (31%) < **Teb**/**Pen** (45%) < **Pen**/**Cyp** (50%). The effect on aromatase activity, which can be attributed to the group effect of triazole mixtures revealed only deviation on the level of statistical error (**Table 1**). The effect of Zn^{2+} (alone) on the CYP19A1 activity was supporting,

the activity increased by another 23%. Therefore, it is surprising that in the mixtures of Zn^{2+} with triazoles there is an inhibitory effect. The inhibitory effect, which can be attributed to the cocktail effect, is usually almost 32% on average (**Table 1**). The mixtures containing triazoles together with Zn^{2+} inhibit aromatase as follows: **Cyp**/Zn^{2+} (12%) < **Teb**/Zn^{2+} (24%) < **Teb**/**Cyp**/Zn^{2+} (30%) < **Teb**/**Pen**/Zn^{2+} (45%) < **Pen**/Zn^{2+} (51%) ~ **Teb**/**Pen**/**Cyp**/Zn^{2+} (52%) ~ **Pen**/**Cyp**/Zn^{2+} (56%).

3.2. Inhibition of CYP3A4

The inhibitory effect of single triazoles to CYP3A4 increases as follows: **Cyp** (23%) < **Pen** (35%) < **Teb** (43%). Therefore, tebuconazole can be considered as moderately strong inhibitor of CYP3A4. The mixtures of triazoles containing tebuconazole are the most effective in CYP3A4 inhibition: **Pen**/**Cyp** (34%) < **Teb**/**Cyp** (36%) < **Teb**/**Pen**/**Cyp** (38%) < **Teb**/**Pen** (43%). The effect to CYP3A4 activity, which can be attributed to the group effect of triazole mixtures revealed only deviation on the level of statistical error (**Table 1**). The presence of Zn^{2+} (alone) does not directly increase CYP3A4 activity (as in the case of CYP19A1), which is consistent with other studies (Kim and Yun, 2005). The inhibitory effect attributable to the cocktail effect of the mixtures is almost 21% on average (**Table 1**). The mixtures containing triazoles together with Zn^{2+} inhibit CYP3A4 as follows: **Cyp**/Zn^{2+} (17%) << **Pen**/**Cyp**/Zn^{2+} (32 %) < **Pen**/Zn^{2+} (36%) ~ **Teb**/**Pen**/**Cyp**/Zn^{2+} (37%) < **Teb**/**Cyp**/Zn^{2+} (39%) < **Teb**/Zn^{2+} (42%) ~ **Teb**/**Pen**/Zn^{2+} (44%).

3.3. Additional inhibitory effect and the reactivity of triazoles with Zn^{2+}

The additional inhibitory effect (*AIE*) was calculated (%) as the difference between the experimental activity (A_{exp}) and the theoretical activity (A_{hypoth}):

$$AIE = A_{exp} - A_{hypoth}$$

The *AIE* on the enzyme activities can be directly addressed to the cocktail (triazoles with Zn^{2+}) or the group (triazoles only) effect. This cocktail or group effect can be explained by the creation of products of the mixtures (cocktails or groups). The *AIE* coming from the group effect of triazoles is in the level of the error (**Fig. SI1**). Therefore, we can consider the group effect of triazoles to CYP19A1 as well as to CYP3A4 as negligible. It means that there are no reaction products, which affect these two enzymes. On the other hand, the *AIE* coming from the cocktail effect of the mixture of a triazole with $ZnCl_2$ is significant.

It is evident that the interaction of triazoles with Zn^{2+} influence their effect to CYP19A1 and CYP3A4. Therefore, it is essential to know which reaction products of triazoles and Zn^{2+} are formed. For this purpose, it is useful to use the gas phase approach to study the variety of possible reactions or complexes using ESI-MS. Of course, the received data must be carefully evaluated because the experiments in the gas phase not always bring the same picture, which is in the liquid phase (Agrawal and Schröder, 2011; Schröder, 2004). It is expected according to the articles published previously (Jakl et al., 2017; Jaklová Dytrtová et al., 2014) that in the presence of some metals the reactivity of triazoles might be modified *via* the creation of complexes or at least by the creation of metabolites.

Let us clarify which triazole complexes in the presence of Zn^{2+} are created and may be responsible for additional decrease of enzyme activities.

3.4. Additional inhibitory effect on aromatase and the triazoles in cocktails with $ZnCl_2$

The *AIE*, which can be attributed to the cocktail effect, is usually more than -32% (**Table 1**). *AIE* of the cocktail higher than -40% was found in these mixtures: (i) **Pen**/**Cyp**/Zn^{2+} and (ii) **Teb**/**Pen**/**Cyp**/Zn^{2+}. *AIE* of the cocktail higher than -30% was found in these mixtures: (i) **Pen**/Zn^{2+} and (ii) **Teb**/**Pen**/Zn^{2+}. All these cocktails are similar in presence of **Pen** and Zn^{2+}.

There is also a little contribution of **Cyp** presence, which probable together with **Pen** creates products (Jakl et al., 2017) influencing the aromatase activity.

The smallest *AIE* is from the **Cyp**/Zn^{2+} mixture, only -9.8%. This contribution differs from the level of error slightly. It means that the **Cyp**/Zn^{2+} adducts change the aromatase activity similarly as the separate contributions of Zn^{2+} and **Cyp** and the cocktail effect might be also negligible. The system consisting of Zn^{2+} and **Cyp** is described in (Jakl et al., 2017). In the presence of Zn^{2+} **Cyp** creates its deprotonated (loss of H^+ from the hydroxyl group) form and in minority (around 1.5 %) decays (loss of the cyclopropyl ring) creating $C_{10}H_8ClN_3O$ fragment. Slightly the minor production of $C_{10}H_8ClN_3$ *via* the cyclopropyl loss can be related with the little contribution to *AIE*. On the other hand, the cocktail effect contributions as *AIE* for the rest of the tested mixtures are significant (**Table 1**).

The highest aromatase *AIE* was in the cocktails containing **Pen** (more than -33%). The system consisting of Zn^{2+} and **Pen** was in detail described in (Kovač et al., 2020). **Pen** in presence of Zn^{2+} is not producing any significant metabolite; only in minority the deprotonated **Pen** (**Pen**-H)$^-$ is produced. Therefore, the aromatase *AIE* might be dominantly provided by the **Pen** complexes. The types of complexes are strongly depended on the reaction mixture content. In presence of $ZnCl_2$ the majority of **Pen** is present in these complexes: $[Zn(\mathbf{Pen})_4]^{2+}$, $[Zn(\mathbf{Pen})_2Cl]^+$, $[Zn(\mathbf{Pen})(\mathbf{Pen}\text{-H})]^+$ and $[Zn(\mathbf{Pen})_2(\mathbf{Pen}\text{-H})]^+$. The stability of these complexes varies from the medium stable $[Zn(\mathbf{Pen})_4]^{2+}$ (159 kJ/mol) to very stable $[Zn(\mathbf{Pen})_2(\mathbf{Pen}\text{-H})]^+$ (271 kJ/mol). It is expected, that the stability of the complexes containing (**Pen**-H)$^-$ is coming from the deprotonation occurred on the chiral carbon (Kovač et al., 2020).

The contribution of the system **Teb**/Zn^{2+} **(Fig. 1)** to *AIE* is -24.1%, which is also significant. Around 10% of **Teb**/Zn^{2+} complexes contain deprotonated **Teb** (**Teb**-H)$^-$. Similarly to **Cyp** (Jakl

et al., 2017), we expect the deprotonation occurs on the hydroxyl group, therefore this deprotonation increases the stability of (**Teb**-H)$^-$ bond in contrast to **Teb**.

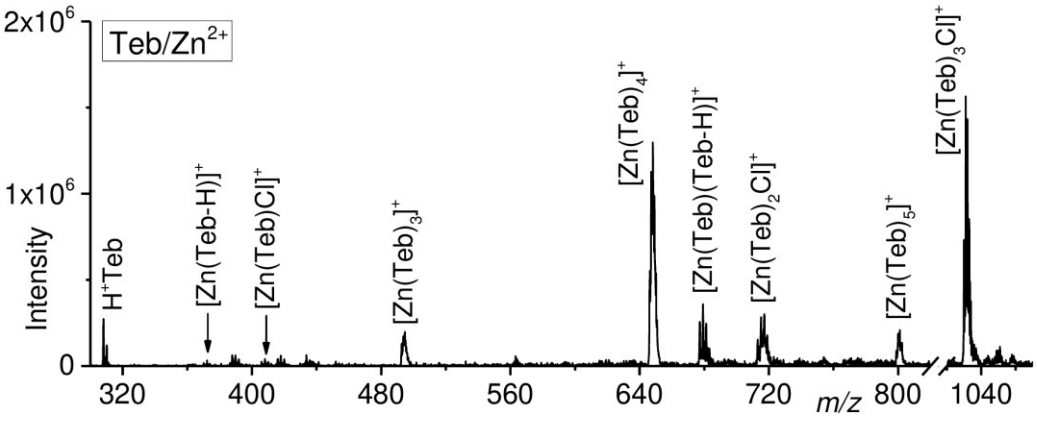


Fig. 1 Full MS spectrum of the mixture of $ZnCl_2$ ($5 \cdot 10^{-5}$ mol/L), tebuconazole (**Teb**, $5 \cdot 10^{-5}$ mol/L) in ethanol/water (1:1).

Therefore, we expect that the *AIE* -24.1% can be explained by the presence of (**Teb**-H)$^-$, which has probably higher inhibition impact to aromatase than the neutral form. The deprotonation of **Teb** as well as **Cyp** might be spontaneous in pH higher than 2 (Konášová et al., 2015), because they are weak bases. Moreover, the presence of dications such as Zn^{2+} supports this tendency *via* creation of stable (more than 200 kJ/mol) complexes (Jaklová Dytrtová et al., 2014). The **Teb**/Zn^{2+} system is also rich (42% from all charged complexes) on double charged complexes ([Zn(**Teb**)$_{3,4,5}$]$^{2+}$). The presence of double-charged complexes is unique among the studied triazole mixtures; other tested mixtures contain the double-charged complexes in minority only.

The system **Teb**/**Cyp**/Zn^{2+} (**Fig. 2**) affects *AIE* about -29.55 %, which is higher than the **Cyp**/Zn^{2+} system (-9.8%) and comparable with **Teb**/Zn^{2+} system (-24.1%). The majority of **Teb** and **Cyp**

is present in three types of complexes: (i) $[Zn(TC)_x]^{2+}$, (ii) $[Zn(TC)_3Cl]^+$ and (iii) $[Zn(TC)_y(TC\text{-}H)]^+$, where TC stands for **Teb** and/or **Cyp** ligands in the complex (triazoles occurrence in complexes explained in SI, **Fig. SI1**), x=3 or 4, y=0 or 1. The $[Zn(TC)_x]^{2+}$, $Zn(TC)_3Cl]^+$, $[Zn(TC)_y(TC\text{-}H)]^+$ and $(HTC)^+$ represent 29%, 51%, 12% and 8% of all signals in the ESI spectra, respectively. In all complexes **Teb** as well as **Cyp** substitutes the central zinc following the Gaussian distribution. **Teb** is preferred as a substituent about 5% in the $[Zn(TC)_3]^{2+}$ cluster and about 12.5% in the $[Zn(TC)_4]^{2+}$ cluster. This evidence is supported by the high incidence of $[Zn(\mathbf{Teb})_{3,4,5}]^{2+}$ in the **Teb**/Zn^{2+} mixture in contrast to the **Cyp**/Zn^{2+} mixture (Jakl et al., 2017). It means that **Teb** has slightly higher tendency than **Cyp** to create the double charged complexes with Zn^{2+}. On the other hand **Cyp** is preferred as a substituent about 4% in the $Zn(TC)_3Cl]^+$ cluster. The metabolites of **Cyp** neither **Teb,** which are formed in presence of $CuCl_2$ (Kovač et al., 2020), are not produced in presence of $ZnCl_2$ under electrospray conditions. The deprotonated **Cyp** and **Teb** in complexes represent approximately 12% from all complexes, which is the similar ratio as for **Teb**/Zn^{2+} system. There is a big difference in *AIE* contribution of the **Cyp**/Zn^{2+} and the **Teb**/**Cyp**/Zn^{2+} which can be addressed to low stability of some Zn/**Cyp** complexes. It seems that one of the **Cyp** enantiomers in the presence of Zn^{2+} has lower stability and decays promptly to $C_{10}H_8ClN_3O$ (Jakl et al., 2017). On the other hand, the presence of **Teb** in the system stabilizes **Cyp** to prevent its decay and $C_{10}H_8ClN_3O$ formation, because its signal is not seen in the spectra of the **Teb**/**Cyp**/Zn^{2+} system (**Fig. 2**).

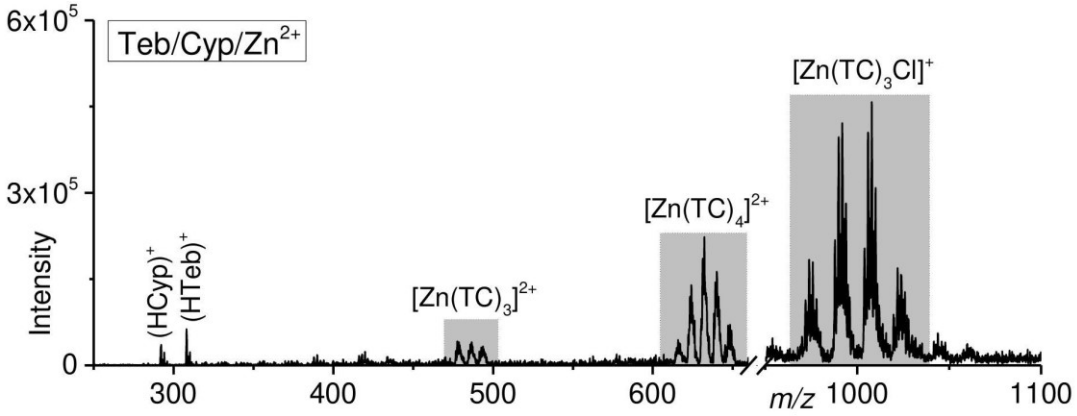


Fig. 2 Full MS spectrum of the mixture of $ZnCl_2$ ($5 \cdot 10^{-5}$ mol/L), tebuconazole (**Teb**, $2.5 \cdot 10^{-5}$ mol/L), cyproconazole (**Cyp**, $2.5 \cdot 10^{-5}$ mol/L) in ethanol/water (1:1). TC stands for **Teb** and/or **Cyp** ligands (see the **SI** for details).

The system **Teb**/**Pen**/Zn^{2+} (**Fig. 3**) decreases the activity of aromatase about additional -36.46%. This is more than **Teb**/Zn^{2+} (-24.4%) or **Pen**/Zn^{2+} (-33.75%) separately or its average. The most stable as well as the most abundant Zn^{2+} complexes contains two triazoles and one chlorine: $[Zn(TP)_2Cl]$, where TP substitutes **Teb** or **Pen** equally. In the spectra are also complexes with deprotonated tebuconazole (**Teb**-H)$^-$ and slightly with deprotonated penconazole (**Pen**-H)$^-$ (Kovač et al., 2020). Because of the high stability especially of the complex $[Zn(\mathbf{Teb})(\mathbf{Pen})Cl]^+$ (220 kJ/mol) we expect that the *AIE* can be contributed *via* its impact to aromatase.

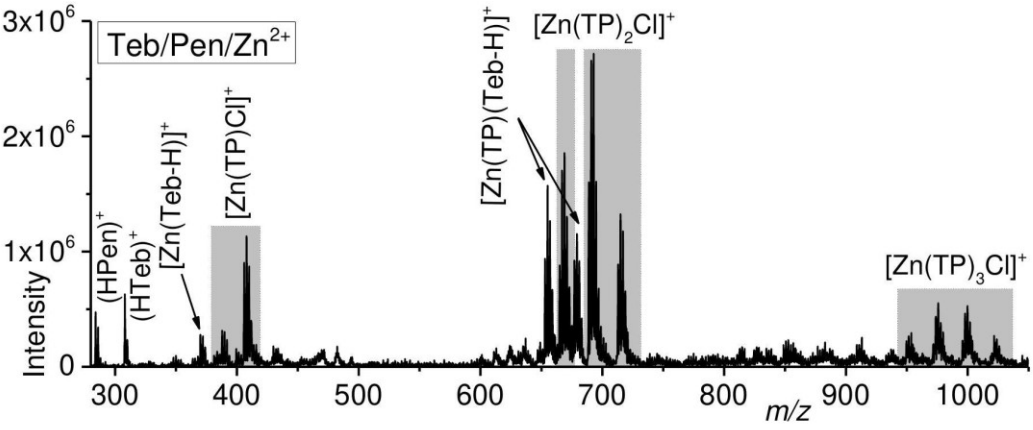


Fig. 3 Full MS spectrum of the mixture of $ZnCl_2$ ($5 \cdot 10^{-5}$ mol/L), tebuconazole (**Teb**, $2.5 \cdot 10^{-5}$ mol/L) and penconazole (**Pen**, $2.5 \cdot 10^{-5}$ mol/L) in ethanol/water (1:1). TP stands for **Teb** and/or **Pen** ligands (see the **SI** for details).

In the system **Pen**/**Cyp**/Zn^{2+} (**Fig. 4**), its *AIE* is -46.08%, not all the important **Pen**/Zn^{2+} complexes are present. Namely $[Zn(\mathbf{Pen})_4]^{2+}$ and $[Zn(\mathbf{Pen})_2(\mathbf{Pen}\text{-H})]^{+}$ are missing. The main reason for their absence is the high amount of **Pen** ligands required – four or three, which are not available. The amount of **Pen** in the **Pen**/**Cyp**/Zn^{2+} reaction mixture is a half of the amount in the **Pen**/Zn^{2+} mixture. Therefore, the highly substituted complexes are less favourable from the thermodynamically point of view. Instead of these highly substituted **Pen**/Zn^{2+} complexes, there were present the **Pen**/**Cyp**/Zn^{2+} complexes; namely $[Zn(\mathbf{Pen})(\mathbf{Cyp}\text{-H})]^{+}$, $[Zn(\mathbf{Pen})(\mathbf{Cyp})Cl]^{+}$. It is interesting that the system **Pen**/**Cyp**/Zn^{2+} decreases the aromatase activity about another 12.33% (from -33.75 to -46.08%, see **Table 1**) in contrast to the **Pen**/Zn^{2+} system. It means that the $[Zn(\mathbf{Pen})(\mathbf{Cyp}\text{-H})]^{+}$, $[Zn(\mathbf{Pen})(\mathbf{Cyp})Cl]^{+}$ complexes have some additional feature increasing the inhibitory effect on aromatase. On the other hand, the additional inhibitory effect of the system **Pen**/**Cyp**/Zn^{2+} is only 2.68 % (from -33.75 % to -36.43%), which is on the level of the error.

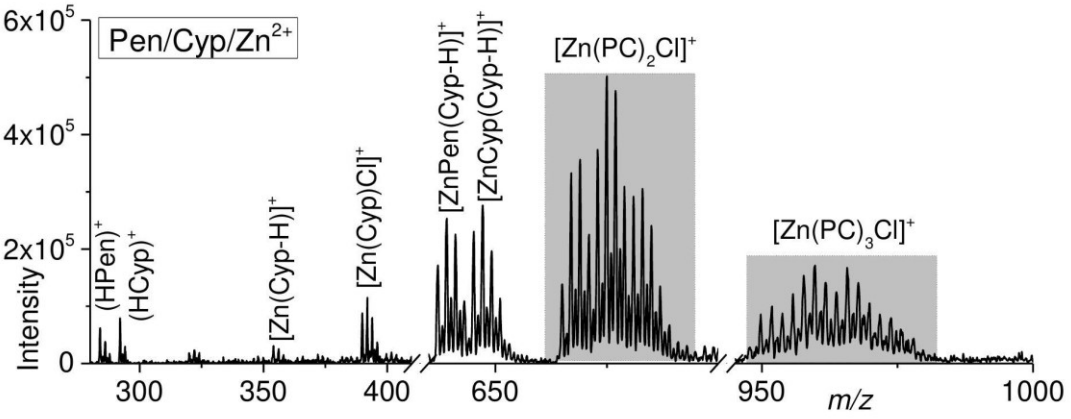


Fig. 4 Full MS spectrum of the mixture of $ZnCl_2$ ($5 \cdot 10^{-5}$ mol/L), cyproconazole (**Cyp**, $2.5 \cdot 10^{-5}$ mol/L) and penconazole (**Pen**, $2.5 \cdot 10^{-5}$ mol/L) in ethanol/water (1:1). PC stands for **Pen** and/or **Cyp** ligands.

Finally, the mixture **Teb**/**Pen**/**Cyp**/Zn^{2+} represents the most complex system here (**Fig. 5**). The *AIE* of this mixture is -46.12%, which is the biggest value among the researched mixtures. Based on previous information, we expect that the major contribution to *AIE* is created by $[Zn(TPC)_xCl]^+$ and $[Zn(TC\text{-}H)(TPC)_y]^+$ complexes, where x is 1, 2 and y is 0, 1 and TPC stands for a variety of **Teb**, **Pen** and/or **Cyp** ligands in the complex and TC for **Teb** and/or **Cyp**.

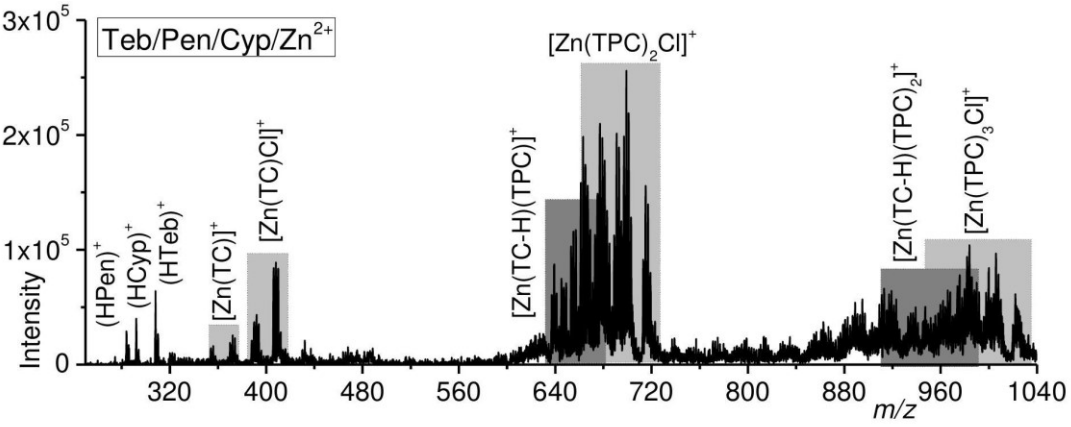


Fig. 5 Full MS spectrum of the mixture of $ZnCl_2$ ($5 \cdot 10^{-5}$ mol/L), tebuconazole (**Teb**, $1.67 \cdot 10^{-5}$ mol/L), cyproconazole (**Cyp**, $1.67 \cdot 10^{-5}$ mol/L) and penconazole (**Pen**, $1.67 \cdot 10^{-5}$ mol/L). TC stands for a variation of **Teb** and/or **Cyp** ligands and TPC for **Teb**, **Pen** and/or **Cyp** ligands.

Fig. 6 shows the most abundant complexes present in the spectrum of the **Teb**/**Pen**/**Cyp**/Zn^{2+} mixture.

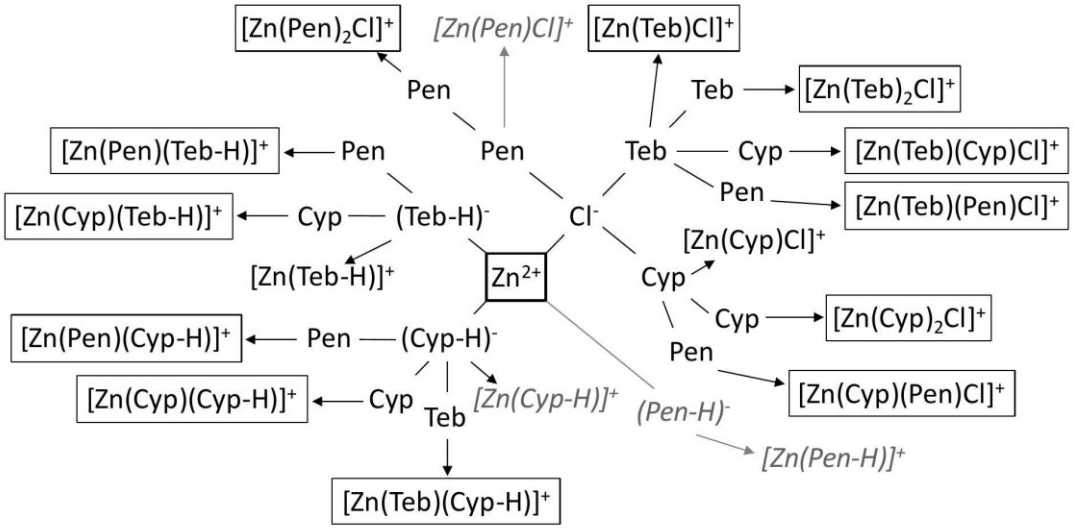


Fig. 6 Scheme of Zn^{2+}-triazole complexes generation; penconazole (**Pen**), cyproconazole (**Cyp**), tebuconazole (**Teb**).

3.5. Additional inhibitory effect on CYP3A4 and the triazoles in cocktails with $ZnCl_2$

Similarly to CYP19A1, the smallest *AIE* effect was observed for the **Cyp**/Zn^{2+} mixture; only -7.55%, which is on the level of the error. On the other hand, the *AIE* contributions to CYP3A4 activity of the other triazole/ Zn^{2+} cocktails are more similar in contrast to CYP19A1 (**Table 1**). The average *AIE* for the rest of the tested mixtures is around to -22.5%. Taking to the account the information from ESI (described in detail in the section above) we suggest that mostly the **Teb** or **Pen** complexes with Zn^{2+} are responsible for *AIE* to CYP3A4. The *AIE* of the **Teb**/**Pen**/Zn^{2+} mixture is highest (-26.48%). Moreover, it seems that the presence of **Teb** and/or **Pen** together with **Cyp** has the stabilizing effect to **Cyp**. Otherwise **Cyp** (one of the enantiomers) in the Zn^{2+} presence easily decays (Jakl et al., 2017), which can be addressed to small *AIE* of the **Cyp**/Zn^{2+} system. From the spectra of the mixture **Teb**/**Cyp**/Zn^{2+} (**Fig. 2**) can be seen the double charged complexes with mixed **Teb** and **Cyp** complexes, as well as the single charged complexes with Cl^- as a counter ion. On the other hand, the complexes containing **Cyp**-H (which are significant in **Cyp**/Zn^{2+} system (Trösken et al., 2006) are not significantly present. Therefore, we consider the complexes with $(\mathbf{Cyp}\text{-H})^-$ do not contribute to the *AIE* contrary to the other Zn^{2+} complexes. In contrast, **Cyp** in the presence of **Pen** creates few complexes containing $(\mathbf{Cyp}\text{-H})^-$ (**Fig. 4**). It corresponds with the second smallest *AIE* contribution of this system (-19.40 %).

4. Conclusion

The experimental activity of CYP19A1 is the lowest in the presence of **Pen** (41%) and of CYP3A4 in the presence of **Teb** (57%) among the tested triazoles. There is no significant effect of triazole mixtures (the group effect) to the activity of both enzymes. On the other hand, the

presence of Zn^{2+} in the mixtures with triazoles brings additional decrease of the enzyme activities although the presence of Zn^{2+} alone increases the activity of CYP19A1 (above 24%) and slightly CYP3A4 (5%).

To compare the cocktail effect of different mixture on the enzyme activities we established the parameter called additional inhibitory effect (*AIE*) calculated as a difference between the experimental and hypothetical enzymatic activity. If the value of *AIE* is positive (in just two cases) the inhibitory effect of the mixture is smaller than expected. On the other hand, if the *AIE* is negative (in most cases) the inhibitory effect of the mixture is higher than expected and can be attributed to the cocktail effect. The cocktail effect can be mostly explained by the creation of complexes or adducts. In the presence of Zn^{2+} there were not observed any metabolites of triazoles. The elevation of the inhibitory effect has to be provided by the deprotonated triazoles ((**Teb**-H)$^-$ and (**Cyp**-H)$^-$ mostly), which are present as ligands in the complexes with Zn^{2+}, or *via* creation of Zn^{2+} complexes with triazoles with Cl^- as a counter ion ($[Zn(TPC)_{1,2,3}Cl]^+$) or double charged complexes ($[Zn(TPC)_{3,4,5}]^{2+}$), where **Teb** (**Cyp**) are preferred as the ligands. TPC stands for a variation of **Teb**, **Pen** and/or **Cyp** ligands in the complex.

The smallest *AIE* for CYP19A1 and CYP3A4 (from the Zn^{2+}/triazole mixtures) was observed for the **Cyp**/Zn^{2+} mixture (-9.8% or -7.55%). This little *AIE* can be explained by low stability of one of the **Cyp** enantiomers in presence of Zn^{2+}. On the other hand, the decay of the **Cyp** enantiomer was not observed in mixtures where **Cyp** beside Zn^{2+} was in the presence of other triazoles (**Pen** or **Teb**). This result corresponds with significantly higher average *AIE* (excluding **Cyp**/Zn^{2+}) of these mixtures (-36% for CYP19A1 and -23% for CYP3A4).

Abbreviations: Cyp, cyproconazole; **Pen**, penconazole; **Teb**, tebuconazole; *RFU*, relative fluorescence units; *AE*, appearance energy; *AIE*, additional inhibitory effect of the cocktail; TC, **Teb** and/or **Cyp**; TP, **Teb** and/or **Pen**; TPC, **Teb**, **Pen** and/or **Cyp**.

Author statement

Jana Jaklová Dytrtová: conceptualization, methodology, investigation, formal analysis, writing, funding acquisition **Kateřina Bělonožníková**: investigation, formal analysis, writing **Michal Jakl**: investigation, formal analysis, writing **Helena Ryšlavá**: conceptualization, methodology, writing.

Funding

J.J.D. thanks to the Czech Science Foundation (project no. 18-01710S) for the financial support.

Competing interests

The authors declare that there are no competing interests associated with the manuscript.

References

Agrawal, D., Schröder, D., 2011. Insight into solution chemistry from gas-phase experiments. Organometallics 30, 32-35.

Balding, P.R., Porro, C.S., McLean, K.J., Sutcliffe, M.J., Marechal, J.D., Munro, A.W., de Visser, S.P., 2008. How do azoles inhibit cytochrome P450 enzymes? A density functional study. J. Phys. Chem. A 112, 12911-12918.

Bhagat, J., Singh, N., Nishimura, N., Shimada, Y., 2021. A comprehensive review on environmental toxicity of azole compounds to fish. Chemosphere 262, 128335.

Brüggemann, R.J.M., Alffenaar, J.W.C., Blijlevens, N.M.A., Billaud, E.M., Kosterink, J.G.W., Verweij, P.E., Burger, D.M., 2009. Clinical relevance of the pharmacokinetic interactions of azole antifungal drugs with other coadministered agents. Clin. Infect. Dis. 48, 1441-1458.

Casida, J.E., 2009. Pest toxicology: the primary mechanisms of pesticide action. Chem. Res. Toxicol. 22, 609-619.

Conley, A., Mapes, S., Corbin, C.J., Greger, D., Walters, K., Trant, J., Graham, S., 2001. A comparative approach to structure-function studies of mammalian aromatases. J. Steroid Biochem. Mol. Biol. 79, 289-297.

Dvořák, Z., 2011. Drug-drug interactions by azole antifungals: Beyond a dogma of CYP3A4 enzyme activity inhibition. Toxicol. Lett. 202, 129-132.

Egbuta, C., Lo, J., Ghosh, D., 2014. Mechanism of inhibition of estrogen biosynthesis by azole fungicides. Endocrinology 155, 4622-4628.

Godamudunage, M.P., Grech, A.M., Scott, E.E., 2018. Comparison of antifungal azole interactions with adult cytochrome P450 3A4 versus neonatal cytochrome P450 3A7. Drug Metab. Dispos. 46, 1329-1337.

Groll, A.H., Townsend, R., Desai, A., Azie, N., Jones, M., Engelhardt, M., Schmitt-Hoffman, A.H., Bruggemann, R.J.M., 2017. Drug-drug interactions between triazole antifungal agents used to treat invasive aspergillosis and immunosuppressants metabolized by cytochrome P450 3A4. Transpl. Infect. Dis. 19, 11.

Jakl, M., Fanfrlík, J., Jaklová Dytrtová, J., 2017. Mimicking of cyproconazole behavior in the presence of Cu and Zn Rapid Commun. Mass Spectrom. 31, 2043-2050.

Jaklová Dytrtová, J., Bělonožníková, K., Jakl, M., Ryšlavá, H., 2020. Triazoles and aromatase: The impact of copper cocktails. Environ. Pollut. 266, 1-8.

Jaklová Dytrtová, J., Fanfrlík, J., Norková, R., Jakl, M., Hobza, P., 2014. Theoretical insight into the stabilization of triazole fungicides via their interactions with dications. Int. J. Mass Spectrom. 359, 38-43.

Jaklová Dytrtová, J., Jakl, M., Schröder, D., Čadková, E., Komárek, M., 2011. Complexation between the fungicide tebuconazole and copper(II) probed by electrospray ionization mass spectrometry. Rapid Commun. Mass Spectrom. 25, 1037-1042.

Jaklová Dytrtová, J., Jakl, M., Schröder, D., Norková, R., 2013. *In situ* generation of copper cations and complexation with tebuconazole in a hyphenation of electrochemistry with mass spectrometry. Int. J. Mass Spectrom. 338, 45-49.

Jaklová Dytrtová, J., Straka, M., Bělonožníková, K., Jakl, M., Ryšlavá, H., 2018. Does resveratrol retain its antioxidative properties in wine? Redox behaviour of resveratrol in the presence of Cu(II) and tebuconazole. Food Chem. 262, 221-225.

Kim, J.S., Yun, C.H., 2005. Inhibition of human cytochrome P450 3A4 activity by zinc(II) ion. Toxicol. Lett. 156, 341-350.

Konášová, R., Jaklová Dytrtová, J., Kašička, V., 2015. Determination of acid dissociation constants of triazole fungicides by pressure assisted capillary electrophoresis. J. Chromatogr. A 1408, 243-249.

Kovač, I., Jakl, M., Fanfrlík, J., Andrushchenko, V., Jaklová Dytrtová, J., 2020. Complexation and stability of the fungicide penconazole in the presence of zinc and copper ions. Rapid Commun. Mass Spectrom. 34, e8714.

Lang, M., Batzl, C., Furet, P., Bowman, R., Hausler, A., Bhatnagar, A.S., 1993. Structure-activity relationships and binding model of novel aromatase inhibitors. J. Steroid Biochem. Mol. Biol. 44, 421-428.

Lepesheva, G.I., Virus, C., Waterman, M.R., 2003. Conservation in the CYP51 family. Role of the B' helix/BC loop and helices F and G in enzymatic function. Biochemistry 42, 9091-9101.

Lynch, T., Price, A., 2007. The effect of cytochrome P450 metabolism on drug response, interactions, and adverse effects. Am. Fam. Physician 76, 391-396.

Norková, R., Jaklová Dytrtová, J., Jakl, M., Schröder, D., 2012. Formation of tebuconazole complexes with cadmium(II) investigated by electrospray ionization mass spectrometry. Water Air Soil Pollut. 223, 2633-2640.

Révész, Á., Milko, P., Žabka, J., Schröder, D., Roithová, J., 2010. Reduction from copper(II) to copper(I) upon collisional activation of $(pyridine)_2CuCl^+$. J. Mass Spectrom. 45, 1246-1252.

Ribas e Ribas, A.D., Spolti, P., Del Ponte, E.M., Zawada Donato, K., Schrekker, H., Fuentefria, A.M., 2016. Is the emergence of fungal resistance to medical triazoles related to their use in the agroecosystems? A mini review. Braz. J. Microbiol. 47, 793-799.

Schmidt, F., Marx-Stoelting, P., Haider, W., Heise, T., Kneuer, C., Ladwig, M., Banneke, S., Rieke, S., Niemann, L., 2016. Combination effects of azole fungicides in male rats in a broad dose range. Toxicology 355, 54-63.

Schröder, D., 2004. Coulomb explosions and stability of multiply charged ions in the gas phase. Angew. Chem.-Int. Edit. 43, 1329-1331.

Trösken, E.R., Fischer, K., Völkel, W., Lutz, W.K., 2006. Inhibition of human CYP19 by azoles used as antifungal agents and aromatase inhibitors, using a new LC-MS/MS method for the analysis of estradiol product formation. Toxicology 219, 33-40.

Yamazoe, Y., Yamada, T., Nagata, K., 2020. Prediction and characterization of CYP3A4-mediated metabolisms of azole fungicides: an application of the fused-grid template* system. Food Saf. (Tokyo) 8, 34-51.

Zarn, J.A., Bruschweiler, B.J., Schlatter, J.R., 2003. Azole fungicides affect mammalian steroidogenesis by inhibiting sterol 14a-demethylase and aromatase. Environ. Health Perspect. 111, 255-261.

Zins, E.-L., Pepe, C., Schröder, D., 2010. Energy-dependent dissociation of benzylpyridinium ions in an ion-trap mass spectrometer. J. Mass Spectrom. 45, 1253-1260.

SUPPORTING INFORMATION

Additional supporting information may be found online in the Supporting Information section at the end of this article.

Supplemental



(It can be accessed online from the original file.)

4 Conclusion

The first part of the doctoral thesis was focused on plant responses to biotic and abiotic stress. In the five manuscripts, we published our results on *Pythium* strains as biological control agents, the impact of heat shock on the course of potyviral propagation, the kinetic parameters of shikimate dehydrogenase from a non-photosynthetic tissue, and the role of foliar treatment with fungicides in the plant growth.

- Even closely related *Pythium oligandrum* strains differed in their properties and effects on plants. The alterations in activities of secreted glycosidases and proteolytic enzymes, and tryptamine production may indicate advantages either for mycoparasitism or plant growth promotion.

- Rapeseed plants, seed-coated with *Pythium* strains, showed major differences in phytohormone levels, increased concentrations of auxin and jasmonates (and salicylic acid for some strains) were found, indicating plant growth promotion as well as readiness for effective defense.

- Heat shock proteins accelerate potyviral propagation. The cytosolic and mitochondrial Hsp70 (~50-75 kDa) persist throughout the developed viral infection. Also, the plant defense response results in increase of salicylic and chlorogenic acids but decrease of quinic acid content. The current research on Hsp70 and viral infection was summarized in the form of a review.

- Shikimate dehydrogenase from the root of *Petroselinum crispum* follows a sequential ordered mechanism, except for three dead-end complexes. Protocatechuic acid is formed as a byproduct, while gallic acid arises non-enzymatically, whereas quinate is not produced. The number of hydroxyl groups influences the inhibition effect of phenylpropanoids, with tannic, caffeic and chlorogenic acids being the most effective shikimate dehydrogenase inhibitors.

- The foliar treatment by triazoles (fungicides) and their mixtures likely induces oxidative stress in tomato plants. The production of some phenolics such as quercetin, *p*-coumaric acid, and hesperidin was significantly increased in triazoles-treated tomato fruit in the first harvest. Most alarming was the decrease of the weight of thin stems and foliage and the concentration of chlorophyll *a* and *b* in leaves in all the triazoles-treated variants.

The second part of the doctoral thesis was dedicated to the antioxidant capacity analyses of medicinal plants and interactions between an antioxidant and a fungicide. We also followed the impact of fungicides on "non-targets", i.e., CYP19A1 (aromatase) and CYP3A4 activities *in vitro*.

- The highest content of total phenolic compounds in aqueous extracts was found in *Agrimonia eupatoria*. In addition to this plant, high antioxidant capacities were also present in *Origanum vulgare* and *Mentha* × *piperita*. The positive correlation between the total phenolic compound content and the antioxidant capacity was strong. All the aqueous plant extracts contain larger amounts of potassium than sodium, which could be beneficial for humans with low NaCl diets.

- The treatment of wine by the fungicide tebuconazole can have unexpected antioxidant protective properties. Tebuconazole shows high affinity for Cu^{2+} which results in the protection of resveratrol. Also, tebuconazole strongly binds to resveratrol and blocks the positions attacked by Cu^{2+}.

- The presence of copper cations together with triazole(s) significantly increases the inhibitory effect on aromatase activity. The highest inhibitory effect (more than 60%) on aromatase activity is produced by cocktails containing penconazole and Cu cations, namely by penconazole/Cu^{2+} and penconazole/tebuconazole/Cu^{2+}. The reactivity of triazoles in groups is not significantly affected by the interactions among them.

- The highest inhibitory effect on CYP3A4 activity was observed for tebuconazole (43%). The additional inhibitory effect on CYP3A4, attributed to the cocktail effect (of triazoles with zinc cations), is usually around 21% on average.

- In the presence of zinc cations, the most inhibiting mixtures on aromatase activity are penconazole/cyproconazole/Zn^{2+} and penconazole/cyproconazole/tebuconazole/Zn^{2+}.

5 References

Agrios GN. 2005. How plants defend themselves against pathogens. *In Plant pathology, Published by Academic Press, Harcourt Brace & Company, San Diego*: 207-48

Al-Rawahi AK, Hancock JG. 1998. Parasitism and Biological Control of *Verticillium dahliae* by *Pythium oligandrum*. *Plant Dis.* 82: 1100-06

Ali-Shtayeh MS, Saleh ASF. 1999. Isolation of *Pythium acanthicum, P. oligandrum*, and *P. periplocum* from soil and evaluation of their mycoparasitic activity and biocontrol efficacy against selected phytopathogenic *Pythium* species. *Mycopathologia* 145: 143–53

Allmang C, Wurth L, Krol A. 2009. The selenium to selenoprotein pathway in eukaryotes: more molecular partners than anticipated. *Biochim. Biophys. Acta* 1790: 1415-23

Aparicio F, Thomas CL, Lederer C, Niu Y, Wang D, Maule AJ. 2005. Virus induction of heat shock protein 70 reflects a general response to protein accumulation in the plant cytosol. *Plant Physiol.* 138: 529-36

Arias M, Paradelo M, López E, Simal-Gándara J. 2006. Influence of pH and soil copper on adsorption of metalaxyl and penconazole by the surface layer of vineyard soils. *J. Agric. Food Chem.* 54: 8155-62

Bak A, Emerson JB. *Cauliflower mosaic virus* (CaMV) Biology, management, and relevance to GM plant detection for sustainable organic agriculture. *Front. Sustain. Food Syst.* 4: 1-21

Balint-Kurti P. 2019. The plant hypersensitive response: concepts, control and consequences. *Mol. Plant Pathol.* 20: 1163-78

Bartwal A, Mall R, Lohani P, Guru SK, Agora S. 2013. Role of secondary metabolites and brassinosteroids in plant defense against environmental stresses. *Plant Growth Regul.* 32: 216-32

Begg GS, Cook SM, Dye R, Ferrante M, Franck P, Lavigne C, Lövei GL, Mansion-Vaquie A, Pell JK, Petit S, Quesada N, Ricci B, Wratten SD, Birch ANE. 2017. A functional overview of conservation biological control. *Crop Prot.* 97: 145-58

Bela K, Horváth E, Gallé Á, Szabados L, Tari I, Csiszár J. 2015. Plant glutathione peroxidases: Emerging role of the antioxidant enzymes in plant development and stress responses. *J. Plant Physiol.* 176: 192-201

Bělonožníková K, Vaverová K, Vaněk T, Kolařík M, Hýsková V, Vaňková R, Dobrev P, Křížek T, Hodek O, Čokrtová K, Štípek A, Ryšlavá H. 2020. Novel insights into the effect of *Pythium* strains on rapeseed metabolism. *Microorganisms* 8: 1472

Benhamou N, Bélanger RR, Rey P, Tirilly Y. 2001. Oligandrin, the elicitin-like protein producedby the mycoparasite *Pythium oligandrum*, induces systemic resistance to *Fusarium crown* and root rot in tomato plants. *Plant Physiol. Biochem.* 39: 681-98

Benhamou N, le Floch G, Vallance J, Gerbore J, Grizard D, Rey P. 2012. *Pythium oligandrum*: an example of opportunistic success. *Microbiology* 158: 2679-94

Benhamou N, Nicole M. 1999. Cell biology of plant immunization against microbial infection: The potential of induced resistance in controlling plant diseases. *Plant Physiol. Biochem.* 37: 703-19

Benhamou N, Rey P, Picard K, Tirilly Y. 1999. Ultrastructural and cytochemical aspects of the interaction between the mycoparasite *Pythium oligandrum* and soilborne plant pathogens. *Phytopathology* 89: 506-17

Bentham AR, De la Concepcion JC, Mukhi N, Zdrzalek R, Draeger M, Gorenkin D, Hughes RK, Banfield MJ. 2020. A molecular roadmap to the plant immune system. *J. Biol. Chem.* 295: 14916-35

Bertini L, Proietti S, Focaracci F, Sabatini B, Caruso C. 2018. Epigenetic control of defense genes following MeJA-induced priming in rice (*O. sativa*). *J. Plant Physiol.* 228: 166-77
Bhagat J, Singh N, Nishimura N, Shimada Y. 2021. A comprehensive review on environmental toxicity of azole compounds to fish. *Chemosphere* 262: 128335
Bhattacharjee S. 2019. Reactive oxygen species in plant biology. *Springer Nature India Private Limited, New Delhi, India* eBook: 1-197
Blokhina O, Virolainen E, Fagerstedt KV. 2003. Antioxidants, oxidative damage and oxygen deprivation stress: a review. *Ann. Bot.* 91: 179-94
Bolhassani A, Agi E. 2019. Heat shock proteins in infection. *Clin. Chim. Acta* 498: 90-100
Bontpart T, Marlin T, Vialet S, Guiraud JL, Pinasseau L, Meudec E, Sommerer N, Cheynier V, Terrier N. 2016. Two shikimate dehydrogenases, VvSDH3 and VvSDH4, are involved in gallic acid biosynthesis in grapevine. *J. Exp. Bot.* 67: 3537-50
Bowyer P, Clarke BR, Lunness P, Daniels MJ, Osbourn AE. 1995. Host range of a plant pathogenic fungus determined by a saponin detoxifying enzyme. *Science* 267: 371-74
Brauer VS, Rezende CP, Pessoni AM, De Paula RG, Rangappa KS, Nayaka SC, Gupta VK, Almeida F. 2019. Antifungal Agents in Agriculture: Friends and Foes of Public Health. *Biomolecules* 9: E521
Brodt S, Six J, Feenstra G, Ingels C, Campbell D, Sustainable, agriculture. Nature Education Knowledge. 2011. Sustainable agriculture. *Nature Education Knowledge* 3: 1
Brown I, Trethowan J, Kerry M, Mansfield J, Bolwell GP. 1998. Localization of components of the oxidative cross-linking of glycoproteins and of callose synthesis in papillae formed during the interaction between non-pathogenic strains of *Xanthomonas campestris* and French bean mesophyll cells. *Plant J.* 15: 333-43
Brožová J. 2002. Exploitation of the Mycoparasitic Fungus *Pythium oligandrum* in Plant Protection. *Plant Prot. Sci.* 38: 29-35
Brunner F, Wirtz W, Rose JK, Darvill AG, Govers F, Scheel D, Nurnberger T. 2002. A beta-glucosidase/xylosidase from the phytopathogenic oomycete, *Phytophthora infestans*. *Phytochemistry* 59: 689-96
Burketová L, Trdá L, Ott PG, Valentová O. 2015. Bio-based resistance inducers for sustainable plant protection against pathogens. *Biotechnol. Adv.* 33: 994-1004
Calil IP, Fontes EPB. 2017. Plant immunity against viruses: antiviral immune receptors in focus. *Ann. Bot.* 119: 711-23
Cao F, Souders II CL, Li P, Pang S, Qiu L, Martyniuk CJ. 2019. Developmental toxicity of the triazole fungicide cyproconazole in embryo-larval stages of zebrafish (*Danio rerio*). *Environ. Sci. Pollut. Res.* 26: 4913–23
Casida JE. 2009. Pest toxicology: the primary mechanisms of pesticide action. *Chem. Res. Toxicol.* 22: 609-19
Cathrin PB, Ghanim M. 2014. Recent advances on interactions between the whitefly *Bemisia tabaci* and begomoviruses, with emphasis on *Tomato yellow leaf curl virus*. *In Plant virus-host interaction, molecular approaches and viral evolution, Edited by R.K. Gaur, P. Sharma, T. Hohn, Published by Academic Press, Elsevier, USA*: 79-103
Caverzan A, Casassola A, Brammer SP. 2016. Antioxidant responses of wheat plants under stress. *Genet. Mol. Biol.* 39: 1-6
Čeřovská N. 1998. Production of monoclonal antibodies to potato virus Y^{NTN} strain and their use for strain differentiation. *Plant Pathol.* 47: 505-09
Čeřovská N, Hoffmeisterová H, Pečenková T, Moravec T, Synková H, Plchová H, Velemínský J. 2008. Transient expression of HPV16 E7 peptide (aa 44–60) and

HPV16 L2 peptide (aa 108–120) on chimeric potyvirus-like particles using *Potato virus X*-based vector. *Protein Exp. Purif.* 58: 154–61
Čeřovská N, Moravec T, Hoffmeisterová H, Plchová H, Poláková I, Dušková M, Šmahel M. 2013. Expression of a recombinant *Human papillomavirus* 16 E6GT oncoprotein fused to N- and C-termini of Potato virus X coat protein in *Nicotiana benthamiana*. *Plant Cell Tiss. Organ Cult.* 113: 81–90
Chen L, Liao H. 2017. Engineering crop nutrient efficiency for sustainable agriculture. *J. Integr. Plant Biol.*: 710-35
Chen Z-F, Ying G-G. 2015. Occurrence, fate and ecological risk of five typical azole fungicides as therapeutic and personal care products in the environment: A review. *Environ. Int.* 84: 142-53
Ciacka K, Tymiński M, Gniazdowska A, Krasuska U. 2020. Carbonylation of proteins—an element of plant ageing. *Planta* 252: 12
Ciríaco da Silva E, Bandeira de Albuquerque M, Dias de Azevedo Neto A, Dias da Silva J, C. 2013. Drought and its consequences to plants – from individual to ecosystem. *IntechOpen* doi: 10.5772/53833
Cona A, Rea G, Angelini R, Federico R, Tavladoraki P. 2006. Functions of amine oxidases in plant development and defence. *Trends Plant Sci.* 11
Conrath U, Beckers GJM, Langenbach CJG, Jaskiewicz MR. 2015. Priming for enhanced defense. *Annu. Rev. Phytopathol.* 53: 97-119
Cordelier S, de Ruffray P, Fritig B, Kauffmann S. 2003. Biological and molecular comparison between localized and systemic acquired resistance induced in tobacco by a *Phytophthora megasperma* glycoprotein elicitin. *Plant Mol. Biol.* 51: 109-18
Costet L, Cordelier S, Dorey S, Baillieul F, Fritig B, Kauffmann S. 1999. Relationship Between Localized Acquired Resistance (LAR) and the Hypersensitive Response (HR): HR Is Necessary for LAR to Occur and Salicylic Acid Is Not Sufficient to Trigger LAR. *Mol. Plant Microbe Interact.* 12: 655–62
Czarnocka W, Karpiński S. 2018. Friend or foe? Reactive oxygen species production, scavenging and signaling in plant response to environmental stresses. *Free Radic. Biol. Med.* 122: 4-20
Deepak SA, Ishii A, Park P. 2006. Acibenzolar-S-methyl primes cell wall strengthening genes and reactive oxygen species forming/scavenging enzymes in cucumber after fungal pathogen attack. *Physiol. Mol. Plant Pathol.* 69: 52-61
Deisseroth A, Dounce AL. 1970. Catalase: Physical and chemical properties, mechanism of catalysis, and physiological role. *Physiol. Rev.* 50: 319-75
Derevnina L, Dagdas YF, De la Concepcion JC, Bialas A, Kellner R, Petre B, Domazakis E, Du J, Wu C-H, Lin X, Aguilera-Galvez C, Cruz-Mireles N, Vleeshouwers VGAA, Kamoun S. 2016. Nine things to know about elicitins. *New Phytol.* 212: 888–95
Dias MC. 2012. Phytotoxicity: An Overview of the Physiological Responses of Plants Exposed to Fungicides. *J. Bot.* 2012: 135479
Dietz K-J. 2016. Thiol-based peroxidases and ascorbate peroxidases: Why plants rely on multiple peroxidase systems in the photosynthesizing chloroplast? *Mol. Cells* 39: 20-25
Ding Y, Sun T, Ao K, Peng Y, Zhang Y, Li X, Zhang Y. 2018. Opposite roles of salicylic acid receptors NPR1 and NPR3/NPR4 in transcriptional regulation of plant immunity. *Cell* 173: 1-14
Djellout H, Raio A, Boutoumi H, Krimi Z. 2020. *Bacillus* and *Pseudomonas* spp. strains induce a response in phenolic profile and enhance biosynthesis of antioxidant enzymes in *Agrobacterium tumefaciens* infected tomato plants. *Eur. J. Plant Pathol.* 157: 269-80

Doehlemann G, Ökmen B, Zhu W, Sharon A. 2017. *Microbiol Spectr.* 5: FUNK-0023-2016
Doubnerová V, Janošková M, Synková H, Šubr Z, Čeřovská N, Ryšlavá H. 2007. Effect of Potato virus Y on activities of antioxidant and anaplerotic enzymes in transgenic *Nicotiana tabacum* L. plants with the gene for P3 protein *Gen. Appl. Plant Physiol.* 33: 123-40
Doubnerová V, Ryšlavá H. 2011. What can enzymes of C_4 photosynthesis do for C_3 plants under stress? *Plant Sci.* 180: 575-83
Drechsler C. 1930. Some new species of Pythium. *J. Wash. Acad. Sci.* X: 398-418
Du J, Verzaux E, Chaparro-Garcia A, Bijsterbosch G, Keizer LCP, Zhou J, Liebrand TWH, Xie C, Govers F, Robatzek S. 2015. Elicitin recognition confers enhanced resistance to *Phytophthora infestans* in potato. *Nature plants* 1: 15034
Duke SO. 2018. Interaction of chemical pesticides and their formulation ingredients with microbes associated with plants and plant pests. *J. Agric. Food Chem.* 66: 7553-61
Dvořák Z. 2011. Drug–drug interactions by azole antifungals: Beyond a dogma of CYP3A4 enzyme activity inhibition. *Toxicol. Lett.* 202: 129-32
Egbuta C, Lo J, Ghosh D. 2014. Mechanism of inhibition of estrogen biosynthesis by azole fungicides. *Endocrinology* 155: en20141561
El-Borollosy AM, Waziri, H.M.A. 2013. Molecular characterization of a cucumber mosaic cucumovirus isolated from lettuce in Egypt. *Ann. Agric. Sci.* 58: 105-09
Elayabalan S, Subramaniam S, Selvarajan R. 2015. Banana bunchy top disease (BBTD) symptom expression in banana and strategies for transgenic resistance: A review. *Emir. J. Food Agric.* 27: 55-74
Espinas NA, Saze H, Saijo Y. 2016. Epigenetic control of defense signaling and priming in plants. *Front. Plant Sci.* 7: 1201
Esquivel B.D., White TD. 2017. Accumulation of Azole Drugs in the Fungal Plant Pathogen Magnaporthe oryzae Is the Result of Facilitated Diffusion Influx. *Front Microbiol* 8: 1320
Faure C, Veyssiere M, Boelle B, San Clemente H, Bouchez O, Lopez-Roques C, Chaubet A, Martinez Y, Bezouska K, Suchanek M, Gaulin E, Rey T, Dumas B. 2020. Long-read genome sequence of the sugar beet rhizosphere mycoparasite *Pythium oligandrum*. *G3-Genes Genom Genet.* 10: 431-36
Feng K, Yu J, Cheng Y, Ruan M, Wang R, Ye Q, Zhou G, Li Z, Yao Z, Yang Y, Zheng Q, Wan H. 2016. The SOD gene family in tomato: Identification, phylogenetic relationships, and expression patterns. *Front. Plant Sci.* 7: 1279
Fletcher RA, Gilley A, Sankhla N, Davis TM. 2000. Triazoles as plant growth regulators and stress protectants. *Hort. Rev.* 24: 56-138
Fotopoulos V, Gilbert MJ, Pittman JK, A.C. M, A.J. B, N. S, J.L. H, L.E. W. 2003. The monosaccharide transporter gene, AtSTP4, and the cell-wall Invertase, Atßfruct1, are induced in *Arabidopsis* during infection with the fungal biotroph *Erysiphe cichoracearum*. *Plant Physiol.* 132: 821-29
FRAC. 2020. Fungal control agents by cross resistance pattern and mode of action. *FRAC Classification of Fungicides* www.frac.info: online. [2021-03-01]
Gabrielova A, Mencl K, Suchanek M, Klimes R, Hubka V, Kolarik M. 2018. The oomycete *Pythium oligandrum* can suppress and kill the causative agents of dermatophytoses. *Mycopathologia* 183: 751-64
Gerbore J, Benhamou N, Vallance J, Le Floch G, Grizard D, Regnault-Roger C, Rey P. 2014a. Biological control of plant pathogens: advantages and limitations seen through the case study of *Pythium oligandrum*. *Environ. Sci. Pollut. Res. Int.* 21: 4847-60

Gerbore J, Vallance J, Yacoub A, Delmotte F, Grizard D, Regnault-Roger C, Rey P. 2014b. Characterization of *Pythium oligandrum* populations that colonize the rhizosphere of vines from the Bordeaux region. *FEMS Microbiol. Ecol.* 90: 153-67
Gergerich RC, Dolja VV. 2006. Introduction to plant viruses, the invisible foe. *Plant Health Instr.*: Online publication.
Gill SS, Tuteja N. 2010. Reactive oxygen species and antioxidant machinery in abiotic stress tolerance in crop plants. *Arch. Toxicol.* 86: 909-30
Godamudunage MP, Grech AM, Scott EE. 2018. Comparison of antifungal azole interactions with adult cytochrome P450 3A4 versus neonatal cytochrome P450 3A7. *Drug Metab. Dispos.* 46: 1329-37
Gorovits R, Czosnek H. 2017. The involvement of heat Shock proteins in the establishment of tomato yellow leaf curl virus infection. *Front. Plant Sci.* 8: 355
Gruhlke MC. 2019. Reactive sulfur species. *In Reactive oxygen, nitrogen and sulfur species in plants: production, metabolism, signaling and defense mechanisms, First Edition. Edited by M. Hasanuzzaman, V. Fotopoulos, K. Nahar, and M. Fujita, Published by John Wiley & Sons Ltd.*: 715-28
Gruhlke MCH, Slusarenko AJ. 2012. The biology of reactive sulfur species (RSS). *Plant Physiol. Biochem.* 59: 98-107
Gülcin I. 2012. Antioxidant activity of food constituents: an overview. *Arch. Toxicol.* 86: 345-91
Guo J, Carrington Y, Alber A, Ehlting J. 2014. Molecular characterization of quinate and shikimate metabolism in Populus trichocarpa. *J. Biol. Chem.* 289: 23846-58
Hammond-Kosack KH, Jones JDG. 2000. Responses to Plant Pathogens. *In Biochemistry & molecular biology of plants, Ediited by Buchanan B.B., Cruissem W., Jones R.L., Published by American Society of Plant Physiologists, Rockville, Maryland, USA.*: 1102-52
Hanley-Bowdoin L, Bejarano ER, Robertson D, Mansoor S. 2013. Geminiviruses: masters at redirecting and reprogramming plant processes. *Nat. Rev. Microbiol.* 11: 777-88
Hasanuzzaman M, Buhyan MHMB, Zulfiqar F, Raza A, Mohsin SMM, Mahmud JA, Fujita M, Fotopoulos V. 2020. Reactive oxygen species and antioxidant defense in plants under abiotic stress: revisiting the crucial role of a universal defense regulator. *Antioxidants* 9: 681
He G, Zhang Z, Sathanantham P, Diaz A, Wang X. 2021. *Brome mosaic virus* (*Bromoviridae*). *In Encyclopedia of virology, volume 3: Viruses as infectious agents: plant viruses, Edited by D.H. Bamford , M. Zuckerman, Published by Academic Press, Elsevier, USA* 3: 252-59
He M, He C-Q, Ding N-Z. 2018. Abiotic stresses: general defenses of and plants and chances for engineering multistress tolerance. *Front. Plant Sci.* 9: 1771
Hefferon K. 2014. Plant virus expression vector development: new perspectives. *Biomed. Res. Int.* 2014: 785382
Henlein M. 2015. Plasmodesmata: channels for viruses on the move. *Methods Mol. Biol.* 1217: 25-52
Herrmann KM, Weaver LM. 1999. The shikimate pathway. *Annu. Rev. Plant Physiol. Plant Mol. Biol.* 50: 473–503
Hibino H, Cabunagan RC. 1986. *Rice tungro-associated viruses* and their relations to host plants and vector leafhoppers. *In Tropical agricultural research series no. 19. Tropical agricultural research center, Japan.*: 173-81
Hilker M, Schmülling T. 2019. Stress priming, memory, and signalling in plants. *Plant Cell Environ.* 42: 753-61
Huang K, Li M, Liu Y, Zhu M, Zhao G, Zhou Y, Zhang L, Wu Y, Dai X, Xia T, Gao L. 2019. Functional analysis of 3-dehydroquinate dehydratase/shikimate

dehydrogenases involved in shikimate pathway in *Camellia sinensis*. *Front. Plant Sci.* 10: 1268
Huey RB, Carlson M, Crozier L, Frazier M, Hamilton H, Harley C, Hoang A, Kingsolver JG. 2002. Plants versus animals: do they deal with stress in different ways. *Integ. Comp. Biol.* 42: 415-23
Hýsková V, Bělonožníková K, Čeřovská N, Ryšlavá H. 2021a. HSP70 plays an ambiguous role during viral infections in plants. *Biol. Plant.* 65: 68-79
Hýsková V, Bělonožníková K, Doričová V, Kavan D, Gillarová S, Henke S, Synková H, Ryšlavá H, Čeřovská N. 2021b. Effects of heat treatment on metabolism of tobacco plants infected with *Potato virus Y*. *Plant Biol.* Online ahead of print: https://doi.org/10.1111/plb.13234
Hýsková V, Bělonožníková K, Šmeringaiová I, Kavan D, Ingr M, Ryšlavá H. 2021c. How is the activity of shikimate dehydrogenase from parsley root regulated and which side reactions are catalyzed? *Phytochemistry* Submitted: March 2021
Hýsková V, Ryšlavá H. 2015. Different roles of ß-N-Acetylhexosaminidase in metabolism. *Biochem. Anal. Biochem.* 4: 215
Ijaz M, Ali Q, Fahad S, Ashraf S, Shahid M, Ahmad S, Hasanuzzaman M. 2019. Role of reactive sulfur species in the oxidative metabolism in plants. *In Reactive Oxygen, Nitrogen and Sulfur Species in Plants: Production, Metabolism, Signaling and Defense Mechanisms, First Edition. Edited by M. Hasanuzzaman, V. Fotopoulos, K. Nahar, and M. Fujita, Published by John Wiley & Sons Ltd.*: 729-42
Ivanov DA, Bernards MA. 2012. Ginsenosidases and the pathogenicity of *Pythium irregulare*. *Phytochemistry* 78: 44-53
Ivanov KI, Eskelin K, Lohmus A, Makinen K. 2014. Molecular and cellular mechanisms underlying potyvirus infection. *J. Gen. Virol.* 95: 1415-29
Ivanov KI, Makinen K. 2012. Coat proteins, host factors and plant viral replication. *Curr Opin Virol* 2: 712-18
Jahnová J, Luhová L, Petřivalský M. 2019. S-Nitrosoglutathione reductase—The master regulator of protein S-nitrosation in plant NO signaling. *Plants* 8: 48
Jakl M, Cavar Zeljkovic S, Kovacs I, Bělonožníková K, Jaklová Dytrtová J. 2021a. Side effects of triazoles on treated crops. *Chemosphere* 277: 130242
Jakl M, Fanfrlík J, Jaklová Dytrtová J. 2017. Mimicking of cyproconazole behavior in the presence of Cu and Zn *Rapid Commun. Mass Spectrom.* 31: 2043-50
Jakl M, Kovač I, Ćavar Zeljković S, Jaklová Dytrtová J. 2021b. Triazole fungicides in soil affect the yield of fruit, green biomass, and phenolics production of Solanum lycopersicum L. *Food Chem.* 351: 129328
Jaklová Dytrtová J, Bělonožníková K, Jakl M, Ryšlavá H. 2020. Triazoles and aromatase: The impact of copper cocktails. *Environ. Pollut.* 266: 115201
Jaklová Dytrtová J, Bělonožníková K, Jakl M, Ryšlavá H. 2021. Cocktail effects of triazoles and zinc on cytochrome 3A4 and 19A. *Food Chem. Toxicol.*: Submitted: February
Jaklová Dytrtová J, Jakl M, Schröder D, Čadková E, Komárek M. 2011. Complexation between the fungicide tebuconazole and copper(II) probed by electrospray ionization mass spectrometry *Rapid Commun. Mass Spectrom.* 25: 1037-42
Jaklová Dytrtová J, Straka M, Bělonožníková K, Jakl M, Ryšlavá H. 2018. Does resveratrol retain its antioxidative properties in wine? Redox behaviour of resveratrol in the presence of Cu(II) and tebuconazole. *Food Chem.* 262: 221-25
Jaleel CA, Gopi R, Panneerselvam R. 2008. Growth and photosynthetic pigments responses of two varieties of Catharanthus roseus to triadimefon treatment. *C. R. Biol.* 331: 272-77
Janků M, Tichá T, Luhová L, Petřivalský M. 2019. Compartmentalization of reactive oxygen species and nitric oxide production in plant vells. *In Reactive oxygen,*

nitrogen and sulfur species in plants: Production, metabolism, signaling and defense mechanisms, First Edition. Edited by M. Hasanuzzaman, V. Fotopoulos, K. Nahar, and M. Fujita, Published by John Wiley & Sons Ltd. 2: 923-45
Jiang S, Lu Y, Li K, Lin L, Zheng H, Yan F, Chen J. 2014. Heat shock protein 70 is necessary for Rice stripe virus infection in plants. *Mol. Plant Pathol.* 15: 907-17
Jockusch H, Wiegand C, Mersch B, Rajes D. 2001. Mutants of tobacco mosaic virus with temperature-sensitive coat proteins induce heat shock response in tobacco leaves. *Mol. Plant Microbe Interact.* 14: 914-7
Jungkunz I, Link K, Vogel F, Voll LM, Sonnewald S, Sonnewald U. 2011. AtHsp70-15-deficient Arabidopsis plants are characterized by reduced growth, a constitutive cytosolic protein response and enhanced resistance to TuMV. *Plant J.* 66: 983-95
Kaddachi I, Souiden Y, Achouri D, Chéour F. 2014. Barley yellow dwarf virus (BYDV): Characteristics, hosts, vectors, disease symptoms and diagnosis. *Int. J. Phytopathol.* 3: 155-60
Kapoor D, Singh S, Kumar V, Romero R, Prasad R, Singh J. 2019. Antioxidant enzymes regulation in plants in reference to reactive oxygen species (ROS) and reactive nitrogen species (RNS). *Plant gene* 19: 100182
Kasiotis KM, Pratsinis H, Kletsas D, Haroutounian SA. 2013. Resveratrol and related stilbenes: Their anti-aging and anti-angiogenic properties. *Food Chem. Toxicol.* 61: 112-20
Keller H, Bonnet P, Galiana E, Pruvot L, Friedrich L, Ryals J, Ricci P. 1996. Salicylic acid mediates elicitin-induced systemic acquired resistance, but not necrosis in tobacco. *Mol. Plant Microbe Interact.* 9: 696-703
Kliebenstein DJ. 2012. Plant defense compounds: systems approaches to metabolic analysis. *Annu. Rev. Phytopathol.* 50: 155-73
Kovač I, Jakl M, Fanfrlík J, Andrushchenko V, Jaklová Dytrtová J. 2020. Complexation and stability of the fungicide penconazole in the presence of zinc and copper ions. *Rapid Commun. Mass Spectrom.* 34: e8714
Kovacs I, Lindmayr C. 2013. Nitricoxide-based protein modification: formation and site-specificity of protein S-nitrosylation. *Front. Plant Sci.* 4: 137
Kravchenko LV, Azarova TS, Makarova NM, Tikhonovich IA. 2004. The effect of tryptophan present in plant root exudates on the phytostimulating activity of rhizobacteria. *Microbiology* 73: 195–98
Kwon Y, Kabir MA, Wang HW, Karuppanapandian T, Monn J-C, Ryu KH, Lee GP, Kim W. 2012. Elimination of pepper mild mottle virus from infected tobacco (*Nicotiana benthamiana* L.) plants by callus culture and the sieving technique. *In Vitro Cell. Dev. Biol. Plant* 48: 595–99
Le Floch G, Rey P, Benizri E, Benhamou N, Tirilly Y. 2003. Impact of auxin-compounds produced by the antagonistic fungus *Pythium oligandrum* or the minor pathogen *Pythium* group F on plant growth. *Plant Soil* 257: 459–70
Le Hesran S, Ras E, Wajnberg E, Beukeboom LW. 2019. Next generation biological control – an introduction. *Entomol. Exp. Appl.* 167: 579-83
Le Roy J, Huss B, Creach A, Hawkins S, Neutelings G. 2016. Glycosylation is a major regulator of phenylpropanoid availability and biological activity in plants. *Front. Plant Sci.* 7: eCollection 2016
Legg J, Winter S. 2021. *Cassava Mosaic Viruses* (*Geminiviridae*). *In Encyclopedia of virology, volume 3: Viruses as infectious agents: Plant viruses, Edited by D.H. Bamford, M. Zuckerman, Published by Academic Press, Elsevier, USA* 3: 301-12
Lepesheva GI, Virus C, Waterman MR. 2003. Conservation in the CYP51 family. Role of the B‘ Helix/BC loop and helices F and G in enzymatic function. *Biochemistry* 42: 9091-101

Levy L, Damsteegt V, Scorza R, Kolber M. 2000. Plum pox potyvirus disease of stone fruits. APSnet Features.: Online
Lherminier J, Benhamou N, Larrue J, Milat M-L, Boudon-Padieu E, Nicole M, Blein J-P. 2003. Cytological characterization of elicitin-induced protection in tobacco plants infected by *Phytophthora parasitica* or Phytoplasma. *Phytopathology* 93: 1308-19
Li S, Sun Q, Wu Q, Gui W, Zhu G, Schlenk D. 2019. Endocrine disrupting effects of tebuconazole on different life stages of zebrafish (*Danio rerio*). *Environ Pollut* 249: 1049-59
Liang D, Andersen CB, Vetukuri RR, Dou D, Grenville-Briggs LJ. 2020. Horizontal gene transfer and tandem duplication shape the unique CAZyme complement of the mycoparasitic oomycetes *Pythium oligandrum* and *Pythium periplocum*. *Front. Microbiol.* 11: 581698
Lico C, Chen Q, Santi L. 2008. Viral Vectors for Production of Recombinant Proteins in Plants. *J. Cell Physiol.* 216: 366-77
Lockhart BE. 2000. Virus diseases of musa in Africa: epidemiology, detection and control. *In International conference on banana and plantain for Africa, International society for horticultural science* 540: 355-59
Lucas WJ. 2006. Plant viral movement proteins: agents for cell-to-cell trafficking of viral genomes. *Virology* 344: 169-84
Ludwig-Muller J. 2011. Auxin conjugates: their role for plant development and in the evolution of land plants. *J. Exp. Bot.* 62: 1757-73
Lushchak VI, Matviishyn TM, Husak VV, Storey JM, Storey KB. 2018. Pesticide toxicity: a mechanistic approach. *EXCLI J.* 17: 1101-36
Ma Y. 2019. Seed coating with beneficial microorganisms for precision agriculture. *Biotechnol. Adv.* 37: 1-11
Magnin-Robert M, Trotel-Aziz P, Quantinet D, Biagianti S, Aziz A. 2007. Biological control of *Botrytis cinerea* by selected grapevine-associated bacteria and stimulation of chitinase and ß-1,3-glucanase activities under field conditions. *Eur. J. Plant Pathol.* 118: 43-57
Mano J, Biswas MS, Sugimoto K. 2019. Reactive carbonyl species: A missing link in ROS signaling. *Plants* 8: 391
Masunaka A, Sekiguchi H, Takahashi H, Takenaka S. 2010. Distribution and expression of elicitin-like protein genes of the biocontrol agent *Pythium oligandrum*. *J. Phytopathol.* 158: 417–26
Mauch-Mani B, Baccelli I, Luna E, Flors V. 2017. Defense priming: an adaptive part of induced resistance. *Annu. Rev. Plant Biol.* 68: 485-512
McGowan J, Fitzpatrick DA. 2017. Genomic, network, and phylogenetic analysis of the oomycete effector arsenal. *mSphere* 2: e00408-17
Meszka B, Bielenin A. 2010. Polyversum WP a new biological prod-uct against strawberry grey mould. *Phytopathology* 58: 13-19
Milani A, Basirnejad M, Shahbazi S, Bolhassani A. 2016. HSP roles as biomarkers and antigens in bacterial and viral infections. *J. Med. Microbiol. Infec. Dis.* 4: 1-7
Miller RNG, Alves GSC, Van Sluys M-A. 2017. Plant immunity: unravelling the complexity of plant responses to biotic stresses. *Ann. Bot.* 119: 681-87
Mohamed N, Lherminier J, Farmer M-J, Fromentin J, Béno N, Houot V, Milat M-L, Blein J-P. 2007. Defense responses in grapevine leaves against *Botrytis cinerea* induced by application of a *Pythium oligandrum* strain or its elicitin, oligandrin, to roots. *Biochem. Cell Biol.* 97: 611-20
Molina-Moya E, Terrón-Camero LC, Pescador-Azofra L, Sandalio LM, M.C. RP. 2019. Reactive oxygen species and nitric oxide production, regulation and function during defense response. *In Reactive oxygen, nitrogen and sulfur species in plants: Production, metabolism, signaling and defense mechanisms, First Edition. Edited*

by M. Hasanuzzaman, V. Fotopoulos, K. Nahar, and M. Fujita, Published by John Wiley & Sons Ltd.: 573-90
Monjane AL, Dellicour S, Harnady P, Oyeniran KA, Owor BE, Bezuidenhout M, Linderme D, Syed RA, Donaldson L, Murray S, Rybicki EP, Kvarnheden A, Yazdkhasti E, Lefeuvre P, Froissart R, Roumagnac P, Shepherd DN, Harkins GW, Suchard MA, Lemey P, Varsani A, Martin DP. 2020. Symptom evolution following the emergence of maize streak virus. *eLife* 9: e51984
Moon JY, Park JM. 2016. Cross-talk in viral defense signaling in plants. *Front. Microbiol.* 7: 2068
Mostofa MG, Ghosh A, Li Z-G, Siddiqui MN, Fujita M, L.-S.P. T. 2018. Methylglyoxal – a signaling molecule in plant abiotic stress responses. *Free Radic. Biol. Med.* 122: 96-109
Muir RM, Ibanez AM, Uratsu SL, Ingham ES, Leslie CA, McGranahan GH, Batra N, Goyal S, Joseph J, Jemmis ED, Dandekar AM. 2011. Mechanism of gallic acid biosynthesis in bacteria (*Escherichia coli*) and walnut (*Juglans regia*). *Plant Mol. Biol.* 75: 555-65
Muller K, Doubnerova V, Synkova H, Cerovska N, Ryslava H. 2009. Regulation of phosphoenolpyruvate carboxylase in PVY^{NTN}-infected tobacco plants. *Biol. Chem.* 390: 245-51
Načeradská M, Mencl K. 2010. Biopreparát s *Pythium oligandrum* při léčbě dermatofytózy koček - kazuistika. *Veterinářství* 60: 559-63
Neill SJ, Desikan R, Hancock JT. 2003. Nitric oxide signalling in plants. *New Phytol.* 159: 11-35
Nicholls C, Altieri M. 2013. Plant biodiversity enhances bees and other insect pollinators in agroecosystems. A review. *Agron. Sustain. Dev.* 33: 257–74
Noctor G, Reichheld J-P, Foyer CH. 2018. ROS-related redox regulation and signaling in plants. *Semin. Cell Dev. Biol.* 80: 3-12
Ortega-Ramirez LA, Rodriguez-Garcia I, Leyva JM, Cruz-Valenzuela MR, Silva-Espinoza BA, Gonzalez-Aguilar GA, Siddiqui MW, Ayala-Zavala JF. 2014. Potential of medicinal plants as antimicrobial and antioxidant agents in food industry: a hypothesis. *J. Food Sci.* 79: R129-R37
Ouyang Z, Li X, Huang L, Hong Y, Zhang Y, Zhang H, Li D, Song F. 2015. Elicitin-like proteins Oli-D1 and Oli-D2 from *Pythium oligandrum* trigger hypersensitive response in *Nicotiana benthamiana* and induce resistance against *Botrytis cinerea* in tomato. *Mol. Plant Pathol.* 16: 238-50
Parween T, Jan S., Mahmooduzzafar S, Fatma T, Siddiqui ZH. 2016. Selective effect of pesticides on plant - a review. *Crit. Rev. Food Sci. Nutr.* 56: 160-79
Patykowski J. 2006. Role of hydrogen peroxide and apoplastic peroxidase in tomato — Botrytis cinerea interaction. *Acta Physiol. Plant* 28: 589-98
Peng M, Kuc J. 1992. Peroxidase-generated hydrogen peroxide as a source of antifungal activity in vitro and on tobacco leaf disks. *Phytopathology* 82: 696-99
Petit A-N, Fontaine F, Vatsa P, Clement C, Vaillant-Gaveau N. 2012. Fungicide impacts on photosynthesis in crop plants. *Photosynth. Res.* 111: 315–26
Petřivalský M, Kubienová L, Tichá T, Luhová L. 2015. S-Nitrosoglutathione reductase: a key regulator of S-nitrosylation in plant development and stress responses. *In Reactive oxygen and nitrogen species signaling and communication in plants, Edited by K.J. Gupta, A.U. Igamberdiev, Published by Springer International Publishing, Switzerland* 23: 283-99
Picard K, Ponchet M, Blein J-P, Rey P, Tirilly Y, Benhamou N. 2000. Oligandrin. A proteinaceous molecule produced by the mycoparasite *Pythium oligandrum* induces resistance to *Phytophthora parasitica* infection in tomato plants. *Plant Physiol.* 124: 379–95

Pieterse CM, Van der Does D, Zamioudis C, Leon-Reyes A, Van Wees SC. 2012. Hormonal modulation of plant immunity. *Annu. Rev. Cell Dev. Biol.* 28: 489-521
Pieterse CMJ, Leon-Reyes A, Van der ENt S, Van Wees SCM. 2009. Networking by small-molecule hormones in plant immunity. *Nat. Chem. Biol.* 5: 308-16
Pieterse CMJ, Van Wees SCM. 2015. Induced Disease Resistance. *In Principles of Plant-Microbe Interactions, Edited by B. Lugtenberg , Published by Springer International Publishing, Switzerland*: 123-33
Plchová H, Moravec T, Hoffmeisterová H, Folwarczna J, Čeřovská N. 2011. Expression of *Human papillomavirus* 16 E7ggg oncoprotein on N- and C-terminus of *Potato virus X* coat protein in bacterial and plant cells. *Protein Exp. Purif.* 77: 146–52
Pogany J, Nagy PD. 2015. Activation of tomato bushy stunt virus RNA-dependent RNA polymerase by cellular heat shock protein 70 is enhanced by phospholipids in vitro. *J. Virol.* 89: 5714-23
Procházková D, Wilhelmová N, Pavlík M. 2015. Reactive nitrogen species and nitric oxide. *In Nitric oxide action in abiotic stress responses in plants. Edited by M. Khan, M. Mobin, F. Mohammad, F. Corpas, Published by Springer International Publishing, Switzerland*
Riah W, Laval K, Laroche-Ajzenberg E, Mougin C, Latour X, Trinsoutrot-Gattin I. 2014. Effects of pesticides on soil enzymes: a review. *Environ. Chem. Lett.* 12: 257-73
Ricci P, Bonnet P, Huet J-C, Sallantin M, Beauvais-Cante F, Bruneteau M, Billard V, Michel G, Pernollet J-C. 1989. Structure and activity of proteins from pathogenic fungi *Phytophthora* eliciting necrosis and acquired resistance in tobacco. *Eur. J. Biochem.* 183: 555-63
Rice-Evans CA, Miller NJ, Paganga G. 1996. Structure-antioxidant activity relationships of flavonoids and phenolic acids. *Free Radic. Biol. Med.* 20: 933-56
Rybicki EP. 2015. A Top ten list for economically important plant viruses. *Arch. Virol.* 160: 17-20
Ryšlavá H, Müller K, Semorádová S, Synková H, Čeřovská N. 2003. Photosynthesis and activity of phosphoenolpyruvate carboxylase in *Nicotiana tabacum* L. leaves infected by *Potato virus A* and *Potato virus Y*. *Photosynthetica* 41: 357-63
Ryšlavá H, Valenta R, Hýsková V, Křížek T, Liberda J, Coufal P. 2014. Purification and enzymatic characterization of tobacco leaf beta-N-acetylhexosaminidase. *Biochimie* 107 263-69
Ryu KH, Hong JS. 2008. Potexvirus. *In Mahy, B.W.J., Van Regenmortel, M.H.V. Encyclopedia of Virology, Academic Press, Elsevier, USA.*: 310-13
Saddhe AA, Malvankar MR, Karle SB, Kumar K. 2019. Reactive nitrogen species: Paradigms of cellular signaling and regulation of salt stress in plants. *Environ. Exp. Bot.* 161: 86-97
Saijo Y, Loo EP. 2020. Plant immunity in signal integration between biotic and abiotic stress responses. *New Phytol.* 225: 87-104
Salas-Marina MA, Silva-Flores MA, Cervantes-Badillo MG, Rosales-Saavedra MT, Islas-Osuna MA, Casas-Flores S. 2011. The plant growth-promoting fungus Aspergillus ustus promotes growth and induces resistance against different lifestyle pathogens in *Arabidopsis thaliana*. *J. Microbiol. Biotechnol.* 21: 686-96
Salaudeen MT, Banwo OO, Kashina BD, Alegbejo MD. 2009. Current status of research on *rice yellow mottle Sobemovirus*. *Arch. Phytopathol. Pflanzenschutz* 43: 562-72
Sankaranarayanan A, Amaresan N. 2020. *Pythium*. *In Beneficial microbes in agro-ecology, bacteria and fungi, Edited by N. Amaresan, M. Senthil Kumar, K. Annapurna, K. Kumar, Published by Academic Press, Elsevier, USA*: 777-92
Satková P, Starý T, V. P, Zapletalová M, Kašparovský T, Činčalová-Kubienová L, Luhová L, Mieslerová B, Mikulík J, Lochman J, Petřivalský M. 2017. Diverse

responses of wild and cultivated tomato to BABA, oligandrin and *Oidium neolycopersici* infection. *Ann. Bot.* 119: 829-40
Schmidt CL, Gründemann D, Groth G, Müller B, Hennig H, Schultz G. 1991. Shikimate pathway in non-photosynthetic tissues identification of common enzymes and partial purification of dehydroquinate hydrolyase-shikimate oxidoreductase and chorismate mutase from roots. *J. Plant Physiol.* 138: 51-56
Schmidt F, Marx-Stoelting P, Haider W, Heise T, Kneuer C, Ladwig M, Banneke S, Rieke S, Niemann L. 2016. Combination effects of azole fungicides in male rats in a broad dose range. *Toxicology* 355: 54-63
Scholthof K-BG. 2004. Tobacco mosaic virus: A model system for plant biology. *Annu. Rev. Phytopathol.* 42: 13-34
Scholthof K-BG, Adkins S, Czosnek H, Palukaitis P, Jacquot E, Hohn T, Hohn B, Saunders K, Candresse T, Ahlquist P, Hemenway C, Foster GD. 2011. Top 10 plant viruses in molecular plant pathology. *Mol. Plant Pathol.* 12: 938-54
Sewelam N, Kazan K, Schenk PM. 2016. Global plant stress signaling: reactive oxygen species at the cross-road. *Front. Plant Sci.* 7: 187
Sharma A, Kumar V, Thukral AK, Bhardwaj R. 2017. Responses of plants to pesticide toxicity: an overview. *Planta Daninha* 37: e019184291
Sharma A, Shukla A, Attri K, Kumar M, Kumar P, Suttee A, Singh G, Barnwal R.P., Singla N. 2020. Global trends in pesticides: A looming threat and viable alternatives. *Ecotoxicol. Environ. Saf.* 201: 110812
Sharma KK, Tripathy V, Rao CS, Bhushan VS, Reddy KN, Jyot G, Sahoo SK, Singh B, Mandal K, Banerjee H, Banerjee T, Bhattacharya S, George T, Beevi N, Sharma K, Tayade A, Gopal M, Walia S. 2019. Persistence, dissipation, and risk assessment of a combination formulation of trifloxystrobin and tebuconazole fungicides in/on tomato. *Regul. Toxicol. Pharmacol.* 108: 104471
Sherwood JL, German TL, Moyer JW, Ullman DE. 2003. Tomato spotted wilt. *Plant Health Instr.* available online: Updated, 2009
Signoret PA. 2008. Cereal Viruses: Maize/Corn. *In Encyclopedia of virology, Edited by B.W.J. Mahy, M.H.V. Van Regenmortel, Published by Academic Press, Elsevier, USA.*: 475-82
Singh A, Prasad SM, Singh RP. 2016. *Plant responses to xenobiotics (eBook), Published by Springer Singapore*
Slámová K, Kapešová J, Valentová K. 2018. "Sweet flavonoids": glycosidase-catalyzed modifications. *Int. J. Mol. Sci.* 19: 2126
Šmidrkal J, Filip V, Melzoch K, Hanzlíková I, Buckiová D, Křísa B. 2001. Resveratrol. *Chem. Listy* 95: 602-09
Soares C, Carvalho MEA, Azevedo RA, Fidalgo F. 2019. Plants facing oxidative challenges—A little help from the antioxidant networks. *Environ. Exp. Bot.* 161: 4-25
Song Z, Pan F, Lou X, Wang D, Yang C, Zhang B, Zhang H. 2019. Genome-wide identification and characterization of Hsp70 gene family in *Nicotiana tabacum*. *Mol. Biol. Rep.* 46: 1941-54
Soshinkova TN, Radyukina NL, Korolkova DV, Nosov AV. 2013. Proline and gunctioning of the antioxidant system in *Thellungiella salsuginea* plants and cultured cells subjected to oxidative stress. *Russ. J. Org. Chem.* 60: 47-60
Spoustová P, Hýsková V, Müller K, Schnablová R, Ryšlavá H, Čeřovská N, Malbeck J, Cvikrová M, Synková H. 2015. Tobacco susceptibility to *Potato virus Y*^{NTN} infection is affected by grafting and endogenous cytokinin content. *Plant Sci.* 235: 25-36
Starý T, Satková P, Piterková J, Mieslerová B, Luhová L, Mikulík J, Kašparovský T, Petřivalský M, Lochman J. 2019. The elicitin ß-cryptogein's activity in tomato is

mediated by jasmonic acid and ethylene signalling pathways independently of elicitin-sterol interactions. *Planta* 249: 739-49
Stiborová M, Doubravová M, Brezinová A, Friedrich A. 1986. Effect of heavy metal ions on growth and biochemical characteristics of photosynthesis of barley *Hordeum vulgare* L. . *Photosynthetica* 20: 418-25
Strasser R. 2016. Plant protein glycosylation. *Glycobiology* 26: 926-39
Synková H, Semorádová S, R. S, Müler K, Pospíšilová J, Ryšlavá, Malbeck J, Čeřovská N. 2006. Effects of biotic stress caused by *Potato virus Y* on photosynthesis in ipt transgenic and control *Nicotiana tabacum* L. *Plant Sci.* 171: 607-16
Szittya G, Silhavy D, Molnar A, Havelda Z, Lovas A, Lakatos L, Banfalvi Z, Burgyan J. 2003. Low temperature inhibits RNA silencing-mediated defence by the control of siRNA generation. *EMBO J.* 22: 633-40
Tahara K, Nishiguchi M, Funke E, Miyazawa S-I, Miyama T, Milkowski C. 2021. Dehydroquinate dehydratase/shikimate dehydrogenases involved in gallate biosynthesis of the aluminum-tolerant tree species *Eucalyptus camaldulensis*. *Planta* 253: 3
Takenaka S. 2015. Studies on biological control mechanisms of *Pythium oligandrum*. *J. Gen. Plant Pathol.* 81: 466-69
Takenaka S, Ishikawa S. 2013. Biocontrol of sugar beet seedling and taproot diseases caused by *Aphanomyces cochlioides* by *Pythium oligandrum* treatments before transplanting. *Jpn. Agric. Res. Q.* 47: 75-83
Takenaka S, Nakamura Y, Kono T, Sekiguchi H, Masunaka A, Takahashi H. 2006. Novel elicitin-like proteins isolated from the cell wall of the biocontrol agent *Pythium oligandrum* induce defence-related genes in sugar beet. *Mol. Plant Pathol.* 7: 325-39
Takenaka S, Nishio Z, Nakamura Y. 2003. Induction of defense reactions in sugar beet and wheat by treatment with cell wall protein fractions from the mycoparasite *Pythium oligandrum*. *Phytopathology* 93: 1228-32
Takenaka S, Tamagake H. 2009. Foliar spray of a cell wall protein fraction from the biocontrol agent *Pythium oligandrum* induces defence-related genes and increases resistance against Cercospora leaf spot in sugar beet. *J. Gen. Plant Pathol.* 75: 340
Takenaka S, Yamaguchi K, Masunaka A, Hase S, Inoue T, Takahashi H. 2011. Implications of oligomeric forms of POD-1 and POD-2 proteins isolated from cell walls of the biocontrol agent *Pythium oligandrum* in relation to their ability to induce defense reactions in tomato. *J. Plant Physiol.* 168: 1972-79
Taxvig C, Vinggaard AM, Hass U, Axelstad M, Metzdorff S, Nellemann C. 2008. Endocrine-disrupting properties in vivo of widely used azole fungicides. *Int. J. Androl.* 31: 170-76
Tenhaken R. 2015. Cell wall remodeling under abiotic stress. *Front. Plant Sci.* 5: 771
Tichá T, Luhová L, Petřivalský M. 2016. Functions and metabolism of S-nitrosothiols and S-nitrosylation of proteins in plants: the role of S-nitrosoglutathione reductase. *In Gasotransmitters in plants: The rise of a new paradigm in cell signaling, Edited by L. Lamattina L., Springer International Publishing, Switzerland*: 175-200
Tohge T, Watanabe M, Hoefgen R, Fernie AR. 2013. Shikimate and phenylalanine biosynthesis in the green lineage. *Front. Plant Sci.* 27: 62
Trösken ER, Fischer K, Völkel W, Lutz WK. 2006. Inhibition of human CYP19 by azoles used as antifungal agents and aromatase inhibitors, using a new LC-MS/MS method for the analysis of estradiol product formation. *Toxicology* 219: 33-40

Tugume AK, Mukasa SB, Valkonen JPT. 2008. Natural wild hosts of *Sweet potato feathery mottle virus* show spatial differences in virus incidence and virus-like diseases in Uganda. *Phytopathology* 98: 640-52
Tuna AL. 2014. Influence of foliarly applied different triazole compounds on growth, nutrition, and antioxidant enzyme activities in tomato (*Solanum lycopersicum* L.) under salt stress. *Aust. J. Crop Sci.* 8: 71-79
Tupec M, Hýsková V, Bělonožníková K, Hraníček J, Červený V, Ryšlavá H. 2017. Characterization of some potential medicinal plants from Central Europe by their antioxidant capacity and the presence of metal elements. *Food Biosci.* 20: 43-50
Turgut-Kara N, Arikan B, Celik H. 2020. Epigenetic memory and priming in plants. *Genetica* 148: 47-54
Turkan I. 2017. Emerging roles for ROS and RNS – versatile molecules in plants. *J. Exp. Bot.* 68: 4413-16
Vaculík P, Plchová H, Moravec T, Hoffmeisterová H, Čeřovská N, Šmahel M. 2015. *Potato virus X* displaying the E7 peptide derived from *human papillomavirus* type 16: a novel position for epitope presentation. *Plant Cell Tiss. Organ Cult.* 120: 671-80
Vaezi A, Fakhim H, Javidnia J, Khodavaisy S, Abtahian Z, Vojoodi M, Nourbakhsh F, Badali H. 2018. Pesticide behavior in paddy fields and development of azole-resistant *Aspergillus fumigatus*: Should we be concerned? *J. Mycol. Med.* 28: 59-64
Valadas J, Mocelin R, Sachett A, Marcon M, Zanette RA, Dallegrave E, Herrmann AP, Piato A. 2019. Propiconazole induces abnormal behavior and oxidative stress in zebrafish. *Environ. Sci. Pollut. Res. Int.* 26: 27808-15
Van Loon LC, Van Strien EA. 1999. The families of pathogenesis-related proteins, their activities, and comparative analysis of PR-1 type proteins. *Physiol. Mol. Plant Pathol.* 55: 85-97
Velásquez AC, Castroverde CDM, He SY. 2018. Plant–pathogen warfare under changing climate conditions. *Curr. Biol.* 28: 619-34
Vesely D. 1978. Studies of the mycoparasitism in rhizosphere of emerging sugar-beet. *Zentralbl. Bakteriol. Naturwiss* 133: 195-200
Vishwakarma A, Kumamri A, Mur LAJ, Gupta KJ. 2018. A discrete role for alternative oxidase under hypoxia to increase nitric oxide and drive energy production. *Free Radic. Biol. Med.* 2018: 40-51
Wallis CM, Galarneau ER-A. 2020. Phenolic compound induction in plant-microbe and plant-insect interactions: a meta-analysis. *Front. Plant Sci.* 11: 2034
Wang M, Liao W. 2016. Carbon monoxide as a signaling molecule in plants. *Front Plant Sci.* 7: 572
Wu X, Valli A, Garcia JA, Zhou X, Cheng X. 2019. The tug-of-war between plants and viruses: great progress and many remaining questions. *Viruses* 11: 203
Yacoub A, Magnin N, Gerbore J, Haidar R, Bruez E, Compant S, Guyoneaud R, Rey P. 2020. The biocontrol root-oomycete, *Pythium Oligandrum*, triggers grapevine resistance and shifts in the transcriptome of the trunk pathogenic fungus, *Phaeomoniella Chlamydospora*. *Int. J. Mol. Sci.* 21: 6876
Yamazoe Y, Yamada T, Nagata K. 2020. Prediction and characterization of CYP3A4-mediated metabolisms of azole fungicides: an application of the fused-grid template* system. *Food Saf.* 8: 34-51
Yan J, Yu H, Li B, Fan A, Melkonian J, Wang X, Zhou T, Hua J. 2019. Cell autonomous and non-autonomous functions of plant intracellular immune receptors in stomatal defense and apoplastic defense. *PLoS Pathog.* 15: e1008094

Zarn JA, Brüschweiler BJ, Schlatter JR. 2003. Azole fungicides affect mammalian steroidogenesis by inhibiting sterol 14 alpha-demethylase and aromatase. *Environ. Health Perspect* 111: 3

Zhou M, Wang W. 2018. Recent advances in synthetic chemical inducers of plant immunity. *Front. Plant Sci.* 9: 1613

Zilli CG, Santa-Cruz DM, Balestrasse KB. 2014. Heme oxygenase-independent endogenous production of carbon monoxide by soybean plants subjected to salt stress. *Environ. Exp. Bot.* 102: 11-16